



**MONASH**  
University

# **The Representation of Drought in Observations and Climate Models**

**David Hoffmann**

Supervisor: Dr Ailie Gallant  
Co-supervisor: Prof Julie Arblaster

A thesis submitted for the degree of  
**Doctor of Philosophy**  
at Monash University in August 2020

School of Earth, Atmosphere and Environment  
Faculty of Science  
Melbourne, Australia

# Copyright

© David Hoffmann, 2020. Except as provided in the Copyright Act 1968, this thesis may not be reproduced in any form without the written permission of the author.

I certify that I have made all reasonable efforts to secure copyright permissions for third-party content included in this thesis and have not knowingly added copyright content to my work without the owner's permission.

# Abstract

Drought is a stochastic natural hazard and an inherent part of climate variability. The evolution of drought occurs over various time scales from sub-seasonal to multi-decadal, which has led to drought being subdivided into different types. In order to comprehensively assess each type and its characteristics, a multitude of drought indices have been developed. Those indices are based on indicators that use land surface and atmospheric variables that identify drought, such as precipitation, soil moisture and evapotranspiration (ET). Due to the complexity of drought development, the lack of long term, widely available soil moisture data and difficulties in estimating ET, those indices include uncertainties in their representation of drought due to the construction of the drought index, and because of the uncertainties in the data used to construct the index. However, these drought indices have not been evaluated on the global scale.

This thesis examined how precipitation and evapotranspiration based indices represent drought in observations and global climate models and if an inclusion of evapotranspiration in a drought index is beneficial. The focus was on agricultural drought, a drought type emerging when precipitation deficits lead to a depletion of soil moisture on seasonal to annual time scales; and flash drought, which is a rapid onset and intensification of agricultural drought within a few weeks. The highly dynamic nature of flash drought as well as the strong land-atmosphere coupling associated with flash drought, present a unique challenge for the prediction and monitoring of this particular type of drought.

This thesis first examined how drought indices represent agricultural drought in observations, given their inherent uncertainties in the data used to calculate them. A number of data sets from different commonly-used sources were procured to compute

the drought indices based on precipitation, ET, or both. Their skill in identifying agricultural drought on time scales from three to twelve months was measured using two soil moisture levels from global land surface models. The research found that in many cases the uncertainties in the variations of the drought indices to the choice of input data were larger in magnitude than the differences between the indices themselves.

The representation of flash drought based on precipitation and ET based indices was assessed using a suite of six global climate models. The performance of the indices relative to soil moisture in the top 10 cm on a 1-month time scale was evaluated in terms of event frequency, rate of change and predictive skill. The results showed that all indices were able to identify flash drought sufficiently within the model's climatology. However, the climate models showed different levels of skill in the detection of flash drought depending on the drought index applied. This was because of differences in the partitioning of energy fluxes from the land surface, highlighting fundamental differences in land-atmosphere interactions within each model.

The analysis from the global climate models were contrasted with observations over Australia. The results showed differences in flash drought frequency in ET-based estimates in the observations compared to the models, as well as in the skill of the concurrent detection of flash drought. These differences in skill were associated with differences in land-atmosphere coupling between global climate models and the observations resulting in different response times of energy and moisture fluxes, which ultimately lead to different representations of flash drought dynamics. The lagging or leading relationship of ET and precipitation to soil moisture resulted in an advanced, concurrent or delayed detection skill with onset in the soil moisture.

Overall this thesis quantified the uncertainties in estimating drought on various time scales and advocates a combination of indices to predict and monitor agricultural and flash drought.

# Publications during enrolment

**Hoffmann, D.**, Gallant, A. J. E., & Arblaster, J. M. (2020). Uncertainties in drought from index and data selection. *Journal of Geophysical Research - Atmospheres*. doi:10.1029/2019JD031946. In press.

Pendergrass, A., Meehl, G., Pulwarty, R., Hobbins, M., Hoell, A., AghaKouchak, A., Bonfils, C., Gallant, A., Hoerling, M., **Hoffmann, D.**, Kaatz, L., Lehner, F., Llewellyn, D., Mote, P., Neale, R., Overpeck, J., Sheffield, A., Stahl, K., Svoboda, M., Wheeler, M., Wood, A. W., & Woodhouse, C. (2020). Flash droughts present a new challenge for subseasonal-to-seasonal prediction. *Nature Climate Change*, 10, 191-199, <https://doi.org/10.1038/s41558-020-0709-0>

# Declaration

This thesis contains no material which has been accepted for the award of any other degree or diploma at any university or equivalent institution and, to the best of my knowledge and belief, this thesis contains no material previously published or written by another person, except where due reference is made in the text of the thesis.

This thesis includes one original article, which has been accepted by a peer-reviewed journal but is not published yet. The ideas, development and writing up of all the paper in the thesis were the principal responsibility of myself, the candidate, working under the supervision of Dr. Ailie Gallant and Prof Julie Arblaster. The published and submitted work constitute the majority of Chapters 3, with minor modifications to the introduction, data and methods sections and section numbers in order to create continuity in the presentation of this thesis.

*Continued on next page →*

Thesis Chapter	Publication Title	Status	Nature and extend of candidate's contribution	Co-author name(s) Nature and % of Co-author's contribution	Co-author(s), Monash student Y/N
3	Uncertainties in drought from index and data selection	in press	Methodology, analysis and writing (90%)	1) Ailie Gallant, input into manuscript (5%)	Yes
				2) Julie Arblaster, input into manuscript (5%)	Yes

The undersigned hereby certify that the above declaration correctly reflects the nature and extent of the student and co-authors contributions to this work.

---

Candidate: David Hoffmann

Date: 20/08/2020

---

Main Supervisor: Dr. Ailie Gallant

Date: 20/08/2020

# Acknowledgements

This project was funded by the Australian Research Council (ARC), with additional support from the ARC Centre of Excellence for Climate Extremes (CE170100023). I also want to thank the NCI and the CMS help team for providing computational support and resources.

Without the support of many people I could not have taken on this PhD project, let alone finished it. First, I must thank Dr. Ailie Gallant, my main supervisor. Ailie has given me great supervision with her expertise in drought research and I appreciate the time and effort she put in to mentor me during this project. Prof. Julie Arblaster has been a great co-supervisor and gave me lots of valuable advice during Ailie's maternity leaves. Not many work with their co-supervisor so closely together and I am glad I had this opportunity.

I am grateful for my colleagues and office mates who made Monash a great place to study. A special thanks to my German fellows Mathias Zeller, Sonja Neske and Christian Stassen who started this PhD journey just half a year earlier and made moving to the other side of the planet so much easier. I also want to thank Bethan White, Stefan Vollgger, Matthias Retsch, David Cooley, Les Toth and Julian Quinting for all the enjoyable bike rides with countless coffees in the picturesque greater Melbourne area to fuel my brain with the oxygen needed for this PhD.

I would like to thank all the staff at Monash University, Silvana Katragadda, Christine Hi, Emily Tran, Robert Oakley, Sook Chor and Ada Han who supported me with all the admin work that a PhD brings along. Special thanks go to Yuzhou Lin for his endless help with additional extensions and organisation during the last couple of months when the COVID19 pandemic hit.

A big thank you to my family, Mama, Papa, Benedikt, Oma, Opa and my friends in Germany, even though far away their support was the backbone of this endeavour. Thank you to all the friends I made in Australia, who showed me their cultural treats including Vegemite, Tim Tams and Footy and made me the coffee snob I am today. And last but not least I want to thank my partner Anna, who supported me throughout my PhD and from halfway onwards even in person, when she made the decision to move to

Melbourne. I couldn't be more grateful for her, especially in the last few weeks during lockdown restrictions when I was busy bringing this project to an end.

# Contents

<b>List of Figures</b>	<b>xii</b>
<b>List of Tables</b>	<b>xxiv</b>
<b>1 Introduction</b>	<b>1</b>
1.1 The Concept of Drought . . . . .	2
1.1.1 Drought Types . . . . .	2
1.1.2 Drought Characteristics . . . . .	7
1.1.3 Drought Indices . . . . .	8
1.1.4 Data for the Analysis of Drought . . . . .	10
1.2 Research Aims . . . . .	13
1.3 Thesis Outline . . . . .	13
<b>2 Data and Methods</b>	<b>15</b>
2.1 Data . . . . .	15
2.1.1 Observational Data . . . . .	15
2.1.1.1 GPCP . . . . .	16
2.1.1.2 CRU TS . . . . .	16
2.1.1.3 UDEL . . . . .	17
2.1.1.4 GPCP . . . . .	17
2.1.1.5 CMAP . . . . .	17
2.1.1.6 AWAP . . . . .	18
2.1.2 Reanalysis Data . . . . .	18
2.1.3 Land Surface Model Data . . . . .	21

2.1.3.1	GLDAS	21
2.1.3.2	AWRA-L	23
2.1.4	General Circulation Model Data	25
2.2	Methods	27
2.2.1	Drought and Evapotranspiration	27
2.2.2	Drought Indices	30
2.2.2.1	The Palmer Drought Severity Index (PDSI)	30
2.2.2.2	The Evaporative Demand Drought Index (EDDI)	32
2.2.2.3	The Standardised Precipitation Index (SPI)	33
2.2.2.4	The Standardised Precipitation Evapotranspiration Index (SPEI)	35
2.2.2.5	The Evaporative Stress Index (ESI)	37
<b>3</b>	<b>Uncertainties in Drought from Index and Data Selection</b>	<b>39</b>
3.1	Preface	39
3.2	Introduction	40
3.3	Data	44
3.3.1	Input variables for the SPI, SPEI and PDSI	44
3.3.2	Soil moisture estimates	44
3.4	Methods	45
3.5	Results	48
3.5.1	Sensitivity of the skill of Drought Indices to Soil Moisture Product	48
3.5.1.1	The sensitivity of drought index skill for upper soil profile (0-10cm)	48
3.5.1.2	The sensitivity of drought index skill for the deeper soil profile (10-40cm)	51
3.5.2	Sensitivity of the Skill of Drought Indices to Index Input Datasets	54
3.5.2.1	Regional Differences in the Sensitivities of the SPI, SPEI and PDSI to Input Datasets	55
3.5.2.2	The sensitivity of drought index skill for shallow soil profile (0-10cm)	57
3.5.2.3	The sensitivity of drought index skill for deeper soil profile (10-40cm)	60

3.5.3	Sensitivity to Input Data versus Choice of Drought Index . . . . .	63
3.6	Discussion . . . . .	66
3.7	Summary . . . . .	69
<b>4</b>	<b>Flash Drought in CMIP5 Models</b>	<b>71</b>
4.1	Preface . . . . .	71
4.2	Introduction . . . . .	72
4.3	Data . . . . .	75
4.4	Methods . . . . .	75
4.5	Results . . . . .	79
4.5.1	Representation of Flash Drought in Drought Indices . . . . .	79
4.5.2	Detection skills of Drought Indices . . . . .	89
4.6	Discussion . . . . .	92
4.7	Conclusion . . . . .	95
<b>5</b>	<b>Flash Drought Detection in Models</b>	
	<b>and Observations over Australia</b>	<b>97</b>
5.1	Preface . . . . .	97
5.2	Introduction . . . . .	98
5.3	Data . . . . .	99
5.4	Methods . . . . .	100
5.5	Results . . . . .	102
5.5.1	Flash drought in AWRA-L . . . . .	103
5.5.1.1	Representation of SSI flash drought in EDDI, ESI and SPI . . . . .	103
5.5.2	Comparison between CMIP5 and AWRA-L/AWAP . . . . .	112
5.5.2.1	Relationships between soil moisture and drought indices	112
5.5.2.2	Differences in flash drought event frequency . . . . .	115
5.5.2.3	Differences in flash drought onset and rate of change . . . . .	117
5.5.2.4	Differences in flash drought detection skills . . . . .	123
5.5.3	Flash drought in AWRA-L using root-zone layer soil moisture . . . . .	126
5.5.3.1	Flash drought frequency in the root-zone layer soil mois- ture . . . . .	127

5.5.3.2	Skill metrics for early flash drought detection and monitoring . . . . .	133
5.5.3.3	Case study – southern Queensland, January 2018 . . . . .	136
5.6	Discussion . . . . .	138
5.7	Conclusion . . . . .	142
<b>6</b>	<b>Discussion and Conclusions</b>	<b>144</b>
6.1	Thesis Summary . . . . .	144
6.2	Discussion and Implications . . . . .	146
6.2.1	Drought indices incorporating ET . . . . .	147
6.2.2	Indices for the prediction and monitoring of drought . . . . .	149
6.2.3	The limitations of LSMs for drought research . . . . .	151
6.3	Future Work . . . . .	153
6.4	Conclusion . . . . .	154
<b>7</b>	<b>Appendix</b>	<b>156</b>
7.1	Appendix Chapter 3 . . . . .	156
7.2	Appendix Chapter 5 . . . . .	159
	<b>References</b>	<b>162</b>

# List of Figures

1.1	Evolution of drought with time. From Zargar et al. (2011). . . . .	3
1.2	Drought characteristics . From Mishra and Singh (2010). D = duration, S = severity, I = intensity, $t_i$ = onset, $t_e$ = cessation, X = drought proxy. . . . .	7
2.1	Global mean soil moisture content climatology for 0-10 and 10-40cm soil layers of CLMv1 and NOAHv1 as well as the scaled and unscaled times series of NOAHv2. The scaling follows the methodology in Hurrell et al. (2008) explained in the Methods section. Serious discontinuity issues in GLDAS v1 and data quality issues in both versions after 1990 as pointed out by Wang et al. (2016b) over China are expected to occur elsewhere, too, leading to periodically big deviations between the LSMs shown above. . . . .	23
2.2	Conceptual AWRA-L grid cell with key water stores and fluxes shown. From Frost et al. (2018). . . . .	24
2.3	Relationship of evapotranspiration (ET) and evaporative demand ( $E_0$ ) during the development of drought starting from wet conditions (energy-limited) on the left and proceeding into dry conditions (water-limited) to the right. From Pendergrass et al. (2020). . . . .	29

2.4	Area-averaged 3-month SPI over Australia calculated from monthly GPCP precipitation data (Schneider et al., 2014) using the original two-parameter gamma probability density function as in McKee et al. (1993) (blue) and the non-parametric empirical probability density function as in Farahmand and AghaKouchak (2015) (orange). Reference period is the entire length of the data set from 1979 to 2013. Shown is the time series from 1990 to 2010. . . . .	35
3.1	Mean correlation of three independent LSM pairings (CLMv1, NOAHv1, NOAHv2) using the 1979-2013 time period and afterwards averaged. Stippling shows statistically significant correlations at the 95% level. . . .	45
3.2	Mean and zonal correlations of varying LSMs for PDSI (a/e), SPI3 (b/f), SPI6 (c/g) and SPI12 (d/h) for whole data distribution (a-d) and drought periods (e-h) of the 0-10cm layer. The zonal average is shown to the right of each plot. Stippling shows statistically significant correlations at the 95% level. . . . .	49
3.3	Explained variance differences of PDSI minus SPI3 (a/e), SPI6 (b/f), SPI9 (c/g) and SPI12 (d/h) calculated with fixed input data from GPCP and NCEP with GLDAS CLMv1, NOAHv1 and NOAHv2 0-10cm for whole distribution (a-d) and drought periods (e-h) defined as PDSI < -2.0 and SPI < -0.8 (1979-2013). Black stippling show where all correlations of the SPI-n with GLDAS are higher than those of the PDSI. Red stippling shows where all correlations of the PDSI and GLDAS LSMs are higher than those of the SPI-n with GLDAS LSMs. . . . .	50
3.4	Mean and zonal correlations of varying LSMs for PDSI (a/e), SPI3 (b/f), SPI6 (c/g) and SPI12 (d/h) for whole data distribution (a-d) and drought periods (e-h) of the 10-40cm layer. The zonal average is shown to the right of each plot. Stippling shows statistically significant correlations at the 95% level. . . . .	52

3.5	<p>Explained variance differences of PDSI minus SPI3 (a/e), SPI6 (b/f), SPI9 (c/g) and SPI12 (d/h) calculated with fixed input data from GPCC and NCEP with GLDAS CLMv1, NOAHv1 and NOAHv2 10-40cm for whole distribution (a-d) and drought periods (e-h) defined as <math>PDSI &lt; -2.0</math> and <math>SPI &lt; -0.8</math> (1979-2013). Black stippling show where all correlations of the SPI-n with GLDAS are higher than those of the PDSI with GLDAS, red stippling where all correlations of the PDSI with GLDAS are higher than those of the SPI-n with GLDAS LSMs. . . . .</p>	53
3.6	<p>Overlap of drought periods between PDSI and SPI-n from 1948 to 2013 showing the number of months for which the PDSI and SPI both indicate drought expressed as a percentage. GPCC precipitation data used for SPI and remaining variables for the PDSI are procured from NCEP Reanalysis II. . . . .</p>	54
3.7	<p>Standardised range of PDSI (a), SPI12 (b) and SPEI12 (c) permutations. First, the range of all permutations at each time step was calculated and afterwards averaged over time. . . . .</p>	55
3.8	<p>PDSI (left), SPEI (middle) and SPI (right) calculated with different precipitation data inputs as listed in Table 2.1 averaged over six different regions defined by Giorgi and Francisco (2000) from 1979 to 2013 (WNA = West North America, AMZ = Amazon, MED = Mediterranean, EAF = East Africa, EAS = East Asia, SAU = South Australia). SAU is modified to include the southern half of Australia only. Data are smoothed with a 12-month running-mean for all indices. PDSI and PET are standardised. The root mean squared error for each region and index is shown in the top left of each time series. The <math>PDSI_{GPCC}</math> and <math>SPI_{GPCC}</math> shown as a solid line represent the ones used for the analyses in Section 3.5.1. PDSI, SPEI and SPI are unitless. . . . .</p>	56

3.9	PDSI (left), SPEI (middle) and PET (right) calculated with different temperature data inputs as listed in Table 2.1 averaged over six different regions defined by Giorgi and Francisco (2000) from 1979 to 2013 (WNA = West North America, AMZ = Amazon, MED = Mediterranean, EAF = East Africa, EAS = East Asia, SAU = South Australia). SAU is modified to include the southern half of Australia only. Data are smoothed with a 12-month running-mean for all indices. PDSI and PET are standardised. The root mean squared error for each region and index is shown in the top left of each time series. The $PDSI_{NCEP}$ and $SPEI_{NCEP}$ shown as a solid line represent the ones used for the analyses in Section 3.5.1. PDSI and SPEI are unitless. . . . .	58
3.10	Mean and zonal correlations of varying input data for PDSI (a/e), SPI3 (b/f), SPI6 (c/g) and SPI12 (d/h) for whole data distribution (a-d) and drought periods (e-h) of the 0-10cm layer. The zonal average is shown to the right of each plot. Stippling shows statistically significant correlations at the 95% level. . . . .	59
3.11	Explained variance differences of PDSI minus SPI3 (a/e), SPI6 (b/f), SPI9 (c/g) and SPI12 (d/h) with varying input data permutations with NOAHv2 0-10cm for whole distribution (a-d) and drought periods (e-h) defined as $PDSI < -2.0$ and $SPI < -0.8$ (1979-2013). Black stippling show where all correlations of the SPI-n with NOAHv2 are higher than those of the PDSI with NOAHv2, red stippling where all correlations of the PDSI with NOAHv2 are higher than those of the SPI-n with NOAHv2. . . . .	60
3.12	Mean and zonal correlation coefficients ( $r$ ) of varying input data for PDSI (a/e), SPI3 (b/e), SPI6 (c/f) and SPI12 (d/g) with GLDAS NOAHv2 for whole data distribution (a-d) and drought periods (e-g) of the 10-40cm layer. The zonal average is shown to the right of each plot. Stippling shows statistically significant correlations at the 95% level. . . . .	61

3.13	Explained variance differences of PDSI minus SPI3 (a/e), SPI6 (b/f), SPI9 (c/g) and SPI12 (d/h) with varying input data permutations with NOAHv2 10-40cm for whole distribution (a-d) and drought periods (e-h) defined as $PDSI < -2.0$ and $SPI < -0.8$ (1979-2013). Black stippling show where all correlations of the SPI-n with NOAHv2 are higher than those of the PDSI with NOAHv2, red stippling where all correlations of the PDSI with NOAHv2 are higher than those of the SPI-n with NOAHv2.	62
3.14	Best correlated indicator for whole distribution with varying LSM (a) and varying input data (c) and drought periods with varying LSM (b) and varying input data (d) of the 0-10cm layer. Stippling indicates where the underlying index is robust against the others, meaning that its max correlation coefficient as well as its mean correlation coefficient is higher than those of the other indices.	64
3.15	Best correlated indicator for whole distribution with varying LSM (a) and varying input data (c) and drought periods with varying LSM (b) and varying input data (d) of the 10-40cm layer. Stippling indicates where the strength of the correlation of the index is robust to varying the input data and LSM.	65
4.1	Time series example of standardised MIROC5 daily 0-10cm soil moisture (SSI, brown), daily aggregated 0-10cm soil moisture over 30 days (dark red) as used in our analyses and monthly root-zone layer soil moisture content up to 1.5m depth (red). The grid cell selected is located in South East Australia at $35.72^{\circ}S$ and $143.4^{\circ}E$ . Dashed lines correspond to the data's 10 <sup>th</sup> and 40 <sup>th</sup> percentile.	76
4.2	CMIP5 ensemble mean of seasonal explained variance of EDDI (top row), ESI (middle) and SPI (bottom) with 0-10cm SSI over the entire historical run length of 138 years. Statistically significant correlations on the 95% level are marked with hatching. The lag/lead at which this highest correlation was detected is shown in figure 4.3. The bottom row shows the annual inter-model spread in the CMIP5 models.	80

4.3	Lag at which the maximum explained variances shown figure 4.2 occurred for EDDI (top row), ESI (middle) and SPI (bottom). Stippling marks where the explained variances are significant at the 95% level. The bottom row shows the annual inter-model spread in the CMIP5 models. . . .	81
4.4	CMIP5 ensemble mean of seasonal FD event frequency expressed as events per decade for EDDI (a-d), ESI (e-h), SPI (i-l) and SSI (m-p) over the entire historical run length of 138 years. Hatching indicates where at least 50% of the CMIP5 models listed in Table 2.4 identified a FD. . . . .	83
4.5	Seasonal CMIP5 inter-model spread of FD event frequency for SPI (a-d), EDDI (e-h), ESI (i-l) and SSI (m-p). The inter-model spread is defined as the ratio of ensemble standard deviation to ensemble mean. Hatching indicates where at least 50% of the CMIP5 models listed in Table 2.4 identified a FD. . . . .	84
4.6	Index values by season according to the USDM at the time of flash drought onset in the SSI for SPI (left column), EDDI (middle) and ESI (right). A category of $\leq ED2$ correspond to the ESI's and SPI's 10 <sup>th</sup> and the EDDI's 90 <sup>th</sup> percentile respectively. Hatching indicates where at least 50% of the CMIP5 models listed in Table 2.4 identified a FD. . . .	86
4.7	Rates of change (RoC) per week from two weeks prior to the onset of FD in the SSI for SPI (left column), EDDI (middle) and ESI (right). Hatching indicates where at least 50% of the CMIP5 models listed in Table 2.4 identified a FD. . . . .	86
4.8	Rates of change (RoC) per week from as in Figure 4.7 but for four weeks prior to the onset of FD in the SSI. . . . .	87
4.9	Rates of change (RoC) per week from as in Figure 4.7 but for six weeks prior to the onset of FD in the SSI. . . . .	87
4.10	Rates of change (RoC) per week from as in Figure 4.7 but for eight weeks prior to the onset of FD in the SSI. . . . .	88

4.11	Hit rate (HR, panel A) and false alarm ratio (FAR, panel B) for SPI (left column), EDDI (middle) and ESI (right). The tolerance window for valid detection is from eight weeks prior to the onset of a flash drought in the soil moisture. Hatching indicates where at least 50% of the CMIP5 models listed in Table 2.4 identified a FD in the SSI. . . . .	89
4.12	As previous Figure 4.11 but the tolerance window has been extend to two weeks after flash drought onset in the soil moisture. . . . .	91
5.1	Time series of daily 0-10, 0-100 and 10-100cm soil moisture expressed in unitless values of the standardised soil moisture index (SSI) for a grid cell in south Queensland. The flash drought observed in this area in January 2018 was subject of Nguyen et al. (2019)'s study. The dashed line represents the 40 <sup>th</sup> (top), the dotted line the 20 <sup>th</sup> (middle) and the dash-dotted line the 10 <sup>th</sup> (bottom) percentile index values. Data was smoothed with a 30 days running mean before standardisation. . . . .	102
5.2	Seasonal explained variance of EDDI (top row) , ESI (middle) and SPI (bottom) with 0-10cm SSI for 1976 to 2018. Stippling marks where the explained variances are significant at the 95% level. The lag/lead at which this highest correlation was detected is shown in figure 5.3. . . . .	103
5.3	Lag at which the maximum explained variances shown figure 5.2 occurred for EDDI (top row), ESI (middle) and SPI (bottom). Stippling marks where the explained variances are significant at the 95% level. . . . .	104
5.4	Seasonal FD event frequency expressed as events per decade for SPI (first column), EDDI (second), ESI (third) and SSI (fourth) over the 39 years of the time period from 1976 to 2018. . . . .	105
5.5	Index categories at the time when a flash drought was detected in the soil moisture (SSI). The values shown are the average of all instances in each season and for each index, SPI (top row), EDDI (middle) and ESI (bottom), over 43 years from 1976 to 2018. White grid cells did not experience soil moisture flash droughts. . . . .	107

5.6	Rates of change (RoC) expressed in "categories per week" for each index in each season. The are calculated as the difference between the index's category at the onset of a flash drought in the soil moisture and the value two weeks prior to that. The result is divided by the number of weeks to achieve a "per week" change unit. The values shown are the average of all instances in each season and for each index, SPI (top row), EDDI (middle) and ESI (bottom), over 43 years from 1976 to 2018. . . . .	108
5.7	As figure 5.6 but for four weeks prior to the onset of flash drought in the SSI. . . . .	109
5.8	As figure 5.6 but for six weeks prior to the onset of flash drought in the SSI. . . . .	109
5.9	As figure 5.6 but for eight weeks prior to the onset of flash drought in the SSI. . . . .	110
5.10	Hit rate (HR, panel A) and false alarm ratio (FAR, panel B) for SPI (left column), EDDI (middle) and ESI (right). Hatching indicates where the SSI identified a flash drought as seen in figure 5.4. Only here are values for HR and FAR possible. Detection rates were determined using a time window around the flash drought detected in the soil moisture of eight weeks prior to the onset in which the indices can yield a hit. . . . .	111
5.11	As described in figure 5.10 above but the time interval is extend by two weeks after the flash drought onset in the SSI happened. . . . .	111
5.12	Cross-correlations for individual CMIP5 models listed in Table 2.4 (columns 1-6), CMIP5 ensemble mean (column 7) and AWRA-L (columns 8). Explained variances are in the y-axis and corresponding lag in days on the x-axis. Graphs are showing the spatial mean of the Australian domain. Positive lag means that the individual index is leading the top 10cm soil moisture while a negative lag means that the index's sign is delayed. . . .	113
5.13	As figure 5.12 but for southern and northern domains of Australia split at the 27°S latitude. Dashed lines represent area averages of explained variances in the south while those for the north are displayed as solid lines.	114

5.14	Area average of Australia of flash drought event frequency per decade for each of EDDI, ESI, SPI and SSI split into season and listed for each CMIP5 model (third to bottom row), CMIP5 ensemble (second row) and AWRA-L/AWAP (first row). Grid cells without any flash droughts occurring were masked out. Black lines represent the 90 <sup>th</sup> percentile confidence interval. . . . .	116
5.15	Area mean across Australia as a whole of index value in dryness/wetness categories from table 2.5 for each of EDDI, ESI, SPI and SSI at the onset of a flash drought in the soil moisture. Split into season and listed for each CMIP5 model (third to last row), CMIP5 ensemble (second row) and AWRA-L/AWAP (first row). Error bars show the standard deviations across the Australian domain. . . . .	119
5.16	As Figure 5.15 but for the northern domain of Australia from 27°S to 9°S.	119
5.17	As Figure 5.15 but for the southern domain of Australia from 44°S to 27°S.	120
5.18	Area average of rates of change (RoC) in units of categories per two-weeks for EDDI, ESI and SPI for 8, 6, 4, and 2 weeks prior to the onset of a flash drought in the soil moisture. Split into season (rows) and ordered for each CMIP5 model (first to sixth columns), CMIP5 ensemble (seventh column) and AWRA-L/AWAP (eighth column). . . . .	121
5.19	As Figure 5.18 but results are shown for southern and northern domains of Australia separated at the 27°S latitude. Dashed coloured lines represent area averages of explained variances in the south while those for the north are displayed as solid lines. . . . .	123
5.20	Spatial mean of hit rate (HR, lighter colours) and false alarm ratio (FAR, darker colours) in percent for EDDI (yellow/gold), ESI (light/dark green) and SPI (light/dark blue). Split into season (columns) and listed for each CMIP5 model (first to sixth row), CMIP5 ensemble (seventh row) and AWRA-L/AWAP (eighth row). Detection rates were determined using a time window around the flash drought detected in the soil moisture of eight weeks prior to the onset in which the indices can yield a hit. . . . .	124
5.21	As figure 5.20 but the time window around the flash drought detected in the soil moisture is extended to two weeks after the onset. . . . .	125

5.22	Seasonal FD event frequency expressed as events per decade for SPI (first column), EDDI (second), ESI (third) and SSI (fourth) over the 39 years of the time period from 1976 to 2018. Values for EDDI, ESI and SPI have not changed to Figure 5.4 as the same definition is used. Flash droughts are defined as a decrease from above the 40th to below the 10th percentile in 14 days. The SSI is calculated using the 0-1m soil layer.	127
5.23	Seasonal FD event frequency expressed as events per decade for SPI (first column), EDDI (second), ESI (third) and SSI (fourth) over the 39 years of the time period from 1976 to 2018. Flash droughts are defined as a decrease from above the 40 <sup>th</sup> to below the 20 <sup>th</sup> percentile in 20 days. The SSI is calculated using the 0-1m soil layer.	128
5.24	Seasonal explained variance of EDDI (top row) , ESI (middle) and SPI (bottom) with 0-100cm SSI for 1976 to 2018. Values above 0.2 are statistically significant on the 95% level and marked with hatching.	129
5.25	Lag at which the maximum explained variances shown figure 5.24 occurred for EDDI (top row), ESI (middle) and SPI (bottom). Stippling marks where the explained variances are significant at the 95% level.	130
5.26	Index categories of SPI at the time when a flash drought was detected in the soil moisture (SSI) are in the first column. Columns two to five show rates of change (RoC) expressed in "categories per week" for each season. They are calculated as the difference between the index's category at the onset of a flash drought in the soil moisture and the value two weeks prior to that. The result is divided by the number of weeks to achieve a "per week" change unit. All values shown are the seasonal average of all instances over 43 years from 1976 to 2018.	132
5.27	As described in figure above but for the EDDI.	133
5.28	As described in figure above but for the ESI.	134

5.29	Hit rate (HR, panel A) and false alarm ratio (FAR, panel B) for SPI (left column), EDDI (middle) and ESI (right). The time interval in which the either the indices can yield a flash drought for a valid hit is within eight weeks prior to the flash drought onset in the soil moisture. Hatching indicates where the SSI identified a flash drought as seen in figure 5.23. Only here are values for HR and FAR possible. . . . .	135
5.30	As described in figure 5.29 above but the time interval is extend by two weeks after the flash drought onset in the soil moisture happened. . . . .	135
5.31	Times series for 0-10cm (brown) and 0-100cm (darkred) SSI from November 2016 to December 2018 for the location $26^{\circ}S$ and $144^{\circ}E$ that was affected by a flash drought in that time period according to Nguyen et al. (2019). Markers show timing of flash drought onset for SSIs, SPI, ESI and EDDI. The dot-dashed line represents their $40^{th}$ and the dashed line their $20^{th}$ percentile. Light grey shaded area covers an eight week time period prior to the onset of a flash drought in the 1m SSI. Dark grey shaded area two week time period after the event onset. . . . .	137
5.32	As figure 5.31 above but with markers removed and time series of SPI, EDDI and ESI added. . . . .	137
7.1	Mean and zonal correlation coefficients ( $r$ ) of varying GLDAS LSMs for SPEI3 (a/d), SPEI6 (b/e) and SPEI12 (c/f) for whole data distribution (a-c) and drought periods (d-f) of the 0-10cm layer. The zonal average is shown to the right of each plot. Stippling shows statistically significant correlations at the 95% level. . . . .	156
7.2	Mean and zonal correlation coefficients ( $r$ ) of varying GLDAS LSMs for SPEI3 (a/d), SPEI6 (b/e) and SPEI12 (c/f) for whole data distribution (a-c) and drought periods (d-f) of the 10-40cm layer. The zonal average is shown to the right of each plot. Stippling shows statistically significant correlations at the 95% level. . . . .	157

7.3	Mean and zonal correlation coefficients ( $r$ ) of varying input data for SPEI3 (a/d), SPEI6 (b/e) and SPEI12 (c/f) with GLDAS NOAHv2 for whole data distribution (a-c) and drought periods (d-f) of the 0-10cm layer. The zonal average is shown to the right of each plot. Stippling shows statistically significant correlations at the 95% level. . . . .	157
7.4	Mean and zonal correlation coefficients ( $r$ ) of varying input data for SPEI3 (a/d), SPEI6 (b/e) and SPEI12 (c/f) with GLDAS NOAHv2 for whole data distribution (a-c) and drought periods (d-f) of the 10-40cm layer. The zonal average is shown to the right of each plot. Stippling shows statistically significant correlations at the 95% level. . . . .	158
7.5	Area median over all of Australia of flash drought event frequency per decade for each of EDDI, ESI, SPI and SSI split into season and listed for each CMIP5 model (top to sixth row), CMIP5 ensemble (seventh row) and AWRA-L/AWAP (eighth row). Black lines represent the 90 <sup>th</sup> percentile confidence interval. . . . .	159
7.6	Area average of north Australia ( $< 27^{\circ}\text{S}$ ) of flash drought event frequency per decade for each of EDDI, ESI, SPI and SSI split into season and listed for each CMIP5 model (top to sixth row), CMIP5 ensemble (seventh row) and AWRA-L/AWAP (eighth row). Grid cells without any flash droughts occurring were masked out. Black lines represent the 90 <sup>th</sup> percentile confidence interval. . . . .	160
7.7	As Figure 7.6 but for south Australia ( $> 27^{\circ}\text{S}$ ) . . . . .	161
7.8	Total count of soil moisture flash drought events longer than 30 days for each season and CMIP5 model/AWRA-L observations. Grid cells with not a single flash drought occurrence are masked out. . . . .	161

# List of Tables

2.1	Utilized Data from ranalysis and observations to calculate drought indices.	20
2.2	Native levels and length of time series of GLDAS CLMv1, NOAHv1 and NOAHv2. Blue shading is the selection/ aggregation for the 0-10cm layer, red shading for the 10-40cm layer. . . . .	23
2.3	Utilized data from off-line land surface models. . . . .	25
2.4	Procured CMIP5 models with their spatial resolution and variables used with their output variable names in square brackets. . . . .	26
2.5	Wetness and drought categories according to the EDDI guidelines stated in Lukas et al. (2017). EDDI is inverted in comparison to SPI, ESI and SSI due to its reciprocal relationship to them. A high evaporative demand and thus positive values correspond to dry conditions for EDDI while e.g. low precipitation and thus negative index values correspond to dry conditions for SPI. The drought categories of EDDI are based on the US Drought Monitor (Svoboda et al., 2002). . . . .	38
4.1	Contingency table. . . . .	78

---

# Chapter 1

## Introduction

---

Drought is an inherent part of climate variability affecting most regions on Earth and is recognized as an environmental disaster (IPCC, 2012; Sheffield and Wood, 2011). In broad terms, drought is the persistence of extreme negative moisture anomalies over a specific region and an extended period of time typically on the order of months or longer (Wilhite and Glantz, 1985; Dracup et al., 1980). This is in contrast to aridity, which is a permanent feature of the climate (Wilhite, 1992). The spatial and temporal extent of drought can vary significantly. They can be short seasonal, intense droughts confined to a small region, for example, the drought in the mid-west of the United States in the summer of 2012 (Rippey, 2015). Yet, drought can also last long and past decadal droughts have covered large parts of a country or region. For example, the "Dust Bowl" drought in the 1930s in the US (Schubert et al., 2004) or the "Millennium Drought" in South East Australia in the beginning of the 21st Century (Van Dijk et al., 2011). The impacts of drought encompass a wide variety of natural and economic sectors such as social security, agriculture, water, energy, tourism, ecosystems, and basic human welfare. These impacts are often significant for a long period making drought one of the most devastating natural disasters on human society (Sheffield and Wood, 2011; Crausbay et al., 2017; Pulwarty and Sivakumar, 2014; Haile et al., 2019). Hence, early warning and detection is crucial to mitigate drought impacts (Pulwarty and Sivakumar, 2014).

Unlike for other natural hazards such as floods, hurricanes and heatwaves, the timing

of onset and cessation of drought is hard to capture. This is because its development is comparatively slow by nature and the concepts of onset and cessation of drought are nebulous (Wilhite, 1992), though it has been recently recognised that drought can occur rapidly, within a few weeks (Svoboda et al., 2002; Otkin et al., 2018; Pendergrass et al., 2020). The processes modulating drought development are complex interactions between the land surface and the atmosphere, which alter water fluxes including precipitation, evaporation, and evapotranspiration (ET) (Hobbins et al., 2017). Changes of these components can be amplified by multiple natural, climatic and anthropogenic drivers such as climate variability/change and land-use changes (Kiem and Franks, 2004; Mishra and Singh, 2010; Sheffield et al., 2012; Seneviratne et al., 2013; Dai and Zhao, 2016; Mukherjee et al., 2018).

The complexity of drought processes and interactions means that drought is, arguably, the least predictable climatic hazard (Mishra and Singh, 2010). However, our understanding and ability to predict drought is also complicated by the myriad of types and definitions. In order to understand the complexity of drought, one must look at their numerous driving mechanisms and their impacts. These features can help to define drought and lead to a multitude of indices to communicate drought levels, depending on the impact of interest (Heim Jr., 2002; Zargar et al., 2011; Mishra and Singh, 2010). Here, we address the concept of drought by discussing a number of topics. We start with the physical processes of drought development including the hydrological cycle as well as its driving energy and water balances. This is followed by a discussion of the definitions of drought before introducing the research aims of this thesis. The structure of this thesis is outlined at the end of this chapter.

## 1.1 The Concept of Drought

### 1.1.1 Drought Types

Unlike many other natural hazards, difficulties arise in terms of defining drought. This is because drought evolves over multiple time scales and its modulating mechanisms stem from complex interactions of atmospheric, land surface and oceanic processes (Mishra and Singh, 2010). While drought is in essence a moisture deficiency, it leads to different impacts on the environment and society over time.

Therefore, [Wilhite and Glantz \(1985\)](#) split drought into four different types cascading through the hydrological cycle. From the shortest (months) to longest (multiple years) time scales, the types of drought have been described as follows and are shown in Figure 1.1. The first sign of drought is a strong shortfall in precipitation in regards to the location's long-term climatology and is termed meteorological drought. Persistent rainfall deficiencies and accompanying clear skies with higher than normal irradiation and temperatures lead to a drying of the root-zone layer. Once, soil moisture in this layer is depleted and crops suffer under water stress reducing the biomass and yield the next stage of drought is reached, agricultural drought or sometimes termed soil moisture drought. The depletion of water in the ground continues into deeper levels with ongoing negative precipitation anomalies and reduces drainage and streamflow to larger water bodies such as rivers, lakes and reservoirs. As runoff and water storage is directly affected, this type is termed hydrological drought. With decreasing levels in reservoirs, the water supply is at some point unable to meet the water demand of the population and industry any

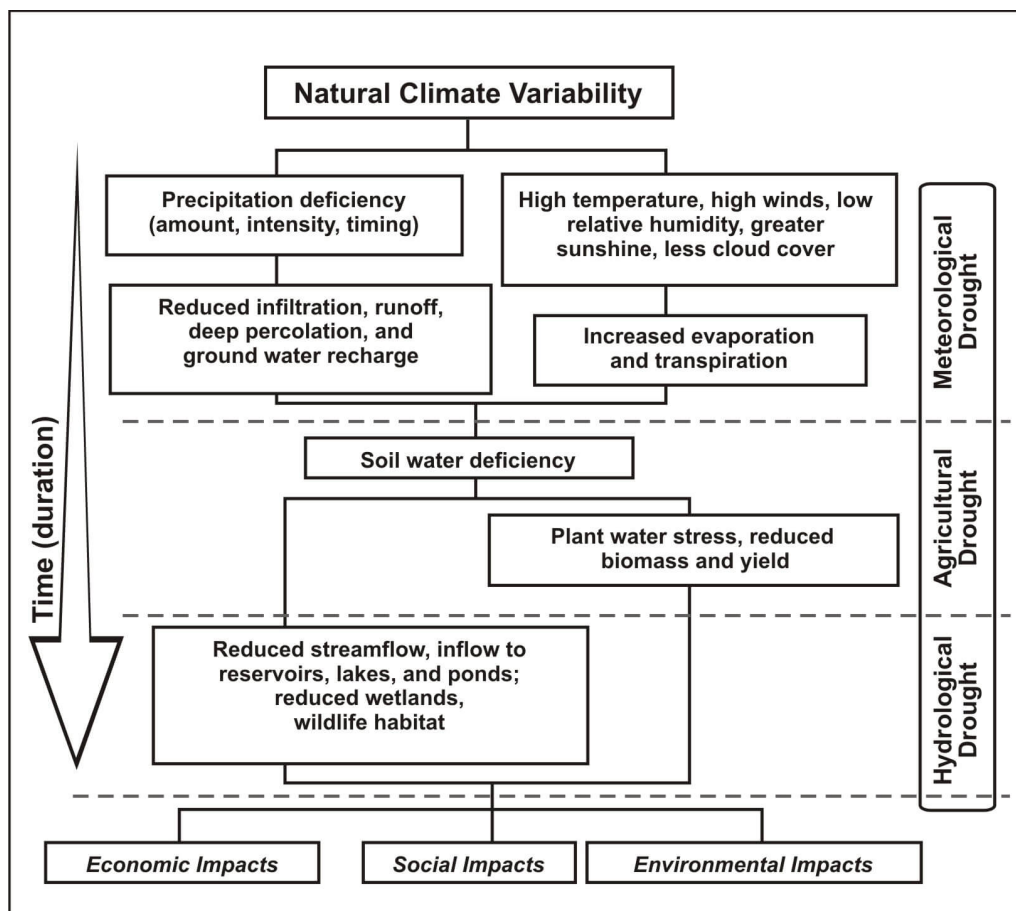


**Figure 1.1:** Evolution of drought with time. From [Zargar et al. \(2011\)](#).

more, which leads to economic and social impacts. Far reaching environmental impacts continue to worsen. This fourth type is termed socio-economic drought.

These four main drought types have been continuously extended over the past two decades and can be seen as subtypes. For example, [Crausbay et al. \(2017\)](#) introduced the ecological drought, an episodic deficit in water availability that drives ecosystems beyond thresholds of vulnerability. Others are groundwater drought ([Van Lanen and Peters, 2000](#)), impacts on groundwater recharge, discharge and levels, and stream health drought, which [Esfahanian et al. \(2016\)](#) describe as a period of time when stream flow deficiency causes irreversible impacts on aquatic/riverine ecosystems.

Another type of drought, which has recently been described is termed “flash drought” ([Doyle, 2018, 2019](#); [Nguyen et al., 2019](#)). The term *flash drought* was first introduced by [Svoboda et al. \(2002\)](#) to describe drought that has features including a rapid onset and intensification in the order of weeks, with substantial impacts on agriculture. The rapidity of flash drought is in contrast to the natural slow development of drought, which usually occurs over months to years. Thus, flash drought classifies as a subseasonal scale drought, posing a new challenge for sub-seasonal to seasonal (S2S, weeks to few months) prediction ([Pendergrass et al., 2020](#)). In essence, a location showing no sign of drought can find itself in the midst of an agricultural drought within several weeks through the rapid depletion of soil moisture from coinciding negative precipitation and above average evaporation. [Otkin et al. \(2018\)](#) and [Pendergrass et al. \(2020\)](#) specify a comprehensive framework for future research on flash drought, suggesting the use of suitable drought indices that reflect the rapidity of flash drought onset within a few weeks.

The rapid intensification of drought conditions during a flash drought has a particularly detrimental effect for the agricultural industry due to the inability to prepare for it; whether it is additional irrigation or delayed seeding of crops or adaptation measures for livestock ([Nguyen et al., 2019](#)). Past flash droughts have been accompanied with significant economic damage such as the 2012 drought in the Midwest US, which had an estimated loss of US\$30 billion ([Rippey, 2015](#)), or the 2018 flash drought event in South Queensland, Australia, with a high mortality in livestock ([Nguyen et al., 2019](#)).

To classify as a flash drought, the root zone layer soil moisture ( $\approx 40\text{-}100\text{cm}$ ) has to be affected ([Otkin et al., 2018](#)). As with other drought types, different definitions have been proposed over the last couple of years. Soil moisture is the primary proxy for

flash drought. Ford and Labosier (2017) proposed a definition whereby root-zone soil moisture has to decline from above the 40<sup>th</sup> to below the 20<sup>th</sup> percentile within 20 days. Their percentiles are based on the “non- drought” and “moderate drought” conditions according to the United States Drought Monitor (USDM, Svoboda et al., 2002, <https://droughtmonitor.unl.edu>). The USDM is a weekly operational product displaying the magnitude and spatial extent of drought in the United States based on a blend of metrics from observations and empirical inputs from regional observers and expert judgement evaluations (Svoboda et al., 2002).

While a precipitation deficiency is required for all types of drought to occur, the accelerated drying of the upper layer soil moisture can be driven additionally by other atmospheric anomalies during flash drought (Hobbins et al., 2017). Surface moisture imbalance associated with drought can be primarily precipitation driven, primarily evaporation (ET) driven or both (Zargar et al., 2011). Low humidity, high winds and temperatures and little cloud cover all increase evaporation which contributes to the rapid drying of the soil layer (Hobbins et al., 2017).

Recent work has highlighted the importance of evapotranspiration for some types of drought like flash drought (Ford and Labosier, 2017; Otkin et al., 2013; Hobbins et al., 2016; McEvoy et al., 2016). However, other studies suggest that precipitation remains the dominant driver and evapotranspiration is a contributor for flash drought (Mo and Lettenmaier, 2015, 2016; Koster et al., 2019). Studies from Mo and Lettenmaier distinguish between two types of flash drought: precipitation driven (Mo and Lettenmaier, 2016) and heatwave driven flash drought (Mo and Lettenmaier, 2015), where the latter is defined by a rapid increase of ET rather than a sudden reduction in precipitation. Mo and Lettenmaier used for their studies a decline in soil moisture to below the 40<sup>th</sup> percentile threshold over a 5-day period to classify flash drought. Even though Otkin et al. (2018) argue that this threshold is not dry enough to quantify as flash drought, their separation highlights the two important drivers for flash drought. While the use of soil moisture is favourable as a direct measure of flash drought and has been used locally in the US (Ford et al., 2015; Ford and Labosier, 2017), its sparse spatial and temporal availability makes flash drought examination challenging on a continuous larger scale. Therefore, atmospheric-based and other land-based variables have been procured to quantify flash drought leading to varying definitions between studies.

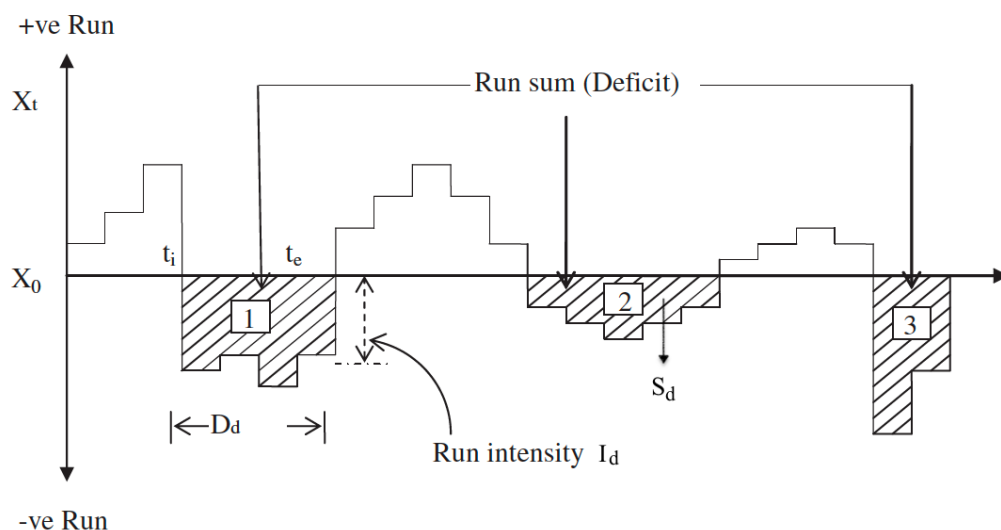
Pendergrass et al. (2020) proposed two definitions for operational use, research and prediction. First, for the United States only, a two-category decrease in the USDM over two weeks and sustained over two more weeks. The second definition for global application employs the Evaporative Demand Drought Index (EDDI, Hobbins et al., 2016), an index estimating the moisture demand in the atmosphere. It is required to increase by 50 percentile within two weeks and also show sustained drought conditions for the following fortnight to fulfil the second definition. Studies from Anderson et al. (2007); Otkin et al. (2013) use anomalous changes in the satellite-derived evaporative stress index, the ratio of actual and potential evapotranspiration (ESI, Anderson et al., 2007), while Nguyen et al. (2019) calculates the ESI from land surface model outputs. Noguera et al. (2020) identifies flash drought through defined anomalous changes in the water balance using the Standardised Precipitation Evapotranspiration Index (SPEI, Vicente-Serrano et al., 2010). Otkin et al. (2014, 2015) developed the Rapid Change Index (RCI) from the ESI to capture the accumulated magnitude of moisture stress changes. Koster et al. (2019) uses reanalysis data to examine flash drought in the Northern Hemisphere but develops their own individual index based on precipitation deficit and excess evapotranspiration.

The variety of definitions and indices shows that there is no consensus yet on what flash drought actually is, other than a rapid intensification of drying. So far, McEvoy et al. (2016) provides the only study which compares different drought indices, namely EDDI, ESI and standardised forms of soil moisture (SSI) and precipitation (SPI, McKee et al., 1993) in a flash drought context. However, this is done for a hand full of flash drought cases in the US without any prescribed conditions to be met. The suitability of those indices in global context and/or with a set definition for flash drought has yet to be examined.

Without relief via widespread precipitation, drought severity increases further and transitions from one type to the next, although each type is not mutually exclusive (i.e. an area can experience more than one type of drought at once). In this thesis, we restrict the scope to the investigation of meteorological and agricultural drought.

### 1.1.2 Drought Characteristics

Drought can be characterised by different features such as intensity, duration, magnitude, severity and spatial extent (Mishra and Singh, 2010). These characteristics are framed by the drought onset and cessation (Dracup et al., 1980). Both, onset and cessation are usually determined by a statistical value representing a threshold under which drought conditions start or end. This threshold can be altered to reflect different levels of drought severity. Figure 1.2 from Mishra and Singh (2010) shows an example of a drought proxy over time, denoted as  $X_t$ . The threshold to identify drought ( $X_0$ ) intersects the drought proxy in those places where the onsets ( $t_i$ ) and cessations ( $t_e$ ) occur. Based on these, the drought characteristics can be determined. The duration ( $D_d$ ) is the time between onset and cessation during which the drought proxy remains under the threshold (longest for drought 2 in Figure 1.2). This can be months, years or even decades. Drought severity ( $S_d$ ) is the cumulative deficiency of the drought proxy over the duration period (highest for drought 1 in Figure 1.2), e.g. in mm for precipitation, while the intensity ( $I_d$ ) describes the maximum deviation of the drought proxy from  $X_0$  at a given time (highest for drought 3 in Figure 1.2). Given the variety of impacts that drought can have, especially over longer time scales, the environment might need several months of above normal precipitation to recover from a drought. Consequently, long lasting



1. Drought with the highest severity;
2. Drought with the longest duration;
3. Drought with the highest intensity

**Figure 1.2:** Drought characteristics . From Mishra and Singh (2010).  $D$  = duration,  $S$  = severity,  $I$  = intensity,  $t_i$  = onset,  $t_e$  = cessation,  $X$  = drought proxy.

droughts can be interspersed by periods of near-normal, or sometimes above normal, rainfall (e.g. due to seasonality) without breaking the drought (Mpelasoka et al., 2008; Gallant et al., 2013).

### 1.1.3 Drought Indices

The different definitions of drought as well as its characteristics, described above, make it challenging to compare and contrast droughts across regions and time. In fact, more than 150 drought indices have been developed to describe drought (Zargar et al., 2011). Indices are based on indicators that use variables influenced by drought such as precipitation, temperature, evaporation, soil moisture, vegetation water content, stream flow/runoff and reservoir storage (Heim Jr., 2002; Zargar et al., 2011). Conveyed as single numeric values, drought indices simplify the complex relationships between these variables and drought in order to evaluate periods of dryness (Dai, 2011b; Mishra and Singh, 2010; Zargar et al., 2011).

Through the incorporation of different meteorological and hydrological variables, drought indices describe different regions or drought characteristics and types, and thus differ on spatial-temporal scales. Therefore, each drought index, whether it is univariate or multivariate, has its strengths and weaknesses as comparisons of several indices in numerous studies reveal (Guttman, 1998; Heim Jr., 2002; Keyantash and Dracup, 2002; Dai et al., 2004; Tsakiris and Vangelis, 2005; Mpelasoka et al., 2008; Zargar et al., 2011; Hao and Singh, 2015; Raible et al., 2017).

Soil moisture deficiency is considered 'truth' for agricultural drought but the difficulty in measuring it accurately across large scales means that meteorological indices are more commonly used. Some drought indices have become well established in climate research such as the Palmer Drought Severity Index (PDSI, Palmer, 1965), which incorporates both precipitation and evapotranspiration variables and the Standardised Precipitation Index (SPI, McKee et al., 1993), which is based on precipitation alone. Using different drought indices to examine the same drought can lead to disagreement in its characteristics, e.g. timing of onset or its duration (Mishra and Singh, 2010). This would occur if, for example, one index defined a drought based on a threshold of precipitation deficit and another used a threshold of soil moisture scarcity. Soil moisture is associated with both precipitation and evapotranspiration (Seneviratne et al., 2010). Some argue that

reliable drought assessment using only precipitation based drought indices is not possible and an extension with evapotranspiration is needed to consider the antecedent precipitation conditions via soil moisture memory, the rate of drying and global warming (e.g. [Tsakiris and Vangelis, 2005](#); [Vicente-Serrano et al., 2012](#)). As a result, studies that have directly examined the characteristics of drought found that using a drought index based on soil moisture or evaporation will change characteristics such as drought duration and intensity compared to using an index based on precipitation alone ([Mpelasoka et al., 2008](#); [Gallant et al., 2013](#)).

Several studies have compared individual or a subset of drought indices to evaluate their reliability on the quest of the universal drought index ([Guttman, 1998](#); [Heim Jr., 2002](#); [Keyantash and Dracup, 2002](#); [Mishra and Singh, 2010](#); [Khalili et al., 2011](#); [Zargar et al., 2011](#); [Vicente-Serrano et al., 2012](#); [Halwatura et al., 2017](#); [Leelaruban et al., 2017](#); [Raible et al., 2017](#)). Those comparisons were performed with in situ or remotely sensed soil moisture observations, stream flow, wells and/or soil moisture estimates from land surface models (LSM), revealing their strength and weaknesses, whether it is their simplicity/complexity, data requirements or being confined and specifically designed for certain areas. Despite the existence of numerous drought indices for each drought category, none of them receives universal acceptance ([Hayes et al., 2011](#)). Only the SPI has been promoted as the reference index for meteorological drought by the World Meteorological Organization (WMO) ([WMO, 2012](#)).

The complexity of the employed algorithms and their implicit approximations in a drought index provide a source of uncertainty. The estimations are necessary to capture processes between the land surface and the atmosphere. Methods incorporated in indices trying to resolve these physical processes without measuring them directly to suit a global application are based on parametrisations. An example is the estimation of potential evapotranspiration, for which various methods exist ([McMahon et al., 2013](#)), such as the Penman-Monteith method ([Monteith, 1965](#)), described later in Chapter 2.2.1. Consequently, differences between those methods yield a source of uncertainty that is embedded in the drought indices ([Trenberth et al., 2014](#); [Dai and Zhao, 2016](#); [Zhan et al., 2016](#)). The reason why different parametrisations and estimates are attempted in the first place is the lack of good *in situ* observational data that delivers a clear state of drought. The following section discussed the issues with *in situ* data and its alternatives.

### 1.1.4 Data for the Analysis of Drought

The quality of drought indices relies on the quality of the input data itself. Hence, reliable, long-term observational data of the specific indicator variable is crucial (Van Loon, 2015). These indicator variables not only encompass measures of the hydrological cycle such as precipitation, evapotranspiration, soil moisture content, stream flow and discharge but also parameters driving physical processes within the cycle such as temperature and radiation. Each of those have a different observational history and as a result, there is a wide range in the quality of the data between different variables.

Drought indices based on soil moisture measurements are ideal since the impacts of agricultural drought are felt by deficiencies of moisture in the root zone. However, in reality, direct soil moisture measurements are rarely employed in drought indices. This is because *in situ* soil moisture observations are sparse in space and time. While considerable efforts are made to expand the soil moisture network and combine stations worldwide to an international soil moisture network (ISMN, Dorigo et al., 2011), it will take time to achieve a network of dense, long lasting records for statistical analyses. Besides drought monitoring, another important purpose of this network is to validate other soil moisture products such as those from satellite observations and land surface models.

Satellite observations of soil moisture are global and several different products exist today but their spectral bands typically capture soil moisture in the first few centimetres of soil only (Karthikeyan et al., 2017). This shallow layer is not necessarily sufficient for capturing drought as it is not necessarily representative of soil moisture storage throughout the root zone. Additionally, calibration techniques and physical limitations, e.g. cloud cover or dense vegetation, leave room for uncertainties (Van Loon et al., 2017).

Land surface models (LSMs) estimate terrestrial water and energy states and fluxes by employing a conceptualization of the physics underlying earth system processes (Pitman, 2003). During recent decades, LSMs have developed from simple, idealized parametrizations to complex, high resolution models able to simulate complex phenomena between the atmosphere and land surface with explicit representations of vegetation and soil types. In operational use, they are either uncoupled and forced by observation-based meteorological fields or are coupled to atmospheric general circulation models (AGCM)

(Koster et al., 2009a). LSMs have been extensively evaluated in their capability to reflect water and energy fluxes (Koster and Suarez, 2001; Dirmeyer, 2011; Prudhomme et al., 2011; Best et al., 2015; Holgate et al., 2016). While LSMs present a globally consistent estimate of soil moisture and show coherent time variability (Koster et al., 2009a; Yuan and Quiring, 2017), being a model, systematic biases persist (Abramowitz et al., 2007). This has especially been found at the dry end of the spectrum where they misrepresent the partitioning of available energy into sensible and latent heat as well as the response of vegetation to water-limited conditions leading to an overestimation of drought (De Kauwe et al., 2015; Ukkola et al., 2016a,b; Milly and Dunne, 2017). Similarly, coupled to AGCMs, systematic biases in evapotranspiration have been identified across the globe in the Coupled Model Intercomparison Project Phase 5 (CMIP5) simulations (Guo et al., 2006; Mueller and Seneviratne, 2014). These are linked to different model parametrisations and model climates causing differences in land-atmosphere coupling (Guo et al., 2006; Ukkola et al., 2018b). The limitations in land-atmosphere processes leads to shortcomings in the models' simulated drought, for example for soil moisture drought intensities (Ukkola et al., 2018a), overamplification of heat extremes (Ukkola et al., 2018b) and a trend towards more severe droughts (Dirmeyer et al., 2013; Seneviratne et al., 2013).

In the absence of a dense, long-running network of soil moisture gauges many drought indices have been developed that are based on other variables that can act as a proxy for soil moisture, for example, precipitation or some combination of precipitation and evapotranspiration. For instance, precipitation has been measured widely for a long time and thus a global network of rain gauges with long-lasting records has been developed (e.g. Chen et al., 2002; Schneider et al., 2014). Similar for temperature records dating back to over a century (Cowtan and Way, 2014). However, uncertainties remain in precipitation and temperature networks associated with the number of long-running stations and aspects of regional coverage, and the level of quality control and interpolation methods. Each play an important role in the accuracy of drought indices (Dai et al., 1997; Stahl et al., 2006; Jones et al., 2009, 2012; Sun et al., 2018).

Problems arise when evapotranspiration is considered for drought evaluation. Not only is it challenging to measure in nature, which is usually done on flux tower sites or using lysimeter, but evaporation and evapotranspiration is also complex to estimate.

Consequently, several methods exist for this purpose (McMahon et al., 2013). Basic approaches, such as the Thornthwaite (Thornthwaite, 1948) approximation, require only temperature to estimate potential evaporation. However, the method has been deemed as too sensitive to increasing global temperatures and overestimates drying (Hobbins et al., 2008). The FAO56 reference crop evapotranspiration is a physical method based on the Penman-Monteith parameterization (Monteith, 1965) for potential evaporation and adopts the characteristics of a well watered hypothetical reference crop. The FAO56 formulation has been widely accepted in drought research (Allen et al., 1998). However, the Penman-Monteith method requires a diverse array of input data, including temperature, precipitation, wind speed, solar radiation and humidity (Allen et al., 1998). Many of these variables are not reliably and widely measured over long periods of time (McVicar et al., 2008; Samani, 2000; Bandyopadhyay et al., 2008; Jones et al., 2009).

Given the data limitations, described above, we provide novel, further efforts to test drought indices for global application, and for the newly emerging subtypes of drought, namely flash drought. This thesis aims to compare the benefits in including evapotranspiration in drought indices for agricultural drought detection given the uncertainties associated with parametrisations and data quality associated with estimating evaporation. We build on previous studies of regional drought by focusing on uncertainties in the representation of drought on the global scale. Whether these uncertainties, which can stem from different input data, override the benefits of the inclusion of evapotranspiration in a drought index is an aim of this thesis.

Only few studies exist that have quantified the value of drought indices to identify flash drought (Otkin et al., 2013; Mo and Lettenmaier, 2015; Otkin et al., 2015; Hobbins et al., 2016; Mo and Lettenmaier, 2016; McEvoy et al., 2016; Koster et al., 2019; Nguyen et al., 2019). These studies are limited to a regional scale and have explored flash drought using observations or reanalysis data only. Therefore, investigating flash drought in global climate models globally using common flash drought indices and evaluating them by comparing them to soil moisture in the models will help to understand if the physical processes in those models are correctly represented. Using the conceptual idea from before, procuring precipitation and evapotranspiration based indices will also shed some light on the driving processes of flash drought in the models and whether a simple index can provide a sufficient detection skill.

## 1.2 Research Aims

This thesis focuses on agricultural and flash drought and how precipitation and evapotranspiration based drought indices represent those in observations and climate models. In summary, the research of this thesis aims to answer the following questions:

1. What are the differences in the representation of soil moisture droughts using drought indices based on E-P balance versus those using precipitation only?
2. How sensitive are drought indices to their input data? How does this sensitivity vary between precipitation-only indices and E-P balance indices?
3. How do different drought indices represent flash drought in a climate model?
4. How well do climate models represent flash drought in Australia?

## 1.3 Thesis Outline

This thesis uses a variety of drought indices to tackle the research questions introduced above. These indices, and the associated data used to compute them, are described in Chapter 2. The fundamental physical processes of evapotranspiration during the development of drought are also described in the same chapter to gain a deeper understanding how drought indices involving ET operate.

The first and second research questions are answered in Chapter 3 which is based on [Hoffmann et al. \(2020\)](#). For this, we procure a number of data sets from different sources for all necessary variables to compute the drought indices PDSI and SPI. Their skill to identify agricultural drought on time scales from three to twelve months is compared to two soil moisture levels from a global land surface model (LSM).

Multiple drought indices, based on precipitation and/or evaporation are used to examine flash drought in climate models in Chapter 4. Here, soil moisture provides the reference as flash drought is a rapid evolving agricultural drought. Using a suite of six global climate models, the performance of the indices relative to the models' soil moisture on a 1-month time scale is evaluated in terms of event frequency, rates of change and prediction skill.

The results from Chapter 4 are contrasted with quasi-observations from observations integrated into an offline LSM in Chapter 5, over the Australian continent. Differences between the representation of flash drought in global climate models and observations are discussed and potential discrepancies in the physical processes leading to flash drought are highlighted. This chapter also analyses the observed drought indices' performance using a deeper soil moisture layer, which was not available for the global climate models. The thesis concludes in Chapter 6 with an overall summary and a discussion of implications and remaining uncertainties and future work.

---

# Chapter 2

## Data and Methods

---

### 2.1 Data

Several data sources are employed throughout this thesis to calculate drought indices and evaluate them. They include observational and reanalysis data as well as data from offline land surface models and global coupled climate models (GCMs). The following section describes the procured data. The variables obtained are summarised in Table 2.1. Descriptions of data processing associated with the analyses in Chapters 3, 4 and 5 is provided in the relevant chapter.

#### 2.1.1 Observational Data

Observational data refers to measurements of atmospheric and land surface variables. Those observations can be *in situ*, e.g. weather station on the ground, or remotely sensed via satellite or radar. These measurements can be in their original form or, more commonly for climate use, many observational networks have been interpolated onto regular grids. Over the past decades the network of measurement stations has grown significantly in number and diversity of variables measured. Due to the relatively straightforward technique, precipitation and temperature are the most frequent and long-term measured variables (Chen et al., 2002; Schneider et al., 2014; Cowtan and Way, 2014).

Correct and reliable observational data is essential for weather forecasts, climate prediction and evaluation of any kind of model trying to reproduce the climate system. However, due to aspects of regional coverage and the number of stations included, the level of quality control, interpolation methods and algorithm imperfections in satellite estimates a multitude of datasets for individual variables has been made available over the past decades (Sun et al., 2018). For this thesis, the following observational datasets have been procured to calculate drought indices and investigate their sensitivity to data input. The datasets are listed in Table 2.1.

#### 2.1.1.1 GPCC

The Global Precipitation Climatology Centre (GPCC) collects and analyses rain gauge data from round 67,200 stations all over the world, mainly from national meteorological agencies (Schneider et al., 2014). The GPCC database covers more than 200 years but the data set requires a minimum of ten uninterrupted years at each station as a quality criterion for the background climatology. The result is the GPCC Full Data version 7 used in this thesis and covers the period from 1901 to the present in monthly increments.

#### 2.1.1.2 CRU TS

The Climate Research Unit (CRU) data set v4.01 comprises a time series (TS) encompasses six climate variables, including temperature and precipitation as used in this thesis (Harris et al., 2014, 2020). The principal sources used for construction of the CRU are monthly CLIMAT messages, exchanged internationally between World Meteorological Organisation (WMO) countries ( $\approx 2400$  stations), obtained as quality-controlled files via the UK Met Office; Monthly Climatic Data for the World (MCDW) summaries ( $\approx 2600$  stations), obtained from the US National Oceanographic and Atmospheric Administration (NOAA) via its National Climate Data Centre (NCDC,  $\approx 1700$  stations); and updates of minimum and maximum temperatures for Australia, obtained from the Bureau of Meteorology (BOM,  $\approx 100$  stations) (Harris et al., 2014, 2020). Due to receiving processed data from these meteorological the CRU TS dataset itself is not homogenised, prompting caution of its use for trend analysis (Harris et al., 2014, 2020).

### 2.1.1.3 UDEL

The University of Delaware (UDEL) has published a fourth version of a high spatial resolution data set which consists of precipitation and temperature (v4.01) and both variables are used in this thesis ([Matsuura and Willmott, 2015](#)). The data set employs station data from a number of sources including a recent version of the Global Historical Climatology Network (GHCN) data set (GHCN2); a version of the Daily GHCN (GHCN-Daily); an Atmospheric Environment Service/Environment Canada archive; data from the Hydrometeorological Institute in St. Petersburg, Russia; Greenland Climate Network data; daily records from the Global Surface Summary of the Day; the National Center for Atmospheric Research (NCAR) daily India data; Nicholson's archive of African precipitation data; Webber and Willmott's South American monthly precipitation station records; and the Automatic Weather Station Project's Greenland station records. Part of the background climatology is taken from [Legates and Willmott \(1990\)](#) unadjusted archive ([Matsuura and Willmott, 2015](#); [Sun et al., 2018](#)). Using a combination of spatial interpolation methods, monthly station data averages are interpolated to gridded fields. An important point is that the stations in dataset were not corrected to mitigate rain-gauge under-catch bias ([Matsuura and Willmott, 2015](#)).

### 2.1.1.4 GPCP

The GPCP precipitation product was first released in 1997 ([Huffman et al., 1997](#)) and version 2 was released in 2002 ([Adler et al., 2003](#)). It is a merged analysis that incorporates a combination of low-orbit satellite microwave, geosynchronous-orbit satellite infra-red, and surface rain gauge observations. The multi-satellite field is merged with rain gauge analyses (over land) by adjusting the satellite estimates to the gauge bias and then combining the (adjusted) satellite and gauge fields to achieve full global coverage and improved quality compared to the individual data sources. With the microwave satellite era starting 1987, the GPCP dataset was extended backward to 1979 using infrared-only satellite data and gauge observations ([Adler et al., 2003](#)).

### 2.1.1.5 CMAP

The Climate Prediction Center (CPC) Merged Analysis of Precipitation (CMAP) is in its approach similar to GPCP but differs in its merging technique. CMAP merges seven in-

dependent sources with different characteristics including gauge observations, estimates inferred from a variety of satellite observations, and the NCEP–NCAR reanalysis data. These sources from satellite and reanalysis are linearly combined and blended in a second step with gauge-based analyses to remove possible biases (Xie and Arkin, 1997).

#### 2.1.1.6 AWAP

In contrast to all other datasets above, the dataset from the Australian Water Availability Project (AWAP) is confined to the Australian continent (Jones et al., 2009). It comprises a high-resolution spatial climate dataset including precipitation, vapour pressure and temperature using topography-resolving analysis methods and an anomaly-based approach to combine *in situ* observations and to achieve a high spatial resolution of  $0.05^\circ \times 0.05^\circ$ . The network coverage of available stations is good with up to 7000 stations for precipitation but declines substantially back in time and is still sparse in the interior of the continent where the accuracy of dataset is limited. This is also due to the deliberate choice of using *in situ* observations only for the analysis as homogeneity issues from including satellite data may cause the dataset to be less applicable to climate change analysis (Jones et al., 2009).

### 2.1.2 Reanalysis Data

The basic idea of reanalysis is to combine assimilated observations and hindcasts to produce a spatially and temporally consistent product. To do so, unchanging ("frozen") state-of-the-art analysis/forecast systems are fed with all available observations every few hours to produce forecasts. Both, observations and forecast can then be combined to one dataset considering the errors of both products using several statistical methods, such as three and four-dimensional variational data assimilation (3D-Var, 4D-Var) and the Kalman filter. The resulting reanalysis of the state of the atmosphere at a particular instant in time is seen as the best estimate. Errors are nested in the forecast models from parametrisations and in observations from changing sources producing artificial variability and trends. Yet, while uncertainties in reanalysis need to be considered carefully when interpreting results, they reflect inter-annual variability in coherence with independent observations for many variables (Kistler et al., 2001). The benefit of reanalysis is the abundance of space and time consistent variables originating for the forecast models in

sub-daily time steps (Kalney et al., 1996; Dee et al., 2011; Sun et al., 2018). For some variables, reanalysis is the only globally coherent dataset available.

Several reanalysis datasets have been developed and are available for use. The ERA Interim (Dee et al., 2011) and NCEP-NCAR Reanalysis I (Kalney et al., 1996) datasets procured for this thesis were designed by the European Center for Medium-Range Weather Forecast (ECMWF) and the National Center for Atmospheric Research (NCAR) and the National Centers for Environment Prediction (NCEP), respectively. Though many other reanalysis products exist, these were chosen as they are widely used.

The ERA Interim reanalysis (ERA-I) is produced with the ECMWF IFS forecast model with three fully coupled components for the atmosphere, land surface, and ocean waves in 60 vertical levels. Observations assimilated from radiosondes, wind profilers, pilot balloons, aircrafts, ships, drifting buoys, land stations and in majority from satellites are fed into the atmospheric 4D-Var analysis in 12-hour cycles. ERA-I spanning from 1979 to 2018 is the successor of ERA-40 and has improved low-frequency variability and stratospheric circulation (Dee et al., 2011).

NCEP-NCAR Reanalysis I (NCEP I) is a first-generation reanalysis product using the NCEP global spectral weather prediction model from 1995 with 28 vertical levels and 3D-Var scheme for spectral statistical interpolation. Observation sources include a similar variety of those in ERA Interim. In contrast to ERA-I, NCEP I is still continued and dates back to 1948, although there were fewer upper-air observations in the first decade (Kistler et al., 2001). NCEP I was used to construct the Princeton Meteorological Dataset (Sheffield et al., 2006) which in turn forces the GLDAS v2 land surface model (see Section 2.1.3.1). Therefore, although NCEP I has a successor, it was procured for this thesis.

Procured variables from these datasets are monthly minimum and maximum temperature (ERA-I), mean temperature (NCEP I), solar insolation, specific humidity and wind speed (both) as listed in Table 2.1.

**Table 2.1:** Utilized Data from reanalysis and observations to calculate drought indices.

Data	Data length	Variables used	Type	Resolution	Reference	Data Source
ERA-Interim	1979-2016	u/v wind speed [ $m/s$ ] Specific humidity [ $kg/kg$ ] Downward shortwave solar radiation [ $W/m^2$ ] Max/min temperature [ $K$ ]	Reanalysis	$0.75^\circ \times 0.75^\circ$	Dee et al. (2011)	This data was provided by ECMWF on their Web site at <a href="https://apps.ecmwf.int/datasets/">https://apps.ecmwf.int/datasets/</a> [Accessed 15 February 2017]
NCEP Reanalysis I	1948-2017	u/v wind speed [ $m/s$ ] Specific humidity [ $g/kg$ ] Downward shortwave solar radiation [ $W/m^2$ ] Mean temperature [ $K$ ]	Reanalysis	$0.75^\circ \times 0.75^\circ$	Kalney et al. (1996)	This data provided by the NOAA/OAR/ESRL PSD, Boulder, Colorado, USA, from their Website at <a href="https://www.esrl.noaa.gov/psd/">https://www.esrl.noaa.gov/psd/</a> [Accessed Febraury 2017 – March 2017]
GPCP v2.3	1979-2015	Precipitation [ $mm/day$ ]	Merged rain-gauge and satellite obs	$2.5^\circ \times 2.5^\circ$	Adler et al. (2003)	
GPCC v7	1900-2015	Precipitation [ $mm/month$ ]	Station observations	$2.5^\circ \times 2.5^\circ$	Schneider et al. (2014)	
CMAP v1706	1979-2017	Precipitation [ $mm/day$ ]	Merged rain-gauge and satellite obs	$2.5^\circ \times 2.5^\circ$	Xie and Arkin (1997)	
UDel AirT and P v4.01	1901-2014	Mean temperature [ $^\circ C$ ] Precipitation [ $cm/month$ ]	Compiled station data. See ref for details.	$0.5^\circ \times 0.5^\circ$	Matsuura and Willmott (2015)	
CRU TS v4.01	1901-2016	Precipitation [ $mm/month$ ] Min/max temperature [ $^\circ C$ ]	Station observations	$0.5^\circ \times 0.5^\circ$	Harris et al. (2014, 2020)	of East Anglia Climatic Research Unit et al. (2017) [Accessed 21 April 2018]
AWAP	1975-2019	Daily precipitation totals [ $mm$ ]	Station observations	$0.05^\circ \times 0.05^\circ$	Jones et al. (2009)	Australian Bureau of Meteorology [Accessed November 2019]

### 2.1.3 Land Surface Model Data

As described in the introduction, long-running *in situ* soil moisture measurements are not available worldwide and satellite measurements of soil moisture are confined to the top few centimetres of soil. Outputs from land surface models (LSM) provide global, gridded estimates of water and energy fluxes and states at the land surface layer for several decades. The procured LSMs in this thesis are now described. The procured variables from the following LSMs are summarised in Table 2.3.

#### 2.1.3.1 GLDAS

NASA's Global Land Data Assimilation System (GLDAS) is a fully physical, global, high-resolution land surface modelling framework that integrates observation-based data products from multiple sources to estimate terrestrial water and energy states and fluxes (Rodell et al., 2004; Rui, 2017). These sources include a number of products from ground and satellite based observational datasets. GLDAS consists in total of four different land surface models, the Community Land Model (CLM), the Mosaic Land Surface Model, NOAH Land Surface model, and the Variable Infiltration Capacity model (VIC) (Rodell et al., 2004). Each model has a different vertical resolution in terms of depth and number/thickness of layers for which details are provided in Rodell et al. (2004) and Table 2.2.

The first version of GLDAS (v1) was forced by multiple datasets. From 1979 to 1993 the models were forced with bias-corrected reanalysis data from European Center for Medium-Range Weather Forecasts (ECMWF); from 1994 to 1999 with bias-corrected reanalysis data from the National Center for Atmospheric Research (NCAR); in 2000 with NOAA/GDAS atmospheric analysis fields and from 2001 to the present day with a combination of NCEP's Global Data Assimilation System (GDAS), CMAP and Air Force Weather Agency datasets (Rui, 2017). Due to inconsistencies in the forcing data sources, which were switched several times in GLDAS v1 and resulted in unnatural trends in 1995-1997, a second generation GLDAS (v2) emerged to improve upon that (Rui, 2018).

The second generation of GLDAS consists of two parts (v2.0 and v2.1) and is only available for the NOAH model. GLDAS v2.0, hereafter NOAHv20, spans from 1948 to 2010 and is forced entirely with the Princeton meteorological dataset, a combined

suite of global observation-based datasets with the NCEP–NCAR Reanalysis I (Sheffield et al., 2006). Other changes made in GLDASv2 include a model version upgrade for NOAH from 2.7 to 3.3, switching to MODIS-based land surface parameter data sets, and initialization of soil moisture over desert (Rui, 2018). The GLDAS v2.1 simulation, hereafter NOAHv21, starts on 1st January 2000 with conditions from NOAHv20 and is updated frequently. In contrast, NOAHv21 is forced with fields from three different datasets which are atmospheric fields from the National Oceanic and Atmospheric Administration (NOAA)/Global Data Assimilation System (GDAS), precipitation from the disaggregated GPCP and radiation from the Air Force Weather Agency’s AGRicultural METeorological modelling system (AGRMET) (Rui, 2018). Due to the initialization of NOAHv21 with conditions of NOAHv20 they can be used as a continuous time series. The simplest way to merge them is to transition from 2.0 to 2.1 either in 2000 or in 2010. Due to different forcing data sets in both versions this simple merging procedure would create some climatological differences so that bias corrections with scaling or CDF matching may be necessary depending on the sensitivity of the application. According to Matthew Rodell (NASA, personal communication) these differences between GLDAS v2.0 and v2.1 are not as large as the differences caused by varying datasets within GLDAS v1.0.

However, to remove those artificial discontinuities caused by those different forcing products a re-scaling method was applied, similar to that described in Hurrell et al. (2008) who applied their methods to sea surface temperature analysis products. We scaled the datasets by re-scaling the NOAHv20 anomalies relative to the mean climatology of NOAHv20 and then adding those monthly anomaly fields onto the NOAHv21 climatology for the same base period of 2000–2010. By comparing anomalies, rather than raw soil moistures, the biases due to the different forcing data sets are removed. The scaled NOAHv20 product was then merged with NOAHv21 in January 2000 to a continuous time series and is further referred to as NOAHv2 (Figure 2.1).

Monthly 1-degree 0–10 cm and 10–40 cm average layer soil moisture output from 1979 to 2016 from the NOAH (GLDASv1 and v2) and CLM (GLDASv1) land surface model are used in this thesis to represent the depth where the majority of total roots from agricultural crops grow (Fan et al., 2016). While NOAH offers those levels individually, the closest layers in CLM to those depth were accumulated as stated in Table 2.2. The

layer depths available for VIC and MOSAIC do not offer these levels in any combination and were therefore not used.

GLDAS has been used in multiple studies to examine changes in terrestrial water storages (Syed et al., 2008; Yang et al., 2013; Mo et al., 2016) and to evaluate drought in regional areas (Spennemann et al., 2015; Agutu et al., 2017; Van Loon et al., 2017; Hameed et al., 2018)

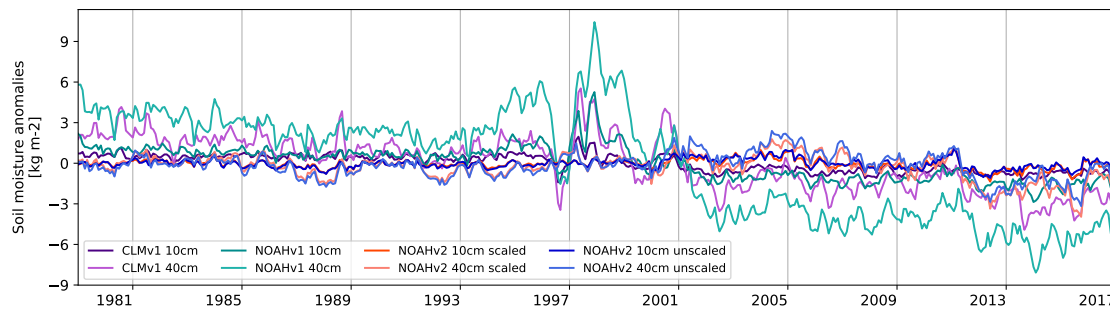


**Figure 2.1:** Global mean soil moisture content climatology for 0-10 and 10-40cm soil layers of CLMv1 and NOAHv1 as well as the scaled and unscaled time series of NOAHv2. The scaling follows the methodology in Hurrell et al. (2008) explained in the Methods section. Serious discontinuity issues in GLDAS v1 and data quality issues in both versions after 1990 as pointed out by Wang et al. (2016b) over China are expected to occur elsewhere, too, leading to periodically big deviations between the LSMs shown above.

**Table 2.2:** Native levels and length of time series of GLDAS CLMv1, NOAHv1 and NOAHv2. Blue shading is the selection/ aggregation for the 0-10cm layer, red shading for the 10-40cm layer.

LSM	Data Length	Layer									
		1	2	3	4	5	6	7	8	9	10
GLDASv1 CLM 2.0	1979- 2017	0- 0.018	0.018- 0.045	0.045- 0.091	0.091- 0.166	0.166- 0.289	0.289- 0.493	0.493- 0.829	0.829- 1.383	1.383- 2.296	2.296- 3.433
GLDASv1 NOAH 2.7	1979- 2017	0- 0.1	0.1- 0.4	0.4- 1.0	1.0- 2.0	-	-	-	-	-	-
GLDASv2 NOAH 3.3	1948- 2017	0- 0.1	0.1- 0.4	0.4- 1.0	1.0- 2.0	-	-	-	-	-	-

### 2.1.3.2 AWRA-L

The Australian Bureau of Meteorology (BOM) has developed the Australian Water Resource Assessment Landscape (AWRA-L, currently version 6) model fed with station and satellite-based observational data to generate those fluxes on a high spatial and temporal resolution (Frost et al., 2018). While the data set is model-based, the data is generated using observations applied to a land surface model and can be seen as 'quasi observations'.

AWRA-L is a one-dimensional, biophysical,  $0.05^\circ$  grid based water balance model, currently in its sixth version (Frost et al., 2018). It was developed by the Commonwealth Scientific and Industrial Research Organisation (CSIRO) and the BOM in order to deliver comprehensive water accounting information across the country. The model is semi-distributed, meaning that the basins are broken down into sub-basin for which the water balance estimates are calculated between the atmosphere, soil, groundwater and surface water stores (Figure 2.2). Each grid cell is divided into three soil layers, top (0-10cm), shallow (10-100cm) and deep (100-600cm), each with a spatially varying maximum water holding capacity.

The water balance is calculated for two hydrological response units (HRU). Those represent the landscape dynamics within an AWRA grid and are, shallow-rooted and deep-rooted vegetation, which differ in their aerodynamic control of evaporation, their interception capacities and in their degree of access to different soil layers limited by their prescribed rooting depth down to 1m and 6m respectively. The HRU is fed with daily climate data sets consisting temperature and precipitation from the Australian Water Availability Project (AWAP, Jones et al., 2009) as well as with remotely sensed solar

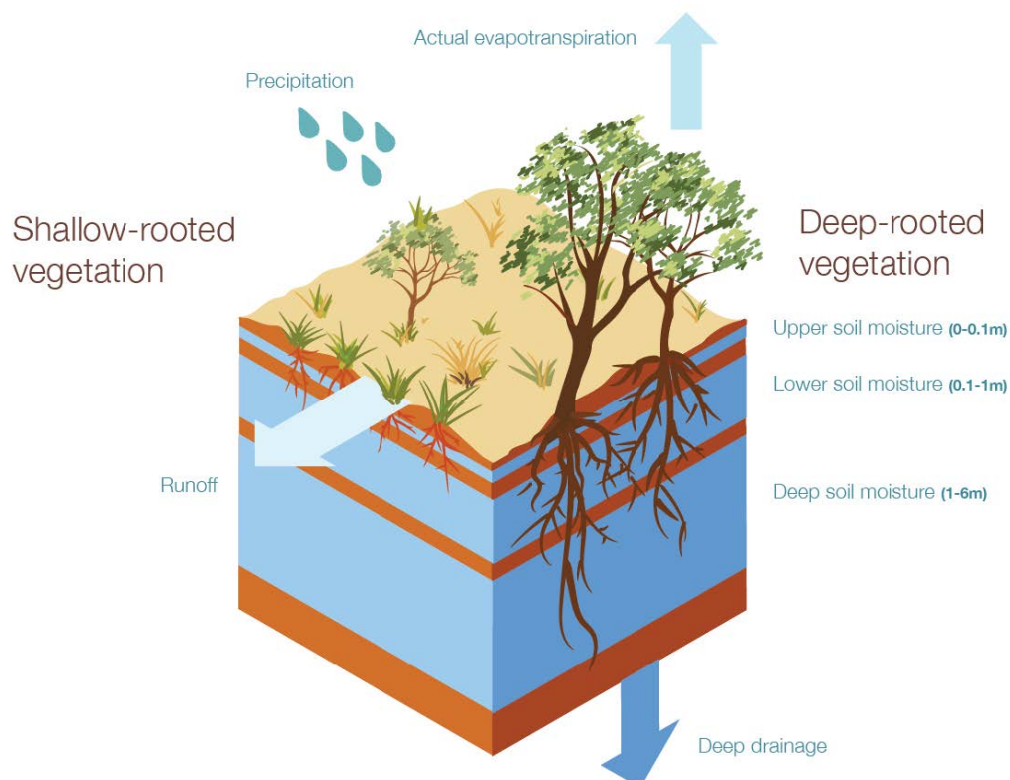


**Figure 2.2:** Conceptual AWRA-L grid cell with key water stores and fluxes shown. From Frost et al. (2018).

radiation since 1990 and site-based wind observations since 1975. Prior to that, a daily varying climatology value was used for radiation ([Weymouth and Le Marshall, 2001](#)) and wind speed ([McVicar et al., 2008](#)). Daily gridded outputs are provided from 1911 onwards in real-time. We limit the time period to 1975 to 2018 due to the use of the wind climatology in earlier years.

AWRA-L v5 has been evaluated by comparing it to data from flux tower sites and soil moisture estimates from in-situ networks and has been found to strongly agree with those in-situ measurements for the top 10cm soil layer ([Holgate et al., 2016](#)) as well as for the deeper 0-100cm soil layer ([Frost et al., 2015](#)).

In this study, the AWRA-L (version 6) water storage values from the top (0–10 cm) and shallow (10-100cm) layer have been utilised. Furthermore, crop reference evapotranspiration (PET) as a direct output from AWRA-L and the ESI, a product calculated only from AWRA-L output data as used in [Nguyen et al. \(2019\)](#) are also used and provided by the Australian Bureau of Meteorology (BOM).

**Table 2.3:** Utilized data from off-line land surface models.

LSM	Data length	Variables used	Resolution	Reference	Data Source
CLMv1 /NOAHv1	1979-2018	Average layer soil moisture [ $kg/m^2$ ]	$1^\circ \times 1^\circ$	<a href="#">Rodell et al. (2004)</a>	<a href="#">Rodell et al. (2007)</a> [Acc. 26 February 2017]
NOAH-v20	1948-2010	Average layer soil moisture [ $kg/m^2$ ]	$1^\circ \times 1^\circ$	<a href="#">Rodell et al. (2004)</a>	<a href="#">Beaudoin et al. (2015)</a> [Acc. 25 September 2018]
NOAH-v21	2000-2017	Average layer soil moisture [ $kg/m^2$ ]	$1^\circ \times 1^\circ$	<a href="#">Rodell et al. (2004)</a>	<a href="#">Beaudoin et al. (2015)</a> [Acc. 25 September 2018]
AWRA-L v6	1975-2019	Fraction of soil moisture fullness [%] Reference PET [ $mm$ ] ESI [ <i>unitless</i> ]	$0.05^\circ \times 0.05^\circ$	<a href="#">Frost et al. (2018)</a>	This data provided by the BOM [Acc. July 2019 – January 2020]

### 2.1.4 General Circulation Model Data

The Coupled Model Intercomparison Project (CMIP) was developed to provide and improve the state of knowledge concerning the science of climate change that were used by the Intergovernmental Panel on Climate Change (IPCC) in its current Fifth Assessment Report (AR5). Simulations used in this thesis are from the 5th phase of CMIP, formally known as CMIP5 ([Taylor et al., 2012](#)). It is a collaborative framework with contributions of atmosphere-ocean general circulation models (AOGCMs) from more than 20 modelling groups worldwide and builds on the previous phases of CMIP. These models

include components that simulate the coupled atmosphere, ocean, land, and sea ice. Improvements over the climate models in previous phases include much greater biological and chemical details. CMIP5 is divided into three categories which define the experiment suites. These are (i) Decadal Hindcasts and Predictions simulations; (ii) "long-term" simulations; and (iii) "atmosphere-only" simulations (Taylor et al., 2012).

The objectives are to evaluate how realistic the models are in simulating the recent past, studying unforced variability, climate change over the historical period, and projected climate change to the end of the century and beyond. Several different experiments are embedded in these categories such as natural forcings, volcanic eruptions, abrupt and gradual CO<sub>2</sub> increases, future projections until 2300 with varying CO<sub>2</sub> emission scenarios and changes to sea surface temperatures or land use to name a few. For this thesis the 'historical run' from the "long-term" simulations is chosen to evaluate and explore flash drought. The historical run is forced by observed atmospheric composition and solar input changes and includes time-evolving land cover to reproduce the climate and variability therein for the period from the industrial revolution starting in 1850 until 2005 (Taylor et al., 2012).

While there are more than 50 models employed in CMIP5, the choice of models is limited by the necessary variables needed for this study. Daily soil moisture output for the length of the historical run caused most constraints leaving only the six models listed in Table 2.4 from the entire CMIP5 models. These models are the Second Generation Canadian Earth System Model (CanESM2), the Commonwealth Scientific and Industrial Research Organisation Mark, version 3.6.0 model (CSIRO Mk3.6.0), the Model for

**Table 2.4:** Procured CMIP5 models with their spatial resolution and variables used with their output variable names in square brackets.

Model	Resolution (lat x lon)	Variables
CanESM2	2.8° × 2.8°	10cm soil moisture [ <i>mrsos</i> ]
CSIRO-Mk3-6-0	1.9° × 1.9°	Max air temperature [ <i>tasmax</i> ] Min air temperature [ <i>tasmin</i> ]
GFDL-CM3		Surface wind speed [ <i>sfcWind</i> ]
GFDL-ESM2G	2.5° × 2.0°	Humidity [ <i>huss</i> ] Surface pressure [ <i>psl</i> ]
GFDL-ESM2M		Downward shortwave solar radiation [ <i>rsds</i> ]
MIROC5	1.4° × 1.4°	Latent heat flux [ <i>hfls</i> ] Precipitation [ <i>pr</i> ]

Interdisciplinary Research on Climate, version 5 (MIROC5) and three models from the Geophysical Fluid Dynamics Laboratory, which are the Earth System Model with Generalized Ocean Layer Dynamics component (GFDL-ESM2G), the Earth System Model with Modular Ocean Model 4 component and the Climate Model, version 3 (GFDL-CM3). One major caveat of all CMIP5 models is that soil moisture on a daily time scale is only available for the 0-10cm layer and thus is not fully representing the root-zone soil layer. However, the highly dynamic changes in moisture availability during the development of a flash drought makes a daily time scale an inevitable necessity. Other procured variables are shown in Table 2.4, and are maximum and minimum air temperature, surface wind speed, humidity, surface pressure, downward short-wave solar radiation, latent heat flux and precipitation. All data is from the historical run providing a common time period of 139 complete years (1867-2005).

## 2.2 Methods

### 2.2.1 Drought and Evapotranspiration

This section outlines the common methods used throughout this thesis. The analysis methods that are specific to each chapter will be described within that chapter.

Drought is defined as a deficiency in moisture at the surface, which can be examined by looking at the water balance. The water balance is driven by precipitation and evapotranspiration (P-ET). Precipitation is straightforward as it is directly measured, but ET is more complicated as direct measurements typically involve computing fluxes of water vapour to the atmosphere. Consequently, to examine the balance we first need to look at how we can estimate ET given the lack of observations.

Evaporation is the process of water removal from the land surface to the atmosphere. It is made up of evaporation from the soil, evaporation from intercepted water and evaporation through the stomates of leaves (transpiration). The combination of these is called evapotranspiration (ET). ET is an important process that cannot be neglected during drought development as it is a significant process depleting water in the soil moisture layer alongside runoff (Hobbins et al., 2017). In fact, besides a small contribution from sublimation, ET is the only way to return water into the atmosphere.

Quantifying ET is challenging due to its various modulating processes from the atmo-

sphere, vegetation and land surface characteristics. To overcome these complications, estimates of ET and the potential ET (PET), similar to evaporative demand  $E_0$ , in combination with moisture availability from a subset of moisture sources is often used in LSMs (Pitman, 2003).  $E_0$  is defined as the maximum rate of ET with unlimited moisture availability. Many techniques have evolved over the years to compute best estimates of  $E_0$  with significantly varying accuracy (McMahon et al., 2013; Swann et al., 2016; Hobbins et al., 2017). The consensus is that it is best to use a fully physical function of radiative and meteorological forcings to compute ET (Allen et al., 1998; McMahon et al., 2013; Hobbins et al., 2017), as in Equation 2.1 (Hobbins et al., 2017) as follows,

$$E_0 = f\{T, q, R_n, U_z, P_a\}. \quad (2.1)$$

Equation 2.1 states that evaporative demand ( $E_0$ ) is a function of temperature,  $T$ , specific humidity,  $q$ , net radiation,  $R_n$ , wind speed,  $U_z$ , and atmospheric surface pressure,  $P_a$ . This framework is commonly employed. For example, the standardized crop reference ET formulation by the American Society of Civil Engineers (ASCE) and the Food and Agriculture Organization of the United Nations (FAO) have provided a widely used estimate of  $E_0$  that is derived from the Penman-Monteith equation (Allen et al., 2005) as in Equation 2.2,

$$E_0 = \frac{0.408\Delta(R_n - G) + \gamma \frac{C_n}{T+273} u_2 (e_s - e_a)}{\Delta + \gamma(1 + C_d u_2)}, \quad (2.2)$$

where  $E_0$  ( $mm \ day^{-1}$ ) is atmospheric evaporative demand;  $\Delta$  ( $kPa \ ^\circ C^{-1}$ ) is the slope of the saturated vapour pressure–temperature curve at the 2-m air temperature ( $^\circ C$ );  $\gamma$  ( $kPa \ ^\circ C^{-1}$ ) is the psychrometric constant;  $U$  ( $m \ s^{-1}$ ) is the wind speed (here specified at a 2-m height);  $R_n$  ( $MJ \ m^{-2} \ day^{-1}$ ) is the net incoming radiation;  $G$  ( $MJ \ m^{-2} \ day^{-1}$ ) is the downward ground heat flux;  $e_s$  ( $kPa$ ) and  $e_a$  ( $kPa$ ) are the saturated and actual vapour pressures, respectively;  $C_n$  ( $kg \ m^{-3} \ s \ day^{-1}$ ) and  $C_d$  ( $s \ m^{-1}$ ) are the “numerator constant” and “denominator constant”, respectively, depending on the reference type and calculation time step with values defined in Allen et al. (2005); and the 0.408 term ( $kg \ MJ^{-1}$ ) represents the inverse of the latent heat of vaporization converting  $E_0$  to daily depth units.

The relation between ET and  $E_0$  under drought is pictured in Figure 2.3. When

moisture availability is plentiful the maximum rate of ET is controlled by the  $E_0$  of the atmosphere, reflecting an energy-limited environment and shown on the left-hand side of the figure. ET increases proportionally with  $E_0$ , for example, with increases in wind speed, radiation or temperature. With continuing negative precipitation anomalies and ongoing high ET soil moisture becomes insufficient to sustain the rate of ET at the same rate as  $E_0$ . Consequently, ET becomes constrained by moisture availability. From there on ET and  $E_0$  start to diverge, reflecting a water-limited environment (Seneviratne et al., 2010). As the sensible heat flux increases,  $E_0$  continues to rise, while ET declines due to a reduction in moisture availability. With time, the rate of drying slows due to a higher water retention in the soil matrix associated with the reduction of ET due to lack of water availability (Seneviratne et al., 2010). The interaction between ET and  $E_0$  is linked across the land surface–atmosphere interface, particularly in drought (Hobbins et al., 2017).

Arguably, the inclusion of ET or an estimate thereof can be useful to monitor and detect agricultural drought. ET provides the second part of the P-ET balance which determines the level of surface moisture.

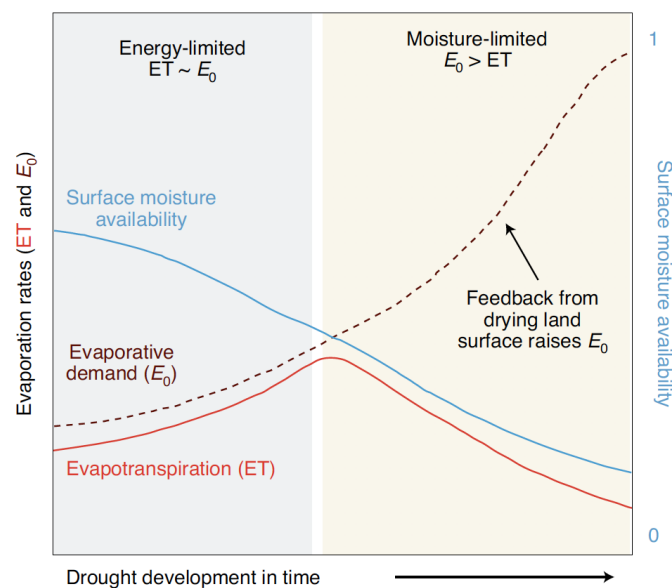


**Figure 2.3:** Relationship of evapotranspiration ( $ET$ ) and evaporative demand ( $E_0$ ) during the development of drought starting from wet conditions (energy-limited) on the left and proceeding into dry conditions (water-limited) to the right. From Pendergrass et al. (2020).

## 2.2.2 Drought Indices

Drought is manifest in different ways and can be identified by atmospheric variables like precipitation, land surface variables such as evaporation or soil moisture, a combination of the two, or on the subsequent effects on the land's surface e.g. vegetation health. Drought indices represent a simplification of these variables, or combinations of variables, to provide a quantifiable estimate of the state of drought. The drought indices used to identify agricultural and flash drought in this thesis are now described.

### 2.2.2.1 The Palmer Drought Severity Index (PDSI)

The Palmer Drought Severity Index (PDSI, [Palmer, 1965](#)) is a well-established drought index. The PDSI was designed to capture meteorological droughts by measuring the departure of moisture balance from normal conditions by using a model of cumulative imbalance of moisture supply and demand at the land surface ([Mishra and Singh, 2010](#)). Its hydrological accounting system includes a two-layer bucket model for soil moisture calculations, taking ET, recharge to soils (R), runoff (RO), water loss to the soil layers (L) and their potential values into account. These fluxes are calculated using precipitation and estimates of ET as model inputs. The water-balance coefficients are then determined for each month,  $i$ , using the average of those water fluxes over the calibration period resulting in the ratio of the long term mean values between a water flux and its potential value as in Equation 2.3,

$$\alpha_i = \frac{\overline{ET}_i}{\overline{PET}_i} \quad \beta_i = \frac{\overline{R}_i}{\overline{PR}_i} \quad \gamma_i = \frac{\overline{RO}_i}{\overline{PRO}_i} \quad \delta_i = \frac{\overline{L}_i}{\overline{PL}_i} \quad (2.3)$$

Where 'P' in the denominator part of each term stands for its potential value. Introduced by [Palmer \(1965\)](#), the climatically appropriate for existing conditions (CAFEC) values describe the conditions needed to maintain normal soil moisture level for a given time. They defined as the product of the potential water flux and its corresponding coefficient from equation 2.3, e.g.  $\alpha_i PET$  for CAFEC evapotranspiration. The sum of all CAFEC water flux values determines the CAFEC precipitation which is the precipitation needed to maintain normal soil moisture levels:

$$\hat{P} = \alpha_i PET + \beta_i PR + \gamma_i PRO + \delta_i PL. \quad (2.4)$$

Equation 2.4 then allows users to estimate precipitation excesses and deficiencies,  $D$ , by subtracting  $\hat{P}$  from the observed precipitation value  $P$ , this is,  $D = P - \hat{P}$ . To account for the different meanings of  $D$  at different locations and times,  $D$  was multiplied by a climatic characteristic constant  $K$  for month  $i$ , which was defined using data from the central United States in Kansas and Iowa:

$$K_i = K_o K'_i = \frac{17.67}{\sum_{i=1}^{12} \overline{D}_i K'_i} K'_i \quad (2.5)$$

where  $K'_i$  in Equation 2.5 is defined as

$$K'_i = 1.5 \log_{10} \left( \frac{\frac{\overline{PET}_i + \overline{R}_i + \overline{RO}_i}{\overline{P}_i + \overline{L}_i} + 2.8}{\overline{D}_i} \right) + 0.5. \quad (2.6)$$

The moisture anomaly index  $Z$  is then the product of the precipitation excesses and deficiencies  $D$  and the climatic characteristic constant  $K$  ( $Z = DK$ ). In a last step  $Z$  is used to calculate the PDSI for time  $t$  ( $X_t$ ):

$$X_t = pX_{t-1} + qZ_t = 0.897X_{t-1} + Z_t/3 \quad (2.7)$$

where  $X_{t-1}$  is the PDSI for the previous month.  $p$  and  $q$  in Equation 2.7 are the duration factors, which determine how sensitive the PDSI is to the monthly moisture anomaly  $Z_t$  and the magnitude of the autocorrelation in the PDSI. Palmer (1965) derived the values of  $p = 0.897$  and  $q = 1/3$  using the linear slope between the length and severity of the most extreme droughts that he studied in Kansas and Iowa (Dai, 2011a).

The original PDSI employed the Thornthwaite equation to calculate ET (Thornthwaite, 1948). However, the Thornthwaite method uses only temperature and has been criticised as this overestimates PET (Hobbins et al., 2008). Sheffield et al. (2012) have shown that the PDSI using the Thornthwaite method responds incorrectly to increasing global temperatures in recent decades and overestimates drought in future climate projections. Being constrained by temperature only, PET increases with increasing temperature (Sheffield et al., 2012). It has been well established that temperature does not uniquely determine the evaporative flux (Penman, 1948; Roderick et al., 2007; Hobbins et al., 2008; Donohue et al., 2010) and studies have shown regional declines in evaporative demand despite generally increasing regional temperatures (Roderick et al., 2009).

Consequently, most applications of the PDSI to date substitute the calculation of PET with the Penman-Monteith formulation, which applies multiple variables to compute PET that are described below (Monteith, 1965).

The PDSI is a complex drought index requiring multiple datasets and various assumptions. As such, standard tools have been developed and are available for use. Jacobi et al. (2013) from the University of Vanderbilt in Tennessee provides several scripts for the individual steps (water balance, PET, Z-Index, etc.) and a main script to select compulsory data for input. However, it only includes the Hamon and Thornthwaite methods to determine the evapotranspiration. Ficklin et al. (2015) improved the tool by incorporating the more accurate method from Penman-Monteith and provided access to their code (<https://github.com/cageo/Ficklin-2015>; Ficklin, personal communication). Their embedded formulation for PET is the same as in Equation 2.2. Using this tool for this thesis, the required input variables are therefore precipitation, temperature, wind speed, humidity and shortwave solar radiation. Moreover, a field constant of available water capacity for the two-layer bucket model needs to be provided for each grid cell.

### 2.2.2.2 The Evaporative Demand Drought Index (EDDI)

The described relationship between ET and drought in the beginning of this chapter is the basis on which the Evaporative Demand Drought Index (EDDI) is built (Hobbins et al., 2016). The index relies on the Penman-Monteith formulation (Eq. 2.2) only and calculates anomalies of  $E_0$ . Assuming that  $E_0$  spikes during the development of drought when the latent heat flux reduces due to diminishing water availability, strong positive values represent this drying process. EDDI is standardised using a non-parametric approach, in which empirically derived probabilities are obtained through an inverse normal approximation to achieve index inter-comparability (Farahmand and AghaKouchak, 2015; Hobbins et al., 2016). This is done by first determining the probabilities of  $E_0$  ( $P(E_{0_i})$ ) dependent on the rank ( $i$ ) of  $E_0$  in the historical time series ( $i = 1$  for minimum  $E_0$ ) and the number of observations ( $n$ ) using the empirical Tukey plotting position:

$$P(E_{0_i}) = \frac{i - 0.33}{n + 0.33}. \quad (2.8)$$

Subsequently, the inverse normal approximation is applied to achieve standardised EDDI values:

$$EDDI = W - \frac{C_0 + C_1W + C_2W^2}{1 + d_1W + d_2W^2 + d_3W^3}, \quad (2.9)$$

where  $W$  depends on the value of  $P(E_{0_i})$ . If  $W$  is  $\leq 0.5$ , then

$$W = \sqrt{-2\ln[P(E_{0_i})]}, \quad (2.10)$$

otherwise, for  $P(E_{0_i}) > 0.5$ ,  $[P(E_{0_i})]$  in equation 2.10 is substituted with  $[1 - P(E_{0_i})]$  and the sign of EDDI is reversed. The remaining constants are  $C_0 = 2.515517$ ,  $C_1 = 0.802853$ ,  $C_2 = 0.010328$ ,  $d_1 = 1.432788$ ,  $d_2 = 0.189269$ , and  $d_3 = 0.001308$ . Similar to other multiscale drought indices such as the SPI (described below), the EDDI can be calculated for an arbitrary time scale prior to standardisation, e.g. 1, 3 or 12-months by aggregating over the time scale of interest so that the value for each month is determined from the previous months. EDDI is used operationally as a drought index in the US and has successfully identified a flash drought in several cases in the US (McEvoy et al., 2016) and diagnosed water stress in west-central Wyoming (McNeeley et al., 2018).

### 2.2.2.3 The Standardised Precipitation Index (SPI)

The SPI (McKee et al., 1993) explicitly specifies drought time scales  $i$  for, typically 3 to 48 months, by comparing precipitation with its multi-year average. This makes the SPI very versatile to investigate short and long-term drought. Hydrological drought caused by long lasting precipitation deficiencies can be examined using the SPI on long time scales such as 24-month while the SPI can also be adapted to just a few months to investigate soil moisture drought (Mishra and Singh, 2010). It is the simplest of all the drought indices applied in this thesis as it only requires precipitation. To calculate the SPI, a location's long-term precipitation record is smoothed with a moving average over a specified time scale so that the value for each month is determined from the previous  $i$  months. The resulting frequency distribution of the time series is then fitted to a two-parameter gamma probability density function:

$$g(x) = \frac{1}{\beta^\alpha \Gamma(\alpha)} x^{\alpha-1} e^{-\frac{x}{\beta}}, \quad (2.11)$$

where  $\Gamma(\alpha)$  is the gamma function,  $x$  is the precipitation accumulation and  $\alpha$  and  $\beta$  the scale parameters of the gamma distribution, which are determined using the maximum likelihood approach (Edwards, 1997). From this, an incomplete cumulative gamma distribution function is derived assuming  $t = \frac{x}{\beta}$  as in Equation 2.12,

$$G(x) = \frac{1}{\Gamma(\alpha)} \int_0^x t^{\alpha-1} e^{-t} dt \quad (2.12)$$

The fact that Equation 2.12 is invalid for zero precipitation makes an extension necessary to account for that, which is  $q + (1 - q)G(x)$ , where  $q$  and  $1 - q$  are the probabilities of zero ( $x = 0$ ) and non-zero ( $x > 0$ ). The resulting complete cumulative probability distribution is then expressed as in Equation 2.13,

$$H(x) = q + (1 - q)G(x). \quad (2.13)$$

Different probability distribution types have been employed in various studies. The most commonly applied are two-parameter gamma and Pearson Type III (Mishra and Singh, 2010). We use the gamma distribution as originally proposed by McKee et al. (1993). The inverse normal approximation is used in a last step to convert the cumulative probability to the standard normal random variable, the SPI, using equations 2.9 and 2.10. The result is a normal distribution with a mean SPI of zero for a specific location and the SPI values representing the number of standard deviations from the mean (McKee et al., 1993). The length of the precipitation record available influences the calculated SPI values considerably due to changes in the shape and scale parameters of the gamma distribution (Wu et al., 2005). Therefore, we have ensured that the precipitation time series is longer than 30 years, which McKee et al. (1993) recommends as the minimum length. The SPI calculated in the presented way was used in Chapter 3.

Instead of the parametric approach, a non-parametric standardised index can be derived using the empirical probability. This can be applied to other drought variables than precipitation too, to obtain inter-comparable indices (Farahmand and AghaKouchak, 2015; Hao and Singh, 2015). Instead of using the Gringorten plotting position as proposed by Farahmand and AghaKouchak (2015), we apply the Tukey plotting position as done by Hobbins et al. (2016) in his formulation of the EDDI. Consequently, the calculations to achieve the non-parametric SPI follow exactly the ones of EDDI in the previous

section after precipitation was averaged over a specified window. This type of the SPI is used in chapters 4 and 5. We used slightly different formulations for two reasons. i) to keep the original formulation from [McKee et al. \(1993\)](#) when comparing to the PDSI with monthly data as done in other studies (e.g. [Guttman, 1998](#); [Vicente-Serrano et al., 2012](#)) and ii) to have inter-comparable indices for flash drought examination as recommended by [Farahmand and AghaKouchak \(2015\)](#). The time series in [Figure 2.4](#) shows that the differences between them are minor.

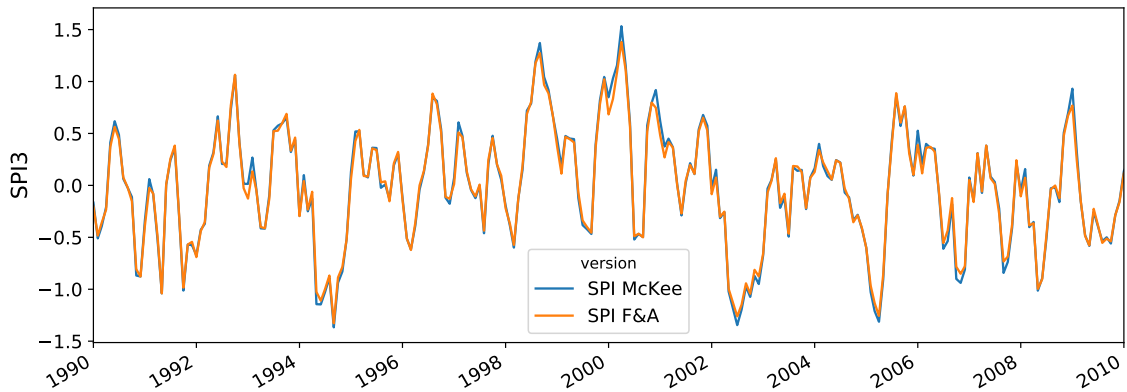


**Figure 2.4:** Area-averaged 3-month SPI over Australia calculated from monthly GPCP precipitation data ([Schneider et al., 2014](#)) using the original two-parameter gamma probability density function as in [McKee et al. \(1993\)](#) (blue) and the non-parametric empirical probability density function as in [Farahmand and AghaKouchak \(2015\)](#) (orange). Reference period is the entire length of the data set from 1979 to 2013. Shown is the time series from 1990 to 2010.

#### 2.2.2.4 The Standardised Precipitation Evapotranspiration Index (SPEI)

The SPEI ([Vicente-Serrano et al., 2010](#)) is in its methodology based on the SPI. However, instead of specifying drought by just precipitation it looks at the difference ( $D$ ) between precipitation ( $P$ ) and PET for month  $i$  as per [Equation 2.14](#):

$$D_i = P_i - PET_i. \quad (2.14)$$

The original formulation from [Vicente-Serrano et al. \(2010\)](#) uses the Thornthwaite method ([Thornthwaite, 1948](#)) to estimate PET. Here, PET is calculated using [Equation 2.2](#) for consistency among the procured drought indices.  $D_i$  values are aggregated over different time scales depending on the drought type or hydrological process of interest. Instead of using a two-parameter gamma distribution as commonly applied on the SPI, the SPEI needs a three-parameter distribution. Precipitation has a lower boundary of

0, whereas the  $D_i$  can be negative when PET exceeds P. [Vicente-Serrano et al. \(2010\)](#) have tested several probability density functions to standardise the  $D$  series and found the three-parameter log-logistic to be the most suitable one due to a better fit for low values. It is expressed as:

$$f(x) = \frac{\beta}{\alpha} \left( \frac{x - \gamma}{\alpha} \right)^{\beta-1} \left[ 1 + \left( \frac{x - \gamma}{\alpha} \right)^{\beta} \right]^{-2}, \quad (2.15)$$

where  $\alpha$ ,  $\beta$ , and  $\gamma$  are scale, shape, and origin parameters, respectively, for  $D$  values in the range ( $\gamma > D < \infty$ ) and are obtained by Equations 2.2.2.4 to 2.17:

$$\beta = \frac{2w_1 - w_0}{6w_1 - w_0 - 6w_2}, \quad (2.16)$$

$$\gamma = \frac{(w_0 - 2w_1)\beta}{\Gamma(1 + 1/\beta)\Gamma(1 - 1/\beta)}, \quad (2.17)$$

$$\gamma = w_0 - \alpha \Gamma\left(\frac{1 + 1}{\beta}\right) \Gamma\left(\frac{1 - 1}{\beta}\right), \quad (2.18)$$

where  $\Gamma(\beta)$  is the gamma function of  $\beta$ .  $w_s$  represents the probability-weighted moments (PWM) of order  $s$  as per Equation 2.19:

$$w_s = \frac{1}{N} \sum_{i=1}^N \frac{\binom{N-i}{s} D_i}{\binom{N-i}{s}}, \quad (2.19)$$

where  $N$  is the number of data points. Equation 2.19 is the updated version from [Beguería et al. \(2014\)](#) who use unbiased PWMs in contrast to the original plotting-positions PWMs in ([Vicente-Serrano et al., 2010](#)).

The probability distribution function of the  $D$  series is given by Equation 2.20:

$$F(x) = \left[ 1 + \left( \frac{\alpha}{x - \gamma} \right)^{\beta} \right]^{-1}. \quad (2.20)$$

The standardised values of the SPEI are then derived using equations 2.9 and 2.10. The result is, just like the SPI, a normal distribution with a mean SPEI of zero for a specific location and the SPEI values representing the number of standard deviations from the mean. The SPEI has been found to be very similar to the SPI for periods with no PET anomalies, but sensitive to increasing temperatures ([Vicente-Serrano et al., 2010](#)).

Due to that [Vicente-Serrano et al. \(2012\)](#) identified a slightly higher skill for drought detection in the boreal summer with abnormal temperature anomalies such as during the 2003 European heat wave event. The SPEI has also lately been used to replicate flash drought using a 1-month time scale ([Noguera et al., 2020](#)).

### 2.2.2.5 The Evaporative Stress Index (ESI)

The SPI, SPEI and EDDI describe atmospheric conditions. While the SPI measures the moisture supply to the land surface, the EDDI gives an estimate of how much moisture the atmosphere demands. The SPEI measures the difference between both. However, neither of them directly estimate the direct response of the land surface.

The ESI ([Anderson et al., 2007](#)) aims to do this. The ESI incorporates PET, indicating atmospheric demand, but also includes actual ET, which is moisture supply from the land's surface. The ESI is defined as the standardised anomaly of the ratio of actual ET to PET ( $r_{ET}$ ) as in Equation 2.21,

$$r_{ET} = \frac{ET}{PET}, \quad (2.21)$$

Studies, e.g. [Otkin et al. \(2013\)](#) and [Nguyen et al. \(2019\)](#) have standardised the ESI using Equation 2.22,

$$ESI = \frac{r_{ET} - \langle r_{ET} \rangle}{\delta(r_{ET})}, \quad (2.22)$$

where  $\langle r_{ET} \rangle$  is the climatology of  $r_{ET}$  and  $\delta(r_{ET})$  its standard deviation over a baseline period. Here, we unify the standardisation process across the indices used in chapters 4 and 5, the ESI is standardised using equations 2.8 to 2.10 so that all indices used in those chapters are comparable.

The ESI calculates both components of  $r_{ET}$  from thermal remote sensing data with the Atmosphere-Land Exchange Inverse model (ALEXI). Alternatively, other measures can be procured for PET and actual ET inputs to retrieve the ESI. This will be described in the methodology of the relevant chapters. As SPI and EDDI,  $r_{ET}$  in Equation 2.21 can be computed over an arbitrary time scale.

For flash drought analyses in chapters 4 and 5, SPI, ESI and EDDI were translated into categories based on their percentile ranks according to the EDDI guidelines ([Lukas et al., 2017](#)) shown in Table 2.5, classifying dry (ED, "EDDI dry") and wet (EW, "EDDI

**Table 2.5:** Wetness and drought categories according to the EDDI guidelines stated in [Lukas et al. \(2017\)](#). EDDI is inverted in comparison to SPI, ESI and SSI due to its reciprocal relationship to them. A high evaporative demand and thus positive values correspond to dry conditions for EDDI while e.g. low precipitation and thus negative index values correspond to dry conditions for SPI. The drought categories of EDDI are based on the US Drought Monitor ([Svoboda et al., 2002](#)).

	Category	Percentile ESI/SPI/SSI	Percentile EDDI	USDM Intensity
Wetness categories	EW4	>98%	<2%	
	EW3	>95%	<5%	
	EW2	>90%	<10%	
	EW1	>80%	<20%	
	EW0	>70%	<30%	
	None			
Drought categories	ED0	<30%	>70%	abnormally
	ED1	<20%	>80%	moderate
	ED2	<10%	>90%	severe
	ED3	<5%	>95%	extreme
	ED4	<2%	>98%	exceptional

wet") conditions. We use these categories to define a consistent state of each index during the onset of a flash drought.

---

## Chapter 3

# Uncertainties in Drought from Index and Data Selection

---

### 3.1 Preface

This section is a reproduction of the paper “Uncertainties in drought from index and data selection” in press in *Journal of Geophysical Research - Atmospheres* by [Hoffmann et al. \(2020\)](#), with section and figure numbers changed to fit the thesis structure. Most of the supplementary material of [Hoffmann et al. \(2020\)](#) is now included in the main text.

This study compares various drought indices, the Palmer Drought Severity Index (PDSI), the Standardized Precipitation Evapotranspiration Index (SPEI), and the Standardized Precipitation Index (SPI), and the uncertainties in each to the input data from which they are derived. The abilities of the PDSI, SPEI and SPI to capture drought periods are assessed through a comparison with soil moisture estimates from two generations of the Global Land Data Assimilation System (GLDAS). This comparison shows that the skill with which a drought index represents variations in soil moisture does not necessarily improve when evapotranspiration is included (i.e. PDSI/SPEI rather than SPI), though this depends on location and the time scale of the drought. The differences in the abilities of the drought indices to represent soil moisture are also compared

to the magnitude of the uncertainty in each index arising from the choice of input data. In many cases, the uncertainties in the variations of the PDSI, SPEI and SPI to the choice of input data are larger in magnitude than the differences between the indices themselves, particularly when considering the dry tails of the distribution. The results show that no one drought index outperforms the others during drought conditions.

## 3.2 Introduction

Drought is an inherent part of climate variability and affects most regions on Earth (IPCC, 2012; Sheffield and Wood, 2011). In broad terms, drought is the persistence of extreme negative moisture anomalies over a specific region and an extended period of time typically on the order of months or longer (Mishra and Singh, 2010; Zargar et al., 2011).

Unlike many other natural hazards, difficulties arise in terms of defining drought (see Chapter 1). This is because drought is a slowly evolving phenomenon (Mishra and Singh, 2010) whose modulating mechanisms stem from complex interactions of atmospheric, land surface and oceanic processes. Moreover, drought is manifest in different ways and can be identified by atmospheric variables like precipitation, land surface variables such as evaporation or soil moisture, a combination of the two, or on the subsequent effects on the land's surface e.g. vegetation health. The broad interpretations of drought into meteorological, agricultural, hydrological and socioeconomic (Wilhite and Glantz, 1985) have led to a multitude of approaches to classify and monitor droughts in terms of their characteristics and hundreds of drought indices have been developed for this purpose (Heim Jr., 2002; Zargar et al., 2011). Each drought index has its unique strengths and weaknesses as comparisons of several indices in numerous studies reveal (Dai et al., 2004; Guttman, 1998; Heim Jr., 2002; Keyantash and Dracup, 2002; Mishra and Singh, 2010; Mpelasoka et al., 2008; Zargar et al., 2011).

A common application of these drought indices is in identifying drought that has an agricultural impact, typically on time scales of 1–12 months. Thus, drought indices based on soil moisture measurements are ideal. However, in reality, direct soil moisture measurements are rarely employed in drought indices. This is because *in situ* soil moisture observations are sparse in space and time. Satellite observations of soil moisture are

global but their spectral bands typically capture soil moisture in the first few centimetres of soil only (Karthikeyan et al., 2017). This shallow layer is not necessarily sufficient for capturing drought as it is not necessarily representative of soil moisture storage through deeper soil layers, including the root zone. In the absence of a dense, long- network of soil moisture gauges many drought indices have been developed that are based on other variables that can act as a proxy for soil moisture, for example, precipitation or some combination of precipitation and evaporation.

Among the most well-established indices used in climate research are the Palmer Drought Severity Index (PDSI, Palmer, 1965), the Standardized Precipitation Index (SPI, McKee et al., 1993) and more recently the Standardized Precipitation Evapotranspiration Index (SPEI, Vicente-Serrano et al., 2010). The SPI estimates drought from precipitation only and is calculated at a location using a distribution of precipitation that has been transformed to a standard normal distribution (i.e. a mean of 0 and standard deviation of 1). The SPEI is mathematically similar to the SPI but estimates drought using water balance, calculated as precipitation minus evapotranspiration. Both indices are multi-scalar, meaning that the time interval on which they are calculated can be adjusted relative to different drought types (e.g. 3, 6 or 12 months). The PDSI employs a simple water balance model, which estimates soil moisture as the difference between precipitation and evapotranspiration. All approaches have their advantages and limitations but their differences can lead to disagreement in some characteristics of drought, e.g. timing of onset or duration (Mishra and Singh, 2010; Zargar et al., 2011).

Mishra and Singh (2010) provide a brief review of the differences in the detection of drought between the PDSI and SPI. Their review suggests that the SPI provides a better representation of soil wetness and is a better indicator of crop production compared to the PDSI. However, Tsakiris and Vangelis (2005) argue that reliable drought assessment is not possible using meteorological drought indices like the SPI and evaporation must be included in order to consider the antecedent water deficit in soil moisture memory. Some argue that temperature is necessary to evaluate changing drought conditions in the future when potential evapotranspiration is likely to increase (Vicente-Serrano et al., 2010). Hence, Vicente-Serrano et al. (2010) developed the SPEI to combine the multi-scalar character of the SPI with the influence of evapotranspiration.

Several studies have compared the PDSI, SPEI and SPI with *in situ* soil moisture

observations and/or soil moisture estimates from land surface models (LSM) to evaluate their reliability. [Narasimhan and Srinivasan \(2005\)](#) compared SPI and PDSI with other soil moisture and evapotranspiration based indices for two watersheds in Texas and found a good positive correlation of around 0.6. [Dai et al. \(2004\)](#) correlated the PDSI with observed soil moisture over several regions worldwide and found good correlations of 0.5–0.7 for those sites. [Spennemann et al. \(2015\)](#) used the SPI to compare it to modelled soil moisture over south eastern South America and found high correlations ( $> 0.7$ ) for longer time scale SPIs in deeper soil layers with seasonal dependencies. [Vicente-Serrano et al. \(2012\)](#) compared PDSI, SPEI and SPI to soil moisture from the international soil moisture network and found that both SPI and SPEI have superior skill over the PDSI to monitor agricultural drought impacts due to their adjustable time scale as found by other studies (e.g. [Zhao et al., 2017](#)). They found that the SPEI performed marginally better than the SPI in the summer season, concluding that the influence of ET cannot be neglected in drought evaluation. [Raible et al. \(2017\)](#) came to the same conclusion for the Mediterranean region when they evaluated the performance of derivatives of SPI, PDSI and SPEI to model simulations over Europe. In contrast [Raible et al. \(2017\)](#) have shown that the SPI is sufficient for Central Europe.

Most studies have evaluated the performance of drought indices to LSM outputs due to globally sparse and temporally short time series of reliable soil moisture observations. As pointed out by [Spennemann et al. \(2015\)](#) and shown by [Ukkola et al. \(2016b\)](#) uncertainty in the soil moisture estimates from LSMs is high and so the evaluation of which “better” represents soil moisture is difficult. In this study, we set the LSMs as the reference for comparison. Despite the LSM’s own implicit biases and errors, which we will discuss later on, a comparison still provides a benchmark for estimating the uncertainty of drought indices to input data. [Koster et al. \(2009a\)](#) pointed out that LSMs, unless all of them are entirely wrong, can “capture the time variations of real-world soil moisture” when forced with realistic meteorological data.

One distinct advantage of the SPI over the SPEI and PDSI is its ease of calculation requiring precipitation as its only variable. These data are available worldwide and are of high veracity. Precipitation data span long periods of time and station networks in most places are relatively dense, providing a good record for the purposes of agricultural drought detection and examining variability and change in drought. The PDSI and SPEI

require additional variables to estimate the ET component via the Penman-Monteith method (Monteith, 1965), formulated as the crop reference ET by the United Nations Food and Agriculture Organisation (FAO) (Allen et al., 1998). The variables employed are namely temperature, solar insolation, humidity and wind speed. Some of these variables are not well measured and globally available. A past criticism of the PDSI was that it was inappropriate to apply the index in regions with extreme variability in rainfall (Mishra and Singh, 2010; Zargar et al., 2011). However, Wells and Hayes (2004) introduced a self-calibrating method for the PDSI to remove fixed climate characteristic coefficients that were based on empirically-derived constants for the United States and this has improved PDSI estimates of drought outside that region. The Penman-Monteith method requires multiple datasets and various assumptions that introduce uncertainties into the PDSI (Dai and Zhao, 2016; Sheffield et al., 2012; Trenberth et al., 2014).

There are distinct differences in how the SPI, SPEI and PDSI represent soil moisture. There are also relative advantages and disadvantages to the calculation of each due to uncertainties in the measurements being used to calculate each index (Dai and Zhao, 2016; Trenberth et al., 2014), as has been outlined above. Whether or not using an index such as the PDSI or SPEI is advantageous for examining drought over a simpler metric like SPI has not been examined in the context of the uncertainty in the data used to compute each index. Therefore, this study highlights the sensitivity of the PDSI, SPEI and SPI to their input data.

The research presented here provides an indication of the uncertainty of three commonly used drought indices to their input data, and compares this to the differences in the way each index detects drought. To do this, we compare the SPI, the SPEI and the PDSI, computed using input data from a number of different sources, including both observations and reanalysis, with multiple modelled global soil moisture products. Given the scarcity of *in situ* soil moisture observations globally, we treat LSMs here as the reference to benchmark the PDSI, SPEI and SPI. The following data section describes them and the obtained soil moisture estimates in detail. The methodology is explained in the third section along with the SPI, SPEI and PDSI methods and the selection of soil depth layers. Results are then provided, divided into sensitivity of indices to input data and soil moisture estimates for two soil depths. Finally, the results are discussed in section 5 and summarised afterwards.

## 3.3 Data

The accuracy of the data sets used to generate the drought indices determines their efficacy. There can be substantial differences between the individual products derived from satellites, weather stations, combinations of the two and from reanalysis products. To assess the sensitivity of the SPI, SPEI and PDSI to their input data sets we computed each drought index from the datasets shown in Table 2.1. These data are now described.

### 3.3.1 Input variables for the SPI, SPEI and PDSI

Monthly precipitation totals are used for the calculation of all three indices. The PDSI and SPEI further require inputs of mean or minimum and maximum monthly temperature, solar insolation, specific humidity and wind speed. These data were sourced from a variety of observational and reanalysis products that are also listed in Table 2.1 and described in detail in Section 2.1. In order to estimate soil moisture content the PDSI also requires the available water capacity (AWC), which is unique for each location, and was obtained from [Webb and Rosenzweig \(1993\)](#). The AWC is a constant, but all other datasets were examined over the period 1979 – 2013.

### 3.3.2 Soil moisture estimates

As described in the introduction, long-running *in situ* soil moisture measurements are not available worldwide. Further, satellite measurements of soil moisture are confined to the top few centimetres of soil. This can be limiting for drought analysis as these top levels of soil moisture can be too responsive to the atmosphere and less indicative of changes in soil moisture throughout the root zone ([Entekhabi et al., 1996](#)).

Instead, for a comparison of drought indices, we employ data from NASA's Global Land Data Assimilation System (GLDAS), which drives four offline land surface models (VIC, NOAH, MOSAIC, CLM) with ground and satellite observation based datasets to estimate terrestrial water and energy states and fluxes ([Rodell et al., 2004](#); [Rui, 2017](#)). The NOAH LSM is also available for the second generation GLDAS which consists of two parts (2.0 and 2.1). The difference to the first generation is an updated NOAH model (2.7 to 3.3) and changes in the forcing data sets due to inconsistencies discovered in GLDAS 1.0. Further details about GLDAS and the merging procedure of the two

GLDAS 2.x parts are outlined in Section 2.1. The second generation GLDAS NOAH LSM is from here on referred as NOAHv2.

For this study, we used monthly 1-degree 0-10 cm and 10-40 cm average layer soil moisture output from 1979 to 2016 from the NOAH and CLM land surface model, from here on referred to as NOAHv1/2 and CLMv1 (Table 2.2). The layer depths available for VIC and MOSAIC do not offer these levels and were therefore not used.

### 3.4 Methods

This study examines differences between the PDSI, SPEI and SPI in their representation of soil moisture from GLDAS LSMs and compares the magnitude of these differences to the uncertainties of the indices to the input data used to calculate the drought indices. Here we look at time variations in soil moisture rather than the magnitude in absolute values to correlate them with SPI and PDSI. In this case, LSMs show very similar information about soil moisture variability over time, despite their large differences in absolute values (Koster et al., 2009a), with similar results found across the three LSMs used in this study (CLMv1, NOAHv1/2) (Figure 3.1). This gives us confidence to use LSMs as an estimated representation of real-world soil moisture and a reference for benchmarking. However, there are shared parametrisations across these three models meaning they are not fully independent.

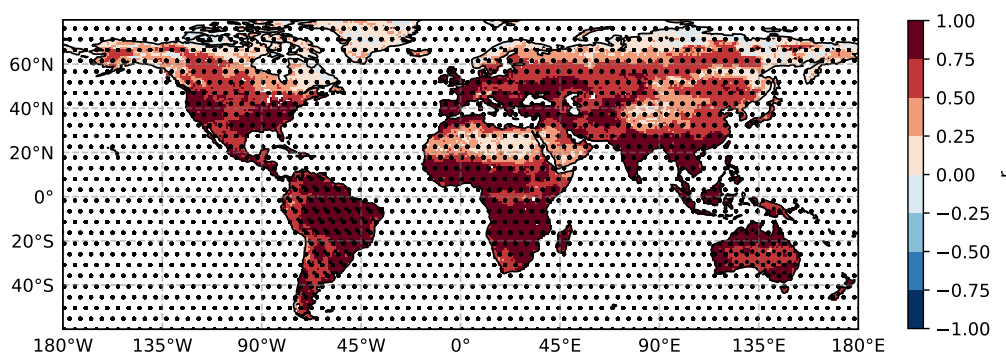


**Figure 3.1:** Mean correlation of three independent LSM pairings (CLMv1, NOAHv1, NOAHv2) using the 1979-2013 time period and afterwards averaged. Stippling shows statistically significant correlations at the 95% level.

As previously described, the SPI fits a precipitation time series to a probability distribution from which a standard normal density distribution is derived (McKee et al., 1993). Here, we compute the SPI on 3, 6, 9 and 12 month time scales to assess seasonal to

annual and inter-annual droughts (McKee et al., 1993).

The SPEI is mathematically very similar to the SPI and is computed for the same time scales. Instead of using only precipitation, its input is the water balance of precipitation minus potential evapotranspiration (Vicente-Serrano et al., 2010).

The PDSI estimates the water supply and demand to restore normal moisture conditions based on the water balance within a two-layer bucket soil model and includes estimates of rainfall, evapotranspiration and soil moisture (Palmer, 1965). Here, the evapotranspiration in the PDSI is computed using the Penman-Monteith method (Monteith, 1965; Allen et al., 1998) which was added by Ficklin et al. (2015) to a Matlab tool developed by Jacobi et al. (2013) (code access via GitHub, <https://github.com/cageo/Ficklin-2015>). More details on the calculation of those indices is presented in Chapter 2.2.

While LSMs consider a variety of soil properties and vegetation types which are important for the rate of soil moisture changes, the indices considered here focus on meteorological drought and either do not account for those characteristics at all (SPI and SPEI) or only for soil properties in a simplistic hydrological model by using prescribed values for water-holding capacity (PDSI).

A comparison between the PDSI, SPEI and SPI and soil moisture is presented in Section 3.5.1. The sensitivity of the verification of the drought indices to the choice of LSM is examined by fixing the input data to the PDSI, SPEI and SPI and comparing these indices to the LSMs described in Section 3.3. The permutation of input data used to calculate the PDSI, SPEI and SPI is fixed to the GPCC for precipitation and the NCEP II reanalysis for the remaining parameters (Table 2.1), which gave the highest global mean correlation of all permutations. The correlations between the PDSI, the SPI and SPEI on a 3, 6, 9 and 12-month time scale and soil moisture are computed at the grid point scale. Soil moisture in the LSMs is approximated for 0-10cm (layer 1) and 10-40cm (layer 2). These are slightly different for each model due to differences in their native levels and are shown in Table 2.2. As the PDSI, SPEI, SPI and soil moisture data are calculated on different scales and have different units, skill is measured using a Pearson correlation.

We use all gridded products in this analysis and to enable comparison all data are bilinearly interpolated to the coarsest common grid of  $2.5^\circ \times 2.5^\circ$  (Table 2.1). We

removed the seasonal cycle from GLDAS and small spatial or temporal data gaps were closed with nearest neighbour values. The spatial domain was limited to  $76^{\circ}N$  and  $58^{\circ}S$  because drought indices do not perform well in high latitudes and where data coverage is poor (Contractor et al., 2019; Zargar et al., 2011). As the start and thus the length of the first and second GLDAS LSM generation varies between 1948 and 1979, only the common period from 1979 onwards was used. The PDSI was calculated and calibrated for this period only as some input data such as ERA Interim also start in this year. For the SPI, a long-term record of more than thirty years is needed by definition (McKee et al., 1993). Thus, the 1979–2013 base period was used for the SPI and SPEI to be consistent with the PDSI.

In Section 3.5.2 the sensitivity of the PDSI, SPEI and SPI to the input data from which they are calculated is examined. The input data are precipitation for the SPI and precipitation, solar insolation, humidity, wind speed and temperature for the PDSI and SPEI. We apply different permutations of these input data sets from different sources listed in Table 2.1 and re-examine the skill of each index in its ability to simulate soil moisture variability by comparing to a soil moisture estimate, the GLDAS NOAHv2 LSM. Hence, statements about the performance of each index indicate how different they are and are relative to the LSM's estimate of soil moisture fluctuations. Given the inherent uncertainties in these soil moisture estimates discussed earlier, we also test the sensitivity by comparing the index values themselves.

In total, there are five permutations of input data possible for the SPI and twelve for the PDSI and SPEI. To account for these differences for the comparison, the PDSI samples were bootstrapped using the same number of replicates as the SPI sample size. This resampling method was performed 1000 times. From this, max/min/mean correlations and spread were computed for the individual indices.

The comparisons between the SPI, SPEI, PDSI and LSM were performed both on the entire dataset and for a subset of drought periods. The drought periods were defined when PDSI and SPI/SPEI values fell below a certain threshold, set at -2.0 and -0.8 respectively. These thresholds were chosen according to the classification of a “moderate drought” from the US Drought Monitor (Svoboda et al., 2002).

## 3.5 Results

This study assesses the effect of uncertainties on the skill of drought indices to approximate modelled soil moisture by a two-stage test. i) testing the uncertainty of the skill of the drought index to soil moisture estimates (Section 3.5.1) and ii) testing the uncertainty of the skill of the drought index to the choice of input data used in the computation of the drought index (Section 3.5.2). The magnitudes of each source of uncertainty are then compared (Section 3.5.3). Sections 3.5.1 and 3.5.2 focus on the differences between PDSI and SPI only as these two indices show the largest contrast.

### 3.5.1 Sensitivity of the skill of Drought Indices to Soil Moisture Product

The skill that each drought index has in capturing variability in soil moisture reanalysis and satellite products is first tested by correlating the drought indices with soil moisture at two levels from the GLDAS products described in Section 3.3. The correlations were performed for each GLDAS LSM individually and the mean of those results is presented here. While these results are relative to modelled soil moisture, comparison to real-world observations can differ and thus the results need to be interpreted with care.

The data sources used to compute the drought indices remain fixed as the GPCC for precipitation and NCEP Reanalysis II for all remaining variables. Those were selected as they have the highest correlation to LSMs. The correlations were produced using the entire sample of PDSI, SPI and soil moisture data (i.e. both wet and dry conditions) as well as only for the lower tails only PDSI and SPI smaller or equal to  $-2.0$  and  $-0.8$  respectively, equating to drought conditions.

#### 3.5.1.1 The sensitivity of drought index skill for upper soil profile (0-10cm)

Figure 3.2 shows the mean correlations between the GLDAS soil moisture products and the SPI-3, 6 and 12 or PDSI, globally for the 0–10cm soil layer. Note, that we have omitted the SPI9 panels for correlation coefficient for space considerations. Maps a) – d) display correlation coefficients ( $r$ ) and significance stippling ( $p < 0.05$ ) for the entire sample of PDSI and SPI with soil moisture data while maps e) – h) only consider drought conditions. Absolute  $r$  between the soil moisture estimate and drought index

reach their maximum around  $r \approx 0.7$  in the subtropical latitudes for the entire sample (Figure 3.2a-d).

For drought conditions,  $r$  is globally weaker in the magnitude of 0.2 – 0.3 compared to the previous scenario with no correlation at all in many places (Figure 3.2e-h). In both cases, the SPI on the shortest time scale of three months (SPI3) has the strongest correlations which are statistically significant at the 95% level in eastern Australia and eastern US. Overall, the SPEI shows similar correlations to the SPI (Figure 7.1).

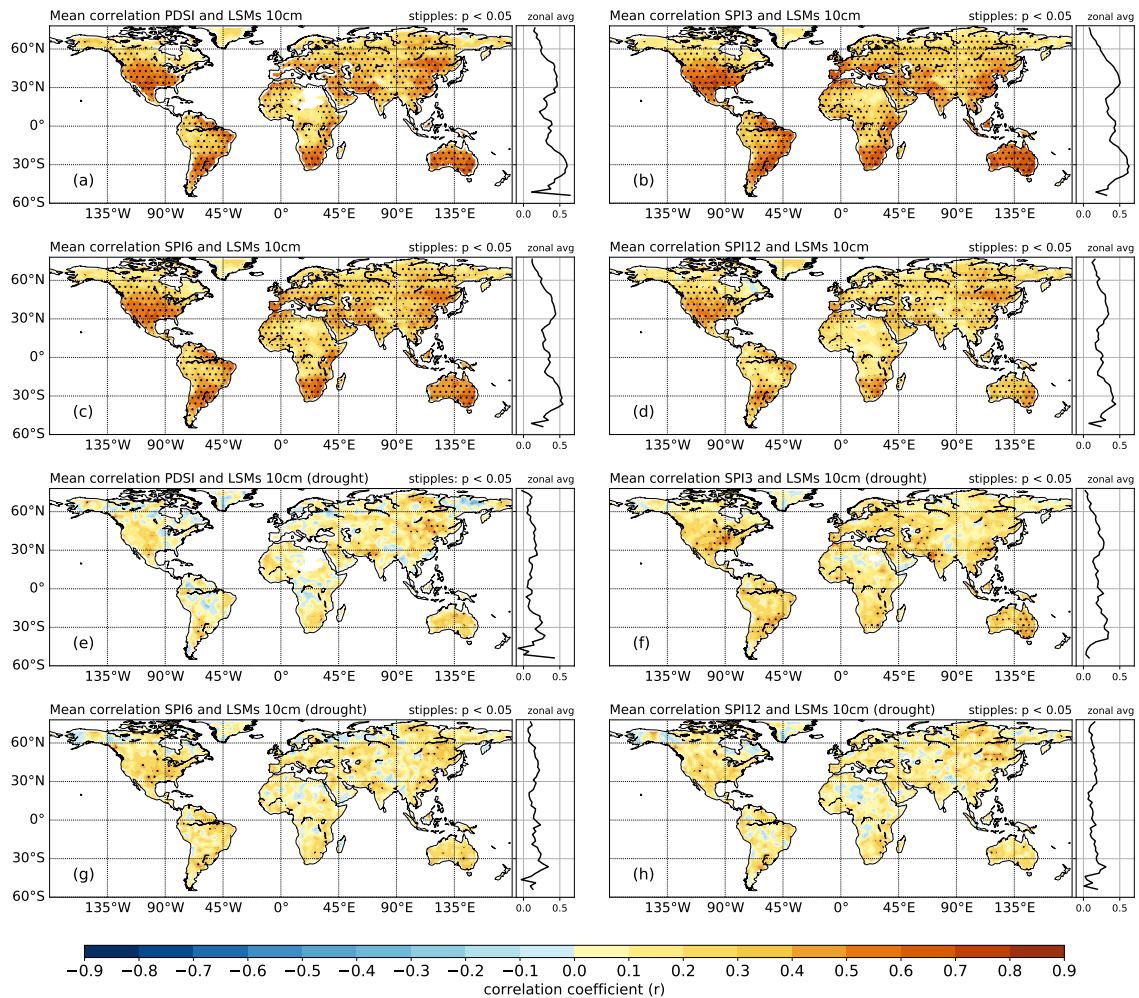


**Figure 3.2:** Mean and zonal correlations of varying LSMs for PDSI (a/e), SPI3 (b/f), SPI6 (c/g) and SPI12 (d/h) for whole data distribution (a-d) and drought periods (e-h) of the 0–10cm layer. The zonal average is shown to the right of each plot. Stippling shows statistically significant correlations at the 95% level

Figure 3.3 shows the difference in the variance explained in the GLDAS soil moisture products by the PDSI and the SPI-n for the 0–10 cm layer of soil, again for all data (a-d) and during drought periods only (e-h). Positive (negative) values indicate that the SPI-n (PDSI) explains a larger amount of variance in the soil moisture product compared

to the PDSI (SPI-n). The stippling shows where the  $r^2$  values show consistency in the sign of the difference regardless of soil moisture product. That is, the SPI (PDSI) index always shows larger  $r^2$  values than the PDSI (SPI) in black (red).

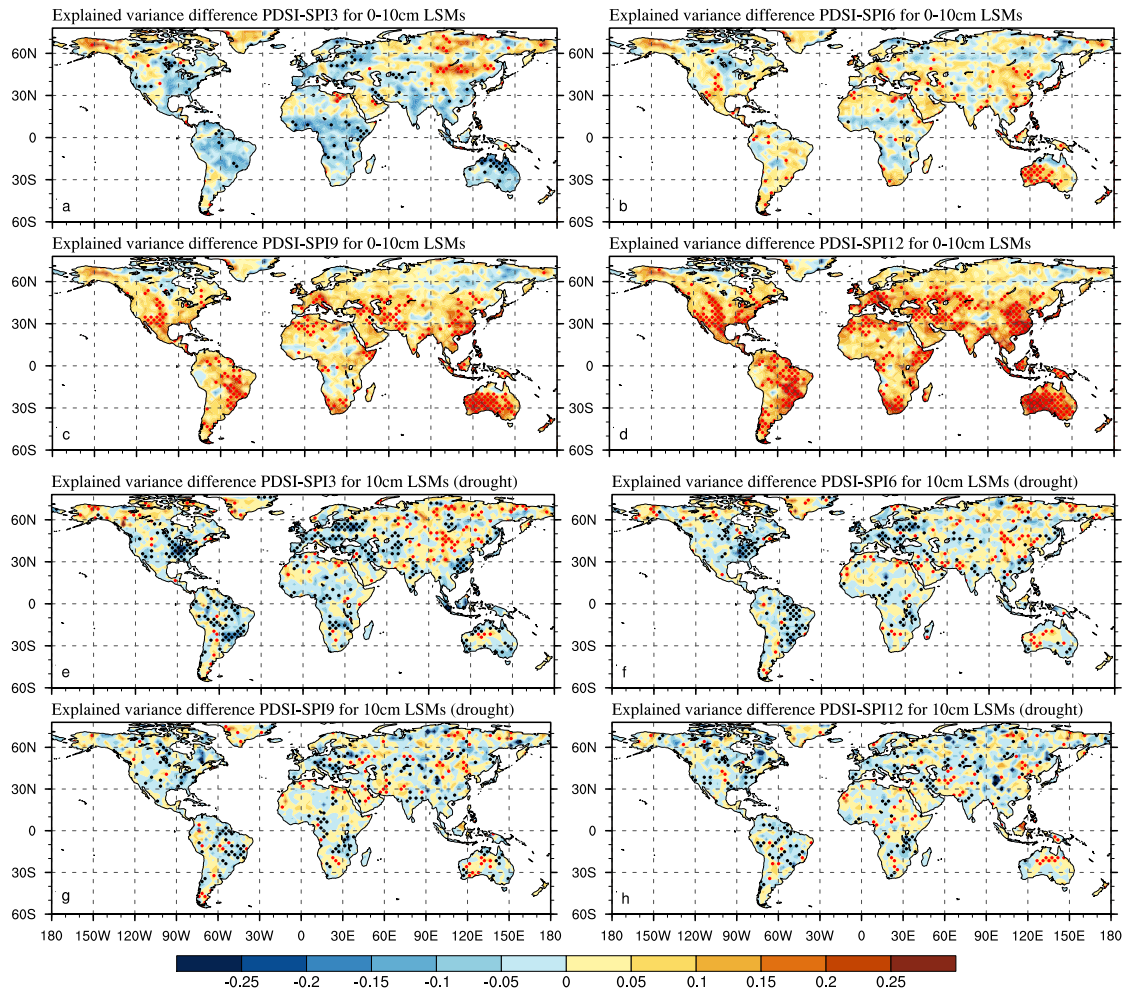


**Figure 3.3:** Explained variance differences of PDSI minus SPI3 (a/e), SPI6 (b/f), SPI9 (c/g) and SPI12 (d/h) calculated with fixed input data from GPCC and NCEP with GLDAS CLMv1, NOAHv1 and NOAHv2 0-10cm for whole distribution (a-d) and drought periods (e-h) defined as  $PDSI < -2.0$  and  $SPI < -0.8$  (1979-2013). Black stippling show where all correlations of the SPI-n with GLDAS are higher than those of the PDSI. Red stippling shows where all correlations of the PDSI and GLDAS LSMs are higher than those of the SPI-n with GLDAS LSMs.

Focussing on the whole data distribution (Figure 3.3a–d), the skill of the SPI versus PDSI changes with the time scale on which the SPI is computed. When the SPI is computed on a three-month time scale, it tends to show better skill than the PDSI in its representation of shallow, modelled soil moisture (0–10 cm) across most of the globe (60%) with the exception of central Asia. In particular, soil moisture variability in drought prone regions in the subtropics such as the southwestern US, Australia and the

Sahel zone are best represented by the SPI3. However, these differences are not robust against the choice of soil moisture model for most locations.

As the time step over which the SPI is computed increases, the skill of the SPI decreases compared to the PDSI, particularly on longer time scales of 9 and 12 months, reducing its global coverage to 21% and 11% respectively. The increase in red stippling in Figures 3.3c and 3.3d indicates that the increase in skill in the PDSI becomes increasingly robust to the choice of reanalysis. In some regions, the PDSI explains an average of over 25% more variance in soil moisture variations compared to the SPI12 (Figure 3.3d). These results show that the inclusion of ET in the drought index is able to better capture long-term soil moisture memory than one based on long-term precipitation variations alone.

The differences in skill decay substantially when drought periods only are examined. Figure 3.3e–h show that the skill of the PDSI and SPI are indistinguishable during drought on longer time scales (e.g. 9 and 12 months, Figure 3.3g and h). Globally, the SPI3 typically shows larger  $r^2$  values than the PDSI that are robust to the choice of LSM as indicated by the black stippling in Figure 3.3e. The differences between the SPI-n and PDSI become smaller when the SPI is computed on the 6, 9 and 12-month time scale (Figure 3.3f, g and h).

### 3.5.1.2 The sensitivity of drought index skill for the deeper soil profile (10–40cm)

For the deeper 10–40cm soil layer the absolute correlations between soil moisture and drought indices are slightly weaker than for the shallow soil layer, but are still moderate ( $r \approx 0.5$ ) and statistically significant ( $p < 0.05$ ) in the subtropics. During drought conditions, they are mainly not significantly correlated (Figure 3.4e–h). The SPEI shows very similar correlations to the SPI (Figure 7.2).

Compared to the 0–10 cm layer, there are more distinct regional differences between the  $r^2$  values for the 10–40 cm soil layer (Figure 3.5). The PDSI becomes increasingly more skilful with 68% of global land areas showing stronger correlations compared to all SPI indices. When the SPI time scale is increased from 3-months to 12-months the pattern of differences is reversed across much of the globe. That is, where the PDSI was most skilful (Figure 3.5a), now the SPI12 shows the greater skill (Figure 3.5d) and

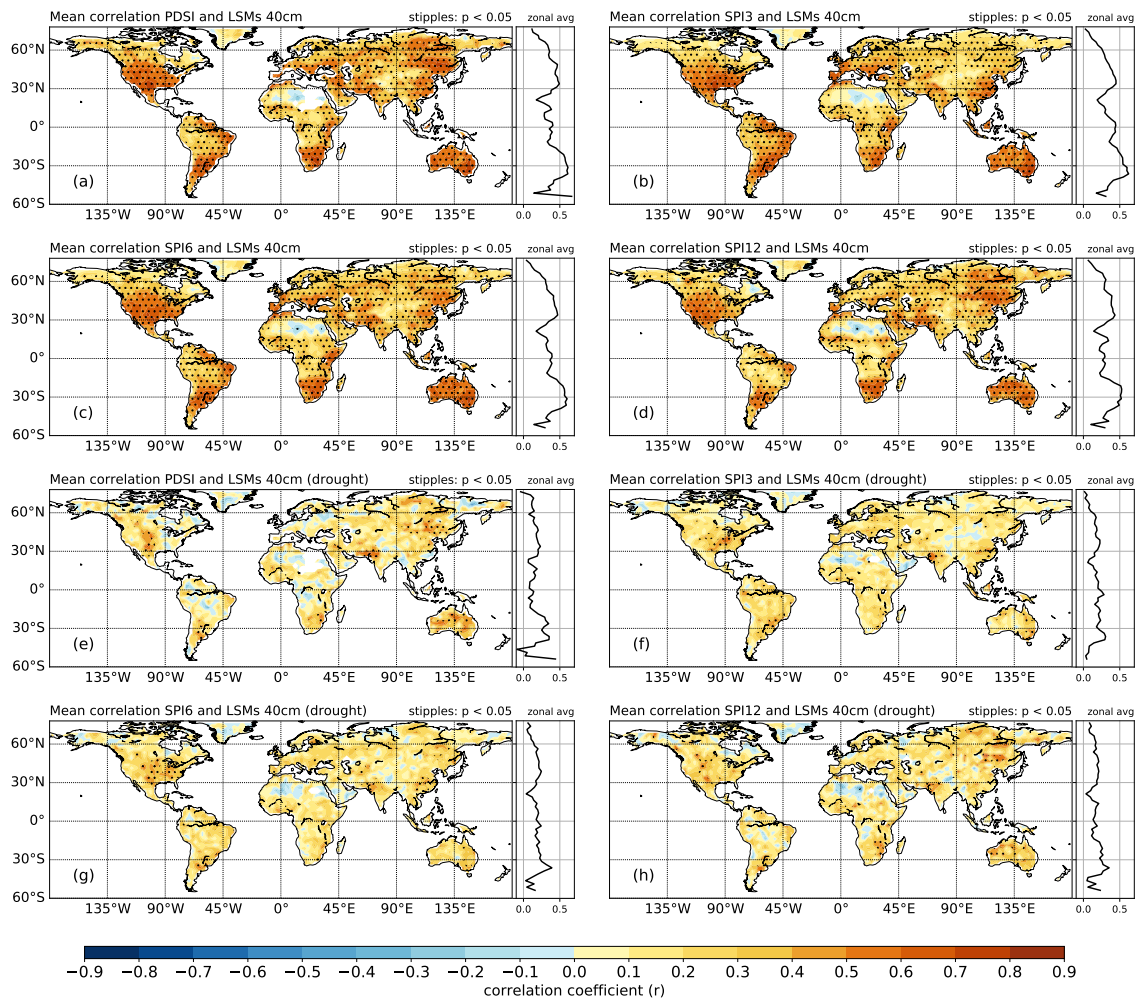


**Figure 3.4:** Mean and zonal correlations of varying LSMs for PDSI (a/e), SPI3 (b/f), SPI6 (c/g) and SPI12 (d/h) for whole data distribution (a-d) and drought periods (e-h) of the 10-40cm layer. The zonal average is shown to the right of each plot. Stippling shows statistically significant correlations at the 95% level.

vice versa.

For drought periods, the land area, where the PDSI shows superior skill decreases to  $\approx 46\%$  but it shows a markedly stronger skill compared to the SPI3 and SPI6 with the exceptions of eastern USA, western Europe and parts of South America and far east Asia. For longer droughts (SPI9 and SPI12), the differences between the PDSI and SPI become small and stippling decreases.

We have shown that the sensitivity of skill for both PDSI and SPI heavily depends on time scale and region for both soil layer depths. In terms of the shallow 0-10cm soil layer, the SPI3 has consistently more skill than the PDSI for combined wet and dry periods. However, neither of each drought indices has substantially more skill than the other when considering drought periods only. Robustness in comparison to the LSMs

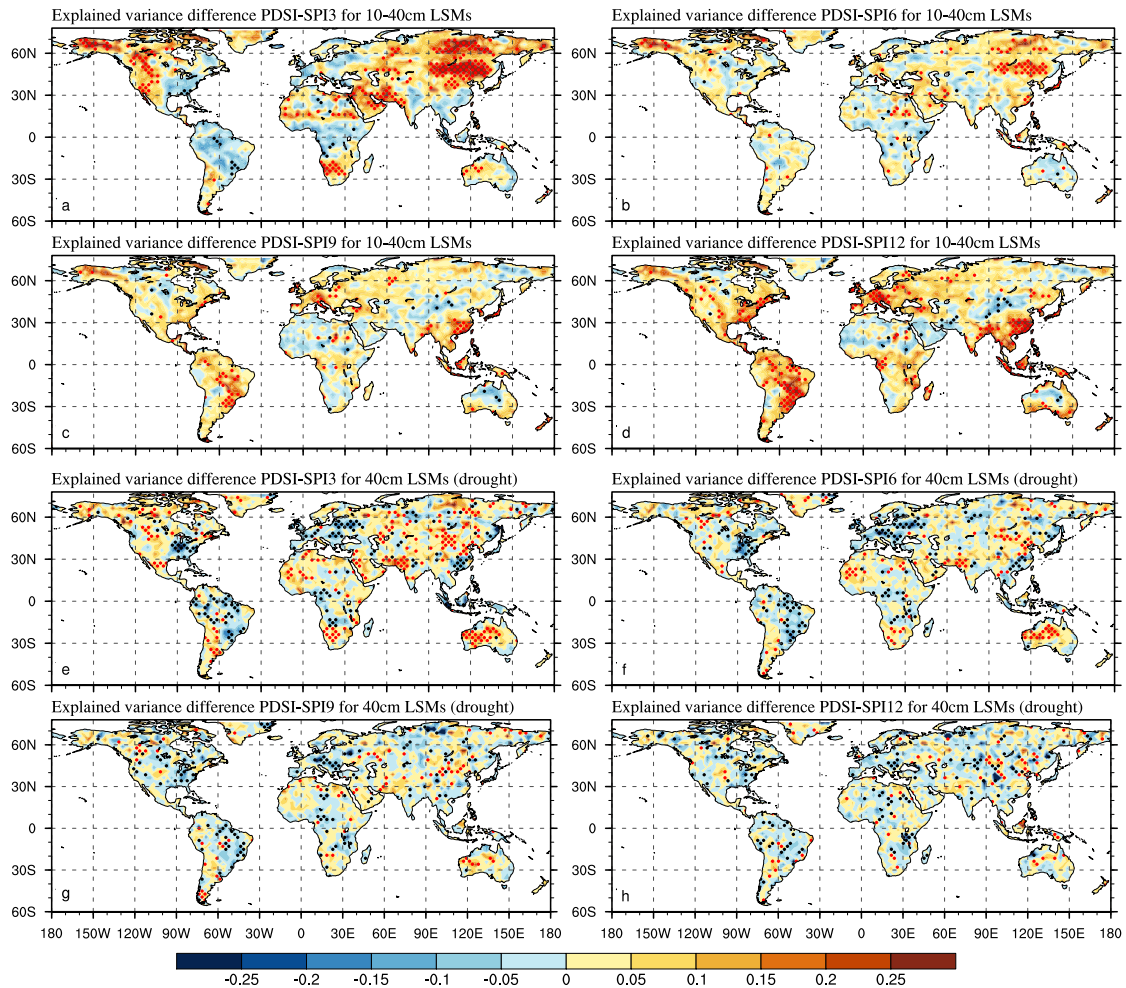


**Figure 3.5:** Explained variance differences of PDSI minus SPI3 (a/e), SPI6 (b/f), SPI9 (c/g) and SPI12 (d/h) calculated with fixed input data from GPCC and NCEP with GLDAS CLMv1, NOAHv1 and NOAHv2 10-40cm for whole distribution (a-d) and drought periods (e-h) defined as  $PDSI < -2.0$  and  $SPI < -0.8$  (1979-2013). Black stippling show where all correlations of the SPI-n with GLDAS are higher than those of the PDSI with GLDAS, red stippling where all correlations of the PDSI with GLDAS are higher than those of the SPI-n with GLDAS LSMs.

is mainly present for drought periods, with regional differences. The skill of the PDSI increases in comparison to the SPI3 for both drought conditions and the entire wet and dry distribution for the deeper 10-40cm layer. In contrast, the SPI increases in skill for six month and longer time scales but with the robustness to the choice of LSM decreasing for both indices.

The differences in timing of drought, expressed as an overlap of drought periods for PDSI and SPI on different time scales (3-, 6-, 9-, 12-month, Figure 3.6), are now examined. Here, drought is defined by the lowest 10th percentile for each of the PDSI and SPI-n in order to have the same sample size for each index. The ratio of overlap

explains how many time steps identified as drought by the SPI were also found in the time series of the PDSI.

The SPI3 shows the least consistency in the detection of drought months compared to the PDSI (Figure 3.6a). This is consistent with previous findings that the PDSI is most representative of drought on near-annual timescales (McKee et al., 1993; Burke and Brown, 2008). Fewer than approximately 60% of the droughts detected by the SPI3 are identified as drought by the PDSI. However, as  $n$  increases for the SPI- $n$  there is a retention of the low frequency signal, which better reflect the slower response of soil moisture discharge and recharge (Burke and Brown, 2008). Figure 3.6c and d show the concurrent occurrence of drought values for the SPI9 and SPI12 exceeding 60% for much of the globe.

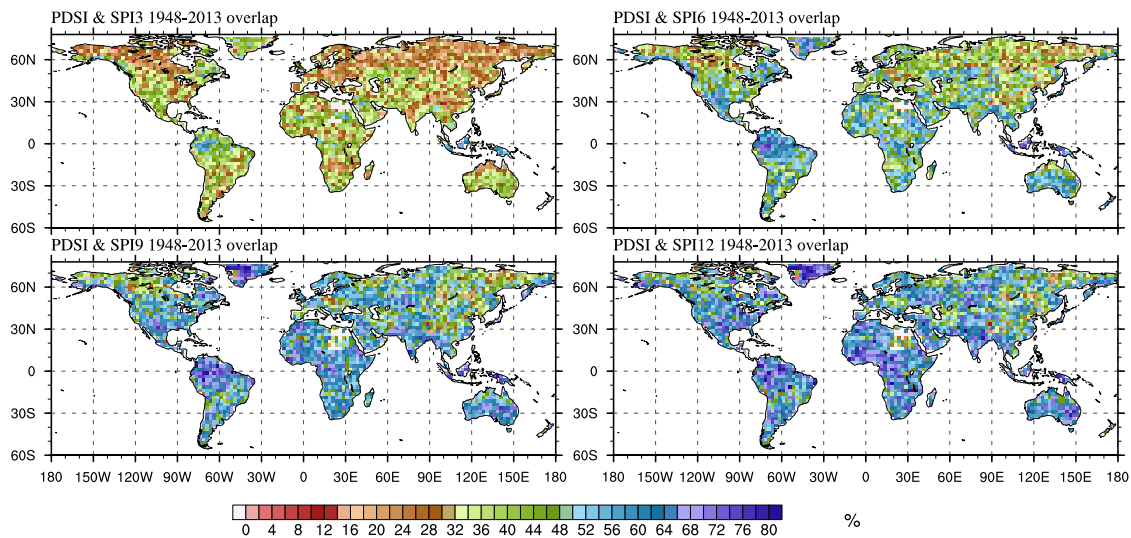


**Figure 3.6:** Overlap of drought periods between PDSI and SPI- $n$  from 1948 to 2013 showing the number of months for which the PDSI and SPI both indicate drought expressed as a percentage. GPCP precipitation data used for SPI and remaining variables for the PDSI are procured from NCEP Reanalysis II.

### 3.5.2 Sensitivity of the Skill of Drought Indices to Index Input Datasets

We now test the sensitivity of the skill of the drought indices to the choice of input data that is used to compute the index. The PDSI, SPEI and SPI are computed using multiple permutations of input data from Table 2.1. The PDSI has been standardised for ease of comparison with other indices. For all indices and regions the intra-index root mean

squared error (RMSE) was computed using all permutations with differing input data. Figure 3.7 provides a global overview of the standardised range between each indices' permutations with higher values indicating greater sensitivity to input data.

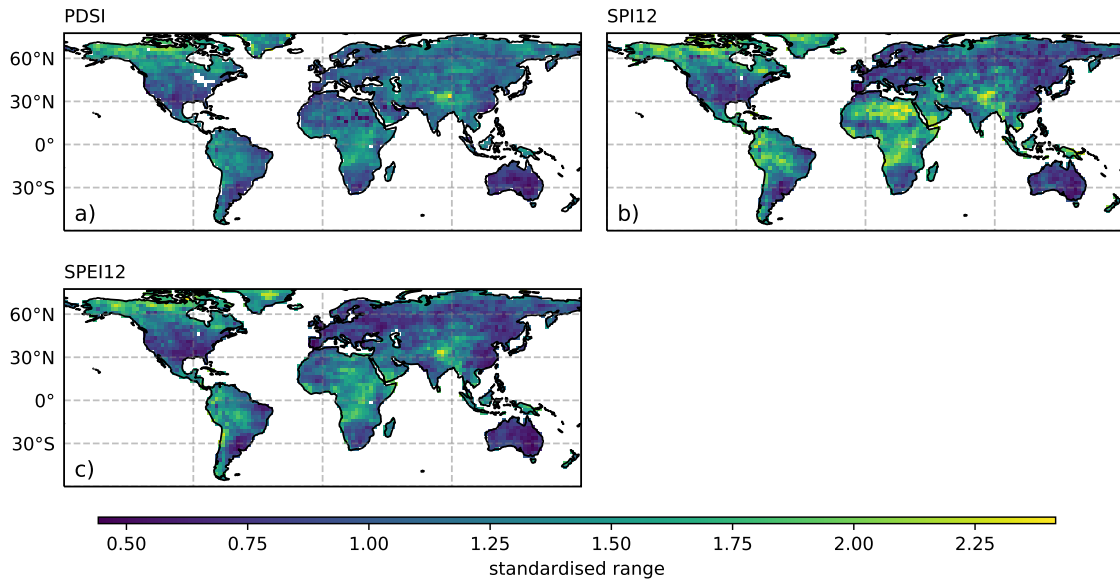


**Figure 3.7:** Standardised range of PDSI (a), SPI12 (b) and SPEI12 (c) permutations. First, the range of all permutations at each time step was calculated and afterwards averaged over time.

### 3.5.2.1 Regional Differences in the Sensitivities of the SPI, SPEI and PDSI to Input Datasets

Based on the findings from the overlap of drought periods, Figure 3.8 shows the sensitivity of SPI12, SPEI12 and PDSI to precipitation input data using examples from drought prone regions around the world, which highlight regional variability. These regions have been guided by those defined by [Giorgi and Francisco \(2000\)](#). All results are smoothed with a 12-month running mean so that the differences can be more readily identified.

The regions selected can be classified by dense or sparse coverage of ground based observations (e.g. [Contractor et al., 2019](#)). Those regions with dense data coverage for those variables used to compute the SPI and PDSI show little sensitivity to the choice of data set, for example, the Mediterranean (MED), Western North America (WNA) and Southern Australia (SAU). Those regions with sparse coverage of ground based observations such as East Africa (EAF), the Amazon (AMZ) and East Asia (EAS) show a stronger dependence on the choice of data set. Some sensitivities are present

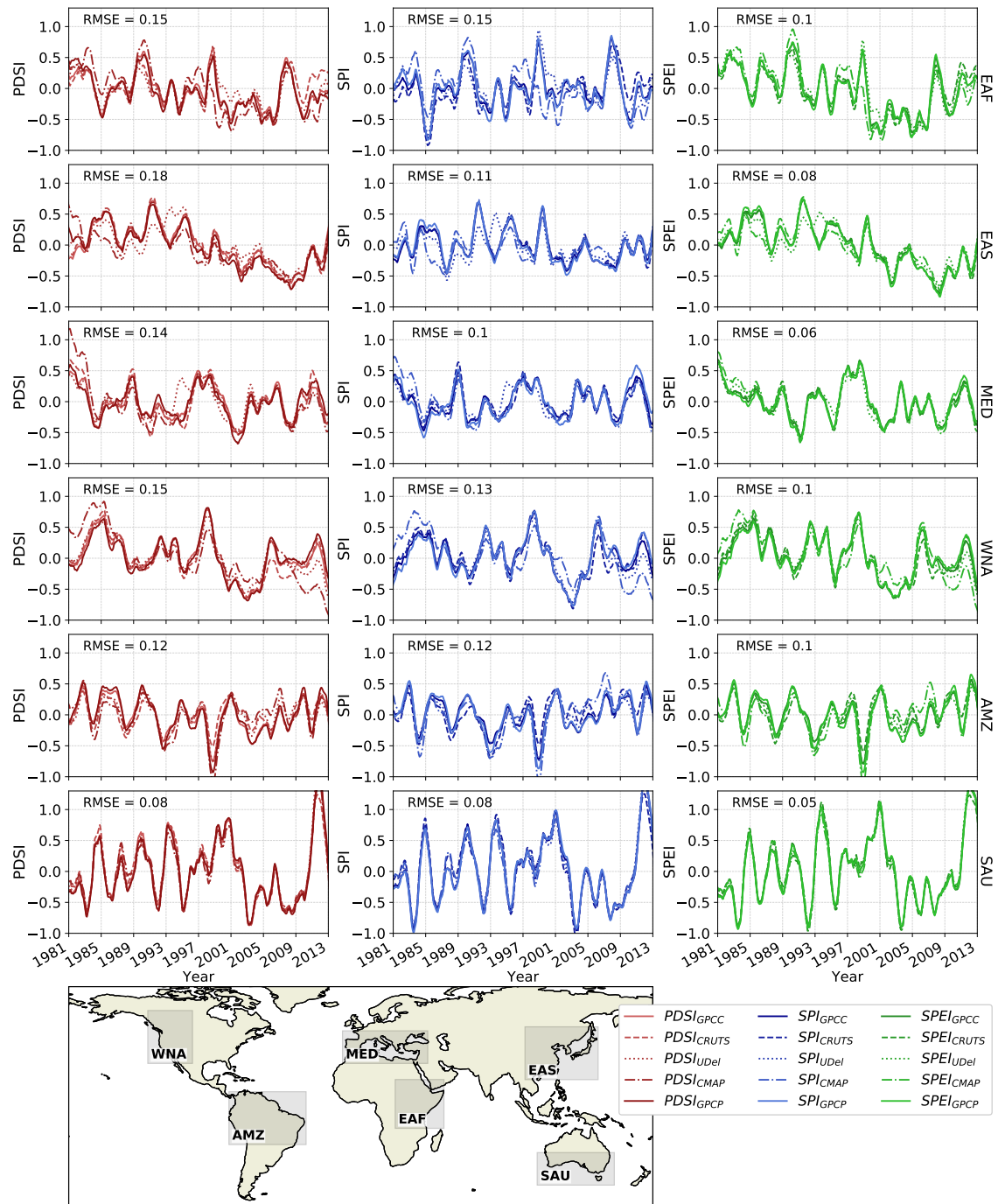


**Figure 3.8:** PDSI (left), SPEI (middle) and SPI (right) calculated with different precipitation data inputs as listed in Table 2.1 averaged over six different regions defined by Giorgi and Francisco (2000) from 1979 to 2013 (WNA = West North America, AMZ = Amazon, MED = Mediterranean, EAF = East Africa, EAS = East Asia, SAU = South Australia). SAU is modified to include the southern half of Australia only. Data are smoothed with a 12-month running-mean for all indices. PDSI and PET are standardised. The root mean squared error for each region and index is shown in the top left of each time series. The PDSI<sub>GPCP</sub> and SPI<sub>GPCP</sub> shown as a solid line represent the ones used for the analyses in Section 3.5.1. PDSI, SPEI and SPI are unitless.

throughout the entire time period whereas other vary only periodically, suggesting that an increase in data coverage over time might act to dampen sensitivity over time.

The largest deviations between the precipitation datasets used to compute the SPI are associated with the CMAP and UDel data set. Both the SPEI and PDSI have more potential sources of uncertainty as they are computed from multiple variables, hence, they show a larger standardised range globally (Figure 3.7).

Those regions where the PDSI is most sensitive to precipitation data are the same as those that are most sensitive for the SPI. However, despite having the same number of input variables as the PDSI, the SPEI has the lowest RMSE of all three indices and the PDSI the highest, with the SPI between the two. When testing the sensitivity of the indices to precipitation, one might expect weaker variability in those indices that are constrained by both evapotranspiration and precipitation. This result suggests that the differences between the SPEI and PDSI are the result of the construction of the water balance model and/or the order of operations of the index.

Although precipitation is a significant source of sensitivity for all indices, the choice of temperature data set also contributes to the sensitivity of SPEI and PDSI (Figure 3.9). However, the PDSI is less sensitive to varying temperature data sets and the RMSE is lower than for precipitation for all regions. For the SPEI in MED, WNA and SAU, the temperature input induces a higher sensitivity in the drought index than precipitation, resulting in a higher RMSE. The greater sensitivity of the SPEI to temperature and the fact that the RMSE of the PDSI is typically smaller than for the SPEI indicates that more weight is given to evapotranspiration in the SPEI drought index compared to the PDSI. Wind speed, specific humidity and downward solar radiation were combined and used from reanalysis data only (NCEP and ERA, not shown) and show only little difference between the two data sets.

### 3.5.2.2 The sensitivity of drought index skill for shallow soil profile (0-10cm)

The skill that each drought index has in capturing variability in soil moisture reanalyses is now tested by correlating the drought indices with a fixed soil moisture product at two levels, using the NOAHv2 from the GLDAS described in Section 3.3.

Figure 3.10 shows the mean correlations between the GLDAS NOAHv2 soil moisture product and the SPI-n or PDSI permutations, globally for the 0–10cm soil layer split

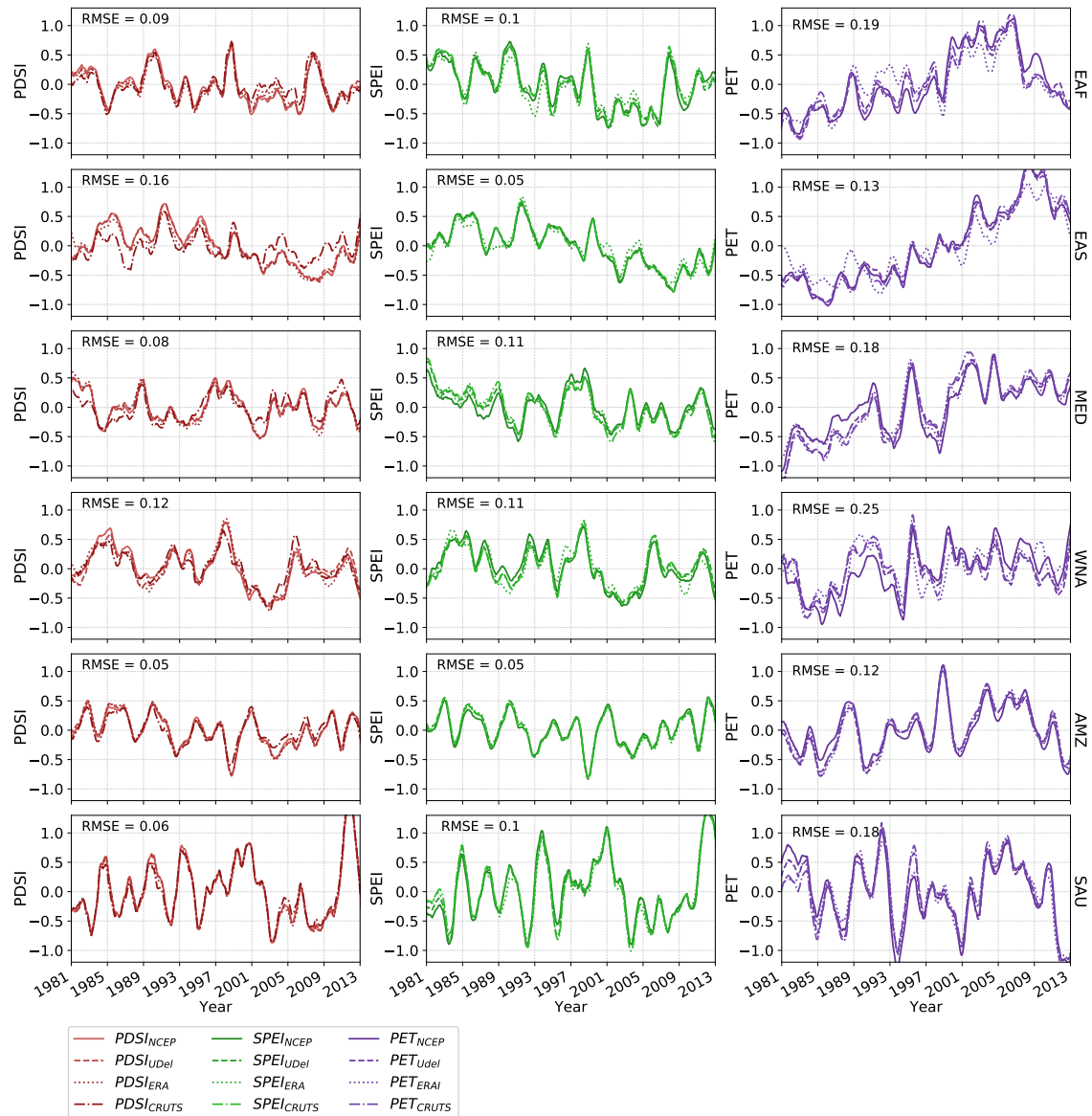


**Figure 3.9:** PDSI (left), SPEI (middle) and PET (right) calculated with different temperature data inputs as listed in Table 2.1 averaged over six different regions defined by Giorgi and Francisco (2000) from 1979 to 2013 (WNA = West North America, AMZ = Amazon, MED = Mediterranean, EAF = East Africa, EAS = East Asia, SAU = South Australia). SAU is modified to include the southern half of Australia only. Data are smoothed with a 12-month running-mean for all indices. PDSI and PET are standardised. The root mean squared error for each region and index is shown in the top left of each time series. The PDSI<sub>NCEP</sub> and SPEI<sub>NCEP</sub> shown as a solid line represent the ones used for the analyses in Section 3.5.1. PDSI and SPEI are unitless.

into the entire sample of PDSI<sub>NCEP</sub> and SPI with soil moisture data in maps a) – d) and drought periods only in e) – h). Absolute  $r$  values between the soil moisture estimate and drought index reach their maximum around  $r \approx 0.7$  in the subtropical latitudes for the entire sample (Figure 3.10a-d). During drought conditions,  $r$  values are overall weaker by 0.2 – 0.3 with no significant correlation (Figure 3.10e-h) except for parts of the US

and eastern Australia. The analyses for the SPEI shows again very similar correlations to the SPI (Figure 7.3).

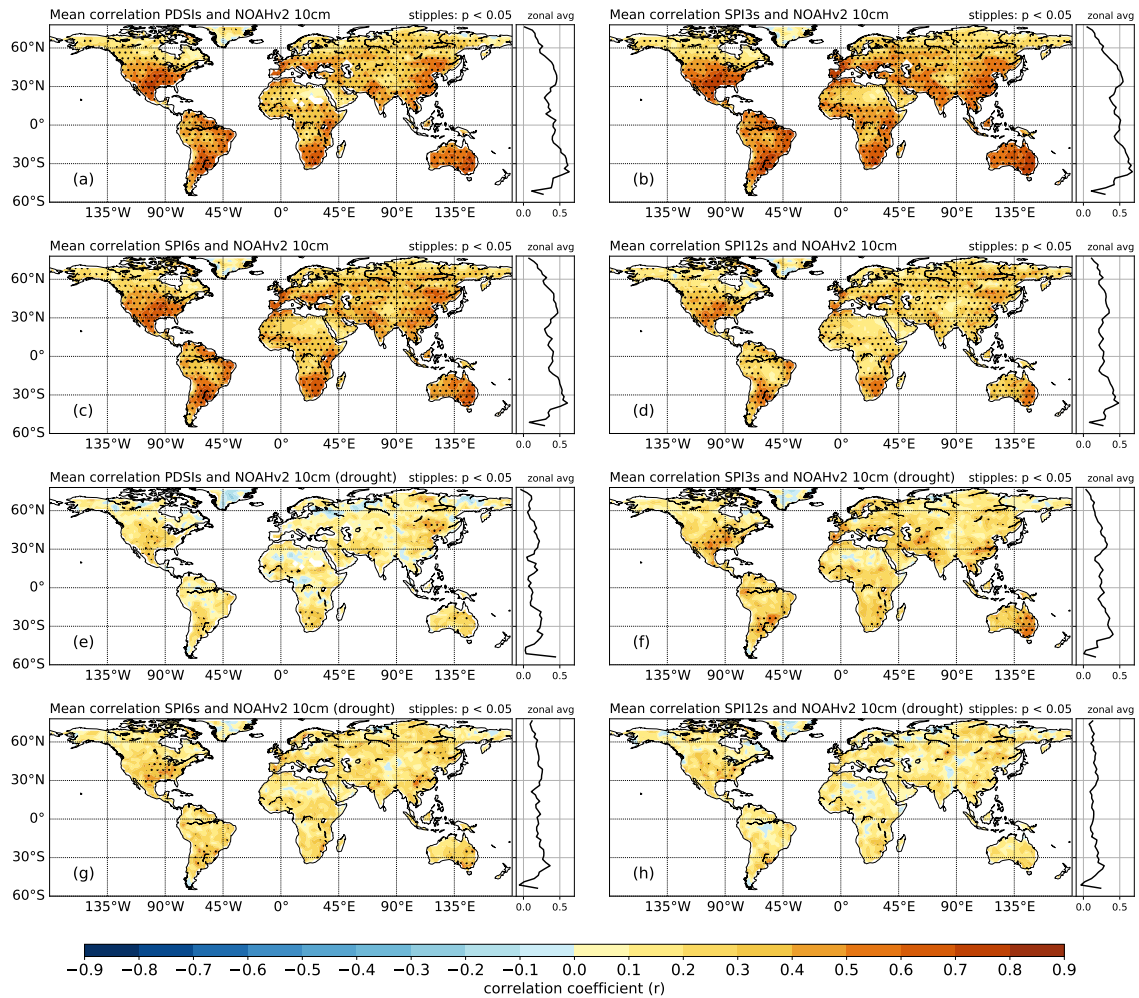


**Figure 3.10:** Mean and zonal correlations of varying input data for PDSI (a/e), SPI3 (b/f), SPI6 (c/g) and SPI12 (d/h) for whole data distribution (a-d) and drought periods (e-h) of the 0-10cm layer. The zonal average is shown to the right of each plot. Stippling shows statistically significant correlations at the 95% level.

Figure 3.11 displays the difference in the variance explained in the GLDAS NOAAv2 soil moisture product by the permutations of PDSI and the SPI-n for the 0–10cm layer of soil. The SPI3 shows the strongest skill for the largest proportion of global land area (70%) and is robust to the choice of input data in various regions across the globe (black stippling). As in Section 3.5.1, the skill decreases as n for SPI-n increases when the whole data distribution is considered (Figure 3.11a-d). This results in gains of robustness for the PDSI in regards to all input data permutations (red stippling).

As before in Section 3.5.1, the correlations of both SPI-n and PDSI with soil moisture weaken globally when drought periods only are considered. The correlations during

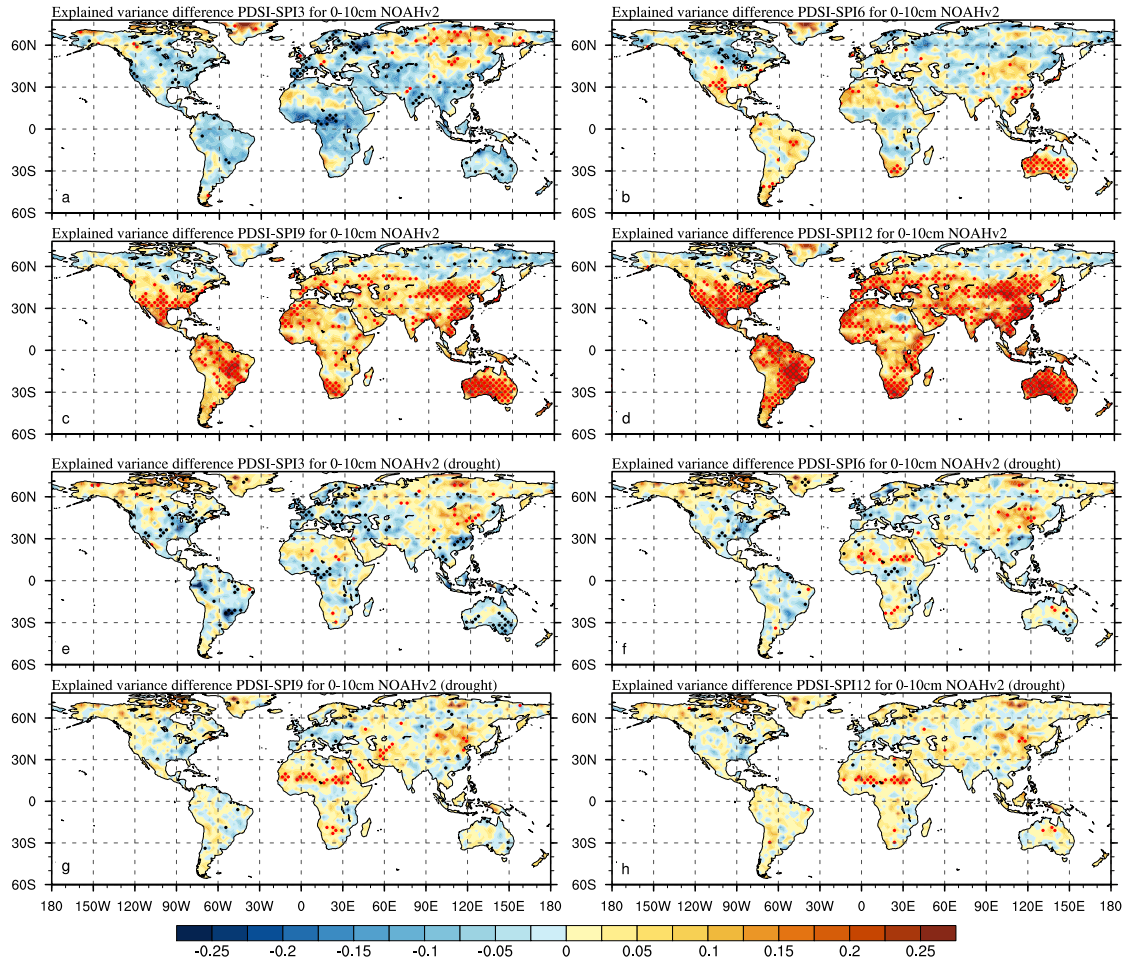


**Figure 3.11:** Explained variance differences of PDSI minus SPI3 (a/e), SPI6 (b/f), SPI9 (c/g) and SPI12 (d/h) with varying input data permutations with NOAHv2 0-10cm for whole distribution (a-d) and drought periods (e-h) defined as PDSI < -2.0 and SPI < -0.8 (1979-2013). Black stippling show where all correlations of the SPI-n with NOAHv2 are higher than those of the PDSI with NOAHv2, red stippling where all correlations of the PDSI with NOAHv2 are higher than those of the SPI-n with NOAHv2.

drought periods remain highest for the SPI3 (67%) compared to longer SPIs and the PDSI (Figure 3.11e-h). Red stippling indicating that the PDSI has consistently a stronger skill independent of input data compared to the SPIs is rare and mainly limited to East Asia and Sahel Africa. This implies that the sensitivities of the SPI and PDSI to input data are larger when compared to the differences in skill between the indices.

### 3.5.2.3 The sensitivity of drought index skill for deeper soil profile (10-40cm)

For the deeper 10-40cm soil layer drought index with the best skill is not as easily determinable. The absolute correlations between soil moisture and drought indices increase for the longer SPI time scales compared to the shallow soil layer (0-10cm) with the

strongest correlations ( $r \approx 0.7$ ) in the subtropics for all indices (Figure 3.12a-d). As before, correlations weaken to mainly insignificant values for drought conditions (Figure 3.12e-h). Again, very similar correlations to are observed for the SPEI compared to the SPI (Figure 7.4).

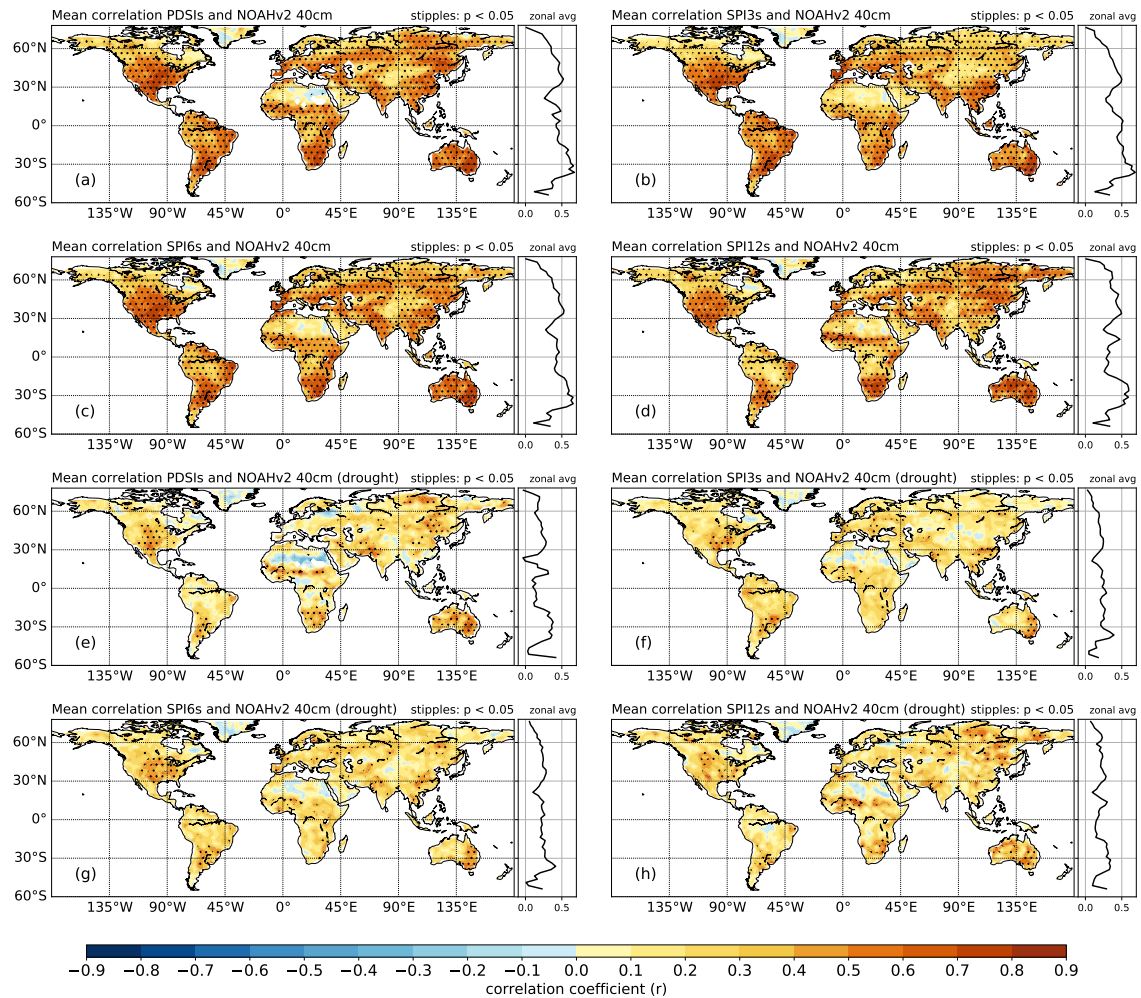


**Figure 3.12:** Mean and zonal correlation coefficients ( $r$ ) of varying input data for PDSI (a/e), SPI3 (b/e), SPI6 (c/f) and SPI12 (d/g) with GLDAS NOAHv2 for whole data distribution (a-d) and drought periods (e-g) of the 10-40cm layer. The zonal average is shown to the right of each plot. Stippling shows statistically significant correlations at the 95% level.

The differences in explained variance between the PDSI and SPI-n change when looking at the 10-40cm soil layer (Figure 3.13a-d). They become partially smaller and/or change sign over North Africa, Eastern Asia and Australia for SPI9 and SPI 12 versus PDSI. An increase is observed over similar parts for SPI3 versus PDSI. Increased differences show that both are more sensitive to the input data for the indices compared to the choice of soil moisture product. Whether the SPI or PDSI is more skilful in capturing soil moisture fluctuations is heavily regionally dependent and can differ significantly

by  $\approx 20\text{-}25\%$  explained variance between both indices, especially when comparing PDSI with SPI3 and SPI12.

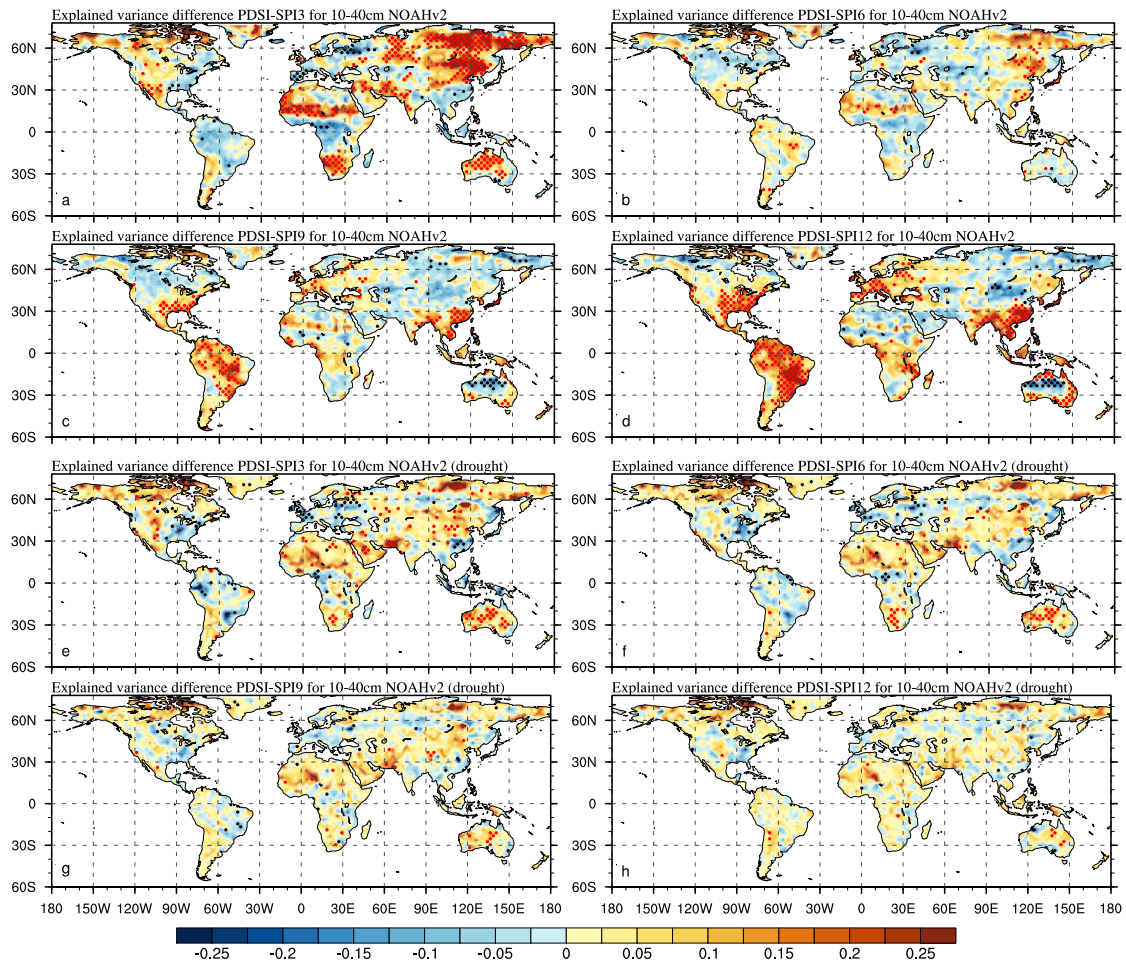


**Figure 3.13:** Explained variance differences of PDSI minus SPI3 (a/e), SPI6 (b/f), SPI9 (c/g) and SPI12 (d/h) with varying input data permutations with NOAHv2 10-40cm for whole distribution (a-d) and drought periods (e-h) defined as  $PDSI < -2.0$  and  $SPI < -0.8$  (1979-2013). Black stippling show where all correlations of the SPI-n with NOAHv2 are higher than those of the PDSI with NOAHv2, red stippling where all correlations of the PDSI with NOAHv2 are higher than those of the SPI-n with NOAHv2.

This continues for differences between PDSI and SPI during drought conditions (Figure 3.13e-h). The spatial pattern as well as the amplitude in differences of explained variance differ marginally from the 10-40cm drought condition results for varying LSMs. However, the noticeable lack of stippling shows the absence of robust skill of each index and consequently a higher sensitivity to their input data.

### 3.5.3 Sensitivity to Input Data versus Choice of Drought Index

The skill of each index in representing soil moisture fluctuations is now assessed using a metric that is defined by the absolute  $r_{max}$  of any permutation for each of SPI and PDSI, presented in Sections 3.5.1 and 3.5.2 and, additionally, SPEI. Time scales of 3-, 6- and 12-month were selected for both SPI and SPEI since the 9-month time scale showed mostly the weakest skill and is generally an uncommon time scale to use.

The metric was computed for the 0–10cm (Figure 3.14) and 10–40cm soil layers (Figure 3.15) using the whole sample (a and c) and drought conditions (b and d). Results are combined in each of the figures showing the sensitivity to LSMs in panels a) and b) and the sensitivity to input data in c) and d) respectively. The stippling in each plot shows where the index associated with  $r_{max}$  is the same as the index that produces the highest mean  $r$  based on all permutations of input data and LSMs. This is regardless of the variance for that index as big deviations between permutations can still have a higher mean  $r$  than another index with smaller variance. Nevertheless, we will call this instance a lower uncertainty for easier differentiation. For those instances where no stippling is present, the mean  $r$  from all permutations using either different input data or LSMs is lower than for other indices. Here, despite having the highest overall correlation for one permutation the variance within all permutations is so big that the  $r_{mean}$  is relatively low compared to another index. All percentages describe the land mass for which the index has the highest correlation compared to other indices.

Figure 3.14 focusses on the shallower 0-10cm soil layer. Here, the PDSI ranks first for the whole data distribution recording the highest skill for 28% of the land mass in regards to sensitivity to LSMs (Figure 3.14a) followed by SPI3 and SPEI3 with each 23%. However, this decreases to 16% when testing the sensitivity to input data (Figure 3.14c) showing a higher skill for SPI3 (29%) and SPEI3 (23%). Seventy-one percent of the area for LSM sensitivity (Figure 3.14a) is overlaid with stippling implying smaller uncertainties due to the choice of index compared to the choice of LSM.

Due to poorer data quality and/or coverage in some regions (e.g. North Africa, equatorial South America and northern Asia) the uncertainty associated with varying the input data leads to robust results for sixty-six percent of the land area as shown by the lack of stippling (Figure 3.14c). Regardless of the sensitivity to LSMs or input data, the SPI3 and SPEI3 generally have the highest skill from the tropics to the mid-latitudes

with the exception of NW North America, South Africa and parts of Asia where the PDSI is best correlated. Throughout, the longer 6- and 12-month time scales of SPI and SPEI covers the least area (3-10%) with some stippling, mainly limited to high northern latitudes where correlations are weak in general.

Limiting the sample to drought conditions defined by values below or equal to -2.0 and -0.8 for PDSI and SPI/SPEI respectively, changes the pattern of the best correlated index to an inhomogeneous mixture of all indices (Figure 3.14c and d). There are very few uniform areas where a single index or time scale clearly has the strongest skill. Exceptions are South East Australia with the SPI3 and East Asia with the PDSI having the highest skill for both  $r_{mean}$  and  $r_{max}$ . Fluctuations in soil moisture during drought conditions are best represented by different SPI and SPEI time scales rather than by the PDSI, which only covers around 17% of the land area for both instances.

The SPI is the only index that covers a greater area with the highest skill for drought identification than for the whole data distribution compared to PDSI and SPEI. Here, the simplicity of the SPI overcomes the ET estimation in the modelled upper layer soil moisture for identifying drought by adjusting its temporal resolution. For drought conditions, uncertainties from varying input data are larger for 48% of the land area (Figure 3.14d) compared to the choice of index, while the uncertainty decreases to 25%

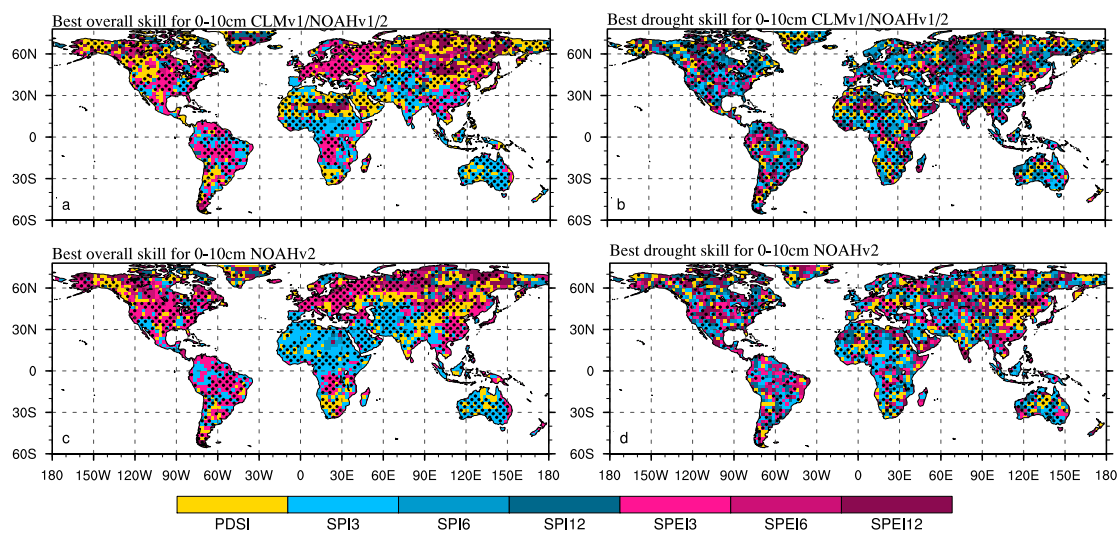


**Figure 3.14:** Best correlated indicator for whole distribution with varying LSM (a) and varying input data (c) and drought periods with varying LSM (b) and varying input data (d) of the 0-10cm layer. Stippling indicates where the underlying index is robust against the others, meaning that its max correlation coefficient as well as its mean correlation coefficient is higher than those of the other indices.

of the land area for LSM sensitivity (Figure 3.14b).

Figure 3.15 shows the most highly correlated index for the deeper 10-40cm soil layer. The results for the whole data distribution (Figure 3.15a and c) are similar to the upper soil layers, previously described. Both SPI and SPEI show more land area where these indices have the strongest correlations (SPI 33%, SPEI 41% for LSMs; SPI 35%, SPEI 44% for input data), compared to the PDSI (26% for LSMs; 21% for input data). Those areas where the PDSI and SPEI showed the strongest skill in the 0-10 cm layer remain mostly unchanged for the 10-40 cm layer. This indicates that ET is an important contributing factor for soil moisture variability in both layers in these regions. Stippling remains unchanged for varying LSMs (Figure 3.15a) and input data (Figure 3.15c) compared to the shallower layer (Figure 3.14a).

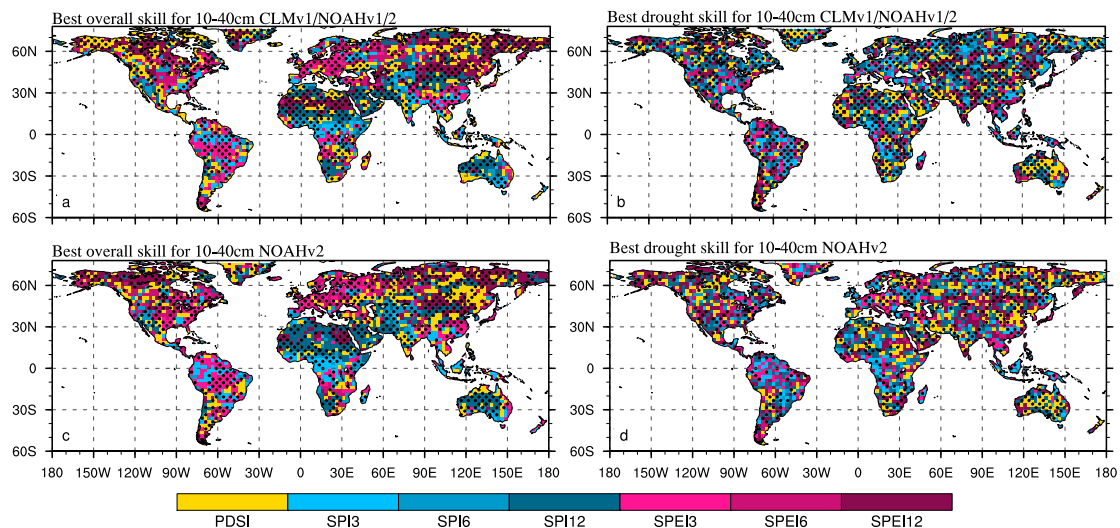


**Figure 3.15:** Best correlated indicator for whole distribution with varying LSM (a) and varying input data (c) and drought periods with varying LSM (b) and varying input data (d) of the 10-40cm layer. Stippling indicates where the strength of the correlation of the index is robust to varying the input data and LSM.

The PDSI is noticeably more skilful in the 10-40 cm layer when compared to the 0–10 cm layer for drought conditions, increasing to 21% of land area coverage for LSMs (Figure 3.15b) and input data (Figure 3.15d). However, the SPI12 is similarly the most skilful index, with 23% of global land area showing the strongest skill in this index with varying LSMs (Figure 3.15b). For the variability in input data (Figure 3.15d), the SPEI12 is ranked first covering 23% of the land mass.

As for the shallow soil layer, the SPI is the only index that shows an increase in grid points where it is the most skilful compared to other indices during drought conditions.

However, it is on par with the SPEI (both 40%) showing that both ET and precipitation are important for drought development in the deeper soil layer. With stronger skill particularly for the 12-month time scale, the SPI is likely integrating land surface feedbacks over time. Stippling for the robustness of the best correlated index remains effectively unchanged with 77% (Figure 3.15b) and 52% (Figure 3.15d) of global land coverage for the two LSMs. Assuming that the NOAHv2 LSM represents soil moisture reasonably, our results show that greater uncertainties stem from the input data rather than from the LSMs to which the indices are compared.

Using a 6- or especially 9-month time scale neither covers seasonal nor annual changes, regardless of drought or non-drought conditions and cover consequently the least area. The inclusion of ET seems to be more important for assessing indices using the entire data distribution, and precipitation becomes increasingly important for when assessing periods of drought.

## 3.6 Discussion

The ultimate goal of this study is (i) to assess the sensitivity of meteorological drought indices to input data and (ii) to examine how well each index represents soil moisture variability in respect to the LSMs capabilities, especially in drought periods, given this uncertainty.

As described in Section 3 the PDSI and SPEI uses a number of meteorological variables to calculate the rate of evapotranspiration and water balance while the SPI uses only precipitation. We showed that the PDSI is most sensitive to variations in temperature and precipitation, which is consistent with [Guttman \(1991\)](#) in [Mishra and Singh \(2010\)](#) who showed seasonal dependence on sensitivity of the PDSI to temperature and precipitation. Differences in the sensitivity between PDSI and SPEI are explained by the construction of the index and its order of operations.

Uncertainties are present in all observational, satellite and reanalysis data sets. The sensitivity of the drought indices to these observational uncertainties is sometimes different between non-drought and drought conditions. This sensitivity yields a larger range of possible correlations between soil moisture estimates and drought indices in regions with poorer observational data coverage, such as Africa and Asia. Although the uncertainties

due to input data are smaller in data rich areas like Europe, North America and Australia, uncertainties are still non-zero and must be considered when employing drought indices.

Past studies have highlighted strong similarities in drought index variations for indices that both include and exclude evapotranspiration ([Vicente-Serrano et al., 2012](#); [Raible et al., 2017](#)). However, we have shown that an additional consideration is whether these differences are significant given the uncertainties in data sources used to generate those indices. The fact that the ET calculations have significantly more variables that are associated with their calculation as compared to temperature, suggests that the uncertainty associated with all variables is likely to be higher than for the SPI, which uses precipitation only. However, this could not be tested here due to a lack of data sets for radiation, wind speed etc.

The PDSI and SPEI include ET, but vary in the complexity of their calculations. Some inferences can be made from the correlations of PDSI and SPI using fixed input data with the GLDAS LSMs. Both indices showed weaker correlations to soil moisture during drought periods, and both showed the highest skill in the subtropics. Correlations for the SPEI yield a very similar picture. This climate zone is usually characterised by a high variability in seasonal rainfall to which all drought indices seem to be very sensitive. High rates of ET due to the high amount of incoming solar radiation and warm temperature create a stronger connection between the upper soil layers and the overlying atmosphere ([Entekhabi et al., 1996](#)). Lack of rainfall leads to a drying of the soil and is eventually accelerated by the evaporative demand of the air mass above and the level of dryness of the soil layer below, making this environment seemingly more advantageous for the PDSI and SPEI. When precipitation occurs, the top centimetres are saturated first and composed with the more rapid drying just mentioned these hydrological fluxes happen on a relatively short time scale of weeks to a few months. Our results show that this high frequency in comparison to deeper soil layers is best represented by the SPI3 and SPEI3. The SPEI generally shows better skill in regions with a more variable ET, where changes between water- and energy-limited conditions occur, such as Europe, SE Asia and parts of North and South America. The SPI in contrast has a higher skill in dry regions where water-limited conditions dominate, such as Australia, SW United States, South Africa and across the Middle Eastern regions to the Indian sub-continent. The water-limited conditions during drought are therefore often better represented by the

SPI in all regions across the globe as shown in the results. However, all indices have little or no inclusion of land surface features such as soil permeability and vegetation, which are important for agricultural and hydrological drought development. The PDSI considers soil properties in a simplistic way by its hydrological accounting system based on a two-layer bucket-type model and relative to field water holding capacity (Palmer, 1965; Webb and Rosenzweig, 1993).

Soil moisture variability in the underlying, deeper 10-40cm layer is dampened as it is less coupled to the atmosphere (Entekhabi et al., 1996). Here, the PDSI would be expected to improve in skill because it applies an approximation of soil moisture balance and soil properties. However, the SPEI and, unexpectedly the SPI on 3-, 6- and 12-month time scales often showed similar or higher skill compared to the PDSI. The adaptation of the SPEI and SPI to diverse environments using different time scales makes them flexible indices. During drought conditions the SPI, predominantly on longer time scales, has the highest skill of any drought index. However, the SPI, as SPEI and PDSI, often lacks robustness to the data uncertainty. Yet, these results suggest that the complexity and/or lack of the multi-scalar characteristic of the PDSI has little advantage over the simplicity of the SPI using precipitation distribution as the only input. Regional studies on SPI correlation with GLDAS (Spennemann et al., 2015; Wang et al., 2015) and river discharge observations (Du et al., 2012) on a much smaller spatial scale support these findings. The inclusion of ET in the SPEI does not show a marked improvement over the SPI for drought conditions in the shallow soil moisture layer. However, the inclusion of ET seems to become increasingly important for deeper layer soil moisture. These considerations must be balanced with the additional uncertainties introduced by the input data associated with the inclusion of ET.

The uncertainties associated with choice of input data in drought indices are significant. However, those uncertainties associated with LSMs must also be considered. Non-linear and site-specific connections of soil-specific water retention characteristics that control soil moisture deficiency vary considerably between environments (Wang et al., 2015). Higher water retention “affects the number, depth and timing of periods of soil moisture shortage” (Halwatura et al., 2017). The rate of soil moisture variability is also tightly bound to the soil matrix and thus reacts differently to ET (Seneviratne et al., 2010). Replicating this in a LSM such as GLDAS can only be an estimate and has to

be considered when interpreting the results. Additionally, to those LSM specific caveats, the assimilated input data driving those models exhibit their own biases as shown in this study by uncertainties using three GLDAS LSMs. (Wang et al., 2016a) have identified serious discontinuity issues over China with temperature and precipitation forcing data when they evaluated GLDAS NOAH v1 and v2 with GRACE terrestrial water storage, which is a remotely sensed, satellite based product. Bias correction in the second version of GLDAS reduces the bias but has a larger mean absolute error than before and both versions face a decline in data quality after 1990. We highlight again that the indications drawn from our analysis are based on modelled soil moisture only. Even though LSMs are able to replicate real-world soil moisture variability to some extent, applying our methods to actual soil moisture observations will most likely lead to slightly different results.

### 3.7 Summary

In this study, we examined the sensitivity of the Palmer Drought Severity Index (PDSI), the Standardised Precipitation Evapotranspiration Index (SPEI) and the Standardised Precipitation Index (SPI) to input data and soil moisture estimates from the GLDAS CLMv1 and NOAHv1 and v2. The aims of the study were two-fold; i) to examine the sensitivity of each index to input data and the associated uncertainty for comparison with soil moisture estimates, and ii) given i), examine the differences between the indices for drought identification. We showed that the choice of input data changes the skill of the drought index such that the differences between the SPI, SPEI and PDSI for drought identification purposes become small in light of the uncertainties. In many cases, the precipitation-only index (SPI) showed greater skill relative to the uncertainty associated with input data when compared to the PDSI and SPEI. This was because of the larger number of inputs needed to compute the ET component of the PDSI, which increased the uncertainty associated with the choice of data set to use as inputs. However, both ET-based indices, PDSI and SPEI can improve their skill for deeper layer soil moisture.

The magnitude of the uncertainty from different input data sets is modulated by the coverage, quality and length of available observations which is typically poor in less developed regions. However, regions associated with good data coverage such as Europe

and North America are not immune to uncertainties. Whether this is regulated by the number of input variables required to compute the individual index remains unclear due to a lack of independent data sources for variables other than precipitation and temperature. The uncertainty in the choice of LSMs also played a significant role in uncertainties in the skill of the drought index. Global evaluation of drought indices remains challenging in the absence of high-quality, long-running, spatially well distributed “true” values of deep soil moisture for examining drought. Hence, we emphasize that our study should be seen as a framework for future evaluation of drought index and data selection.

---

## Chapter 4

# Flash Drought in CMIP5 Models

---

### 4.1 Preface

Drought is a natural hazard occurring near globally. The evolution of drought occurs over various time scales from sub-seasonal to multi-decadal. The variety of time scales has led to drought being subdivided into different types. A newly emerging term, 'Flash drought' describes the rapid onset of drought on a sub-seasonal to seasonal time scale (S2S). It is of particular interest for agriculture as it can rapidly deplete soil moisture for crop growth within several weeks. To better understand the driving processes of flash drought, we evaluate the importance of evaporative demand by comparing three different drought indices that estimate this hazard using meteorological and hydrological parameters from the CMIP5 suite of models. We apply the Standardised Precipitation Index (SPI), which is a popular drought index due to its simplicity; the Evaporative Demand Drought Index (EDDI), which provides an estimate of the rate of drying; and the Evaporative Stress Index (ESI), which connects atmospheric and soil moisture conditions by taking the ratio of actual and potential evapotranspiration (ET). Results show moderate to strong relationships ( $r^2 > 0.5$ ) between drought indices and soil moisture, especially in drought-prone regions. We found that all indices are able to identify flash drought sufficiently within the model's climatology. However, there is significant inter-model spread of the flash droughts identified.

## 4.2 Introduction

Drought describes the persistence of extreme negative moisture anomalies over a specific region and an extended period of time from sub-seasonal to multi-decadal time scales (Mishra and Singh, 2010). The impacts on such different time scales vary broadly and affect the hydrological cycle, landscape, society and economy. This makes it challenging to provide a uniform definition which applies to all circumstances. Consequently, drought has been categorised into five different types which develop over time as moisture deficiency intensifies. From the shortest (months) to longest (multiple years) time scales, the types of drought have been described as follows. Meteorological, a strong shortfall in precipitation in regards to the location's long term climatology; agricultural, drying soil moisture affecting plant health; hydrological, reduced groundwater, river and reservoir levels; economic, when water supply cannot meet water demand of industry and population (Wilhite and Glantz, 1985); and, ecological drought, an episodic deficit in water availability that drives ecosystems beyond thresholds of vulnerability (Crausbay et al., 2017). Without relief via widespread precipitation, drought severity increases further and transitions from one type to the next, although each type is not mutually exclusive (i.e. an area can experience more than one type of drought at once).

Recently, a sixth drought type has been proposed to the scientific community, named "flash drought" (FD) and is described as drought with a rapid onset and intensification (Otkin et al., 2018; Svoboda et al., 2002). This is classified as a sub-seasonal scale drought and poses a new challenge for sub-seasonal to seasonal (S2S, weeks to few months) prediction (Pendergrass et al., 2020). Flash drought has been described in detail in Chapter 2. Essentially, it is characterised by the rapid intensification of drought conditions in the root-zone soil layer (Otkin et al., 2018).

As with other drought types, difficulties arise in establishing a definition for FD identification. Soil moisture is the primary proxy for FD. Ford and Labosier (2017) proposed a definition whereby root-zone soil moisture has to decline from above the 40<sup>th</sup> to below the 20<sup>th</sup> percentile within 20 days. Studies from Mo and Lettenmaier distinguish between two types of FD: precipitation driven (Mo and Lettenmaier, 2016) and heatwave driven FD (Mo and Lettenmaier, 2015), where the latter is defined by a rapid increase of ET rather than a sudden reduction in precipitation. Even though Otkin

et al. (2018) argue that these percentile based thresholds for soil moisture (below 40<sup>th</sup> prctl over a 5-day FD) are not dry enough, this separation highlights the two important drivers for FD. Pendergrass et al. (2020) proposed two definitions for operational use, research and prediction. First, for the United States only, a two-category decrease in the United States Drought Monitor (USDM, <https://droughtmonitor.unl.edu/AboutUSDM/WhatIsTheUSDM.aspx>) over two weeks and sustained over two more weeks. The second definition is for global application and requires a 50 percentile increase in the Evaporative Demand Drought Index (EDDI, Hobbins et al., 2016) within two weeks and also sustained drought conditions for the following fortnight. Other studies do not specifically define thresholds but are rather based on standard anomalies or rates of change within a given period of the individual index used (McEvoy et al., 2016; Nguyen et al., 2019; Otkin et al., 2018).

Based on the above, drought indices that account for those processes responsible for drying conditions have been used to examine flash drought in several regional studies in the US (Otkin et al., 2013; Hunt et al., 2014; Ford et al., 2015; McEvoy et al., 2016; Otkin et al., 2016; Ford and Labosier, 2017), China (Wang et al., 2016a; Zhang et al., 2017) and Australia (Nguyen et al., 2019). Those used in this study are briefly summarised here, with more detail provided in section 2.2.2.

The simplest index and widely used in drought research is the Standardised Precipitation Index (SPI, McKee et al., 1993). The SPI compares precipitation to its climatological average. However, the SPI ignores the ET component which is described as being responsible for the rapid onset and intensification of a flash drought (Otkin et al., 2018; Pendergrass et al., 2020). In contrast, the Evaporative Demand Drought Index (EDDI, Hobbins et al., 2016) calculates the evaporative demand of the atmosphere ( $E_0$ ), an estimate of the crop reference evapotranspiration or potential evapotranspiration ( $ET_0$ ). It incorporates influences from temperature, radiation, wind speed and humidity and thus only accounts for the moisture demand. Another index, which seem to overcome the caveats of both EDDI and SPI and combines both moisture fluxes is the Evaporative Stress Index (ESI; Anderson et al., 2007). By incorporating  $ET_0$  it is connected to atmospheric drying conditions, yet also takes the surface moisture supply into account by using actual ET. The ESI is simply defined as the standardised anomaly of the ratio of actual ET to  $ET_0$ . McEvoy et al. (2016) showed that EDDI identifies drought over

the southern continental US and is consistent with identification from the SPI, ESI and a standardised soil moisture index (SSI).

However, whether the connection between low precipitation (e.g. SPI), actual ET (ESI) and  $ET_0$  (EDDI) is replicated globally is unknown. [Nguyen et al. \(2019\)](#) noted in their observational study over Australia that certain regions can be strongly affected by factors other than rainfall and temperature such as soil memory and water capacity as well as plant types, vapour pressure and wind speed. It is important to know the regions where this relationship is apparent. The outcome from a global ET and non-ET based index comparison will show the importance of ET for FD on a sub-seasonal time scale. No study has yet achieved this globally, nor has any study examined FD in coupled climate models globally. Especially in terms of FD frequency and seasonal distribution, with the known caveat that land-atmosphere interactions are not necessarily well represented in those models ([Lorenz et al., 2016](#); [Seneviratne et al., 2013](#); [Ukkola et al., 2018a,b](#); [Yuan and Quiring, 2017](#)). CMIP5 models can give us an idea of the relationships between precipitation, ET and soil moisture and how each of the models handles this. There is an urgent need to evaluate climate models to help constrain future projections of FD ([Pendergrass et al., 2020](#)).

This chapter examines the occurrence of FD in coupled climate models from the Coupled Modelled Inter-comparison Project phase five (CMIP5, [Taylor et al., 2012](#)) which are described in the next section. To do so, we first define FD based on percentiles in [4.4](#) and apply those percentiles to the upper layer soil moisture to produce a global climatology of FD event frequency, shown in [4.5](#). Drought index values at the onset of a FD detected in the soil moisture and their rates of change prior to that will provide information on how sensitive the chosen drought indices are to soil moisture variability. Additionally, we apply the same definition on the drought indices themselves. From this we calculate the detection skills for each index to infer their prediction capabilities. Looking at the inter-model spread provides insight as to how the individual CMIP5 models differentiate from another in terms of FD frequency, sensitivity and detection skills. The findings from these analyses are discussed in [4.6](#) and summarised in [4.7](#).

### 4.3 Data

The model outputs from six CMIP5 (Taylor et al., 2012) models listed in Table 2.4 in Section 2.1 were analysed as they provide all necessary data for this study on a daily time scale to calculate the drought indices on a global scale. Several variables are required to calculate, however, daily soil moisture output was the limiting factor for the selection of CMIP5 models listed. One major caveat of all CMIP5 models is that soil moisture on a daily time scale is only available for the 0-10cm layer and thus is not fully representing the root-zone soil layer. However, the highly dynamic changes in moisture availability during the development of a FD makes a daily time scale an inevitable necessity. All data is from the historical run providing a common time period of 139 complete years (1867-2005).

### 4.4 Methods

As introduced before, the SPI, EDDI and ESI are used for this study. Potential evapotranspiration (PET), which is an equivalent to evaporative demand ( $E_0$ ), for both EDDI and ESI is based on the crop reference evaporation formulation from Allen et al. (1998). PET requires input data of minimum and maximum temperature, radiation, wind speed and humidity. The actual evaporation needed for the ESI was derived from the latent heat flux directly output from the model. Evaporation expresses the amount of water lost from a surface in units of water depth (m) and can also be expressed in terms of energy received per unit area ( $Wm^{-2}$ ) (Allen et al., 1998). Hence, latent heat flux can be directly converted into water depth per time unit (here  $m s^{-1}$ ) using Equation 4.1:

$$E = \frac{LE}{\lambda\rho_w}, \quad (4.1)$$

where  $LE$  is the latent heat flux,  $\lambda$  the latent heat of vaporisation and  $\rho_w$  the density of water. Both  $\lambda$  and  $\rho_w$  are set as constants using  $2.45 \text{ MJ kg}^{-1}$  and  $1000 \text{ kg m}^{-3}$ . No data processing was needed for the SPI input as it only uses precipitation. We use all data in daily resolution to compute the indices.

As daily rainfall, evaporative demand and actual evaporation undergo naturally strong fluctuations on short time scales, their input data is aggregated (SPI and EDDI) or

averaged (ESI) over 30 days to achieve a 1-month time scale. Strong daily fluctuations are also present in the top 10cm soil moisture layer as exemplified by the brown line in figure 4.1 for SE Australia. This can be limiting for our analysis as this top level can be too responsive to the atmosphere and less indicative of changes in soil moisture in the root zone layer at a depth of  $\approx 1\text{m}$  (Entekhabi et al., 1996). Additionally, the bulk of root matter in a mature corn field is typically below 10cm (Fan et al., 2016). The agricultural impacts from a 0-10cm flash drought are therefore considerably smaller compared to one in 40cm or 1m depth. Depending on the soil type and quantity of precipitation as well as the partitioning into run-off and percolation, the lag between top and root-zone layer soil moisture can vary significantly and the signal is dampened (Ford and Quiring, 2014). Deep soil moisture variations are shown for MIRC05 monthly 1.5m soil moisture as a red line in figure 4.1. Consequently, soil moisture was also aggregated over the same time period of 30 days as EDDI and SPI to achieve a more similar variability to the root-zone layer soil moisture as displayed by the dark red line.

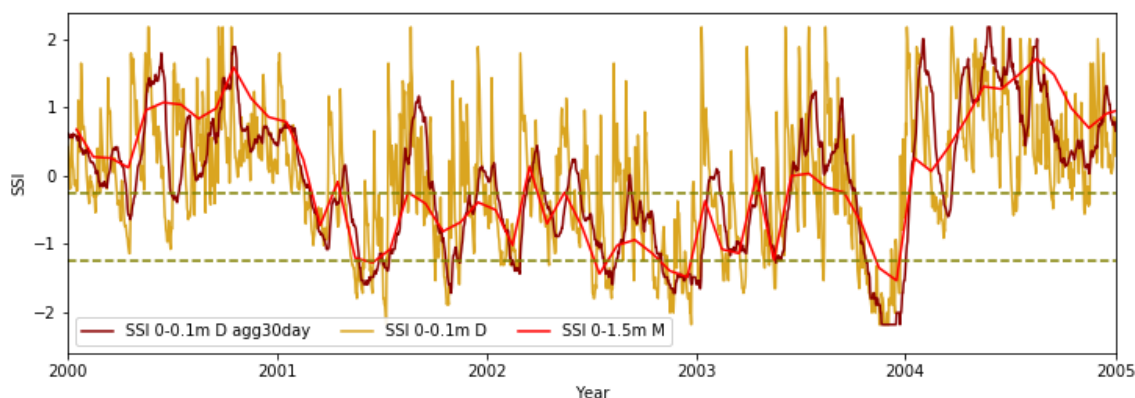


**Figure 4.1:** Time series example of standardised MIROC5 daily 0-10cm soil moisture (SSI, brown), daily aggregated 0-10cm soil moisture over 30 days (dark red) as used in our analyses and monthly root-zone layer soil moisture content up to 1.5m depth (red). The grid cell selected is located in South East Australia at  $35.72^{\circ}\text{S}$  and  $143.4^{\circ}\text{E}$ . Dashed lines correspond to the data's  $10^{\text{th}}$  and  $40^{\text{th}}$  percentile.

All drought indices are standardised and we further apply the standardisation to soil moisture values to generate a Standardised Soil moisture Index (SSI). We use a non-parametric approach by Farahmand and AghaKouchak (2015) to achieve inter-comparable indices. The resulting values were then translated into drought categories according to the EDDI guidelines (Lukas et al., 2017), which is based on the USDM (Svoboda et al., 2002) to quantify their severity and to simplify comparisons with other studies. The categories and their criteria are listed in Table 2.5 and range from "ED4"

- exceptionally dry to "EW4" - exceptionally wet with "None" representing normal conditions. FD events in soil moisture are treated as "truth" and are detected using a percentile definition, defined next.

As a FD is an extreme event, its occurrence should be relatively rare in a time series analysis. To establish an appropriate definition, we initially use that from [Ford and Labosier \(2017\)](#), who define FD as "periods when the pentad-average 0–40 cm volumetric water content declines from at least the 40<sup>th</sup> percentile to below the 20<sup>th</sup> percentile in 4 pentads [20 days] or less". Their percentiles are based on the "non-drought" and "moderate drought" conditions according to the USDM ([Svoboda et al., 2002](#)).

However, some adjustments to this definition were necessary for this study as flash drought frequency exceeded more than ten FD events per decade in each season for much of the global domain, which is too frequent compared to observational studies. Although we attempted to imitate the dynamics of deeper layer soil moisture using CMIP5 10cm soil moisture content by smoothing the time series with a four week running mean, [Figure 4.1](#) shows that the variability in the SSI is still overestimated compared to the deeper soil layers. Thus, the high frequency of FD events is likely associated with the responsiveness of the upper 10cm soil moisture to the atmospheric layer above ([Entekhabi et al., 1996](#)). Consequently, we adjusted the FD definition by lowering the percentile defining the onset of an FD to the 10<sup>th</sup> (USDM "severe drought") and the time period in which the rapid decline has to occur to 14 days, which is closer to the proposed definition for operations in the United States by [Pendergrass et al. \(2020\)](#), requiring a two-category change in the US Drought Monitor in two weeks.

This resulted in most locations registering a few FD events per decade, which is closer to what is expected from the regional observational studies ([Koster et al., 2019](#); [Zhang et al., 2018](#); [Ford and Labosier, 2017](#)). The FD terminates once soil moisture is restored to the 40<sup>th</sup> percentile or above. These thresholds were derived empirically as there is no previous study which applied the [Ford and Labosier \(2017\)](#) formulation on a top 10cm soil moisture level. Additionally, only FD events with a duration longer than four weeks were examined since shorter events in the upper layer do not necessarily penetrate deeper into the soil profile on shorter time scales ([Ford and Quiring, 2014](#)). Effectively, the root zone layer soil moisture ( $\approx 40\text{-}100\text{cm}$ ) has to be affected for a FD

to happen (Otkin et al., 2018).

In order to examine differences of flash drought dynamics within the CMIP5 model group, we look at the inter-model spread. The inter-model spread is defined as the ratio of ensemble standard deviation to ensemble mean. A value  $\ll 1$  implies that the inter-model differences are much smaller than the mean and vice versa for  $\gg 1$ . This measure was applied to the co-variability of drought indices to soil moisture and the FD event frequency and will provide information to what extent the models agree or disagree on their relationship between soil moisture, precipitation and ET.

Once the time series of FD events have been created for all drought indices, the ability of the index to detect flash drought was assessed. This was achieved using a contingency table commonly used to assess the accuracy of weather forecasts. The statistical measures of false alarm ratio (FAR) and hit rate (HR) were determined. The HR represents the success of the index to capture flash drought events. The higher the HR the more events are correctly detected by the particular index. The FAR in contrast shows the proportion of times the indices failed to predict flash drought, that is when the index yields a flash drought but it doesn't occur in the soil moisture. A high percentage value shows that the index detects many flash droughts that do not occur in the soil moisture. A contingency table (Table 4.1) gives the required parameters to calculate those skills, which is a 2x2 matrix of forecast/event pairs for the dichotomous non-probabilistic verification situation.

**Table 4.1:** Contingency table.

		Observations (SSI)		Marginal totals forecast
		Yes	No	
Forecast (EDDI,ESI,SPI)	Yes	a	b	a+b
	No	c	d	c+d
		a+c	b+d	n=a+b+c+d
		Marginal totals observations		

Here, EDDI, ESI and SPI are treated as the event forecast while SSI represents the event observation. 'Yes' and 'No' dictate whether an FD event was observed. As atmospheric drying conditions precede the drying signal in the soil profile, a tolerance time window of eight weeks prior to the FD detected in the soil moisture is applied for

the drought indices. From the contingency table, HR and FAR are defined as follows:

$$FAR = \frac{b}{a + b} \quad (4.2)$$

$$HR = \frac{a}{a + c}, \quad (4.3)$$

where  $a$  is the number of occurrences when the forecast index correctly detected a FD within the four/eight weeks prior to a FD in the observations,  $b$  when the forecast index detected a FD but none were observed and  $c$  when the forecast index did not detect a FD which was actually observed.

## 4.5 Results

### 4.5.1 Representation of Flash Drought in Drought Indices

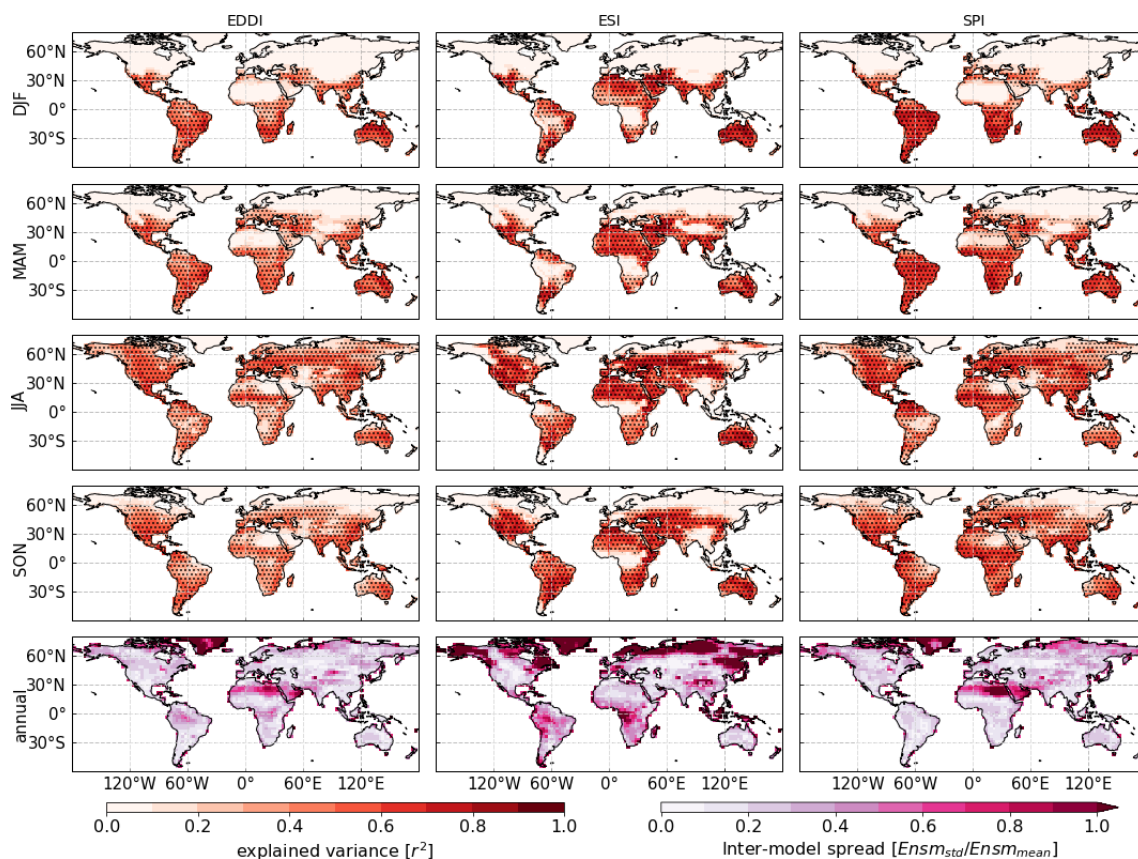
The SSI represents the “true” occurrence of FDs in the CMIP5 models and the ESI, EDDI and SPI are tested as proxies for capturing these events. Correlating the latter three indices with the SSI using a global Pearson correlation indicates the relationship between them during all conditions, not just drought. The correlations were computed as cross-correlations where each drought index was moved along the time axis relative to the soil moisture from -14 to +14 days in two day increments.

Figure 4.2 shows the maximum explained variance while figure 4.3 displays its corresponding lag or lead. The CMIP5 ensembles of all proxies represent the soil moisture fluctuations very well with explained variances of 0.4 to 0.8 with the ESI having generally the strongest relationship. This mainly encompasses regions from the subtropics to the mid/high latitudes where variability in precipitation and ET are largest and environments are often water-limited. Natural seasonal variations in soil moisture, such as a frozen state, affect the correlations across the northern higher latitudes ( $45 - 60^\circ N$ ) whereas subtropical regions, especially in the Southern Hemisphere have a far more consistent relationship between soil moisture and precipitation/ET throughout the year.

The inter-model spread of the six CMIP5 models is significant, predominantly in arid regions for SPI and EDDI and in the tropics and higher latitudes for ESI (Figure 4.2 bottom row). This suggests that the correlations between drought indices and soil moisture vary largely between the individual models causing the high inter-model spread

and consequently a weak overall correlation for the ensemble mean.

The high correlations of the ESI are often associated with a lag time of -2 to -10 meaning that its signal is delayed in regards to the SSI and the ESI responses to changes in the soil moisture. EDDI often has a small lead time of 2-4 days in significant correlated regions but is also sometimes lagging the soil moisture changes behind, e.g. Southern Australia in MAM. Precipitation shows a lead time of 2 to 12 days for the SPI with the longer lead occurring during the colder season. The inter-model spread in the bottom row of figure 4.3 highlights further discrepancies in the CMIP5 models in addition to differences in correlations outlined above. The lead time of precipitation is consistent within the CMIP5 model suite as indicated by an inter-model spread of 0 to 0.4 for the global domain. In contrast, huge differences exist for the EDDI in subtropical regions in the Southern Hemisphere and especially for the ESI exceeding an inter-model spread of two. This means that the difference between the models is twice as large as the mean.



**Figure 4.2:** CMIP5 ensemble mean of seasonal explained variance of EDDI (top row), ESI (middle) and SPI (bottom) with 0-10cm SSI over the entire historical run length of 138 years. Statistically significant correlations on the 95% level are marked with hatching. The lag/lead at which this highest correlation was detected is shown in figure 4.3. The bottom row shows the annual inter-model spread in the CMIP5 models.

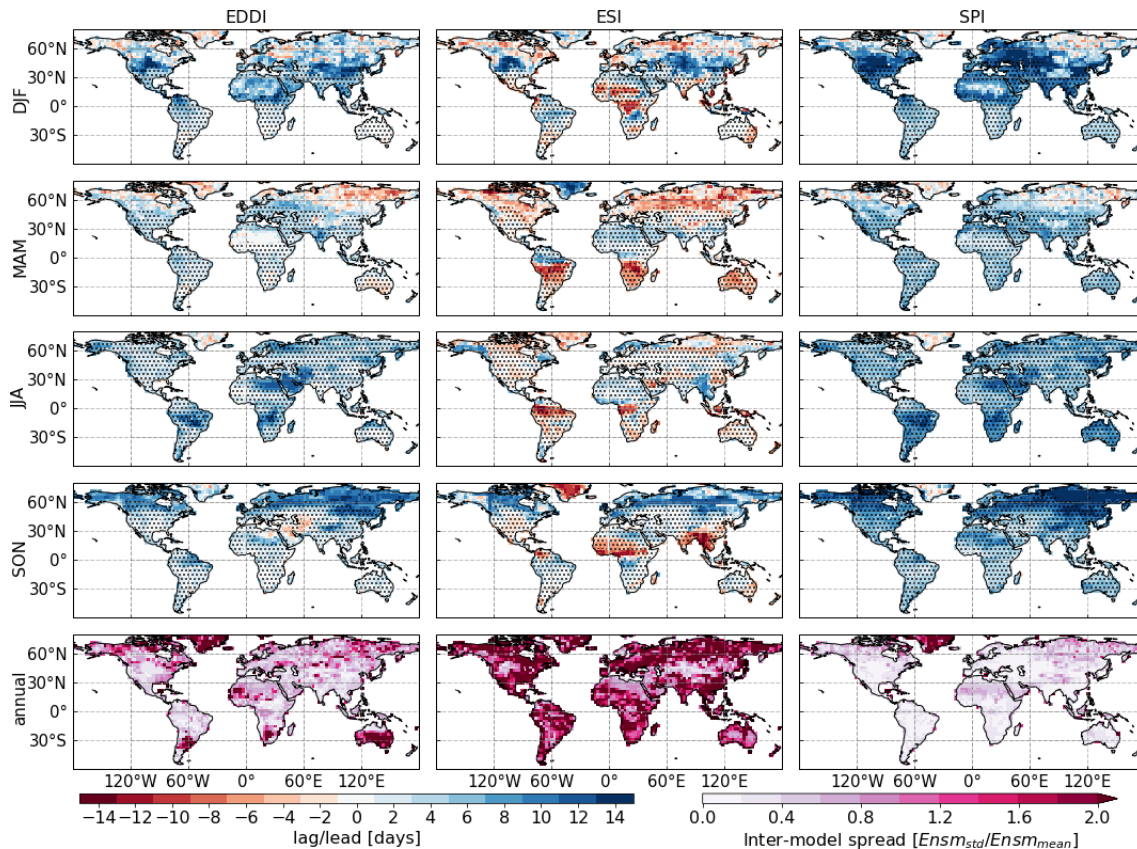


**Figure 4.3:** Lag at which the maximum explained variances shown figure 4.2 occurred for EDDI (top row), ESI (middle) and SPI (bottom). Stippling marks where the explained variances are significant at the 95% level. The bottom row shows the annual inter-model spread in the CMIP5 models.

The large inter-model spread highlights the discrepancies in land-atmosphere processes in CMIP5 models as outlined in the introduction. To which degree the inter-model spread is confined to the partitioning and timing of energy fluxes which drive potential and actual ET remains unknown since issues with pedo-transfer functions in land surface models are well known (Pitman, 2003; Van Looy et al., 2017) and contribute to the inter-model spread.

The climatology of FD events in the CMIP5 ensemble mean was produced using the SSI (Fig. 4.4m-p). The FD events are fairly evenly distributed across the globe and can theoretically happen in almost all environments throughout the year, predominantly during the warm seasons when evaporation is naturally higher and precipitation less variable than during the cold season. Seasonal hot spots are present in South Africa, South America and Australia during the austral summer season while SE Asia, Africa's Sahel zone and parts in Northern North America are more affected by FD during the boreal spring. Koster et al. (2019) have identified a similar pattern but with slightly lower

frequency of FD events in the Northern Hemisphere due to using a different definition during the April to September 1980-2017 period using MERRA-2 reanalysis data of root-zone soil moisture. The similarity between our climatology and that from [Koster et al. \(2019\)](#) provides some confidence that the definition we have set is reasonable. The differences in soil moisture depth of 10cm in our data versus 100cm in Koster's prohibits us from simply applying their definition.

Next, we applied the FD thresholds that were established using the SSI to the times series of the other indices to create an FD climatology for each index (Fig. 4.4a-l) and compare them to the SSI.

Generally, the ESI shows a similar event frequency to SSI. Yet, it has some incongruences in the NH around  $40-50^{\circ}N$  where it detects a high event frequency in comparison to the rest of the global domain, especially during the winter season. Tropical regions between  $10^{\circ}N/S$  are characterised by a low event frequency, presumably because rainfall in the tropics is always relatively reliable. Subtropical regions have the highest event frequency (Fig. 4.4i-l).

The SPI FD frequency is a factor of 2.5 larger than the SSI. The EDDI shows only relatively few areas with fewer than eight events/decade and exceeds 12 events/decade in North Africa and high latitudes. This means that a flash drought occurs on average once every year. Both the SPI and EDDI show similar climatologies of FDs for all seasons and even detect many FDs in the high latitudes during the winter season which counteracts the reasoning for a lower SSI FD frequency before. The high FD frequencies of EDDI and SPI are in contrast to the ESI which barely detects flash droughts in the high latitudes in any model as the frozen ground does not release moisture for evaporation and the environment is energy-limited with ET and  $ET_0$  in a parallel interaction. Generally, FD event frequency shows a similar range in the EDDI, ESI and SPI climatology but with different base values where the climatology for FD events is highest for EDDI, lowest for ESI and SPI between them.

The FD event frequency can vary considerably between the CMIP5 models, shown as the inter-model spread in Figure 4.5. Inter-model spread is defined as the ratio of model ensemble mean to ensemble standard deviation. A value  $> 1$  means that the inter-model differences are larger than the ensemble mean. For example, a spread of 2 would mean that the difference between the models is twice as large as the mean.

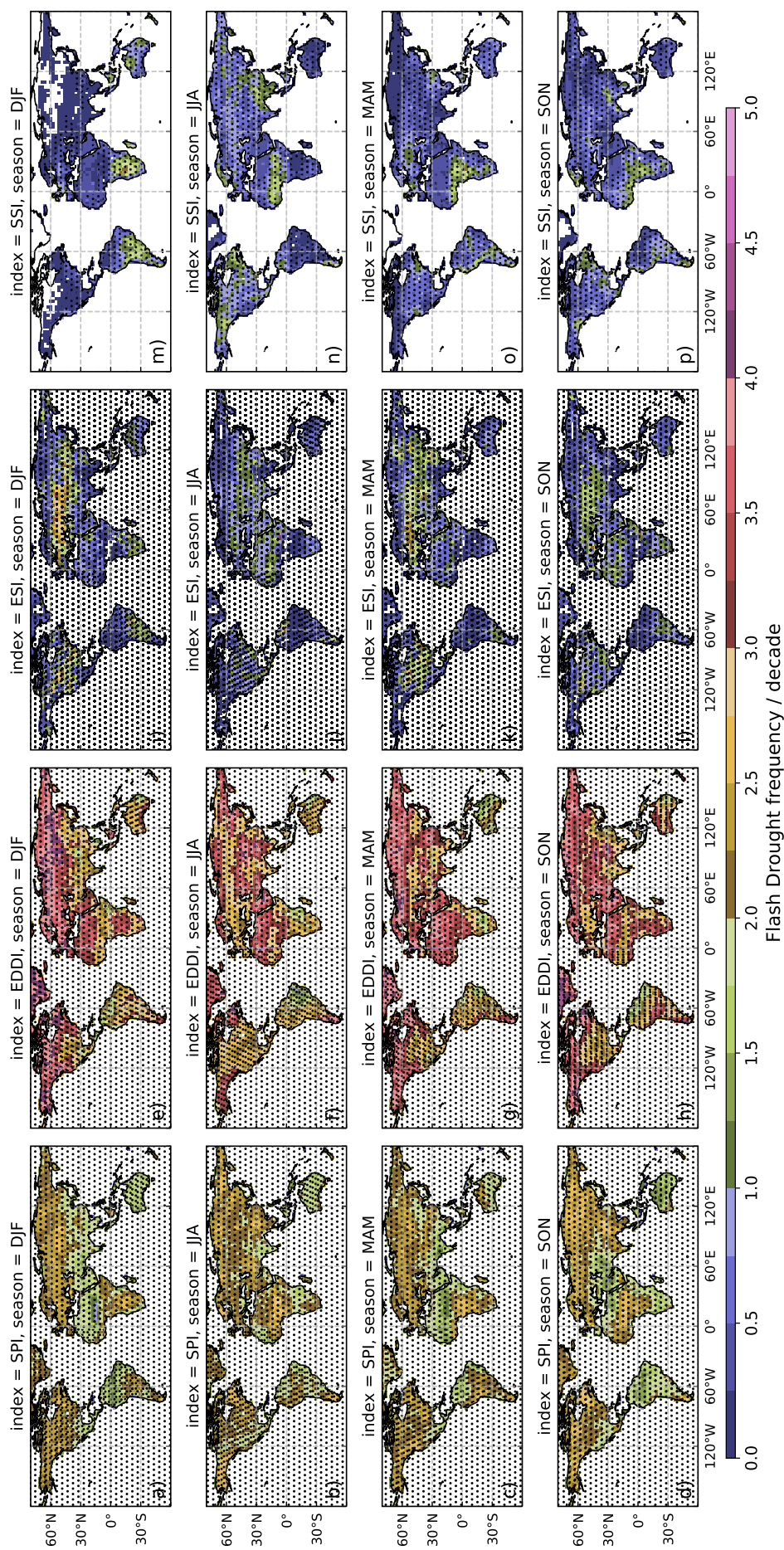


**Figure 4.4:** CMIP5 ensemble mean of seasonal FD event frequency expressed as events per decade for EDDI (a-d), ESI (e-h), SPI (i-l) and SSI (m-p) over the entire historical run length of 138 years. Hatching indicates where at least 50% of the CMIP5 models listed in Table 2.4 identified a FD.

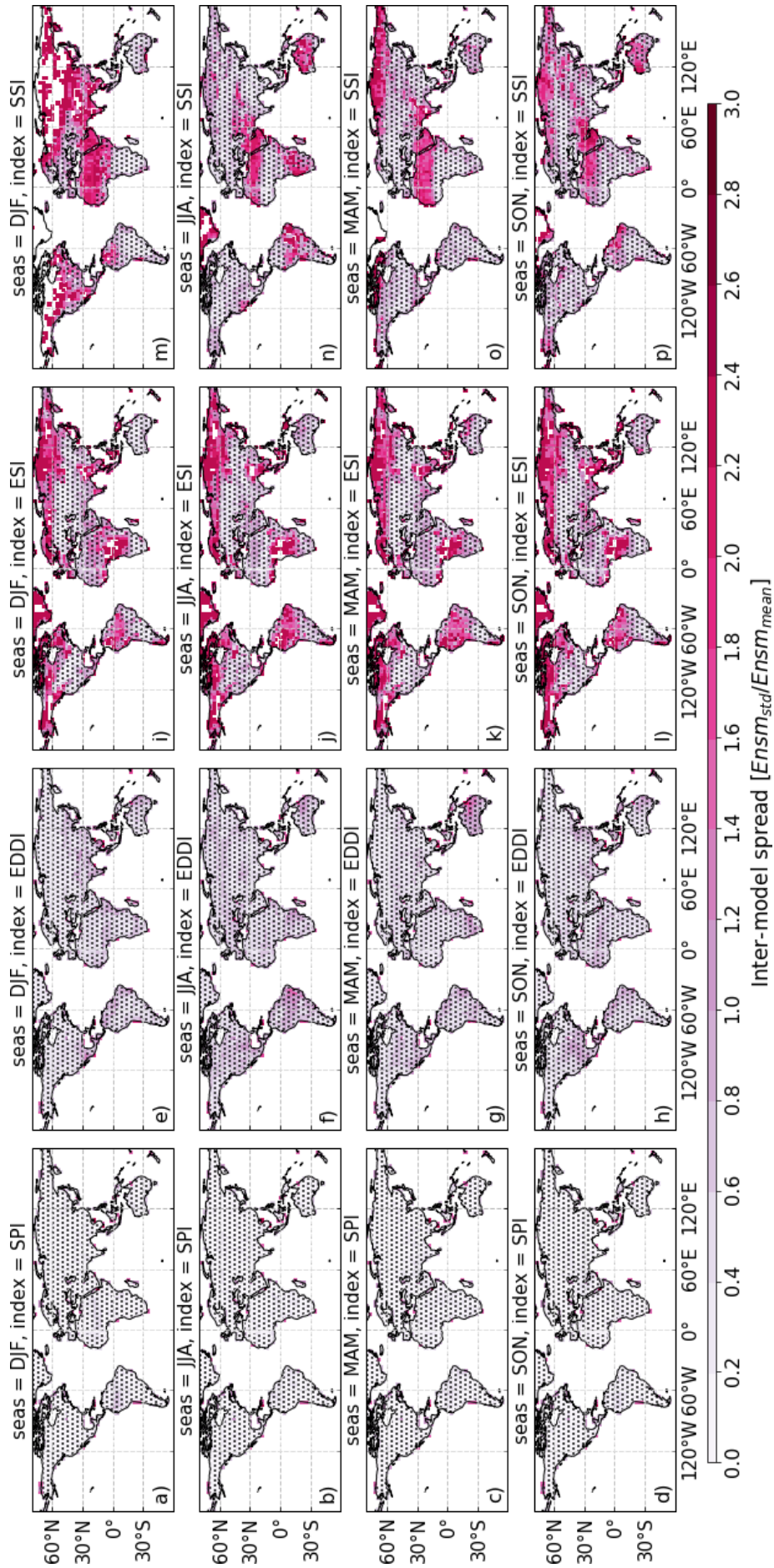


**Figure 4.5:** Seasonal CMIP5 inter-model spread of FD event frequency for SPI (a-d), EDDI (e-h), ESI (i-l) and SSI (m-p). The inter-model spread is defined as the ratio of ensemble standard deviation to ensemble mean. Hatching indicates areas where at least 50% of the CMIP5 models listed in Table 2.4 identified a FD.

Regionally, the spread exceeds the number of events of the ensemble mean for ESI and SSI, highlighting large inter-model differences compared to mean number of events. The discrepancies in arid regions and high latitudes are most prominent, with a spread of 2-3 events per decade. This is mainly driven by the fact that here, less than 50% of the models detected a FD at all. Slightly better model agreement is present in the subtropics and mid-latitudes where hatching is present. The inter-model spread for EDDI is more homogeneous and slightly lower with around 0.8 compared to hatched regions (>50% of models show flash drought here) in the ESI and SSI with around 1.2. While the spread in ESI and SSI is driven by differences between all models of similar magnitudes, the spread for EDDI is heavily weighted by a significantly higher FD event frequency (by a factor of four) in the CanESM2. The frequency is more similar, but still higher, compared to the SPI FD frequency if CanESM2 is excluded. Of all indices the SPI has the fewest differences between models across the global domain and seasons, implying that a significant source of the spread is coming from the land surface models or land-atmosphere coupling. Another possibility is that the inter-model spread is caused by those atmospheric variables (e.g. humidity, wind etc) that are used to generate PET. However, the inter-model spread in the EDDI is less than for ESI and flash drought, suggesting that atmospheric variables make less contribution to the spread than land surface variables.

The coincidence of the FDs in the climatologies of EDDI, ESI and SPI with those detected in the soil moisture shows whether the index is appropriate for FD monitoring and detection. We examined this by picking the flash droughts identified in the soil moisture by the SSI, our reference, and looked at the representation of these events by EDDI, ESI and SPI in a two-fold way. First, the index value at the onset of the FD, which is when the 10<sup>th</sup> percentile in soil moisture is surpassed and second, the rate of change (RoC) in the drought index 2-6 weeks prior to the onset. Figure 4.6 shows the first metric for SPI, ESI, and EDDI as absolute values for each season. A category of ED2 ("severe drought") corresponds to the 10<sup>th</sup> (90<sup>th</sup> for EDDI) percentile which is observed for all indices across the globe and all seasons where FD is detected by the SSI.

Here, the SPI shows the highest sensitivity to flash droughts in the soil moisture, shown as the strongest negative values for both the RoC and index value at the onset. This is consistent throughout all seasons. While EDDI and ESI also show a consistent

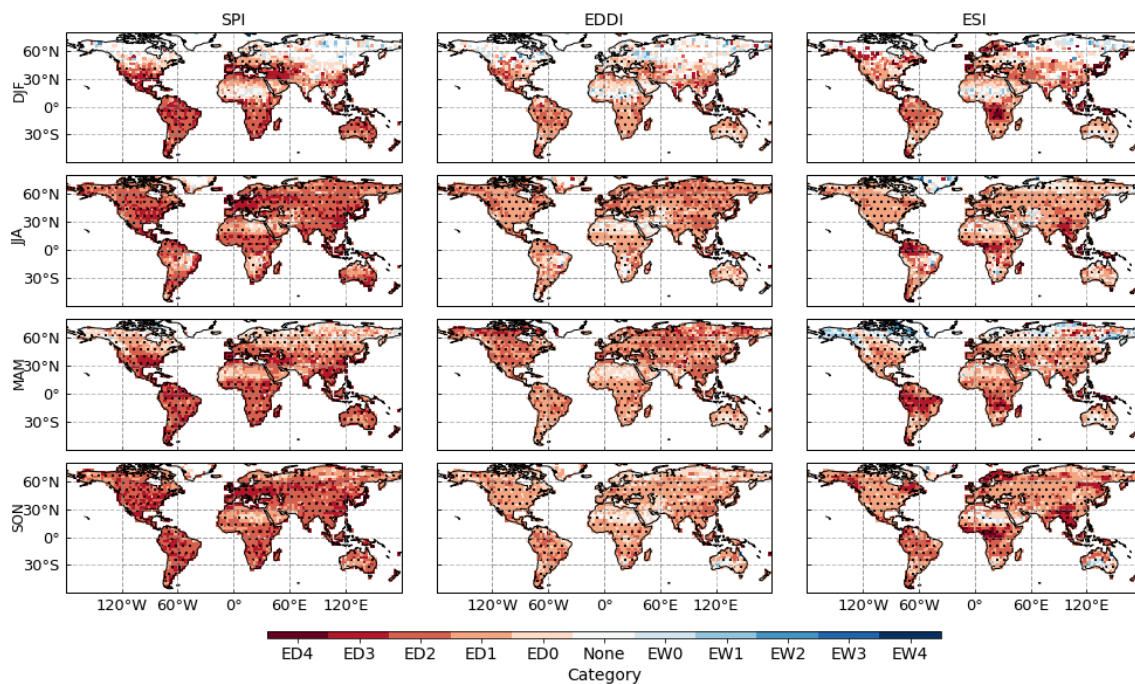


**Figure 4.6:** Index values by season according to the USDM at the time of flash drought onset in the SSI for SPI (left column), EDDI (middle) and ESI (right). A category of  $\leq \text{ED2}$  correspond to the ESI's and SPI's 10<sup>th</sup> and the EDDI's 90<sup>th</sup> percentile respectively. Hatching indicates where at least 50% of the CMIP5 models listed in Table 2.4 identified a FD.

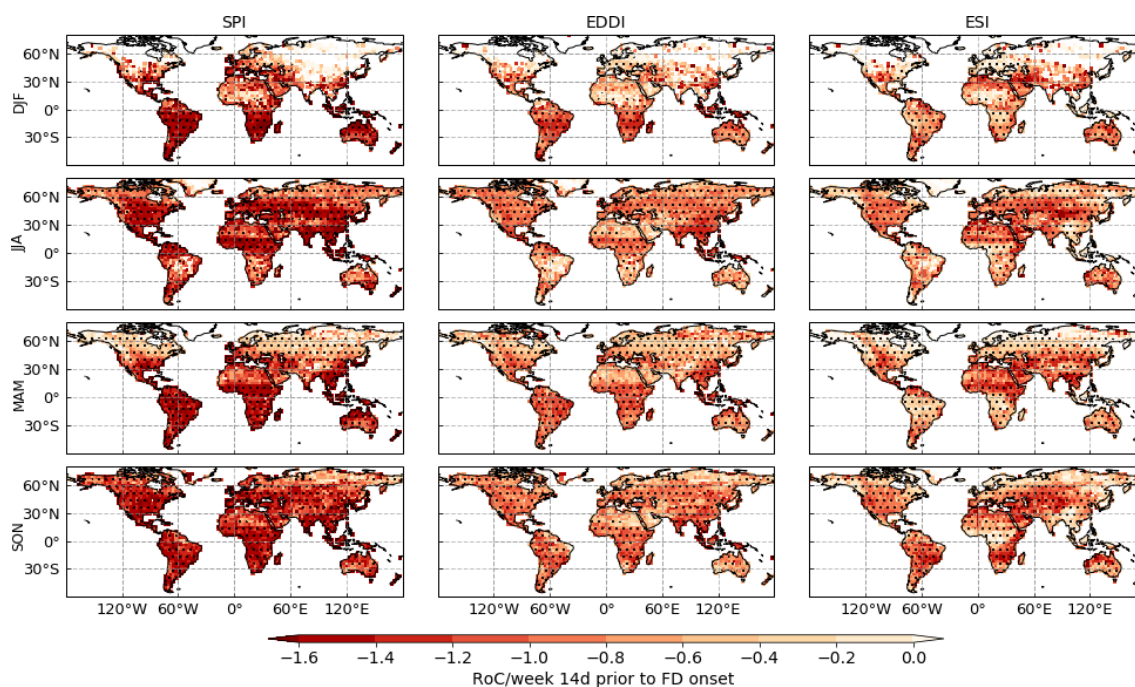


**Figure 4.7:** Rates of change (RoC) per week from two weeks prior to the onset of FD in the SSI for SPI (left column), EDDI (middle) and ESI (right). Hatching indicates where at least 50% of the CMIP5 models listed in Table 2.4 identified a FD.

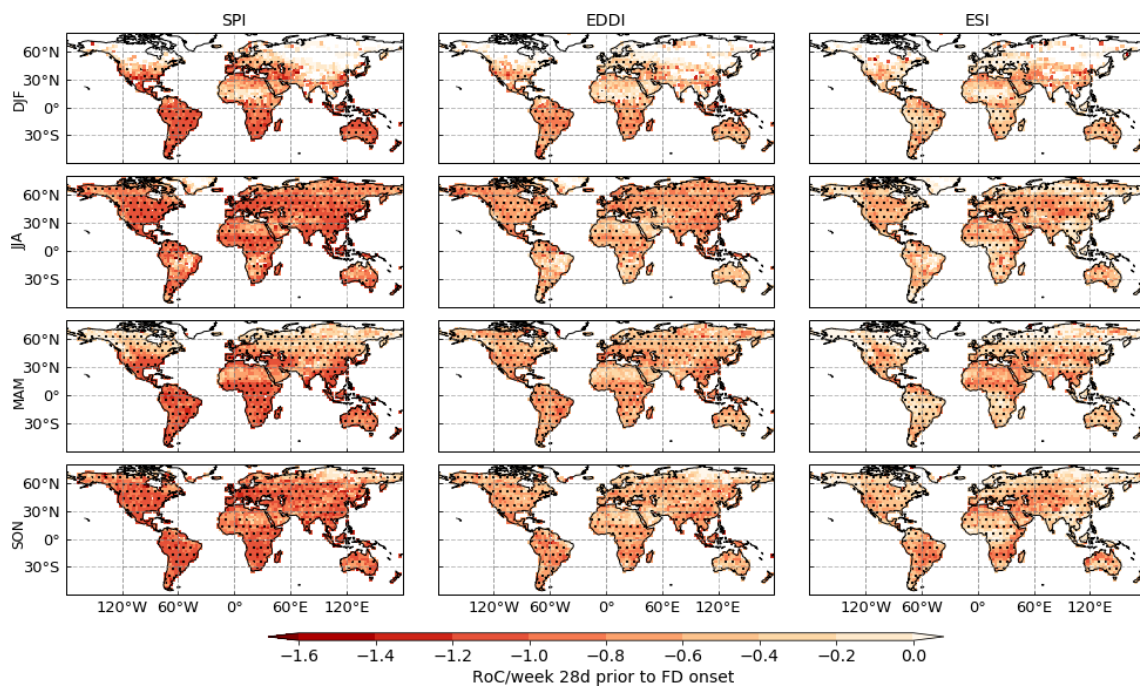


**Figure 4.8:** Rates of change (RoC) per week from as in Figure 4.7 but for four weeks prior to the onset of FD in the SSI.

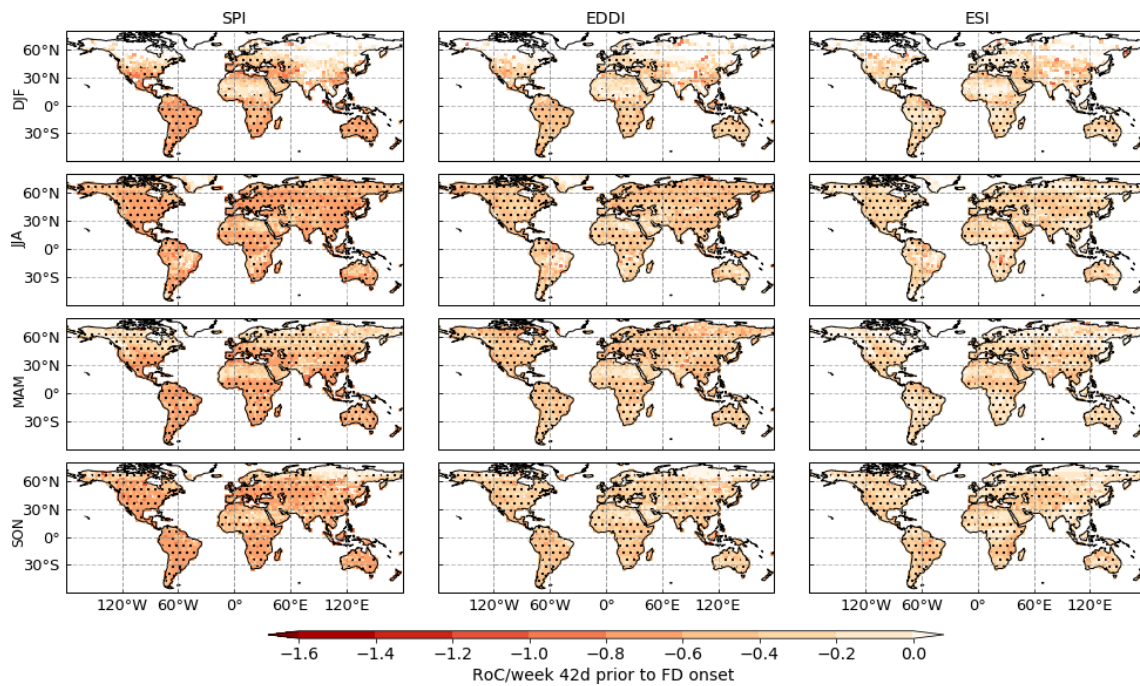


**Figure 4.9:** Rates of change (RoC) per week from as in Figure 4.7 but for six weeks prior to the onset of FD in the SSI.

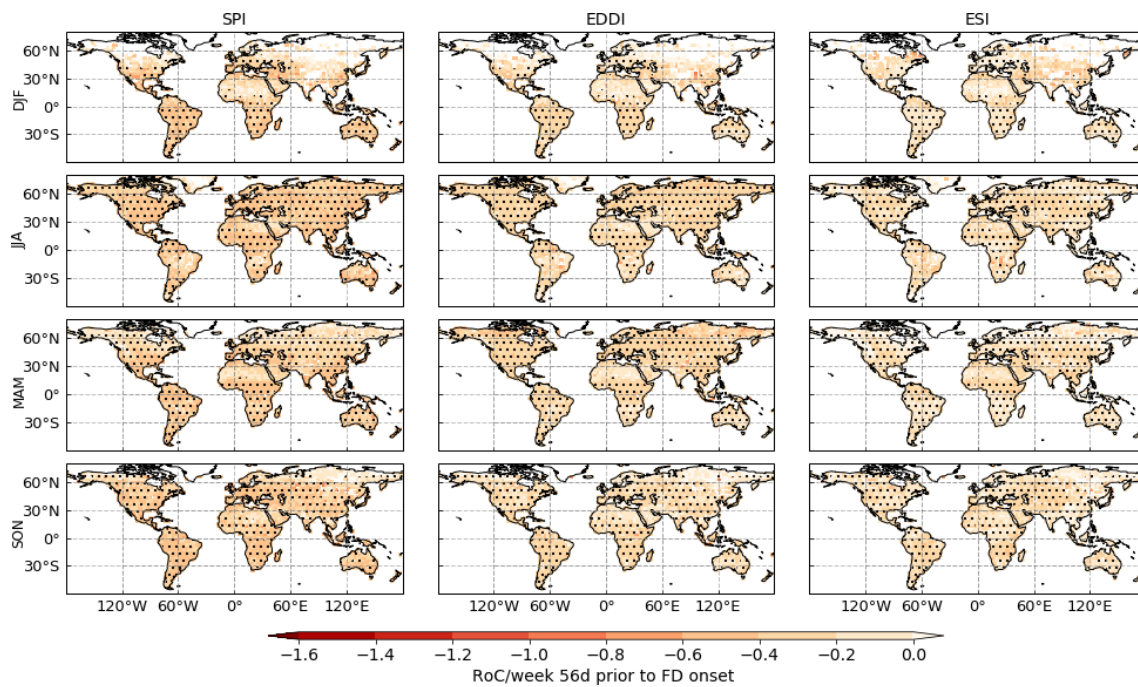


**Figure 4.10:** Rates of change (RoC) per week from as in Figure 4.7 but for eight weeks prior to the onset of FD in the SSI.

strong decline (increase for EDDI) of close to one category per week in the two weeks prior to the FD onset in the soil moisture, their absolute values at the onset itself are regionally much weaker than those of the SPI. This includes subtropical regions where FD is an imminent threat to agriculture, for example Australia and Eastern South America. Overall, this implies that all indices capture FD identified by soil moisture. Yet, in conjunction with the lag/lead times in the correlation, it seems that FDs are primarily driven by precipitation and the signal in the evaporation does not occur until later.

The RoC shows how quickly the drying intensifies several weeks before the onset of a FD. Figure 4.7 displays that change over the two weeks prior to the onset. The change of each index per week over the two week period is compared to the change over four (Fig. 4.8), six (Fig. 4.9) and eight weeks (Fig. 4.10). Again, the SPI has consistently stronger changes prior to the onset of the FD event than ESI and EDDI. These changes are highest for all indices from two weeks to the onset and decay when longer periods are considered. This indicates that the movement into a flash drought is rapid in the models, with the greatest drying in the two weeks prior to drought onset. While the RoC is consistently negative across all models, showing a drying signal in all indices, the actual index values for ESI and EDDI are regionally on the wet side, especially for the GFDL models in subtropical regions of the Southern Hemisphere, which modifies

the ensemble mean accordingly to weaker values. Here, the land atmosphere coupling between GFDL models and CSIRO-Mk3-6-0, CanESM2 and MIROC5 differs the most when it comes to the timing of the ET response signal to the soil moisture.

### 4.5.2 Detection skills of Drought Indices

Using the FD climatologies from all indices, we estimate the event detection skill for each of EDDI, ESI and SPI with the contingency table described in section 4.4. Panel A of Figure 4.11 shows the HR for each index split into seasons with an 8-week tolerance window prior to the observed FD event applied. The hatching shows where at least 50%

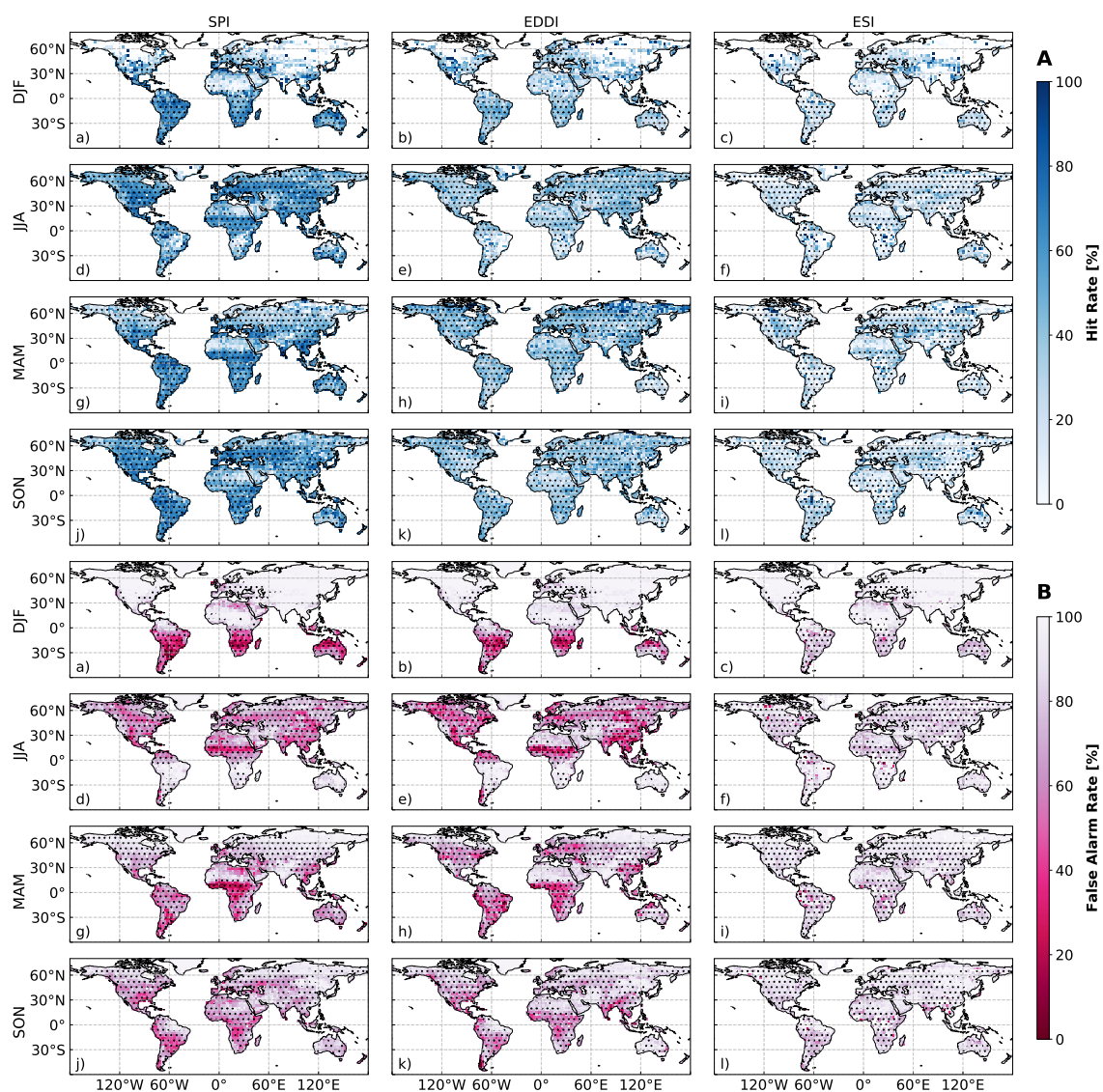


**Figure 4.11:** Hit rate (HR, panel A) and false alarm ratio (FAR, panel B) for SPI (left column), EDDI (middle) and ESI (right). The tolerance window for valid detection is from eight weeks prior to the onset of a flash drought in the soil moisture. Hatching indicates where at least 50% of the CMIP5 models listed in Table 2.4 identified a FD in the SSI.

of the CMIP5 models have marked a FD in the SSI. Only these regions are discussed.

The SPI consistently showed the highest HR globally throughout all seasons with around 60% to 80% of flash droughts detected in the SSI, also detected by the SPI. The EDDI and ESI have a significantly weaker HR with 40% to 60% and around 20% respectively. The larger HR for the SPI could be the result of the high responsiveness of the top soil layer to rainfall. Deeper soil layers might reveal differences in the HR between the SPI and the two evaporation based indices. However, as previously outlined, this data is not available at the temporal resolution required for analysis.

The high HR for the SPI is consistent across all models. The EDDI HR is generally weaker in the CanESM2, despite its gross overestimation of EDDI FD frequency. Theoretically, an overestimation of the frequency should increase the chances of an FD in the EDDI coinciding with one from the SSI, but this is not the case. This suggests that many high RoC in the EDDI (i.e. sudden, high PET) are not coinciding with similarly rapid soil moisture depletion. Instead, they must occur during times when soil moisture is not showing severe drying conditions illustrating issues with the land-atmosphere coupling in extreme conditions for this particular model. For the ESI, the HR is very low in all GFDL models contributing to the overall low HR in the ensemble mean given that the GFDL models represent 50% of the ensemble (3/6 models). CanESM2, CSIRO-Mk3-6-0 and MIROC5 generally show HRs of greater than 50% for the ESI.

Consequently, the above results are also embodied in the FAR (Fig. 4.11 panel B) as a high HR usually means a low FAR and vice versa. However, with a significantly higher detection of FD events in the index than in the soil moisture a high HR will come at the cost of a high FAR. While FAR for EDDI are very similar to the ones of the SPI (around 40%), the FAR of the ESI is considerably weaker with around 80% in hatched areas. The FAR for EDDI is largely driven by the high departures of FD frequency in CanESM2. The seasonally varying FAR for SPI and EDDI are caused by their relatively uniform distribution of FDs over all seasons, whereas FDs in the soil moisture mainly occur during the warm season. During the colder season EDDI and SPI might still detect the soil moisture FD but their event frequency in general is too high. The over detection of FD in the cool season is less apparent in the HR and FAR for the ESI. Even though the FD frequency identified in the ESI is very similar to the SSI and would yield a low FAR if the HR was good, but they tend to happen slightly after the FD occurred in

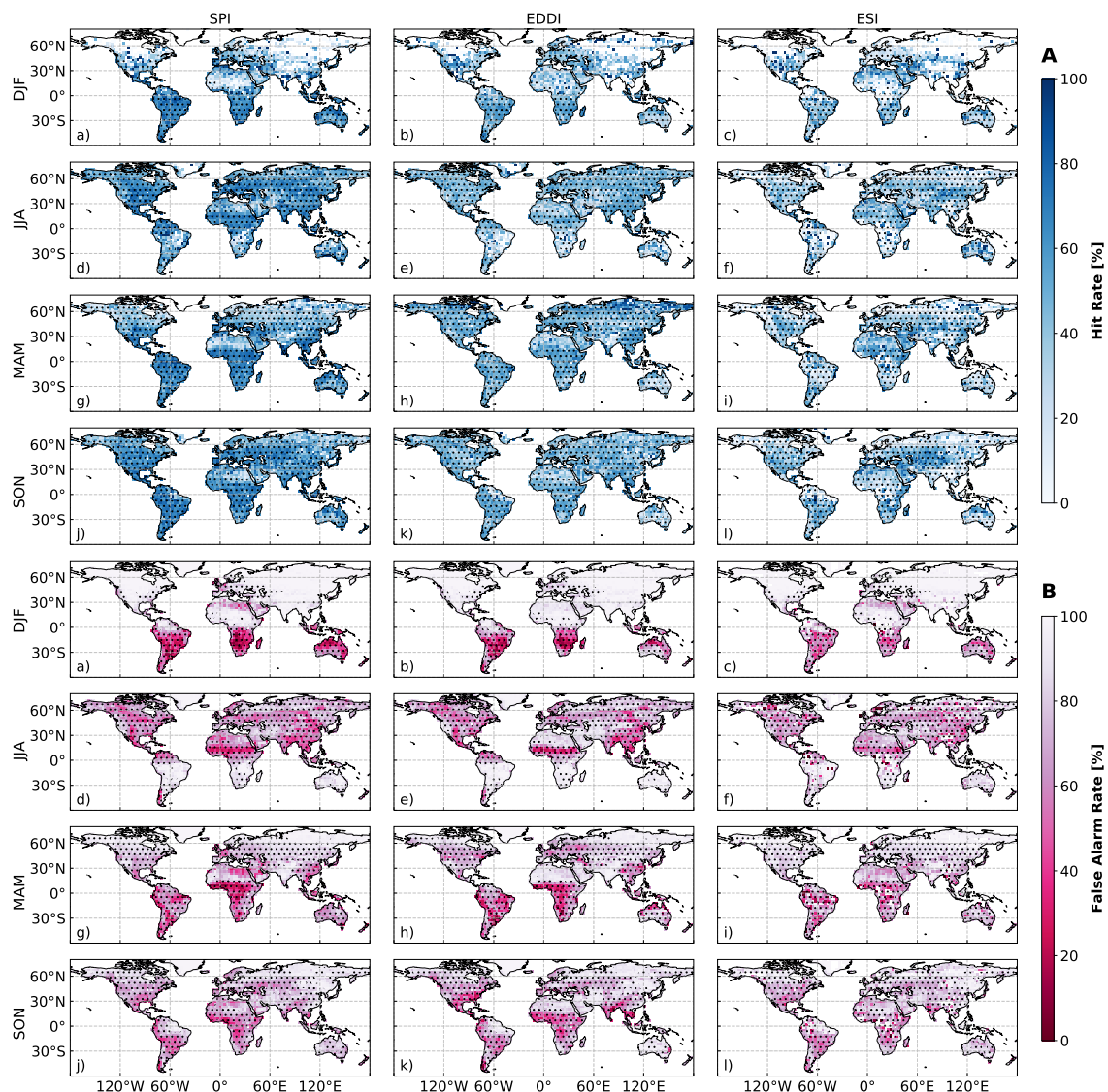


**Figure 4.12:** As previous Figure 4.11 but the tolerance window has been extended to two weeks after flash drought onset in the soil moisture.

the soil moisture for which the high responsiveness in top 10cm soil layer is likely to be responsible. As a result, both detection skills are very weak. However, this varies between the individual CMIP5 models more than HR and FAR for EDDI and SPI.

The results for the ESI improve when the detection window is extended to two weeks after the flash drought occurred in the soil moisture (Fig. 4.12). This time, flash droughts detected in the ESI are a result of a flash drought in the SSI, and thus showing a lag, are captured as well. ESI HRs improve by approximately 20 to 30% for the CMIP5 ensemble (right column), again showing the highest HRs in CanESM2, CSIRO-Mk3-6-0 and MIROC5. Similarly, there is a concurrent drop in the FAR. EDDI also improves its HR by about 10 to 20% but there are no differences for the SPI due to its continuous

leading signal. While the ESI's HR now closely matches the one of EDDI, both are still weaker than the SPI's HR. The markedly improving skill for the ESI, and to some extent for the EDDI, for the two week extension of the detection window to post SSI FD onset implies that both indices are less skilful for FD prediction but are rather useful for FD monitoring. For the top 10cm soil moisture, the SPI is the best index for FD prediction.

## 4.6 Discussion

The goal of this chapter was to examine the occurrence of flash drought in CMIP5 models and to evaluate how well various drought indices represent FDs in comparison to the models' soil moisture.

The characteristics found in EDDI, ESI and SPI provide information about the processes related to FD in the upper 10cm soil moisture level. Of those three indices, the ESI showed the closest flash drought event frequency to the SSI. As the ESI uses the latent heat flux, it has a direct link to the available moisture since it is a measure for evaporation from the land surface. When available moisture in the land surface depletes, incoming energy from shortwave radiation is increasingly partitioned into sensible heat, which increases the atmospheric temperature and tends to increase  $ET_0$ . Over time, this can create a water-limited condition in the absence of significant rainfall (Hobbins et al., 2016). This is when the ESI starts to decrease as actual evaporation cannot match  $ET_0$  anymore. As long as available moisture is sufficient in an energy-limited condition, ESI cannot decrease because ET is defining the upper limit of  $ET_0$  (Anderson et al., 2007). Therefore, ESI detects FD frequency similarly to the SSI. However, the response in the ESI is delayed as an increase in  $ET_0$  caused by increasing temperature (e.g. advection) initially results in an increase of ET due to their parallel relation during energy-limited conditions (Hobbins et al., 2017). The lag in the cross-correlation as well as the weak rates of change are evident for this delay.

The EDDI should be coupled to available moisture as well due to the immanent relation between  $ET_0$  and ET. The initial response of  $ET_0$  to changing synoptic conditions leading to higher temperatures and lower humidity is again amplified by an increase in sensible heat flux during the development of a drought. This is especially the case in regions of high net radiation and where seasonal changes between water-limited and

energy-limited regimes exist (Koster et al., 2009b). On the other hand, high  $ET_0$  caused by an increased forcing parameter such as wind speed, can also occur without increasing the risk of drought as long as soil moisture supply is sufficient, which can offset the increased moisture demand (Otkin et al., 2018). EDDI is also less reliable in energy-limited environments where ET and  $ET_0$  are positively correlated (McEvoy et al., 2016). As a result of different driving mechanisms, EDDI shows the highest frequency for the occurrence of flash drought.

Precipitation alone, represented by the SPI, sits between EDDI and ESI in terms of event frequency. A sharp decrease in precipitation may not necessarily lead to a flash drought, especially not during the cold season when ET is low or when a surplus in precipitation was received prior to the decline. The SPI can produce large oscillations on short time scales of just a few days due to the episodic nature of rainfall. Thus each prominent drop in precipitation will likely result in a flash drought event even though the environmental conditions are not showing any sign of drought. Since both, precipitation deficiency and high anomalies of ET can occur independently without causing the soil moisture to decline significantly (Otkin et al., 2018), especially in the root-zone layer for which CMIP5 does not provide a daily measure, the absolute number of FD events is overestimated by SPI and EDDI.

The strong negative values expressed in categories according to the USDM and strong RoC indicates that severe and ongoing negative precipitation anomalies cause flash drought events. This ascribes that precipitation has a primary role for priming a flash drought, as shown by the SPI. Arguably, a precipitation deficiency is a common feature in all drought types and might not be unique enough to characterise a FD (Otkin et al., 2018), also indicated by the overestimation of FD in the SPI itself. While this just represents the overall picture suggesting that precipitation is the primary driver for FD, the RoC for those indices can vary for individual FD events. This is consistent with findings from Koster et al. (2019) who ascribed the importance of ET to the development of FD but identified its overall contribution as “small relative to the contribution of precipitation deficits”. It would also support the separation into heatwave- and precipitation driven FD (Mo and Lettenmaier, 2016, 2015), whereas FDs primarily caused by a precipitation deficit would occur more frequently.

The relationship of precipitation,  $ET_0$  and ET with the top 10cm soil moisture as

discussed above dictates their utility for flash drought prediction. Precipitation as the moisture supply is closely correlated with top 10cm soil moisture variability and can practically not lag the soil moisture signal. Consequently, the prediction skill of the SPI is highest, which achieved an HR of around 70% in regions where at least half of the CMIP5 models detected a FD in the soil moisture. EDDI detects only half of the soil moisture FD (HR  $\approx$ 50%), showing the primary contribution of precipitation to the development of FD and the longer response time of increasing  $ET_0$  from the sensible heat flux.

The weak skill of the ESI of around 30%, limits its initial positive impression based on the very similar FD event frequency and co-variability to the SSI. However, extending the detection window to two weeks after the FD onset in the SSI showed an increase in the HR of the ESI. This suggests that the ESI is rather a tool for flash drought monitoring than early warning which is inconsistent with what is found in the literature of observed case studies. [Nguyen et al. \(2019\)](#) detected a lead time of about one month for the ESI, and similar lead times were described in studies from [Otkin et al. \(2013, 2015\)](#). The HR for EDDI also increases, yet not as much as for the ESI. In contrast, a lead time of up to two months was shown for the EDDI to detect FD in the summer of 2012 in the US ([McEvoy et al., 2016](#)). The difference to the studies from [Nguyen et al. \(2019\)](#), [Otkin et al. \(2013, 2015\)](#) and [McEvoy et al. \(2016\)](#) is that the here applied definition is stricter. Signals in the indices might occur sooner when simply examining times series but they might just not hit our threshold one or two months in advance.

However, the fact that we are limited to the upper 10cm soil layer shortens the response time of the soil moisture signal to atmospheric conditions and hinders the comparison with these studies, which either focus on the root-zone layer of around 1m depth or deeper or only investigate specific FD cases and do not determine detections skills explicitly. Consequently, the lead of EDDI and ESI in reference to the deeper soil layers is offset by the fast response of the upper most soil layer. Moreover, the flash droughts in the upper 10cm do not necessarily penetrate deep enough into the ground to affect the root zone layer. Our chosen minimum duration of 30 days is purely arbitrary and might be too short.

The results described here need to be seen in the light of CMIP5 models and their underlying limitations as mentioned in the introduction (4.2). The CMIP5 analysis must

be considered with the imposed land surface model for each of the climate models in mind. Their formulations will have geographically- and seasonally-varying biases dependent on the land fluxes and states they produce. The overall lowest spread for SPI and EDDI FD event frequency in comparison to ESI and SSI confirms again the model's discrepancies in land-atmosphere interaction to reflect the latent heat flux and available moisture correctly compared to atmospheric conditions such as precipitation. The consistent higher frequency occurrence of FD identified by the EDDI (Fig. 4.4 e-h) might also be indicative of an overestimation of  $ET_0$  caused by an excessive sensible heat flux. An overestimation of evaporative droughts similar to our findings has been observed in LSMs by Ukkola et al. (2016a). Their results show that LSMs systematically miscalculate the partitioning of sensible and latent heat flux. An overestimation of sensible heat would directly lead to an increased  $ET_0$  causing EDDI to increase more rapidly. An underestimated latent heat flux, and thus ET, during water-stressed conditions would in turn decrease the ESI unproportionally but slow down the drying pace of the soil moisture. The first case would also yield a FD more rapidly in the ESI whereas the second case does not in the SSI. A comparison of CMIP5 to regional land surface reanalysis data in the next chapter will show if the overestimation of PET is also present in an offline LSM.

## 4.7 Conclusion

This chapter has examined the flash drought event frequency globally in CMIP5 models using three drought indices. Flash droughts were identified using soil moisture and the detection of flash droughts was compared using indices that measure precipitation, evaporative demand and evapotranspiration as included in the SSI, SPI, EDDI and ESI respectively. This analysis determined the detection capabilities of the indices. We provided information on the use of these indices as an early warning tools for flash drought detection, based on the improvement in our metrics using leads and lags between the indices and the SSI. The analyses were performed using a suite of six CMIP5 models, which included a range of representations in land-atmosphere feedbacks.

Our findings show that the SPI and EDDI overestimate flash drought event frequency, while the ESI shows a similar frequency to those flash droughts detected in modelled soil

moisture directly. The data from the CMIP5 models show less agreement in the results of event frequency for SSI and ESI which is caused by the models' flaw of different land-atmosphere interactions as shown in other studies. Consequently, the results show that the ESI, while a useful index for the detection and monitoring of flash drought, cannot provide an early warning capability. On the other hand, SPI and to some extent EDDI are capable of early detection in the models at lead times of over a week in some cases. However, they also have relatively high false alarm rates associated with their overestimation of FD event frequency. The results vary between the individual models, especially for the ESI, highlighting that these results might be a function of the different land surface models and coupling.

The results presented here are for the top 10cm layer of soil only. Being confined to the upper 10cm soil layer due to the daily time scale available from the selected CMIP5 models limits the result's application to actual FD events which are defined by the impact on the root-zone layer soil moisture (Otkin et al., 2018). However, as described in Section 4.3, soil moisture for the deeper layers was not available at the daily time step necessary for the analysis of flash drought. Future CMIP generations with more frequent root-zone layer soil moisture outputs would help to investigate this further. All thresholds and time periods specified for FD identification in this study were empirically derived after testing the definition from Ford and Labosier (2017) as not suitable for the top 10cm layer. Consequently, modifying them based on a newly published FD perspective paper from Pendergrass et al. (2020) could lead to more comprehensive results at least for the EDDI, which was used as a reference in that publication. As our study is a first in identifying FD in CMIP5 models, our approach will serve as an example for future studies. Further investigation is urgently needed using observational data in order to determine whether the detection capabilities of ESI, EDDI and SPI in the CMIP5 models are representative of reality.

---

## Chapter 5

# Flash Drought Detection in Models and Observations over Australia

---

### 5.1 Preface

Flash droughts, defined as a rapid decline in soil moisture from non-drought to severe drought conditions in a matter of weeks, are a potential threat for Australia because of their high agricultural impacts. Vulnerability to flash drought is largely due to the continent's large variability in precipitation and high evaporation rates. Understanding the physical processes causing flash drought is key for developing a suitable tool for flash drought detection and early warning. The highly dynamic nature and strong land-atmosphere coupling of flash drought present a unique challenge for the prediction and monitoring of this particular type of drought. In models, characteristics of the land surface schemes such as soil water retention capabilities characterised by soil type and vegetation cover, play an important role in soil moisture variability and the development of flash drought but are highly localised. Consequently, these characteristics can only be parametrised in a model. Chapter 4 has shown that CMIP5 models show different levels of skill in flash drought detection using different drought indices based on partitioning of energy fluxes from the land surface, highlighting fundamental differences in land-atmosphere interactions between different models. Here, we compare those results to

the same metrics derived from the Bureau of Meteorology's land surface observational reanalysis data, computed from the water balance model AWRA-L. The results show differences in flash drought frequency and in the skill of the detection of flash drought using the SPI, EDDI and ESI indices. These differences in skill are associated with differences in land-atmosphere coupling in CMIP5 and the observations/reanalysis. This leads to different response times of energy and moisture fluxes, which ultimately lead to different representations of flash drought dynamics. Due to the limitations of available soil moisture data in CMIP5 to the daily 0-10cm soil layer only, we use daily 0-10cm and 0-100cm root-zone level soil moisture of AWRA-L in a second analysis to examine the differences and similarities between both layer depths. For the root-zone layer soil moisture, the skill of flash drought detection in ET-based indices increases markedly compared to the shallow soil layer while precipitation remains a strong early indicator for flash droughts.

## 5.2 Introduction

Drought has always been particularly challenging for monitoring and prediction due to the complexity of its causal mechanisms and land-atmosphere interactions ([Mishra and Singh, 2010](#); [Pulwarty and Sivakumar, 2014](#)). Prediction is particularly challenging for so-called "flash drought" ([Svoboda et al., 2002](#)) because of its sudden onset and rapid intensification over as few as a couple of weeks. This sub-seasonal time scale is challenging for research as well as current drought-coping mechanisms implemented in policies ([Pendergrass et al., 2020](#)). In order to improve prediction, a better understanding of the compound and cascading physical processes associated with flash drought is needed, especially with the likely increase in drought with a warming future climate ([Seneviratne et al., 2012](#)). Global coupled models offer some insight into drought processes and how they are represented by particular models. The results from six CMIP5 ([Taylor et al., 2012](#)) models in the previous chapter show that they differ widely in their representation of flash drought, possibly caused by differences in the interactions and feedbacks of land-atmosphere processes ([Koster et al., 2004](#); [Guo et al., 2006](#)).

In this chapter, we use the results found in the CMIP5 models (Chapter 4) and compare them to observational and reanalysis data over Australia using common drought

indices, which are discussed in the previous chapter and presented in more detail in Section 2.2.2. We use the term reanalysis for some data, as they are still based on modelled data that are fed with observations as no direct observations are available (see Section 5.3).

While drought can affect most regions on Earth (Mishra and Singh, 2010), regions in the subtropical high-pressure belt, such as Australia, are of particular interest for flash drought due to their high variability in rainfall and high evaporative rates year-round (Seneviratne et al., 2010). Drought is a reoccurring characteristic in Australia's climate and has been well investigated in terms of characteristics, climate drivers and variability (Verdon-Kidd and Kiem, 2009; Ummenhofer et al., 2011, 2009; Mpelasoka et al., 2008; van Dijk et al., 2013; Gallant et al., 2013). However, there have been few studies on Australian flash drought (Nguyen et al., 2019), making them an under-studied phenomenon in Australia. Nguyen et al.'s case-specific research examined the January 2018 flash drought in South Queensland using the ESI; the standardized anomaly of the actual evapotranspiration to potential evapotranspiration ratio (see Section 2.2). They showed that the ESI might be a capable tool for flash drought monitoring as its change anomalies tend to lead the event by up to one month.

Comparing the CMIP5 models to observation hand reanalysis provides information on the efficacy of the models and on flash drought dynamics. Section 5.3 provides a brief description of the land surface model and the procured inputs. Section 5.4 discusses some details of the drought indices computations and how they differ for this particular study from the previous chapter. The results are presented in Section 5.5, separated into flash drought in AWRA-L and the comparison to CMIP5. Additional analyses concerning the root-zone layer is discussed in section 5.6, followed by concluding remarks in section 5.7.

## 5.3 Data

The procured CMIP5 models and corresponding outputs used to calculate the indices are identical to those used in Chapter 4 and listed in Table 2.4. For the comparison with results from AWRA-L and AWAP data, the domain was simply cropped to the extent of the Australian continent.

The Australian Bureau of Meteorology (BOM) has developed the Australian Water Resource Assessment Landscape (AWRA-L, currently version 6, see Chapter 2.1 for details) model fed with station- and satellite-based observational data to generate ET fluxes on a high spatial and temporal resolution (Frost et al., 2018). While this is practically still model-based, the data is generated using observations from AWAP, a high-resolution spatial climate dataset using *in situ* observations from gauges spread across Australia (Jones et al., 2009, see Chapter 2.1 for details), applied to a land surface model. The model output was compared with AWRA-L data interpolated to a common grid of  $2.5^\circ \times 2.5^\circ$  over all Australian land points.

AWRA-L v5 has been evaluated by comparing it to data from flux tower sites and soil moisture estimates from *in-situ* networks and has been found to strongly agree with those *in-situ* measurements for the top 10cm soil layer (Holgate et al., 2016) as well as for the deeper 0-100cm soil layer (Frost et al., 2015).

In this study, the AWRA-L (version 6) water storage values from the top (0–10 cm) and shallow (10-100cm) layer have been utilised. Furthermore, crop reference evapotranspiration (PET), precipitation and the ESI, as used in Nguyen et al. (2019) were provided by the BOM. The ESI uses the sum of evaporation and transpiration for ET and PET from the AWRA-L model output to calculate their ratio.

## 5.4 Methods

The methods employed to calculate SPI and EDDI are explained in detail in Chapter 2. Essentially, the SPI solely requires precipitation from which it simply compares it to its multi-year average. The same methodology is applied to soil moisture to calculate the standardised soil moisture index (SSI). EDDI is calculated from potential ET (PET), which has been calculated by the BOM using the Penman-Monteith equation as stated in Allen et al. (1998) and was introduced in Section 2.2.1. While EDDI, SSI and ESI use output from AWRA-L, the SPI is calculated from AWAP precipitation.

Daily SPI, ESI, EDDI and SSI outputs from the CMIP5 models and AWRA-L/AWAP have been smoothed with a moving average over 28 days to reduce the noise from strong daily fluctuations, especially in precipitation and PET. This smoothing also makes the data directly comparable to the ESI computed by Nguyen et al. (2019), who computed

daily running means of ET and PET over 4-week windows before standardisation. All data were then standardised using a non-parametric approach by [Farahmand and AghaKouchak \(2015\)](#) to make all indices inter-comparable (see Section 2.2.2.2). Those were then translated into categories based on the percentile ranks according to the EDDI guidelines shown in Table 2.5, Section 2.2, classifying dry (ED, "EDDI dry") and wet (EW, "EDDI wet") conditions. We use these categories to define a consistent state of each index during the onset of a flash drought.

The definition for a flash drought remains the same as in Chapter 4 and is explained in more detail in Section 4.4 of that chapter. That is a decrease in the soil moisture (SSI) from above the 40<sup>th</sup> to below the 10<sup>th</sup> percentile within 14 days, which is a modification of a definition from [Ford and Labosier \(2017\)](#) and corresponds to a two-category change in EDDI categories as proposed in a definition by [Pendergrass et al. \(2020\)](#) for operational use in the United States. This definition is applied to the daily 0-10cm AWRA-L soil moisture level. Additionally, we look at the flash drought results in the AWRA-L data using the deeper 0-100cm soil layer. [Otkin et al. \(2018\)](#) describe this layer as needing to be affected for a flash drought to occur. An AWRA-L based comparison using two definitions on different soil depths will show how the detection skill of the drought indices change and will give implications if the top 10cm can be sufficient to detect flash drought. For the deeper layer, we can also make use of the original flash drought definition from [Ford and Labosier \(2017\)](#), which is a decrease in root-zone layer soil moisture from above the 40<sup>th</sup> to below the 20<sup>th</sup> percentile within 20 days. The thresholds differ to account for the delayed propagation of precipitation into deeper soil layers which dampens the signal ([Entekhabi et al., 1996](#)) (Figure 5.1).

The result is a flash drought climatology for each index from which we derive the flash drought event frequency per decade for each season in the same way as was achieved for the CMIP5 models in Chapter 4. The SSI from the AWRA-L is used as the reference variable for flash drought. Using those climatologies, we determine the category of each of EDDI, ESI and SPI at the onset of a flash drought as defined using the SSI as well as the rates of change for two, four, six and eight weeks prior to the onset. The change in categories per week identifies the time period in which the specific index decreases the most.

Flash droughts defined using each of the drought indices were compared using the

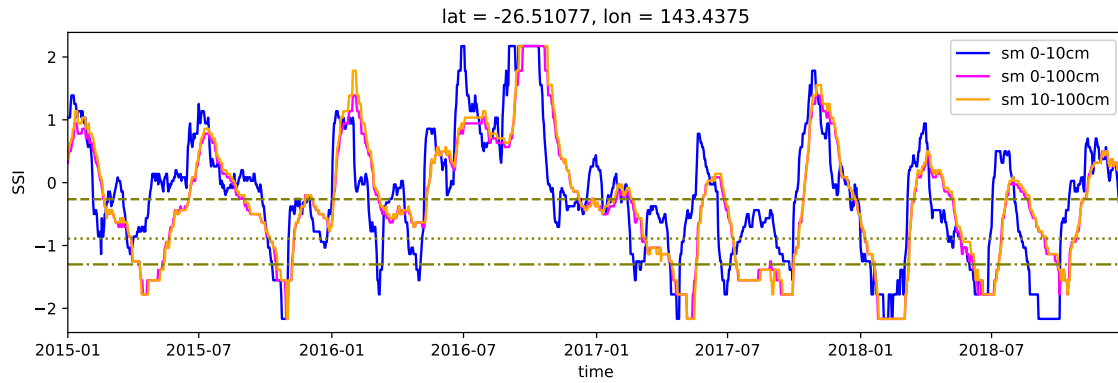


**Figure 5.1:** Time series of daily 0-10, 0-100 and 10-100cm soil moisture expressed in unitless values of the standardised soil moisture index (SSI) for a grid cell in south Queensland. The flash drought observed in this area in January 2018 was subject of [Nguyen et al. \(2019\)](#)'s study. The dashed line represents the 40<sup>th</sup> (top), the dotted line the 20<sup>th</sup> (middle) and the dash-dotted line the 10<sup>th</sup> (bottom) percentile index values. Data was smoothed with a 30 days running mean before standardisation.

same dichotomous forecast metrics as in Chapter 4. False alarm rate (FAR) and hit rate (HR) are computed from the parameters of a contingency table (Table 4.1) using equations 4.2 and 4.3 respectively. Results from AWRA-L and CMIP5 were compared in terms of their FD event frequency, representation of soil moisture flash droughts in EDDI, SPI and ESI and rates of change as well as detection skills of those indices. The additional analyses of the 0-100cm AWRA-L soil layer is handled independently but compared to AWRA-L's 0-10cm soil layer in regard to the mentioned metrics. The flash drought of January 2018 in southern Queensland as discussed by [Nguyen et al. \(2019\)](#) will serve as an example.

We compare AWRA-L v6 and CMIP5 on a grid-cell basis. Therefore, all AWRA-L, AWAP and ESI are bilinearly regridded from their native fine resolution grids of  $0.05^\circ \times 0.05^\circ$  to  $2.5^\circ \times 2.5^\circ$  to match the common grid size of CMIP5 before we conduct the analysis.

## 5.5 Results

First, the event frequency of flash drought using AWAP observations and AWRA-L reanalysis over the Australian domain are examined. The results are then compared to those from CMIP5 models shown in Chapter 4. An AWRA-L and AWAP internal comparison of top (0-10cm) versus shallow (10-100cm) soil moisture levels based on a flash drought case study from January 2018 are then presented.

### 5.5.1 Flash drought in AWRA-L

#### 5.5.1.1 Representation of SSI flash drought in EDDI, ESI and SPI

The variance explained ( $r^2$ ) between the AWRA-L EDDI, ESI and SPI with the top 10cm SSI at the grid point level was computed for each season and is presented in Figure 5.2. Overlaid stippling shows where  $r^2$  shows significant similarities at the 95% level. Across seasons, the SPI displays the highest  $r^2$  values of around 0.7 to 0.9, meaning that soil moisture in the top 10cm is heavily dependent on precipitation variability. Both the EDDI and ESI have weaker co-variability with the SSI and vary more between the seasons than the SPI, which only loses some skill in the north of the continent in the winter season (JJA), which is the climatologically dry time of the year with no or very little rainfall. During this time of year, ESI and EDDI also have their weakest skill and only show significant correlations in a band between around 30°S and 20°S. Moving into the spring season (SON), the correlations increase towards the south while the north is still in the dry season. During the summer (DJF), most of the continent shows

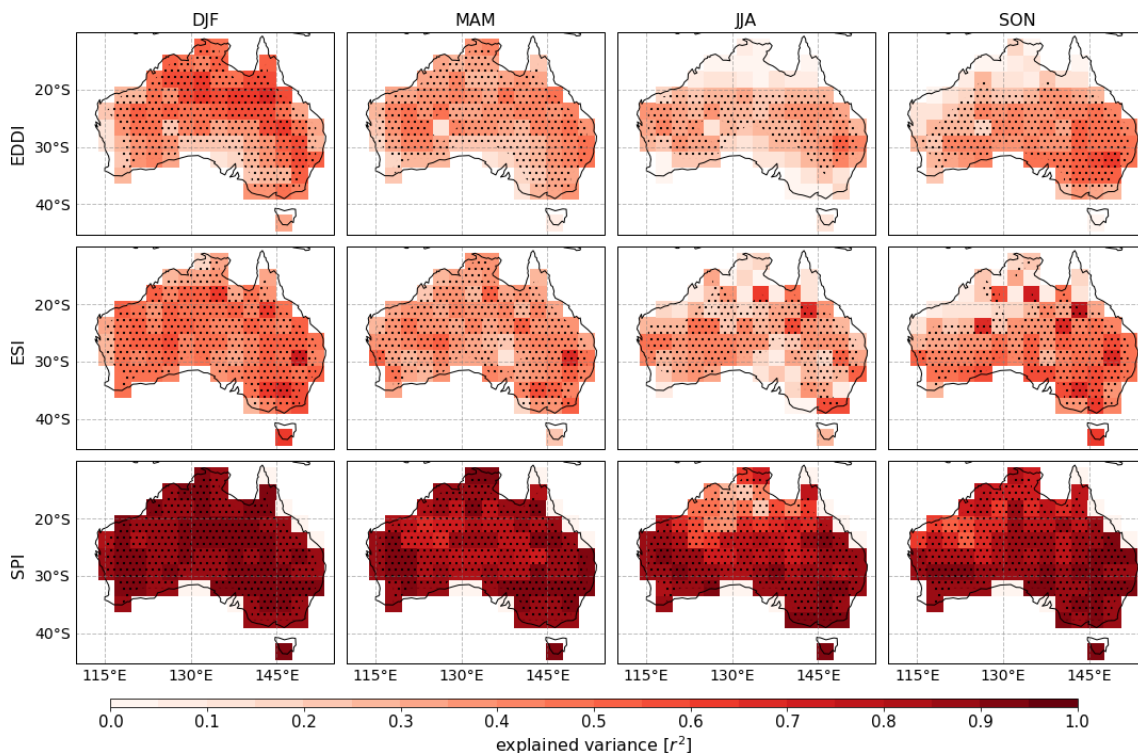


**Figure 5.2:** Seasonal explained variance of EDDI (top row) , ESI (middle) and SPI (bottom) with 0-10cm SSI for 1976 to 2018. Stippling marks where the explained variances are significant at the 95% level. The lag/lead at which this highest correlation was detected is shown in figure 5.3.

5.5. Results

statistically significant similarities between all three indices and the SSI. Subsequently, the skill slightly decreases again during the autumn season (MAM). Generally, the ESI has a slightly better skill over southern Australia, than the EDDI.

The correlations in Figure 5.2 show the maximum cross-correlation when each drought index was moved along the time axis relative to the SSI from -14 to +14 days in two day increments. Figure 5.3 shows the lag at which the maximum correlation in Figure 5.2 occurred. A negative lag means that the signal in the particular index is delayed, a positive lag that it is leading the SSI signal. Obviously, soil moisture cannot respond to the precipitation before it occurs, hence, a negative lag for SPI is not possible. However, as the top soil layer receives the precipitation directly and loses its moisture quickly when rain eases, there is also little to no lead time and most of the domain has a lag of zero days. For the EDDI, the response in the SSI is also typically concurrent with exception of the southern half of the continent during MAM and JJA, where a small delay of 2-4 days is observed. Here, ET is less sensitive to changes in soil moisture and the shallow top soil layer might lose its water mostly through runoff than through evaporation. The ESI is in a stark contrast to EDDI and SPI as it shows a lag of 4 to 14 days to the top

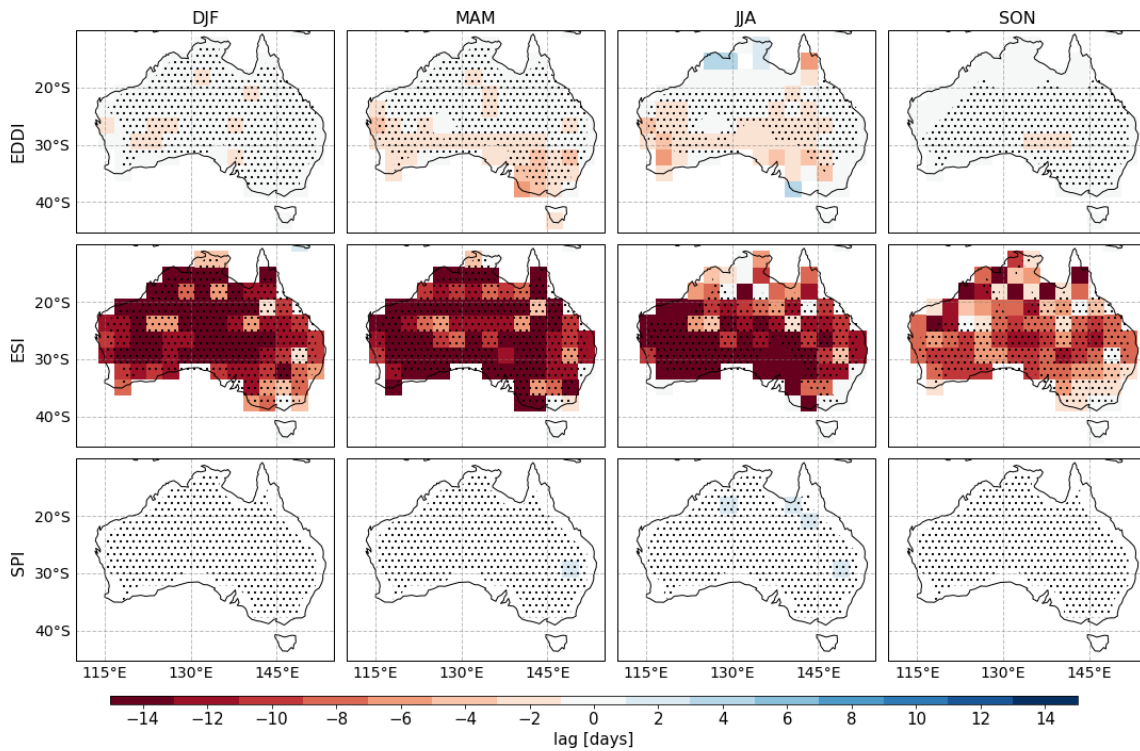


**Figure 5.3:** Lag at which the maximum explained variances shown figure 5.2 occurred for EDDI (top row), ESI (middle) and SPI (bottom). Stippling marks where the explained variances are significant at the 95% level.

5.5. Results

10cm soil moisture level. This persists throughout all seasons with a slightly smaller lag of 4-8 days during spring. The ESI's actual ET from AWRA-L also takes plant conditions into account. This means that ET being modulated not only from atmospheric conditions, but also from plant roots accessing deeper level moisture and so continuing transpiration, regardless of the upper level soil moisture.

Figure 5.4 shows the frequency of flash drought events per decade for each season and index in the upper 10cm soil moisture level when the condition of a decrease from above the 40<sup>th</sup> to below the 10<sup>th</sup> percentile within 14 days is applied to each grid cell of the indices' time series. It is noticeable that the ESI in the third column of the figure identified the fewest flash droughts with many grid cells remaining empty. It is followed by the EDDI which yields mostly between 0.5 to 2 events per decade for each season with little variability throughout the year. The EDDI tends to identify more flash droughts

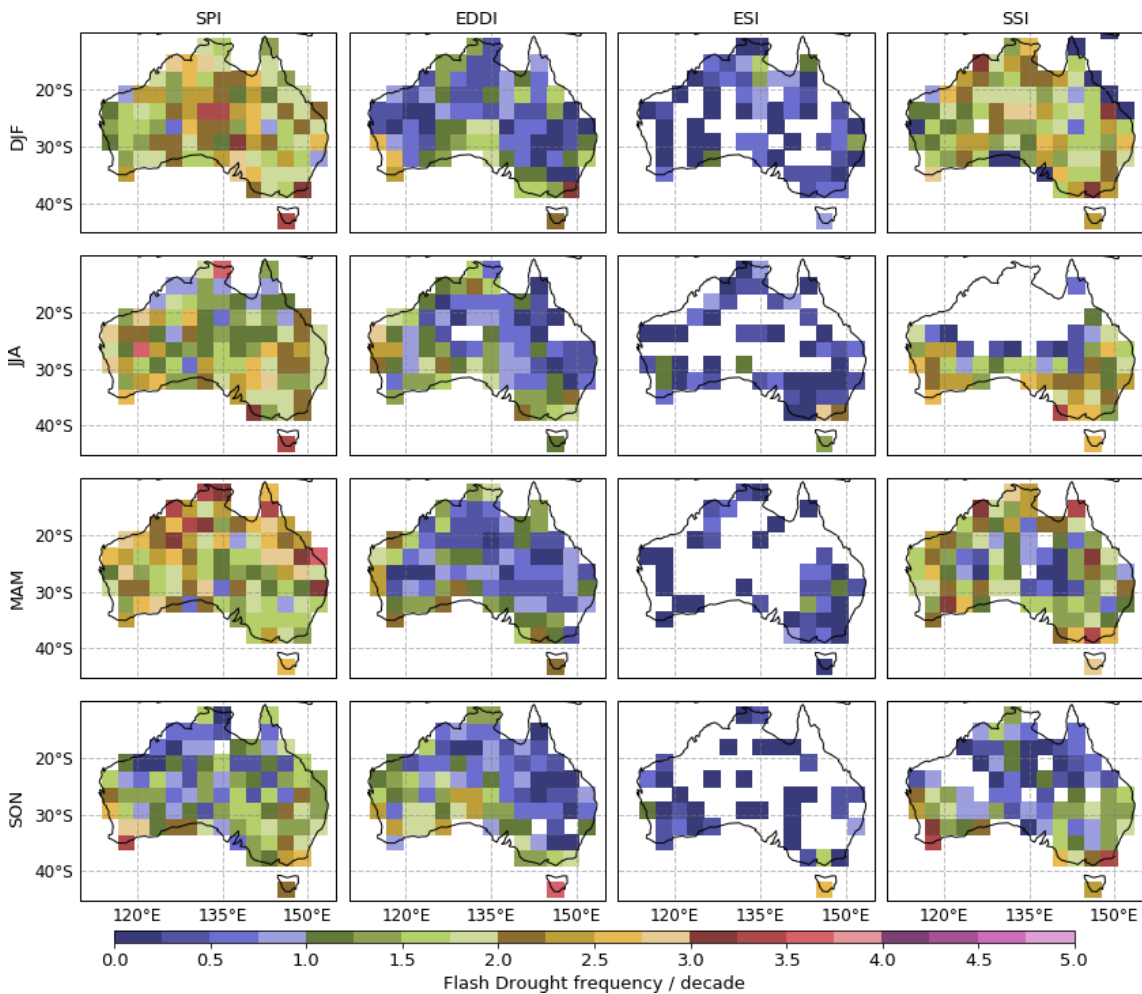


**Figure 5.4:** Seasonal FD event frequency expressed as events per decade for SPI (first column), EDDI (second), ESI (third) and SSI (fourth) over the 39 years of the time period from 1976 to 2018.

in the west and south of Australia with few in the northeast and east. Flash droughts in the SPI are generally more frequent with up to 3.5 events per decade for some grid cells but also present a stronger seasonality. In the SPI, flash drought events are more frequent in DJF and MAM and least in SON, with a north-south gradient. In fact, of all indices the distribution and pattern of event frequency of the SPI is closest to the SSI based on the top 10cm of soil, particularly for SON and DJF. This is particularly the case for SON and DJF. Flash droughts do not occur north of 25°S in the dry season in the SSI but they do in the SPI and EDDI. However, assessing those in the dry season would be inappropriate.

The coincidence of flash droughts in soil moisture and the EDDI, ESI and SPI provide an indication of their skill for flash drought monitoring and detection. We examined this by selecting the flash droughts identified in the soil moisture using the SSI. We then compared how the events in the SSI were represented by the EDDI, ESI and SPI in a two-fold way. First, by comparing the index category (Table 2.5) at the onset of the flash drought in the SSI, which is when the 10th percentile in soil moisture is surpassed represented by a drought category of ED2; and second, the rate of change (RoC) in the drought index 2-6 weeks prior to the onset of the flash drought as defined by the SSI.

Figure 5.5 displays the mean drought category in the SPI, EDDI and ESI on the day of flash drought onset in the SSI. The indices are masked by the occurrence of flash droughts in the SSI as only those instances can be examined. The aforementioned lag of the ESI means that it descends into dry conditions later than in the SSI. In fact, the ESI is typically still in neutral to wet categories on the day the flash drought was detected in the SSI (bottom row). These results are independent of the season. The EDDI mostly reaches ED0 (abnormally dry) to ED1 (moderately dry) with the exception of JJA where slightly more neutral conditions are observed in the south of the country. Due to its strong co-variability with the SSI, the SPI shows consistently dryer categories than ESI and EDDI. These are mainly ED2 (severely dry), which correspond to the lower 10<sup>th</sup> percentile of the index and thus qualify as a flash drought. Based on this, the SPI shows the best representation of flash drought in the upper level soil moisture when looking at the onset values. This applies across all seasons.

Figure 5.6 displays the RoC per week of each index from 14 days prior until the onset of the flash drought in the top 10cm soil moisture. A strong, negative RoC indicates

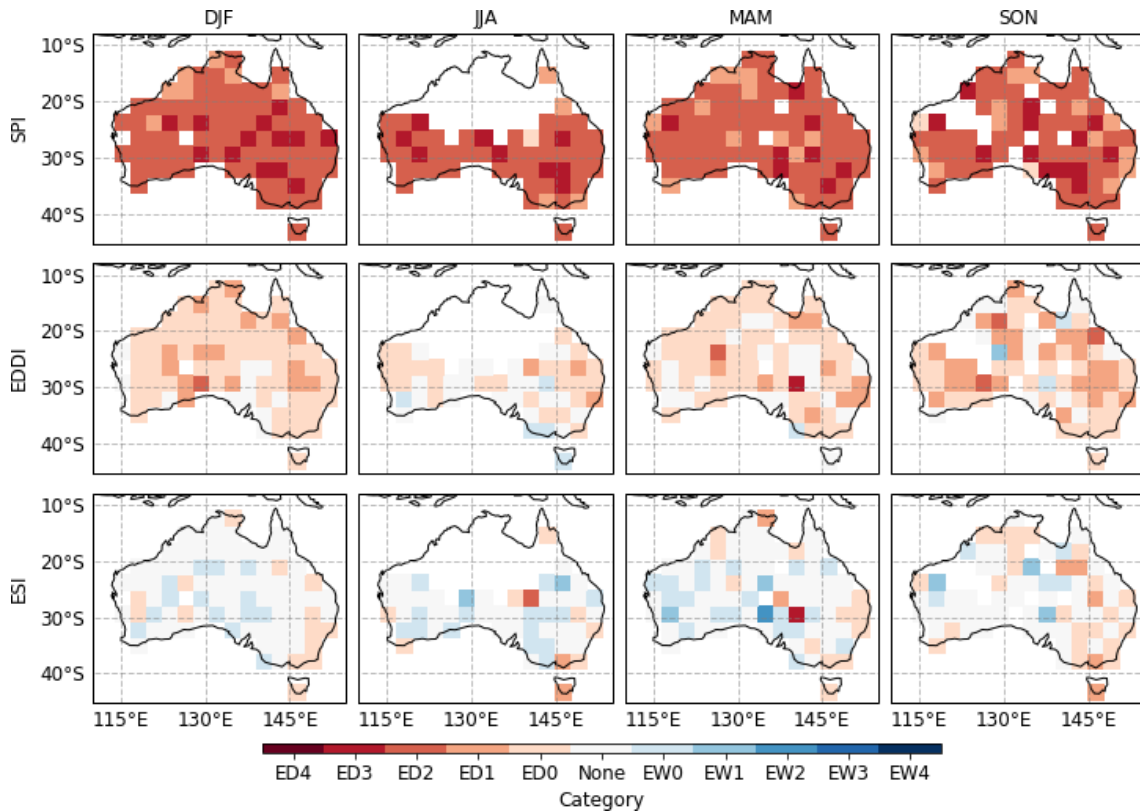


**Figure 5.5:** Index categories at the time when a flash drought was detected in the soil moisture (SSI). The values shown are the average of all instances in each season and for each index, SPI (top row), EDDI (middle) and ESI (bottom), over 43 years from 1976 to 2018. White grid cells did not experience soil moisture flash droughts.

rapidly changing conditions towards drying. With the very dry conditions shown by the SPI at the onset of the flash drought, it is no surprise that it also shows the strongest RoC per week in comparison to EDDI and ESI. However, all indices show their strongest decline in the two weeks prior to flash drought onset. The average RoC magnitude is smaller when longer time periods, such as four, six and eight weeks are considered (Figures 5.7, 5.8, 5.9), showing that the intensification in drying in all indices is most prominent in the two weeks prior to flash drought onset. This means that all indices capture the rapid intensification of dry conditions. Again, there are few differences between seasons.

Using the flash drought climatologies from each of the EDDI, ESI and SPI, we estimate the event detection skill using the contingency table (Table 4.1) described in Section 4.4 of Chapter 4. We calculated the ratio of instances when an index yields a flash drought in the eight weeks before the flash drought was detected in the SSI. This gives us the hit ratio (HR). The false alarm rate (FAR) is determined by the ratio of instances when the index yields a flash drought but none was observed in the SSI in the

5.5. Results

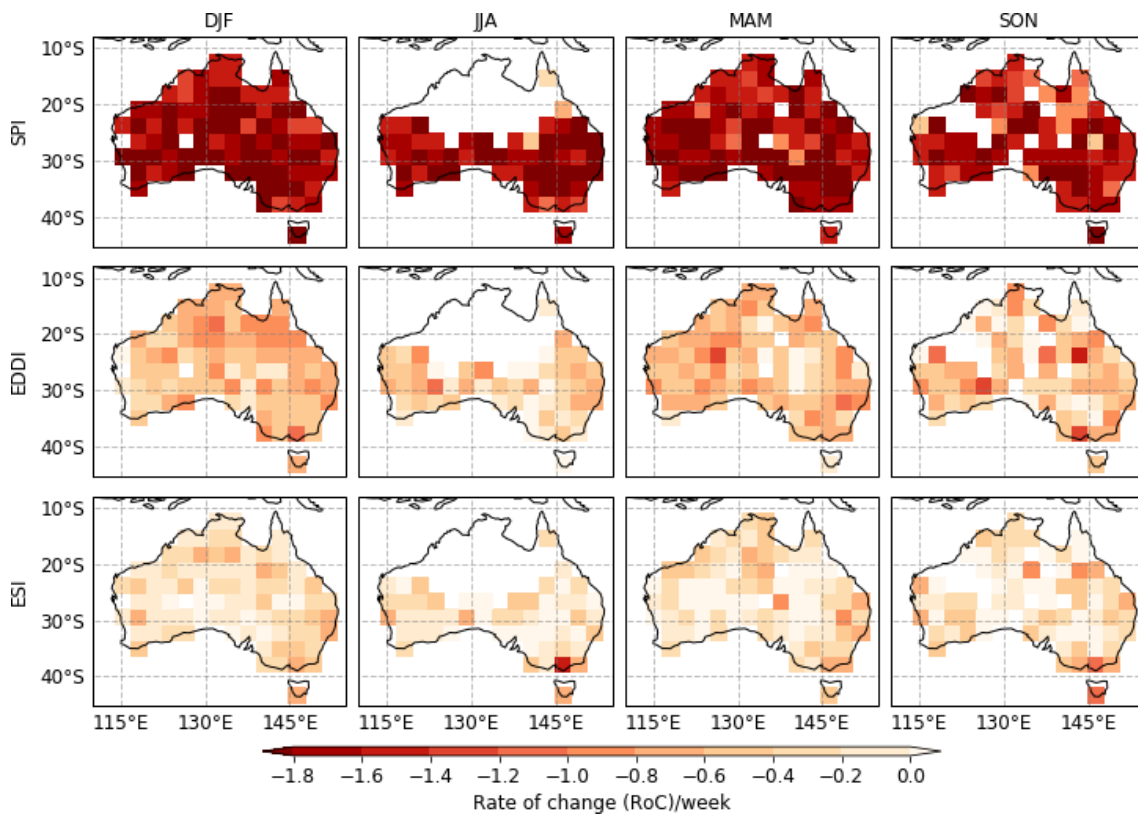


**Figure 5.6:** Rates of change (RoC) expressed in "categories per week" for each index in each season. The are calculated as the difference between the index's category at the onset of a flash drought in the soil moisture and the value two weeks prior to that. The result is divided by the number of weeks to achieve a "per week" change unit. The values shown are the average of all instances in each season and for each index, SPI (top row), EDDI (middle) and ESI (bottom), over 43 years from 1976 to 2018.

eight weeks following flash drought onset in the index. Panel A of Figure 5.10 shows the HR for each index split into seasons while panel B presents the FAR. Ideally, the index should have a high HR and a low FAR in order to be a capable flash drought prediction tool. This is represented by a darker colour for each detection skill metric in Figure 5.10.

The good agreement between SPI and SSI found previously, supports the result in Figure 5.10 that the SPI has the highest HR and lowest FAR in comparison to the EDDI and ESI. However, the magnitude of the skill metrics change across the country and there are also seasonal variations. For example, while the HR in some parts of the southeast of Australia is around 70% in JJA, MAM and to some extent in DJF, its magnitude halves in these regions during SON. The austral spring season is generally characterised by a weaker skill over the whole Australian domain. The EDDI and ESI both have significantly weaker HRs and much higher FARs compared to the SPI in all seasons, with around 0-10% and 60-100% respectively. The strong delay of the ESI in regards to the

5.5. Results

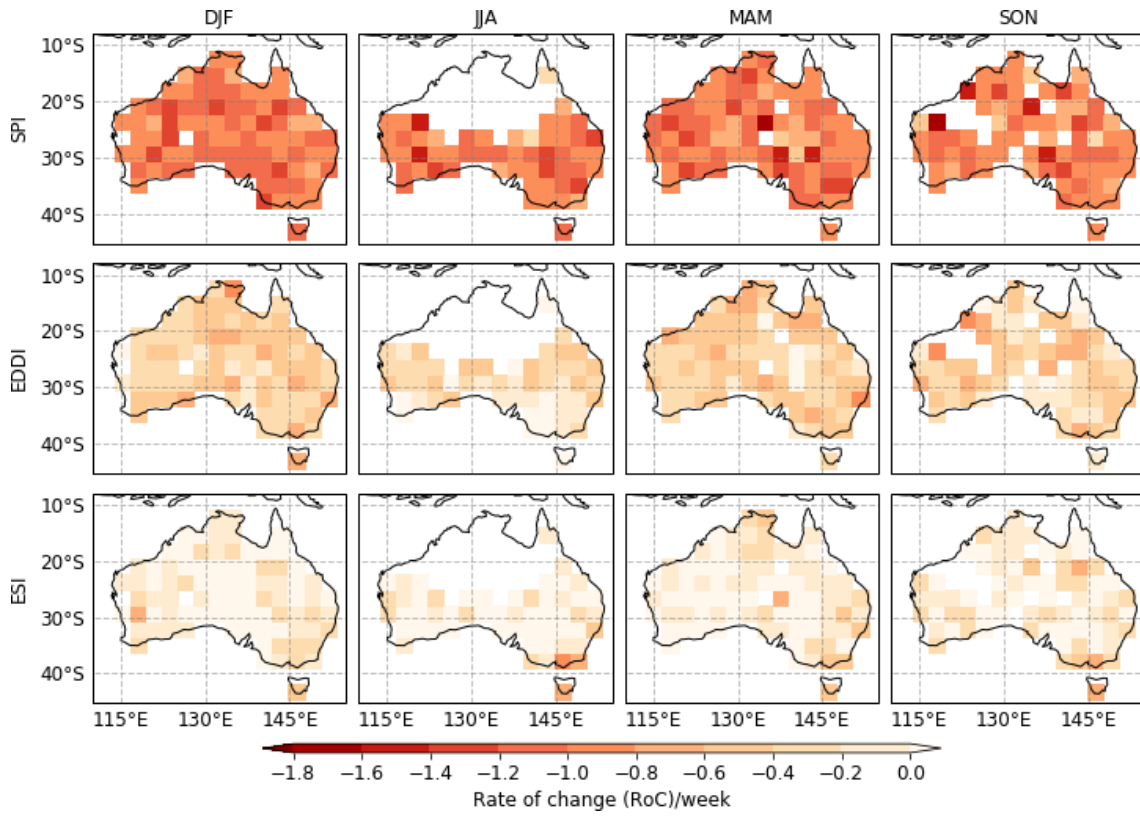


Figure 5.7: As figure 5.6 but for four weeks prior to the onset of flash drought in the SSI.

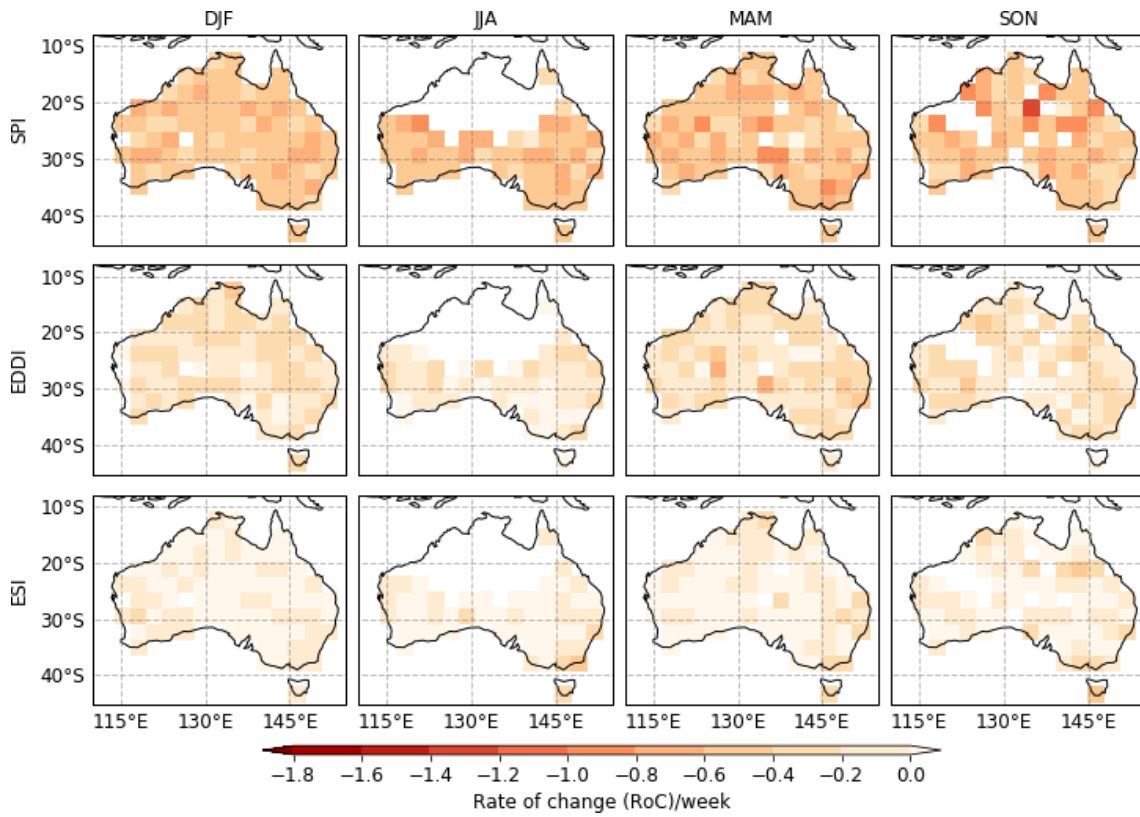
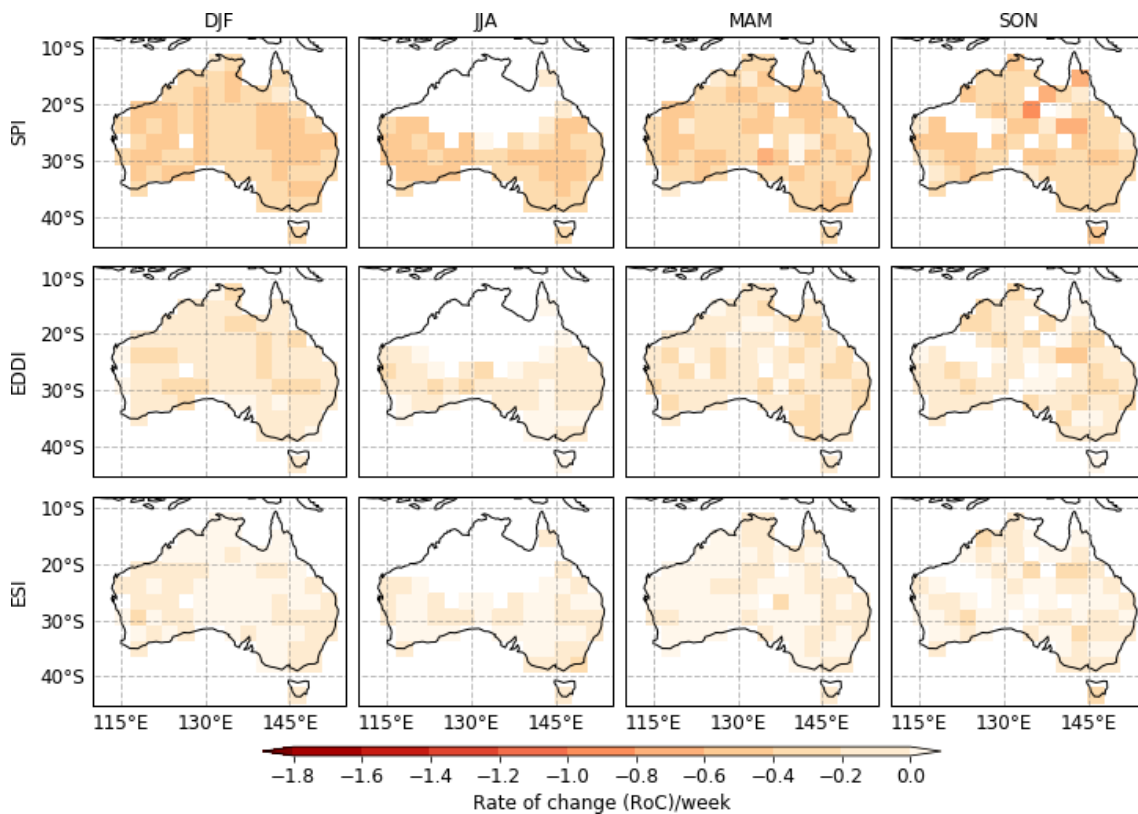


Figure 5.8: As figure 5.6 but for six weeks prior to the onset of flash drought in the SSI.

5.5. Results



**Figure 5.9:** As figure 5.6 but for eight weeks prior to the onset of flash drought in the SSI.

top 10cm SSI shows that flash droughts in the upper level of soil cannot be detected in the ESI before they are detected in the SSI. This is due to the modulation of ET in the ESI from plants accessing deeper soil moisture. Additionally, the flash drought event frequency as computed from the ESI is extremely low across the entire domain and events in the ESI are absent in many places hindering any detection. The EDDI is able to predict a low fraction of 20% of the soil moisture flash drought in the east of Australia during DJF and MAM. Here, despite the low HR, the FAR is comparatively low due to the index's low flash drought event frequency in this area.

Extending the tolerance window for detection to within two weeks after the FD onset in the SSI shows few changes (Figure 5.11). In some instances, across the Australian domain the HR of the EDDI improves by approximately 20-30% during DJF and SON. However, improvements in flash drought detection in the ESI are limited to only a hand full of grid cells, with the increase in HR reaching a maximum of around a 20% improvement. The modest improvements are because there is a long lag in the ESI of more than two weeks on average, meaning that even with a larger tolerance window of 2 weeks, flash droughts are still not detected at time of onset in the SSI. Further, the

5.5. Results

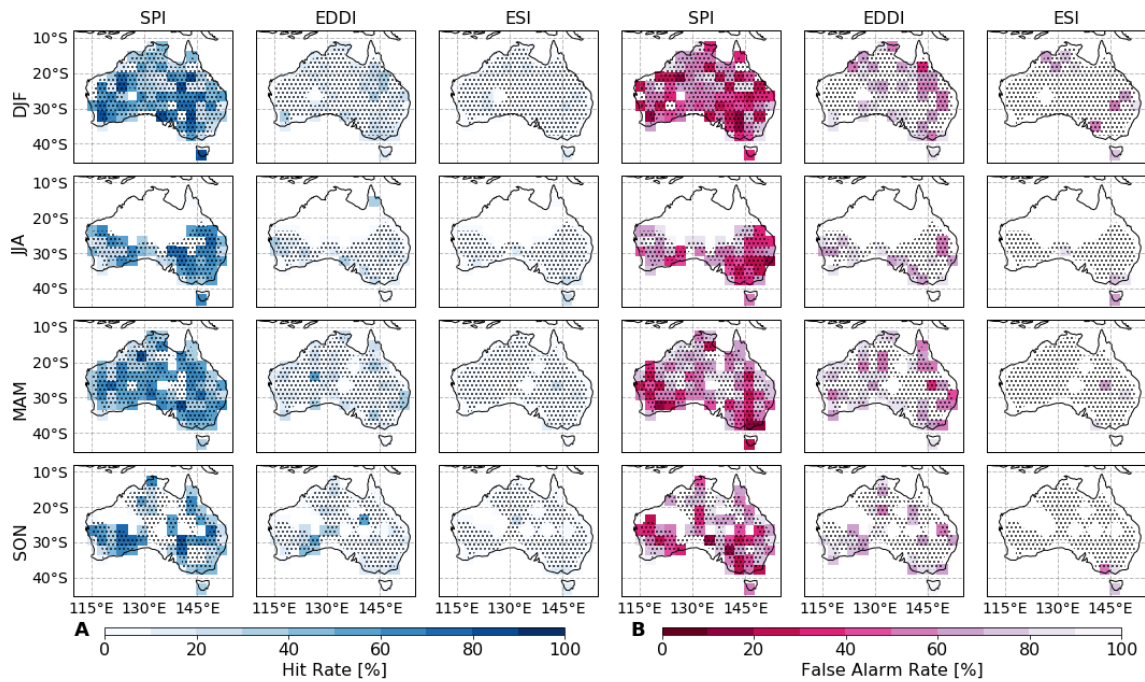


**Figure 5.10:** Hit rate (HR, panel A) and false alarm ratio (FAR, panel B) for SPI (left column), EDDI (middle) and ESI (right). Hatching indicates where the SSI identified a flash drought as seen in figure 5.4. Only here are values for HR and FAR possible. Detection rates were determined using a time window around the flash drought detected in the soil moisture of eight weeks prior to the onset in which the indices can yield a hit.

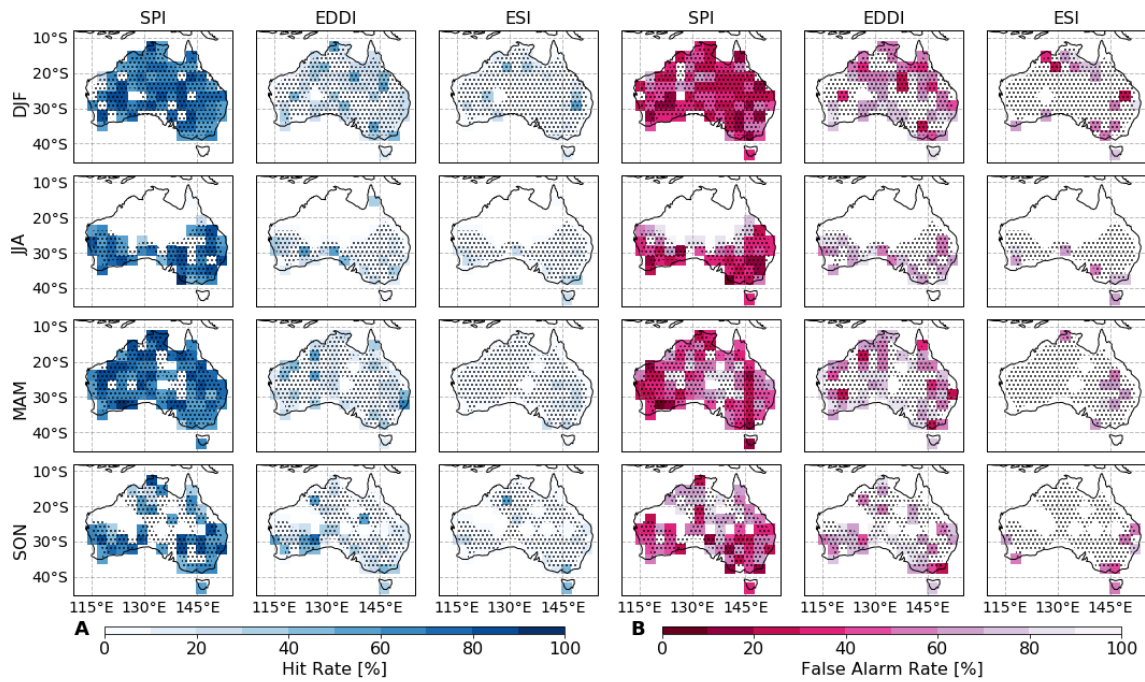


**Figure 5.11:** As described in figure 5.10 above but the time interval is extended by two weeks after the flash drought onset in the SSI happened.

ESI event frequency is small compared to the SSI, restricting the HR because of the differences in the sample sizes of the events from each index.

Expanding the tolerance window to 2 weeks post-flash drought onset in the SSI did not markedly improve the HR and FAR for the EDDI, despite its short lag of 0 to 6 days with the SSI. This suggests that ET is not necessarily the dominant first order effect leading to drying in the top 10cm layer and suggests that other processes, e.g. runoff and percolation, play a significant role.

Interestingly, with the increased tolerance to include the 2 weeks post-onset, the HR of the SPI increases and its FAR decreases. However, there was no temporal lag for the cross-correlation between the SSI and SPI. This suggests that some FDs in the SSI can occur in situations when there is strong persistence in a precipitation time series. Here, while the SSI has dried sufficiently to induce a flash drought, the change in the SPI is coincidentally larger post-FD onset, rather than prior to the FD onset due to persistence of low rainfall anomalies. These few occasions could be accompanied with the strong increasing rates of PET and hence, the occasions when EDDI was a strong contributor to the FD.

Our results show that the SPI has the highest skill for the prediction and early detection of flash drought in the top 10cm soil layer. The results show that the EDDI and ESI underestimate flash drought event frequency when compared to events computed directly from the SSI. Further, any signal that is apparent in the EDDI and ESI lags the SSI signal.

## **5.5.2 Comparison between CMIP5 and AWRA-L/AWAP**

### **5.5.2.1 Relationships between soil moisture and drought indices**

In this section, we show a comparison between the AWRA-L/AWAP analysis in [5.5.1](#) and the CMIP5 analysis in [Chapter 4](#) to evaluate the representation of flash drought in coupled climate models. All of the following figures show the area average of each metric for Australia. This is calculated by taking the mean of each metric, e.g. the mean of the explained variance in all grid cells over the Australian continent. First, the direct and lag correlations between the top 10cm soil moisture and each of SPI, EDDI and ESI are examined.

Figure 5.12 visualises the cross-correlation between the SSI and each index averaged over the Australian domain. The lags and leads are offsets from -14 to +14 days. The graphs show the magnitude of the co-variability on the y-axis and the lead or lag time of the co-variability with the SSI on the x-axis. There are distinct inter-model differences between the CMIP5 models and also between the between CMIP5 models and the AWRA-L/AWAP. The differences within the CMIP5 models have been discussed in the previous chapter. Here, we focus on the differences between models and observations/reanalysis. In AWAP (last column in Figure 5.12), the cross-correlation for the SPI spikes at a lag of 0 and falls sharply with non-zero leads/lags. Its shape remains unchanged and reaches the highest explained variance of all indices with correlations of 0.7 to 0.8 throughout the year. These correlations show the strong relationship between precipitation and soil moisture in the upper 10 cm of soil. Both the ESI and EDDI show much lower explained variances of 0.3 to 0.5 and 0.1 to 0.3 respectively. The lag at which the EDDI correlates best with the SSI is less obvious than for the SPI, while the ESI shows a maximum over several lag times with no distinct spike. The ESI reaches its highest correlation at lag times of 7 (SON) to 14 days (DJF, MAM).

The characteristics in the observations/reanalysis, just described, show stark differ-

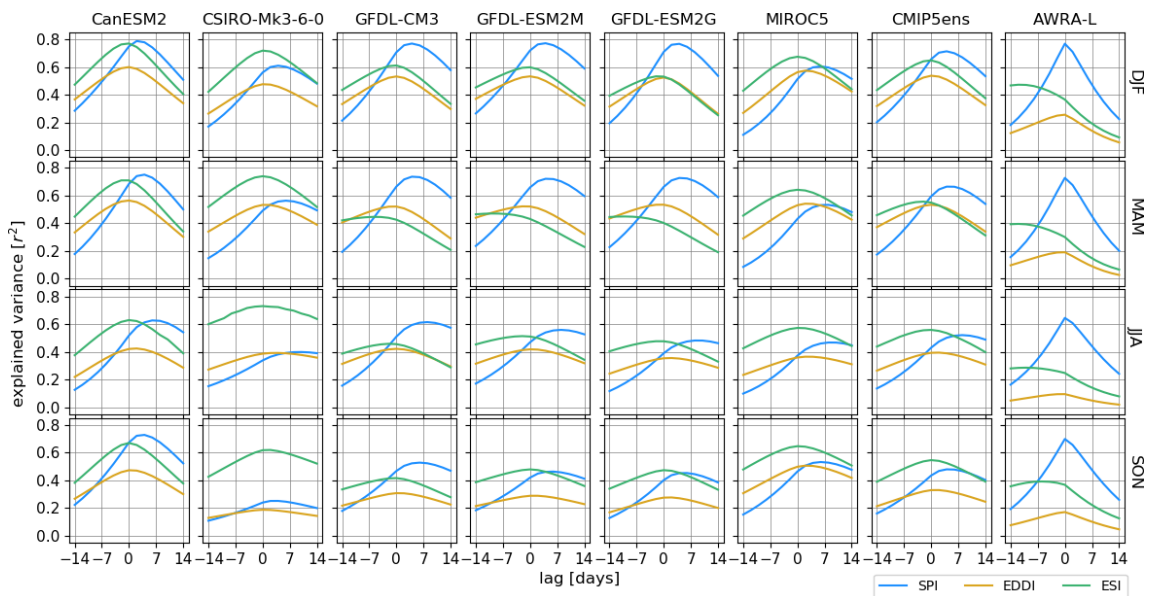


**Figure 5.12:** Cross-correlations for individual CMIP5 models listed in Table 2.4 (columns 1-6), CMIP5 ensemble mean (column 7) and AWRA-L (columns 8). Explained variances are in the y-axis and corresponding lag in days on the x-axis. Graphs are showing the spatial mean of the Australian domain. Positive lag means that the individual index is leading the top 10cm soil moisture while a negative lag means that the index's sign is delayed.

ences to the CMIP5 ensemble mean (second last column in Figure 5.12). Both ET driven indices, the EDDI and ESI, have higher explained variances than the observations in all seasons. The EDDI reaches 0.3 (SON) to 0.55 (DJF, MAM) with a mostly unchanged lag of -2 to 0 days. The ESI reaches maximum correlations of 0.55 to 0.65. However, in contrast to the observations, the ESI has a lag of around a couple of days at most in CMIP5, which is comparable to the EDDI in the models. The ESI is also better correlated to the SSI than the SPI in JJA and SON. The SPI computed from the CMIP5 data shows a weaker correlation to soil moisture when compared to the observations in all seasons. The distinct peak at 0 days also changes to a more flattened curve and has been shifted towards positive leads of 4 to 8 days.

To account for the subtropical climate in the north and the temperate climate in the south of Australia and hence potentially different processes for flash drought, we split the continent in two halves at 27°S latitude (Alexander and Arblaster, 2009). Figure 5.13 shows the area average of explained variance of the northern and southern domain as solid and dashed lines respectively. The AWRA-L/AWAP data have a stronger coupling (by >0.1 larger  $r^2$ ) of the SPI and ET with the SSI in the south during JJA/SON and SON respectively, compared to the north of Australia. In contrast, the CMIP5 model average shows stronger couplings of all indices with the SSI during DJF in the north than in the south. A stronger response is also visible in the south during JJA and SON

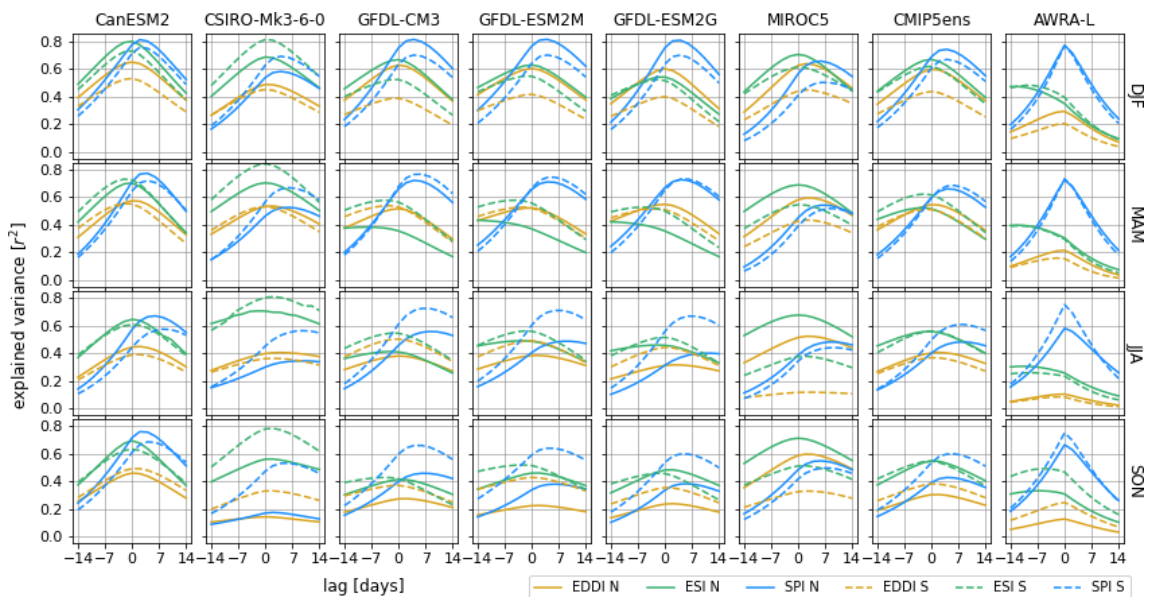


**Figure 5.13:** As figure 5.12 but for southern and northern domains of Australia split at the 27°S latitude. Dashed lines represent area averages of explained variances in the south while those for the north are displayed as solid lines.

for the SPI. Only minor changes in  $r^2$  ( $<0.1$ ) are observed in other seasons. However, larger variations are present for the individual models, even showing changes between north and south in opposite directions. For example, while CanESM2 and MIROC5 indicate stronger coupling of all indices but especially ET with SSI in the south during all seasons, all other models only agree with that change in DJF but are showing the opposite change from MAM to SON. The lag and lead times remain mostly unchanged for all models and observations/reanalysis.

The above provides some insight to the CMIP5 models. The first is that the response of ET to the soil moisture compared to AWRA-L of ET is overestimated in CMIP5 while the direct effect of precipitation on the upper 10cm soil layer is underestimated as indicated by differing lag/lead times and explained variances in comparison to AWRA-L. The lag in the CMIP5 models is shorter and the relationship is stronger between soil moisture and ET while the lead is longer for precipitation but weaker related to soil moisture compared to AWRA-L/AWAP. This could be caused by drizzle every day leading to an underestimation of precipitation variability. In this case ET becomes more "important" because the soil is always a bit damp implying that the modulation in soil moisture is coming more from ET than from precipitation. These results show the relative differences between CMIP5 models and AWRA-L in the importance of ET and precipitation without implying right or wrong.

### 5.5.2.2 Differences in flash drought event frequency

The above differences between the AWRA-L and CMIP5 models show fundamental differences in precipitation and surface fluxes driving soil moisture variability. Consequently, the differences in the representation of the processes fundamental to flash drought are manifest as differences in flash drought event frequency between the models and the AWRA-L reanalysis. The area averaged flash drought event frequency over Australia is shown in 5.14 for each index and model, with the corresponding 90<sup>th</sup> confidence interval displayed by the black line. Only grid cells with at least one flash drought in the climatology were considered, and the confidence interval is computed as the range from the 5th to 95th percentile of frequencies at the grid box level. Taking the mean of all grid cells, rather than mandating they must have at least one flash drought, yields much lower values for ESI and SSI in those instances, where the majority of the grid cells never

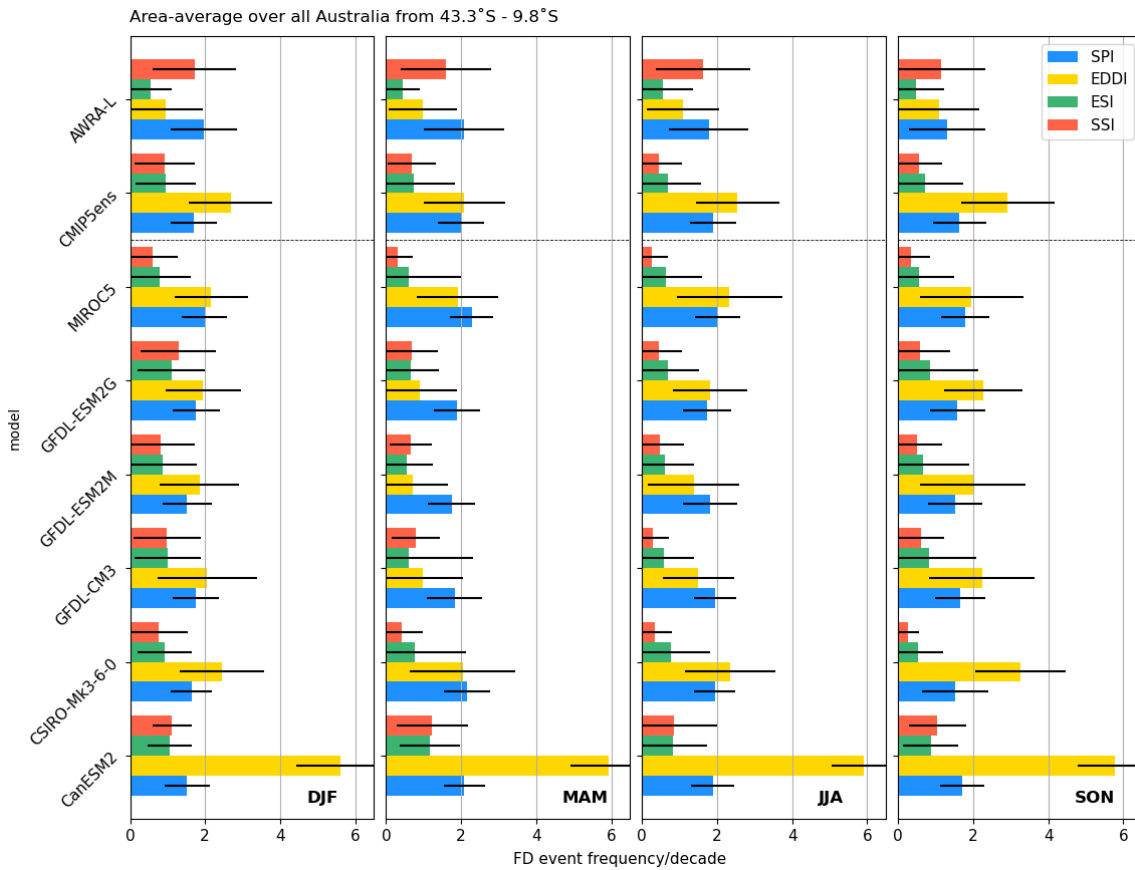


**Figure 5.14:** Area average of Australia of flash drought event frequency per decade for each of EDDI, ESI, SPI and SSI split into season and listed for each CMIP5 model (third to bottom row), CMIP5 ensemble (second row) and AWRA-L/AWAP (first row). Grid cells without any flash droughts occurring were masked out. Black lines represent the 90<sup>th</sup> percentile confidence interval.

experienced a flash drought. Including all grid cells, the median across the continent is zero (see Figure 7.5 in the appendix).

As shown in Chapter 4 and also identified by Mueller and Seneviratne (2014), CMIP5 models overestimate evaporative drought, meaning that they misrepresent the partitioning of energy fluxes from the land surface and ascribe too much weight to the sensible heat flux driving PET. This is reflected in the CMIP5 ensemble’s flash drought event frequency for the EDDI, for which there are 2-3 events per decade, which is double to three times higher than what is found in the AWRA-L reanalysis (Figure 5.14). The CMIP5 ensemble mean is heavily modulated by the CanESM2, which detects almost six events per decade in each season. However, half of the models exceed the EDDI flash drought frequency in AWRA-L by some degree with the exception of the GFDL models in JJA.

Similarly, the event frequency for the ESI is less than 0.5 events per decade in the

AWRA-L reanalysis, but is larger in the CMIP5 ensemble – around 0.5 to 1 events per decade. However, the differences between the models and observations/reanalysis are considerably smaller for the ESI than the EDDI. Considering all grid cells, the area averaged ESI event frequency drops to close to zero for AWRA-L reanalysis because most grid cells in Australia do not experience a flash drought (Figure 7.5). However, this is not the case for CMIP5 models and flash droughts are identified by the ESI over a larger geographical extent.

The area average of the event frequency of the SSI in the CMIP5 ensemble is less than half that of the AWRA-L reanalysis. This suggests that the discharge of moisture in the top 10cm soil layer happens on shorter time scales in the AWRA-L compared to the CMIP5 models. Reasons for the higher discharge could be from a higher moisture flux into deeper soil layers or an increased moisture uptake from vegetation compared to CMIP5 models.

The flash drought frequency computed from the SPI is similar in magnitude for the CMIP5 and AWRA-L data, and is around 1.5 to 2 events per decade. However, while the area average is fairly similar, the 90<sup>th</sup> confidence interval for CMIP5 models is larger than in AWRA-L/AWAP, represented by the black lines in Figure 5.14, suggesting much higher rainfall variability in the observations compared to the models. This larger spatial variability in rainfall is also apparent in the confidence intervals for the SSI (Figure 5.14), again highlighting the strong connection between soil moisture and rainfall.

Splitting the Australian continent into a northern and southern domain along the 27°S latitude shows that slightly more flash drought events are identified in the south but the spatial variability remains similar (see Figs 7.6 and 7.7 in the appendix).

While there is relatively good agreement in precipitation flash drought between CMIP5 and observations, there are clear differences in flash drought event frequency in the ESI and especially SSI and EDDI due to the way the models represent land surface coupling.

### 5.5.2.3 Differences in flash drought onset and rate of change

The lags associated with the times of maximum correlation between the EDDI, ESI and SPI, and soil moisture determines their magnitude at the onset of a flash drought, where the flash drought is defined using the SSI. The median value in each index at the time

of onset of flash drought (i.e. the median as computed from all flash drought events) is calculated for all grid cells independently, when at least one flash drought was detected in the SSI. The median was taken due to the small sample size of flash drought events in many regions for most models and AWRA-L reanalysis and hence to avoid potential skewness (see Figure 7.8 in appendix). The bars shown in Figure 5.15 represent the area average category of those values according to Table 2.5. A more neutral to wet category, e.g. >ED0, implies that the index has not progressed to abnormally dry conditions at the time of onset of flash drought in the SSI. This could be because the response in the index is lagging the soil moisture, or that soil moisture is not strongly coupled to the index. The latter would mean that, for example, ET is not a significant cause of the rapid depletion of soil moisture associated with a flash drought.

A category of ED2 – ED4 represents values below the 10<sup>th</sup> percentile for SPI and ESI and above the 90<sup>th</sup> percentile for EDDI and qualifies as a flash drought onset in the index itself. However, this does not mean that the particular index identified a flash drought for all instances as this metric does not consider the rapidity of change in the index. Equally, large spatial variability can modify the area average value. Therefore, the 90<sup>th</sup> percentile confidence interval is shown as black lines for each bar, where a short line indicates that the category of most grid cells are around the median value. Long lines show the opposite, for example that the indices in some areas are closely coupled to soil moisture in some or are lagging behind more than in others, reflecting largely different categories across the domain.

The CMIP5 models shows some similarities between particular groups of models. The first group encompasses the GFDL models and the second all other models, namely MIROC5, CSIRO-Mk3 and CanESM2. The latter group mainly shows categories of ED1 and drier for all indices with SPI often surpassing ED2. In other words, all indices show a strong drying associated with a lack of precipitation or increased PET. In contrast, the GFDL group only shows the SPI in moderate to severe dry conditions (ED1 to ED2). Both the EDDI and especially the ESI are mostly around the neutral position (None), or slightly leaning towards dryness, represented by a None to ED0 category. For SON, the ESI and partially the EDDI for all GFDL are even on the wet side of the distribution. This indicates that in the GFDL models ET is less important in lowering soil moisture compared to the other models. However, the large range of the 90<sup>th</sup> percentile

5.5. Results

confidence interval in the ESI and EDDI, spanning from ED2 to EW2 indicates that there are very large differences across the Australian domain.

The differences in the median onset categories between the different models becomes more evident when splitting the continent into a northern and a southern domain along the 27°S latitude line. All GFDL models show vastly different onset categories for EDDI and ESI across all seasons in the northern domain compared to the southern domain. While both indices reside on the dry side of the distribution during DJF and

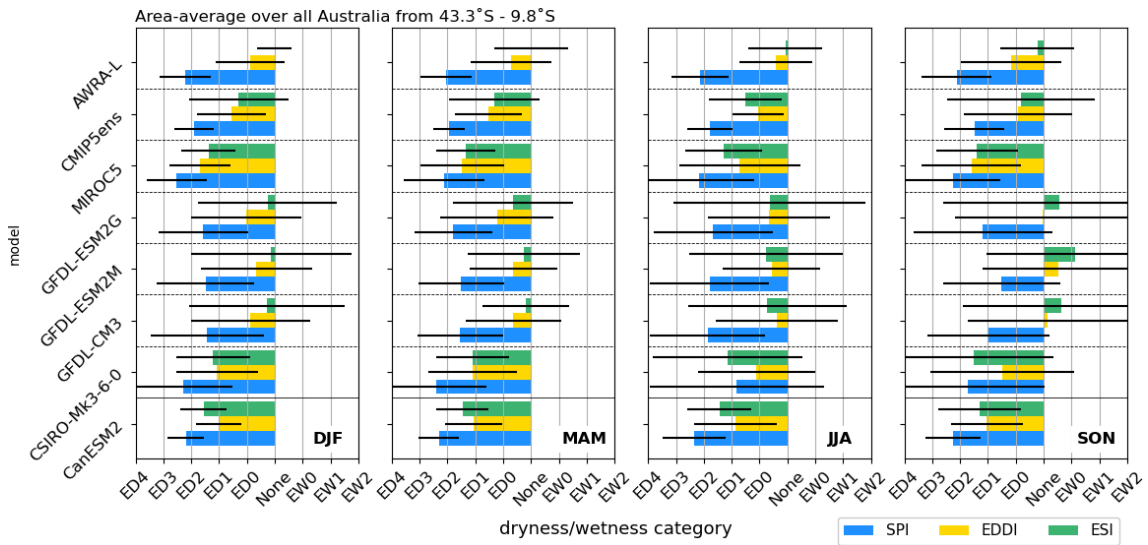


**Figure 5.15:** Area mean across Australia as a whole of index value in dryness/wetness categories from table 2.5 for each of EDDI, ESI, SPI and SSI at the onset of a flash drought in the soil moisture. Split into season and listed for each CMIP5 model (third to last row), CMIP5 ensemble (second row) and AWRA-L/AWAP (first row). Error bars show the standard deviations across the Australian domain.

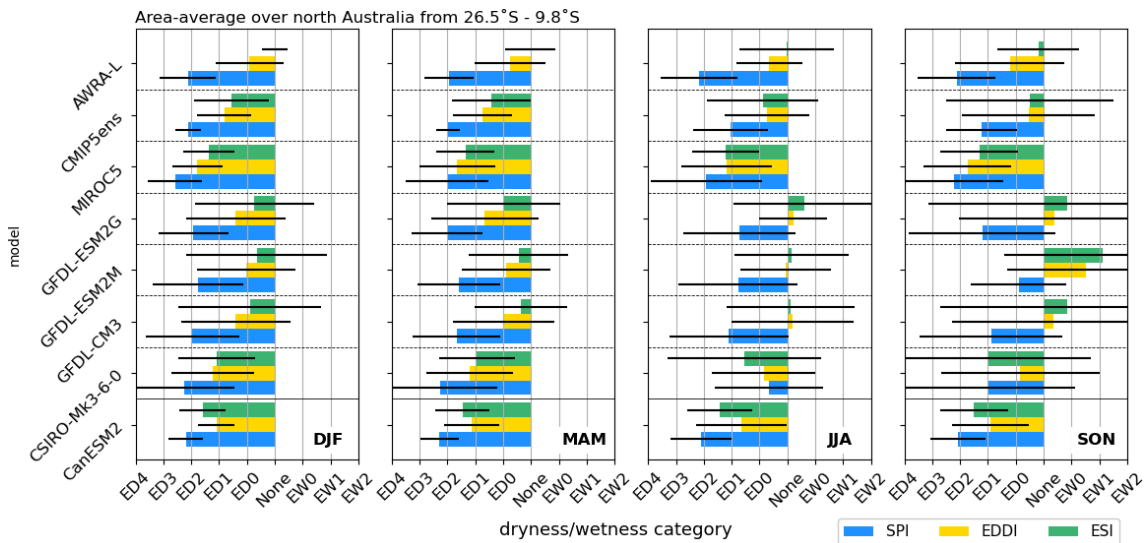


**Figure 5.16:** As Figure 5.15 but for the northern domain of Australia from 27°S to 9°S.

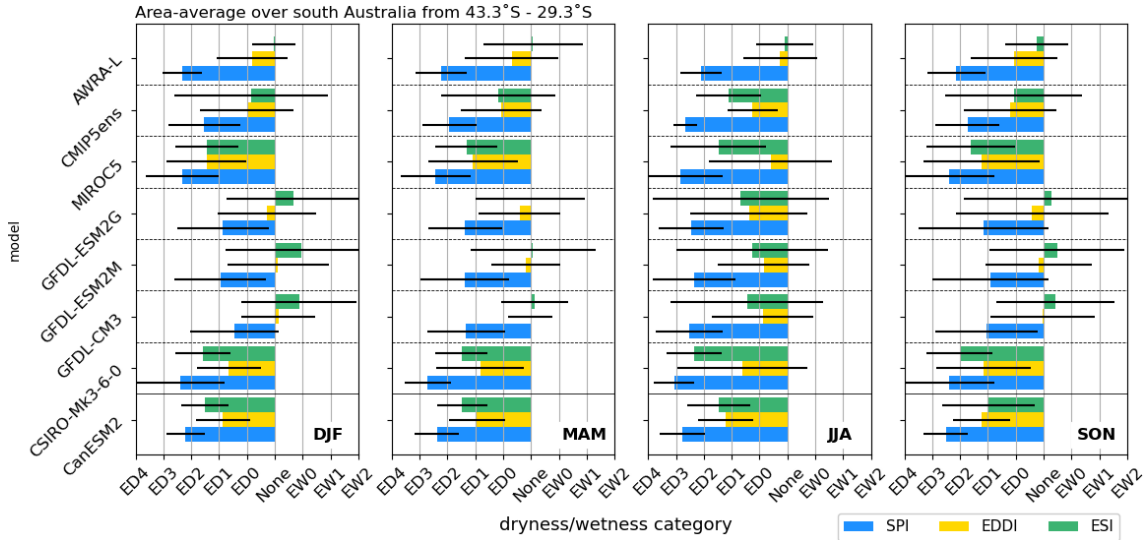


**Figure 5.17:** As Figure 5.15 but for the southern domain of Australia from  $44^{\circ}S$  to  $27^{\circ}S$ .

JJA for the northern domain, SON is characterised by abnormally wet conditions at the onset of a flash drought in the soil moisture (Figure 5.16). The opposite applies to the southern domain (Figure 5.17). ESI onset categories show wet conditions in DJF and around neutral in all other seasons. Despite the split into north and south, large confidence intervals still indicate sizeable differences in onset categories across the domains. Here, the GFDL models seem to overestimate the influence of ET for some regions and underestimate it for others. All other models and AWRA-L/AWAP observations show only little differences between domains.

Comparing the AWRA-L and AWAP for all of Australia shows that the observations and reanalysis have some similarities to both groups of CMIP5 models. The SPI in AWAP shows an area average category of ED2 in all seasons implying a strong lack in precipitation at the onset of a flash drought in the soil moisture. This result aligns well with those found in MIROC5, CanESM2 and CSIRO-Mk3-6-0. In contrast to the SPI and the suite of these three CMIP5 models, both EDDI and ESI of AWRA-L reanalysis shown only weak drying signals with area average categories for the EDDI of around ED0 and neutral conditions (None) for the ESI. As seen in Figure 5.6 in section 5.5.1 almost no grid cells show a significant drying of the ESI and are between ED0 and EW0 during all seasons resulting in an area average of around None and thus making it almost invisible in Figure 5.15. Here, AWRA-L has similarities to the GFDL model suite, which also ascribe a subordinate role to ET at the onset of a flash drought in soil moisture. The relatively small confidence interval in comparison to the GFDL models indicates this

smaller spatial variability across the Australian domain. The shorter lag for EDDI results in slightly drier values for this index. However, the EDDI categories still do not represent flash drought at the time of onset. Only the SPI resembles a category of ED2 that represents flash drought onset. The SPI also has the least spatial variability, implying that precipitation is the main driver for flash drought in most regions of Australia. The split into north and south changes only vary little for all indices in AWRA-L/AWAP (Figs. 5.16 and 5.17).

The rate of change (RoC) within a certain period leading to flash drought onset highlight the changes in the SPI, EDDI and ESI associated with the rapid drying of soil moisture. This is represented by the reference curve in figure 5.18 showing a two category decline per two weeks. This is, at eight weeks prior to the onset the RoC will be 0.5 and at four weeks prior it will be one. At two weeks prior to the flash drought onset in the soil moisture the RoC reaches two categories in accordance to our flash drought definition. If the curves for EDDI, ESI and SPI are lying on or below this reference, their RoC would meet the criteria for flash drought detection at the same time as the soil moisture. An earlier detection would shift the curve to the left while a delayed response would shift it to the right.

All of those scenarios are present in Figure 5.18. Again, splitting the models in the

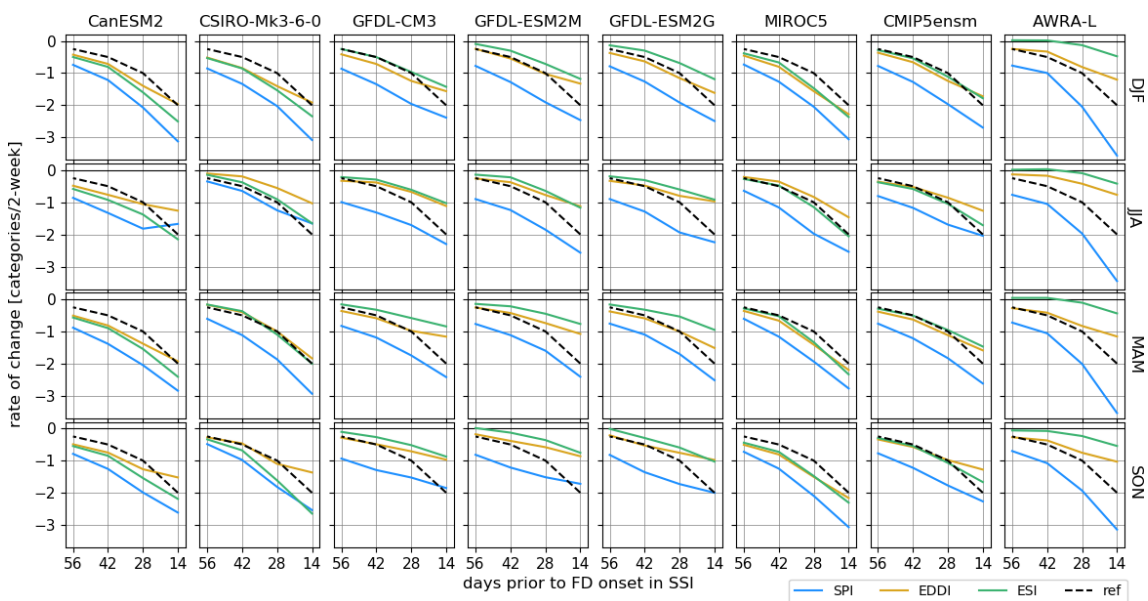


**Figure 5.18:** Area average of rates of change (RoC) in units of categories per two-weeks for EDDI, ESI and SPI for 8, 6, 4, and 2 weeks prior to the onset of a flash drought in the soil moisture. Split into season (rows) and ordered for each CMIP5 model (first to sixth columns), CMIP5 ensemble (seventh column) and AWRA-L/AWAP (eighth column).

GFDL and non-GFDL models highlights different characteristics. In the GFDL models, the neutral to only slightly dry categories for EDDI and ESI at the time of flash drought onset in the SSI are linked to slow RoCs (columns 3-5). This suggests that the contribution of increasing ET to flash drought in the GFDL models is small. Instead, only the curves for SPI show rapid drying, suggesting that precipitation is the main driver of flash drought in these models. While the strong changes in the SPI are also present in CanESM2, CSIRO-Mk3-6-0 and MIROC5, those models also show a stronger RoC for EDDI and ESI with their curves much closer to the reference line or below. Thus, ET is a more important component for flash droughts in the non-GFDL models.

Differences between northern and southern domains are displayed in Figure 5.19 are generally small, however, some models show some distinct differences. That is, for example, the GFDL model suite, which manifests greater RoCs for all indices during JJA but smaller ones during DJF and MAM in the south compared to the north. Yet, only the SPI lies entirely below the reference line in both domains and all seasons. Another distinct difference between north and south is observed in the CSIRO model. While mostly all indices for both domains lay underneath the reference line indicating a strong drying that qualifies for a flash drought yield in the index, this is not the case for the northern domain in JJA. Here, SPI, EDDI and ESI are above the reference line and hence only indicate insufficient drying for a flash drought. In this case, flash drought in the soil moisture would not be detected by any of the indices.

The Australia averaged RoCs for EDDI and ESI are weakest in the reanalysis and observations of AWRA-L and AWAP compared to all models. (Figure 5.18). The long lag of the ESI with soil moisture in the reanalysis, discussed previously, suggests that the ESI intensifies towards a stronger negative change much later than in the soil moisture and that it significantly lags the onset of flash drought in the SSI. Interestingly, the change in the SPI in the observations is much stronger than in any of the models with the exception of MIROC5 in DJF and SON, reaching a decrease of more than three categories in each season. This adds to the body of evidence that in AWRA-L, precipitation is a more important factor driving flash drought as compared to ET. Differences between the northern and southern domain in the observations/reanalysis are even more subtle than for any of the CMIP5 models (Figure 5.19). In both domains, precipitation is the main contributor to flash drought in the top 10cm soil moisture level.

5.5. Results

Generally, the dynamics found in the observations and reanalysis are not fully represented by any model. While the onset values of EDDI, ESI and SPI in the GFDL models are relatively close to those in the observations and reanalysis, their spatial distribution and progression of the indices differ considerably.

5.5.2.4 Differences in flash drought detection skills

The results described thus far provide valuable information about the skill of the indices in their detection of flash drought as defined from soil moisture. The results from most CMIP5 models and from AWRA-L/AWAP, suggest that precipitation is the strongest driver of flash drought, supporting [Koster et al. \(2019\)](#). Thus, our evidence shows that the SPI would be able to provide the earliest detection of a flash drought in the upper 10 cm of soil moisture. The slight lag in the EDDI and more prominent delay in the ESI limit their capabilities for prediction and early detection, and this is especially true in the AWRA-L data.

The skill of flash drought detection in terms of Hit Rate (HR) and False Alarm Rate (FAR) at the time of flash drought onset, as defined using soil moisture, is shown in [Figure 5.20](#). The bars display the area-averaged HR and FAR over Australia where at least one flash drought was detected in the soil moisture, taking the average of the values

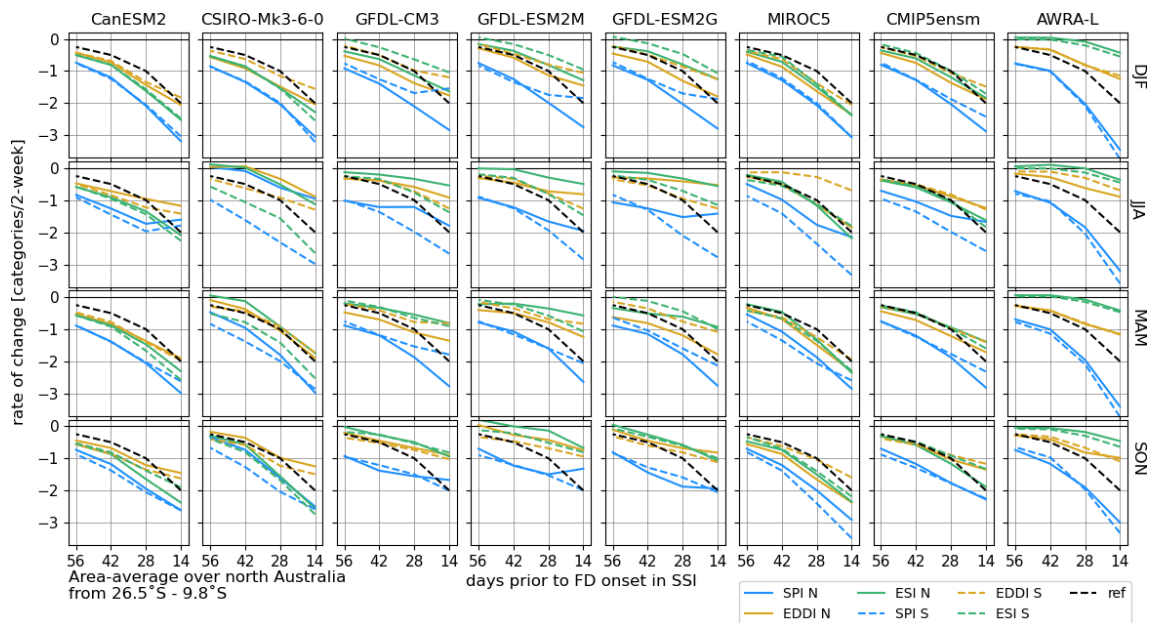


**Figure 5.19:** As [Figure 5.18](#) but results are shown for southern and northern domains of Australia separated at the 27°S latitude. Dashed coloured lines represent area averages of explained variances in the south while those for the north are displayed as solid lines.

5.5. Results

over all grid cells. The error bars indicate the variability in magnitude of the HR and FAR across the domain as the 90<sup>th</sup> percent confidence interval. Thus, the spread shows that the skill of each index varies widely between regions when the error bar is large, and only small differences in the skill are detected across the domain when the error bar is small. Both HR and FAR can sum to more than 100% due to an overestimation in the flash drought event frequency by the SPI, ESI or EDDI index.

Most noticeably in Figure 5.20 is that the FAR is consistently higher than the HR for all models and in the AWRA-L/AWAP data. There are only some exceptions for SPI in CanESM2 during DJF, JJA and SON when the HR exceeds the FAR. In general, the early detection rate of flash drought in the top 10cm soil moisture is highest for the SPI, exceeding 50%. The ESI and EDDI only detect about a quarter to a third of events. However, the comparatively high HR for EDDI and ESI in MIROC5 with 50% to 60% is on par with the SPI and suggests that the response of ET to the soil moisture is quicker

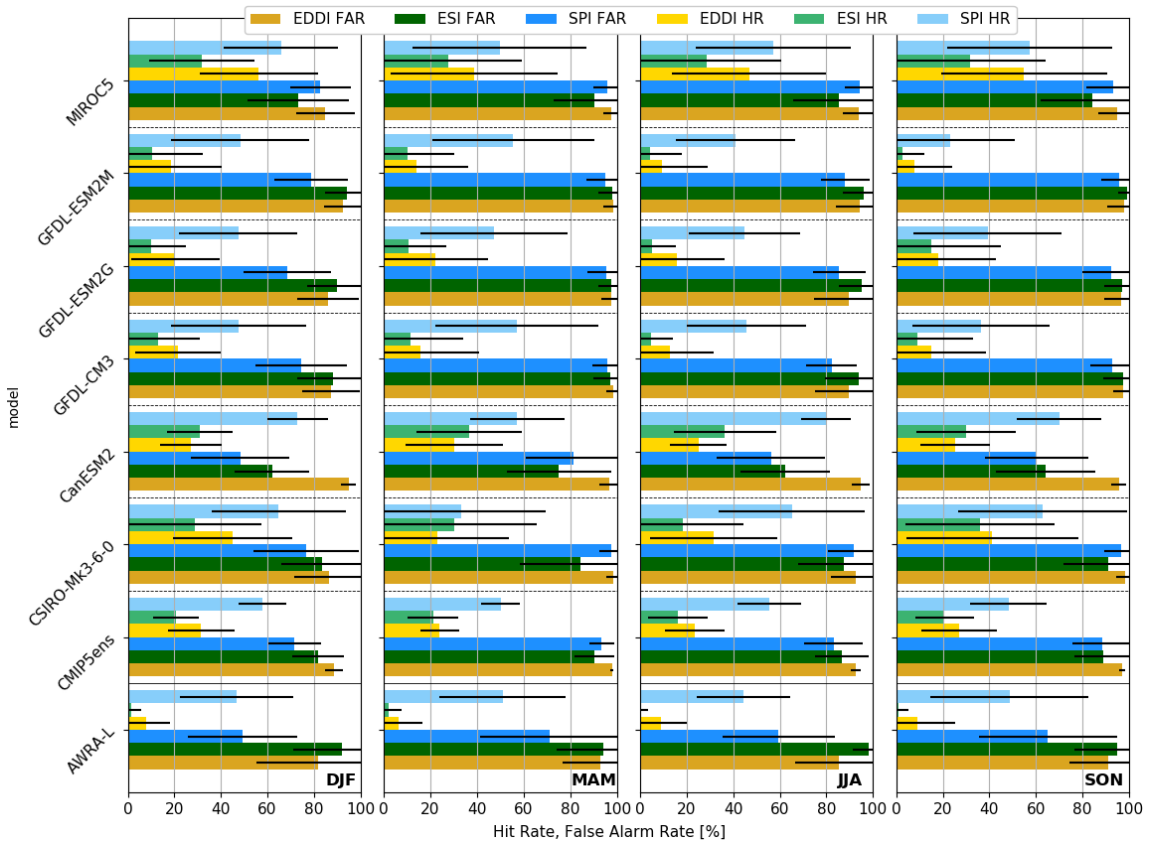


**Figure 5.20:** Spatial mean of hit rate (HR, lighter colours) and false alarm ratio (FAR, darker colours) in percent for EDDI (yellow/gold), ESI (light/dark green) and SPI (light/dark blue). Split into season (columns) and listed for each CMIP5 model (first to sixth row), CMIP5 ensemble (seventh row) and AWRA-L/AWAP (eighth row). Detection rates were determined using a time window around the flash drought detected in the soil moisture of eight weeks prior to the onset in which the indices can yield a hit.

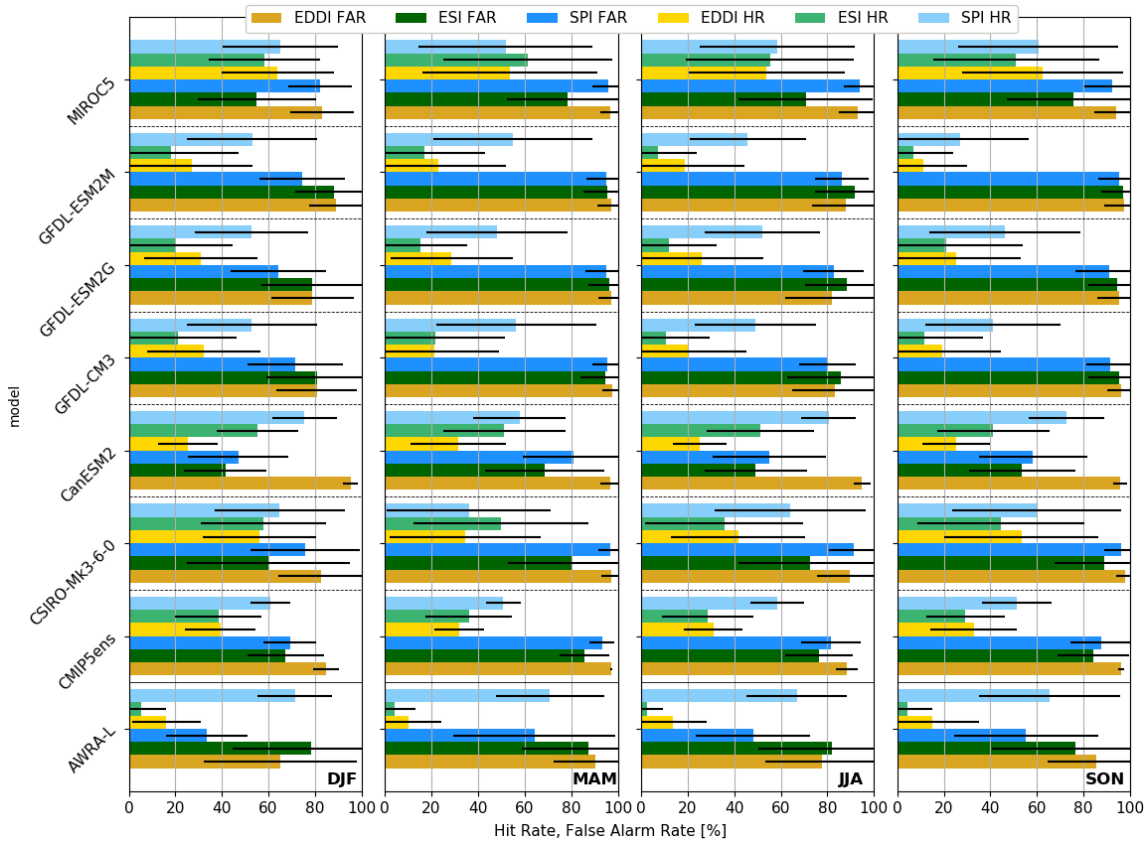


**Figure 5.21:** As figure 5.20 but the time window around the flash drought detected in the soil moisture is extended to two weeks after the onset.

in this than in other models.

The comparison to AWRA-L/AWAP shows that the response time of ET to soil moisture levels is too short in CMIP5 since the HR in the observations/reanalysis is very low with only around 10% for EDDI and less than 5% for ESI confirming the findings of the previous chapter. Yet, the results from AWRA-L have to be considered with its underlying water balance model in mind. The delay in the detection of ET-based indices in CMIP5 can be improved by extending the detection window to two weeks after the flash drought occurred in the soil moisture (Figure 5.21). Expanding the detection window improves the skill most noticeable for ESI in MIROC5 and CanESM2 during DJF and JJA. However, the skill for the ESI still remains low in AWRA-L since the average delay for ESI to the soil moisture is two weeks or longer and the flash drought event frequency is significantly lower than the SSI. Despite a very short lag of only a couple of days, the HR and FAR did not improve markedly for the EDDI because of its similarly low event frequency.

When compared to AWRA-L/AWAP, the skill values of flash drought detection by

the EDDI and the ESI are too high in the CMIP5 models due to the stronger land-atmosphere coupling in the CMIP5 models, and hence an overestimation of ET. However, the overestimation of the strength of the coupling varies between the individual models. There is a stronger consensus between the CMIP5 models and AWAP observations when the SPI is used for flash drought detection. This consensus, and the fact that the HR is highest and FAR lowest for most models and for the observations, suggests that the SPI is the most suitable tool for flash drought detection in the upper 10cm soil layer in a predictive sense. That is, the SPI registers a flash drought much earlier and closer to true flash drought onset as compared to the ET-based indices. The following section will show if this holds when using the deeper 0-100cm soil moisture layer.

### 5.5.3 Flash drought in AWRA-L using root-zone layer soil moisture

The major caveat of the analyses above and in Chapter 4 is that we were only able to consider the top 10cm soil moisture for flash drought identification since CMIP5 only offers this layer on a daily time scale. Monthly values of deeper layer soil moisture cannot be examined using current flash drought definitions that are based on strong changes over just two weeks. Past flash drought studies only used the root-zone layer with depths up to 50-100cm to shape definitions (Ford and Labosier, 2017; Otkin et al., 2018) or use it as a measure for reported flash droughts (Otkin et al., 2016; Nguyen et al., 2019). Consequently, other studies to compare our results to, computed using near-surface soil moisture, do not exist.

In order to compare our findings in a meaningful way and to determine if the top 10cm soil layer might be sufficient for flash drought evaluations, we conducted the analysis just presented in 5.5.2 on the total 0-100cm root-zone layer soil moisture content from AWRA-L. This is first performed using the 40<sup>th</sup> to <10<sup>th</sup> percentile drop within 14 days for a direct comparison to the above findings, hereafter called Definition 1. Subsequently, we use the proposed definition from Ford and Labosier (2017) with a more gentle decline from 40<sup>th</sup> to <20<sup>th</sup> in 20 days is used for comparison with previously published research, hereafter called Definition 2.

5.5.3.1 Flash drought frequency in the root-zone layer soil moisture

Applying Definition 1 to the SSI calculated from the 0 - 100cm soil moisture level reduces the event frequency from 1 - 3 events per decade to 0.5 - 1.5 events per decade in each season with the majority of the Australian domain remaining without any registered events (Figure 5.22). Values for EDDI, ESI and SPI do not change but are shown again in the figure for convenience. The very low sample size shows that Definition 1 is too strict for the lower level soil moisture. Thus, our modified definition is not applicable to the root zone soil moisture as the fluctuations are damped in comparison to the top 10cm soil layer as seen in Figure 5.1.

We then applied Definition 2, which is consistent with past studies (Ford and La-

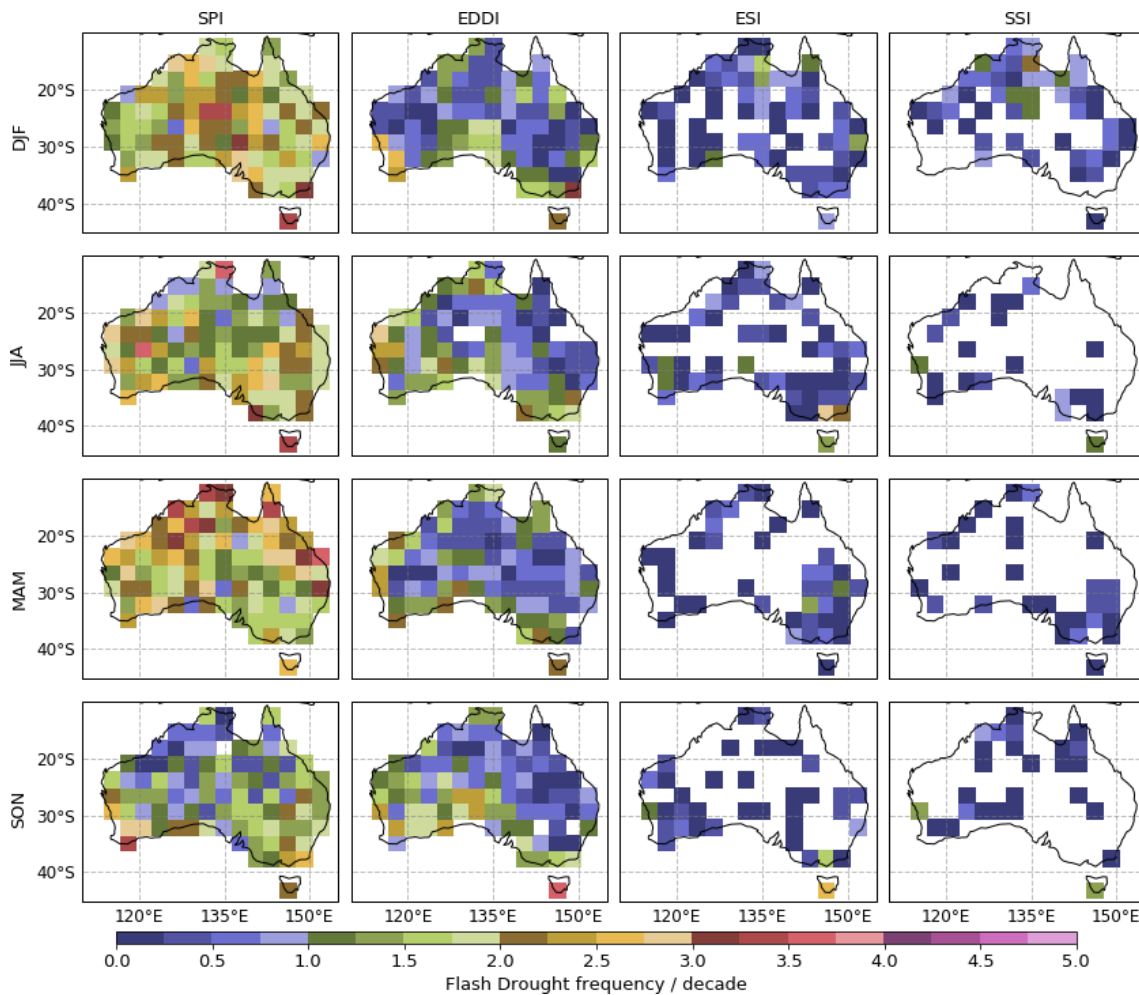


**Figure 5.22:** Seasonal FD event frequency expressed as events per decade for SPI (first column), EDDI (second), ESI (third) and SSI (fourth) over the 39 years of the time period from 1976 to 2018. Values for EDDI, ESI and SPI have not changed to Figure 5.4 as the same definition is used. Flash droughts are defined as a decrease from above the 40th to below the 10th percentile in 14 days. The SSI is calculated using the 0-1m soil layer.

5.5. Results

bosier, 2017). Figure 5.23 shows changes to the event frequency not only for the SSI but also for EDDI, ESI and SPI since the threshold for the lower percentile and the rate of change has been altered, as described previously. The gentler decline over a longer time yields more flash droughts in all indices.

Figure 5.23 shows significant increases in flash drought event frequency of about 50 to 400% when Definition 2 is applied. The previously sparsely distributed flash drought events in the ESI in Figure 5.22 are now present in almost all grid cells with a frequency of 1-4 events per decade. This is about the same range that is observed in the SSI. Fewer events during the dry season in the north of the country (JJA) and more during the wet season (DJF) as well as a higher frequency in the SE in autumn (MAM) agree well between ESI and the SSI. Flash drought event frequency in the EDDI and SPI is a

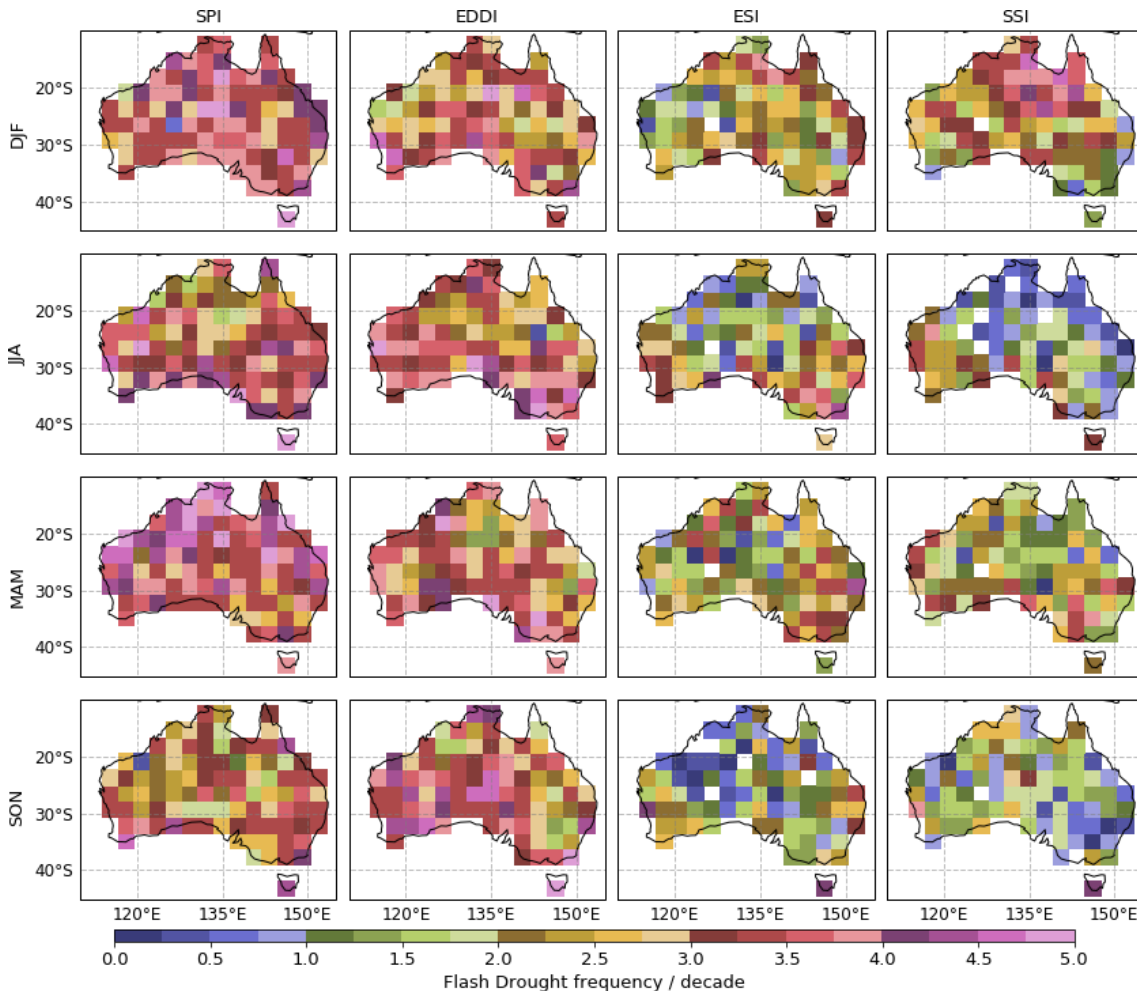


**Figure 5.23:** Seasonal FD event frequency expressed as events per decade for SPI (first column), EDDI (second), ESI (third) and SSI (fourth) over the 39 years of the time period from 1976 to 2018. Flash droughts are defined as a decrease from above the 40<sup>th</sup> to below the 20<sup>th</sup> percentile in 20 days. The SSI is calculated using the 0-1m soil layer.

5.5. Results

factor of 1.5 to 2 higher than in the ESI and SSI reaching around 2-5 events per decade for much of the domain. The spatial patterns of the EDDI and SPI also correspond less with the pattern described for ESI and SSI. From this initial analysis, it seems that the ESI is the most promising index for flash drought detection, though coincidence of events has not yet been established. The skill in the ESI has also been shown for the United States by Otkin et al. (2013, 2015) who compared the ESI with the top 2m soil moisture profile, precipitation and crop condition data during flash drought periods.

The close relation between ESI and soil moisture based on the flash drought event frequency is supported by a very high explained variances of around 0.7 to 0.8 displayed in 5.24. This is about 0.4 higher compared to the top 10cm layer 5.2. The strong correlations prevail for the whole domain throughout the year and only eases to  $\approx 0.3$  during JJA and SON in the NW and far SE. In contrast to the increased co-variability for the ESI, the SPI shows weaker correlations with values of around 0.5, which is 0.3 to 0.4 weaker compared to the 0-10cm soil layer. However, the SPI still shows significant correlations for much of the domain except for the North in JJA (which corresponds to the dry season there). Interestingly, the co-variability between EDDI and SSI does

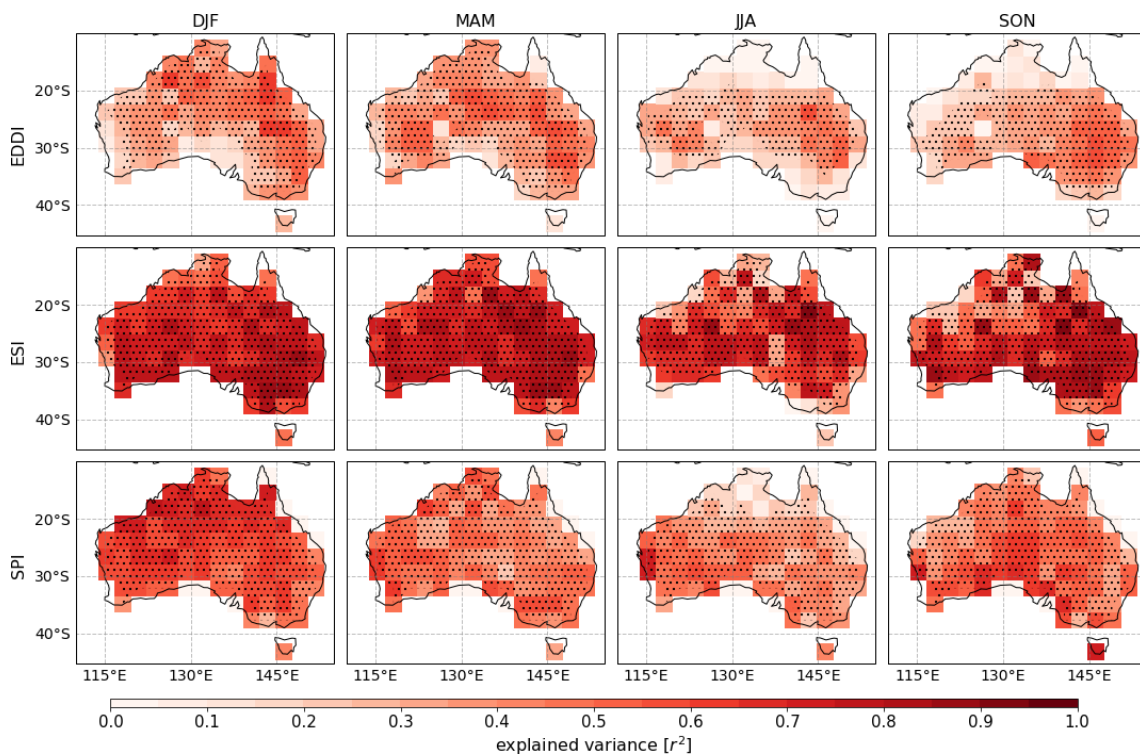


**Figure 5.24:** Seasonal explained variance of EDDI (top row) , ESI (middle) and SPI (bottom) with 0-100cm SSI for 1976 to 2018. Values above 0.2 are statistically significant on the 95% level and marked with hatching.

5.5. Results

not change markedly between the 0-10cm and 0-100cm soil layers. The pattern remains unchanged with higher actual explained variances of 0.5 in the North and East during DJF and MAM and in the E/SE in SON and only significant correlations between 20° and 30°S.

The explained variances shown are the strongest found in a cross-correlation which displaces the time series of the drought indices 0 to 14 days in each direction relative to the SSI time series. This is done in two day increments to achieve a test for lag and lead times. The lag/lead times at which the presented explained variances were detected are displayed in Figure 5.25. The lags and leads shown are relative to the soil moisture, meaning that the index leads soil moisture if a positive number occurs and vice versa the particular index is lagging soil moisture in the case of a negative number.

The EDDI shows similar lags/leads for the 0-100 cm soil layer as for the 0-10 cm shallow soil layer shown in Figure 5.3. However, the EDDI's displacement in time relative to the SSI changes slightly from a slight lag of 2-4 days to 0 or a lead of around 2-4 days. The maximum correlation of the SPI with SSI develops to a long lead of 6-12 days of the SPI as compared to the shallow soil layer, which had a near-zero lead/lag.

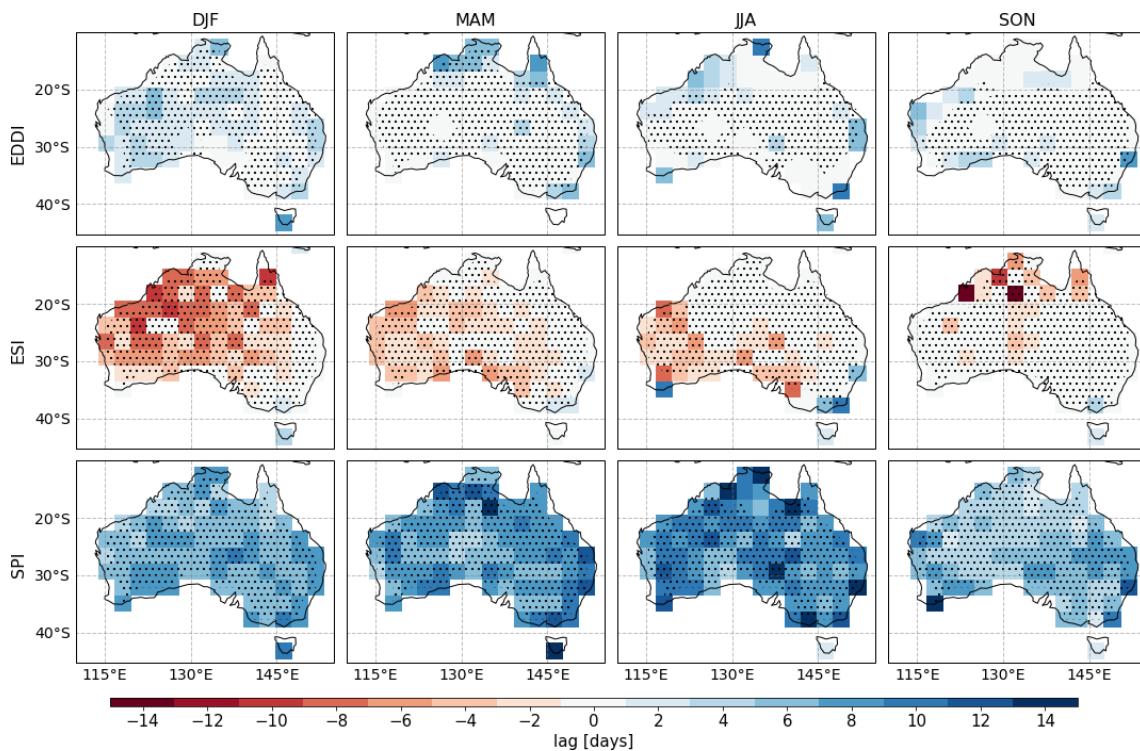


**Figure 5.25:** Lag at which the maximum explained variances shown figure 5.24 occurred for EDDI (top row), ESI (middle) and SPI (bottom). Stippling marks where the explained variances are significant at the 95% level.

This shows that the signal of precipitation at the surface takes on the order of a week to permeate through to deeper soil layers. Similarly, the long lag of ESI in the shallow soil layer changes to a weaker, but seasonally and regionally dependent, lag. The lag of the ESI to SSI is zero for most of the domain from MAM to SON with exception of the west and south in MAM and JJA. A lag of around one week is still present in DJF, except in the southeast.

These results highlight that the dynamics in the deeper layer soil moisture are more closely related to the ESI than SPI or EDDI (Otkin et al., 2013, 2018). The contribution of the transpiration rate from plants included in the actual ET of the ESI delivers information about the soil moisture level in this 0-100cm soil layer as the plants access the soil moisture in that depth. Flash drought may be defined using soil moisture, but in reality is denoted by agricultural or ecological impacts (Nguyen et al., 2019; Pendergrass et al., 2020), to which ESI may be better tuned.

The different relationships between the indices and soil moisture in the deeper part of the soil column have an effect on the rates of change of each index prior to the onset of a flash drought in the soil moisture. Due to the long lead time of the SPI's relationship with deeper soil moisture content, the SPI shows a strong RoC earlier than two weeks before flash drought onset in the SSI, reaching an Australia-wide average of -0.4 at two weeks, -0.5 at four and -0.45 categories per week at six weeks prior to the onset. However, regional and seasonal differences in RoC between indices increase the closer they approach flash drought onset (Figure 5.26). As only droughts were selected that last for at least 30 days, the SPI category is still very low with ED1 to ED2 at the onset of flash drought in the SSI, reflecting the lowest 20<sup>th</sup> and 10<sup>th</sup> percentile respectively despite its long lead time. However, neither the RoCs nor the onset values are as strong as they were for the top 10cm layer, which is unsurprising given the closer connection of the upper level of soil moisture to the overlying atmosphere.

For the EDDI, there are few changes to the value at onset and the RoC prior to onset when compared to the 0-10cm soil layer. Flash drought values at the onset in the SSI are still mostly ED0 to ED1 indicating only abnormally to moderately dry conditions (first column in Figure 5.27). However, the EDDI changes little in the lead up from two to eight weeks before the onset with around 0.1 to -0.6 categories per week (positive change for EDDI as it is inverted to ESI and SPI).

5.5. Results

The RoC in the ESI intensifies in the two weeks prior to the onset of flash drought, which is not observed in the EDDI and SPI. The ESI's relatively weak category of ED0 or even None at the onset of the flash drought in the SSI (first column in Figure 5.28) shows only abnormally dry or average conditions and highlights the lag in the index compared to soil moisture content.

Comparing the onset values of EDDI, ESI and SPI using Definition 2 for flash drought in the 0-100 cm soil layer with those using Definition 1 for the 0-10 cm soil layer means that a direct comparison is not possible. Therefore, we concentrated on comparing the RoC in the SPI, EDDI and ESI prior to flash drought onset in the SSI. In the 0-100 cm soil layer, the strong negative changes in the SPI earlier on signal a strong decline in moisture supply from precipitation, while the later intensifying ESI implies a shortage in transpiration. The EDDI sits somewhere in the middle of both showing a consistent

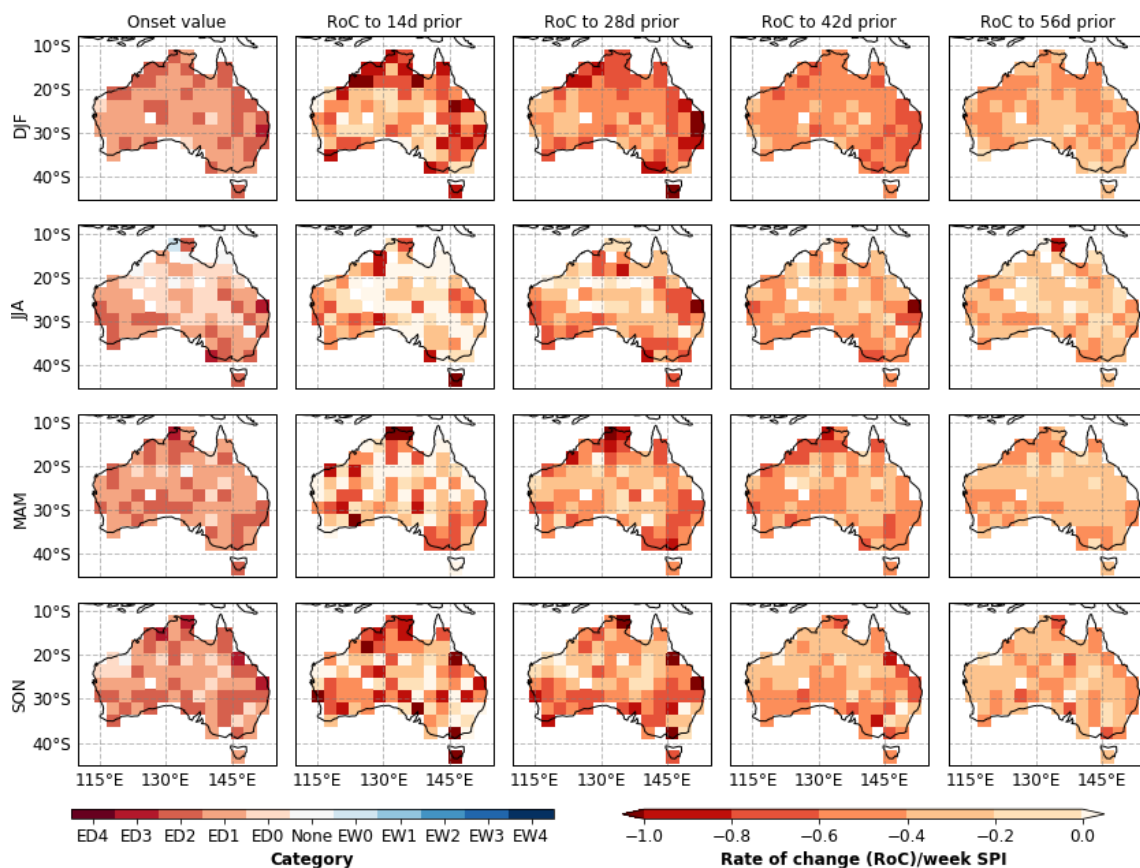


**Figure 5.26:** Index categories of SPI at the time when a flash drought was detected in the soil moisture (SSI) are in the first column. Columns two to five show rates of change (RoC) expressed in "categories per week" for each season. They are calculated as the difference between the index's category at the onset of a flash drought in the soil moisture and the value two weeks prior to that. The result is divided by the number of weeks to achieve a "per week" change unit. All values shown are the seasonal average of all instances over 43 years from 1976 to 2018.

5.5. Results

negative trend in ET. The differences in flash drought event frequency due to the change in flash drought definition, and the representation of the events in the deeper layer soil moisture by EDDI, ESI and SPI, have an inevitable impact on their forecast skill metrics.

5.5.3.2 Skill metrics for early flash drought detection and monitoring

When applied to the deeper soil layer, the ability of the indices to detect a flash drought before it occurs in the soil moisture changes most noticeably for the EDDI (Figure 5.29). During DJF and SON, the hit rate (HR) of the EDDI increases from an area-average of around 8% to 31% for flash droughts computed from the shallow and deeper soil layers respectively. The changes in the HR of the SPI for the deeper soil layer are mixed. While the HR for the SPI generally improves over the whole domain in DJF from an area average of approximately 45% to 60%, the SPI's HR decreases in MAM and JJA to less than 30% in the interior of the continent. During MAM and JJA, the Australia-wide area average HR of the SPI decreases from 50% to 40% between the upper and total column soil layers respectively. The FAR remains at a similar level to the shallow soil layer for

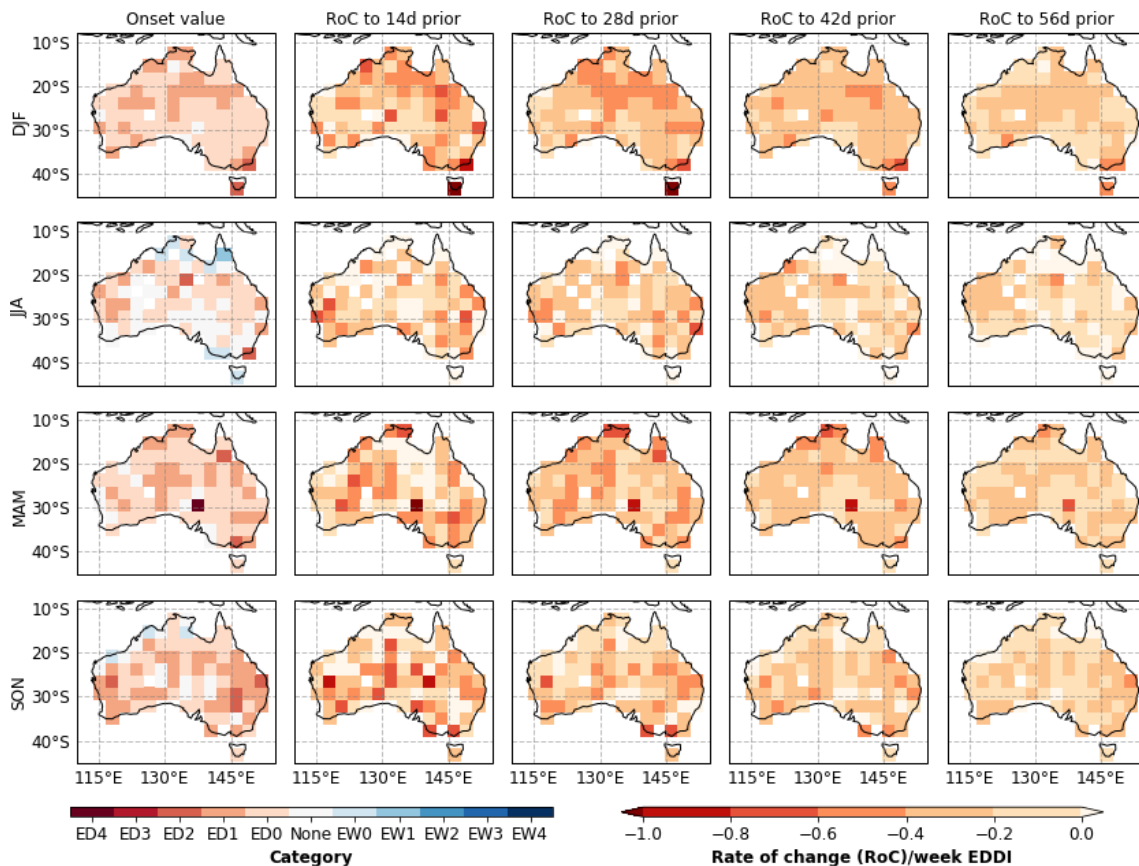


Figure 5.27: As described in figure above but for the EDDI.

5.5. Results

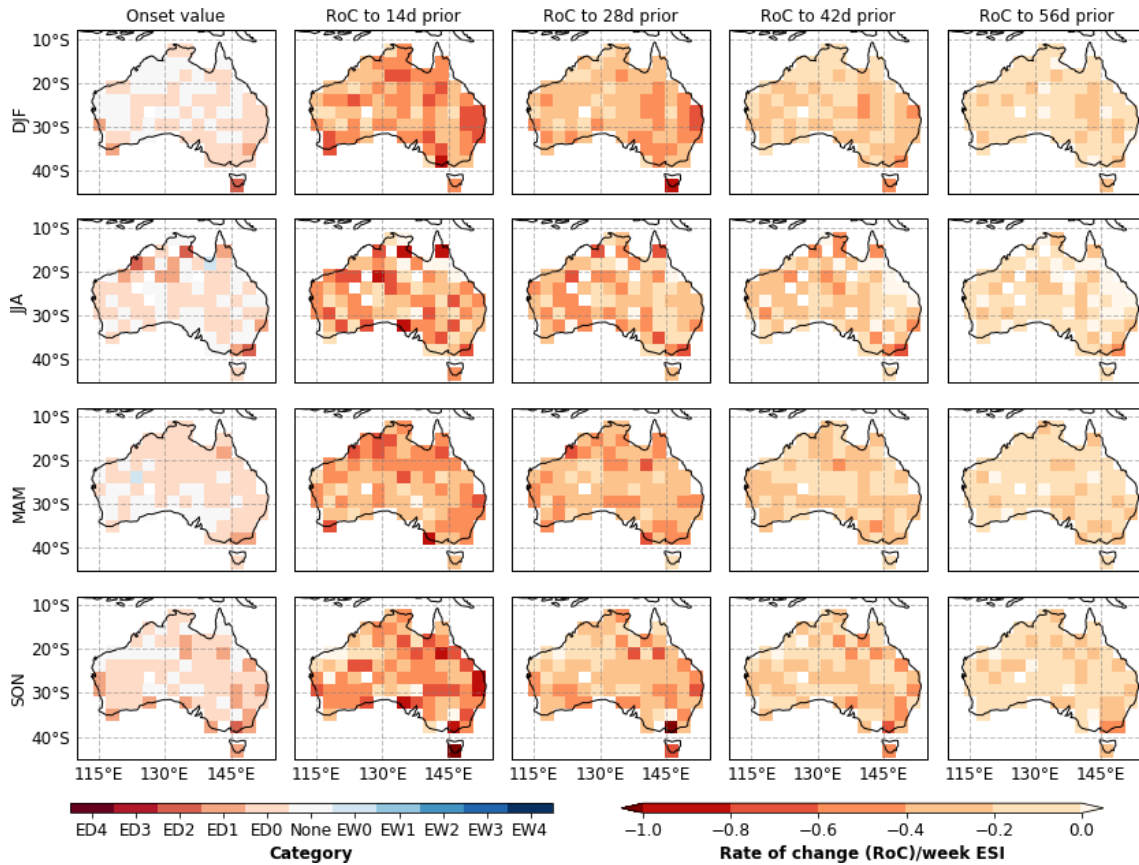


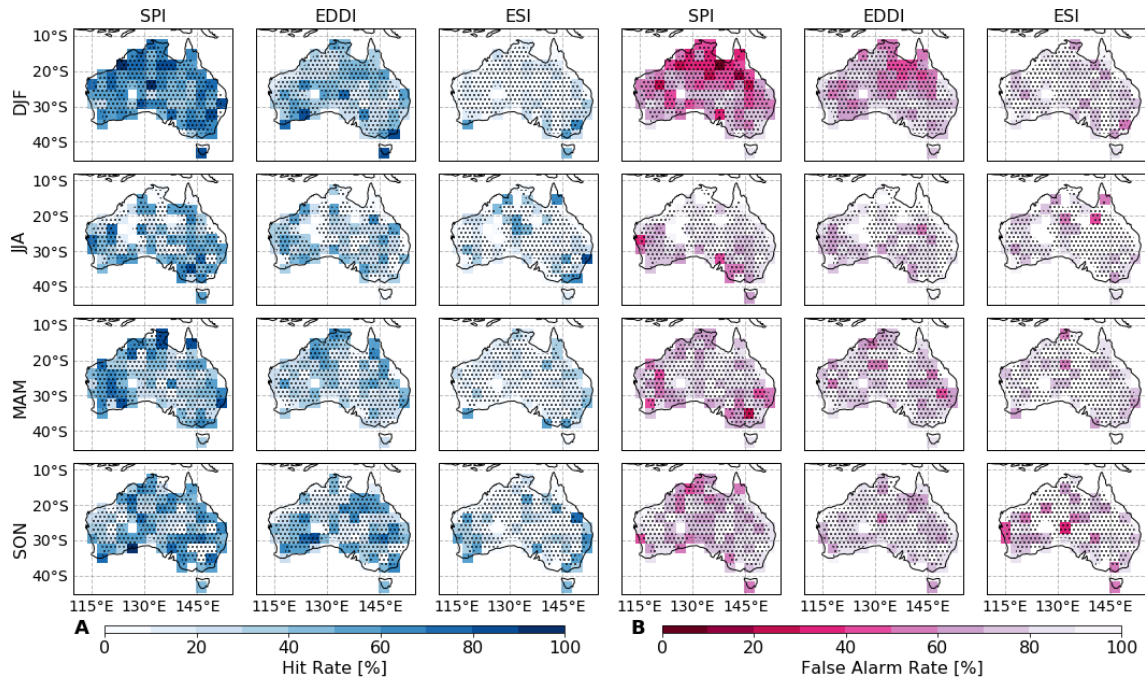
Figure 5.28: As described in figure above but for the ESI.

the EDDI and SPI with an Australia wide average of 85% and 70% respectively. The HR of the ESI improves for only some grid cells, showing that its lag, even though it is shorter than for the shallow soil layer, prohibits flash drought detection concurrently with 0-100 cm soil column. Improvements are limited to the southeast coast in all seasons and western Australia in SON resulting in an increase of the area-average HR from 1% to 14%. Consequently, the ESI's FAR is still very high and ranges between approximately 70% to 100% (90% confidence interval) for flash drought detection in the 1m soil layer.

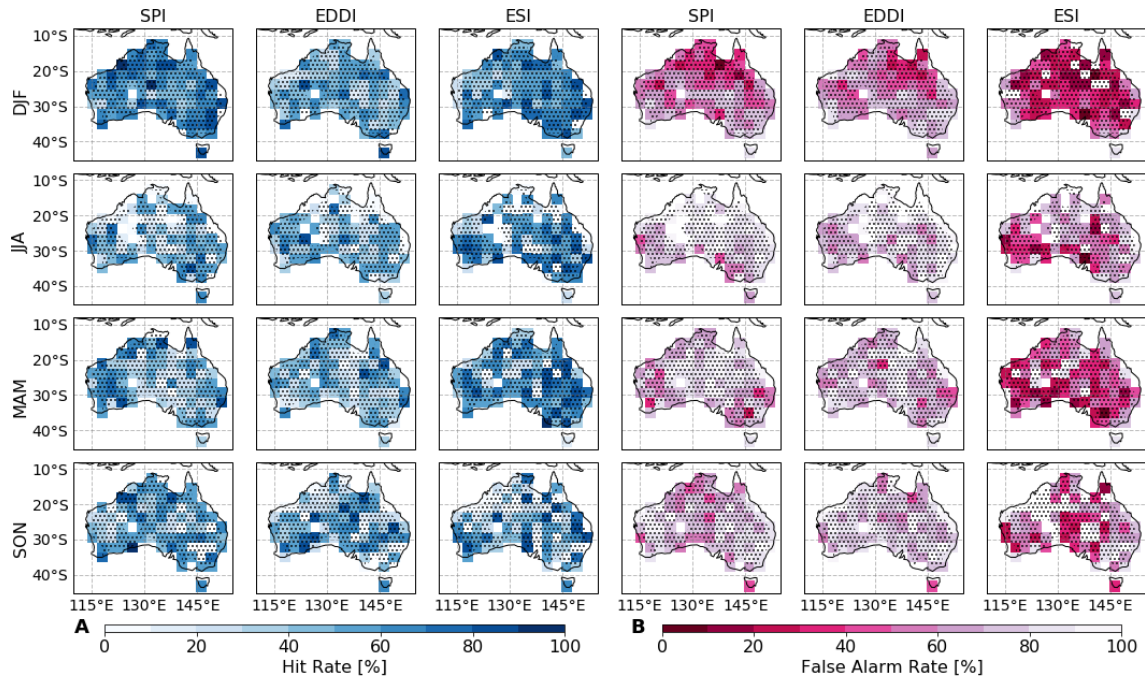
We test the sensitivity to our definition of flash drought onset by relaxing the time interval in which we define onset. This is, we define flash drought onset as the 2 week period after the SSI first falls below the required threshold for a flash drought. This relaxed criteria will show if the lag in the EDDI and ESI are able to provide skilful detection of events near to their commencement. A small delay could still be useful for management and decisions making purposes.

Figure 5.30 displays the HR and FAR with this extended definition of 'onset' applied. It is immediately evident that the detection skill for the ESI markedly improves. In DJF,

5.5. Results



**Figure 5.29:** Hit rate (HR, panel A) and false alarm ratio (FAR, panel B) for SPI (left column), EDDI (middle) and ESI (right). The time interval in which the either the indices can yield a flash drought for a valid hit is within eight weeks prior to the flash drought onset in the soil moisture. Hatching indicates where the SSI identified a flash drought as seen in figure 5.23. Only here are values for HR and FAR possible.



**Figure 5.30:** As described in figure 5.29 above but the time interval is extend by two weeks after the flash drought onset in the soil moisture happened.

the HR reaches values that are similar to the SPI, detecting around 60% of the flash droughts in the SSI on average. During JJA and MAM, the HR of the ESI exceeds that of the SPI by about 15% on average also reaching around 55% on average, even around 85% (90<sup>th</sup> percentile value) in some areas in the southeast. Further, the ESI often outperforms the EDDI and SPI when the extended definition of 'onset' is applied. This is because there are also comparatively low FAR values for the ESI, decreasing from an area-average of previously 90% in all seasons to 60% in JJA and only 30% in DJF. Both the SPI and EDDI have FAR values of 60% to 85% due to little improvements in the HR with the two week extension.

Here, we show that the climatological frequency of flash drought in the ESI was most similar to the SSI in the 0-100cm soil layer. The low FAR values of the ESI confirm that the flash droughts detected by the ESI are mostly the same as those in the SSI. This makes the ESI a reliable index for monitoring. However, though there is high skill, the lag in the ESI shows that it is less suitable for the early detection of flash drought as it does not highlight the event until around 2 weeks or longer after its onset in the soil moisture.

The results presented here show that the SPI is the most suitable index for *early detection* because of its high HR and the fact that it leads the SSI by around a week. However, the SPI also has a high FAR over much of Australia. Thus, a multi-index approach to detection and monitoring would be most appropriate. For example, determining flash drought risk using the SPI, but following a potential onset via monitoring using the ESI.

### 5.5.3.3 Case study – southern Queensland, January 2018

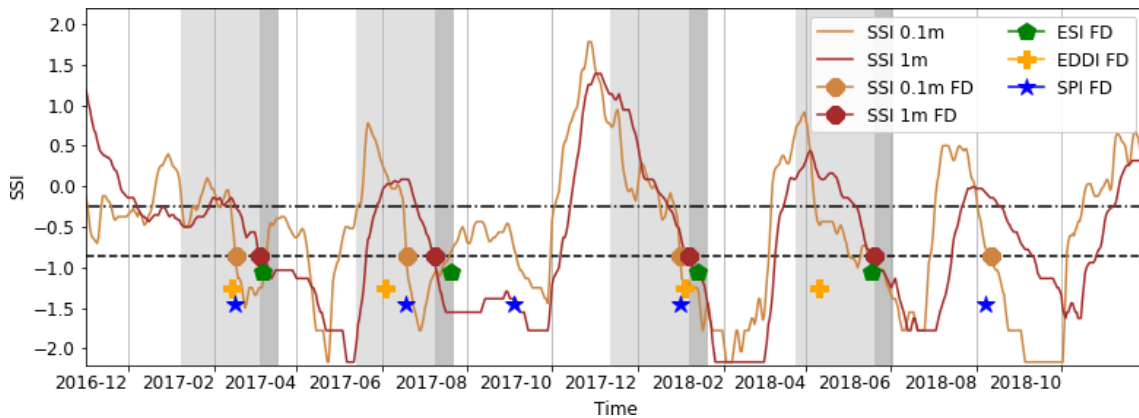
To further examine the utility of the various indices for flash drought detection and monitoring, we apply them to a known flash drought that occurred in southern Queensland in January 2018 (Nguyen et al., 2019).

Figure 5.31 shows the development of the SSI for 0-10cm (brown) and 0-100cm (dark red) from November 2016 until December 2018 with their respective 40<sup>th</sup> (black dot-dashed) and 20<sup>th</sup> (black dashed) percentiles for a single grid cell that is representative of the area (26°S, 144°E). Markers shown in the same colour represent the onset of a flash drought in each of the layers when the decline between the two percentile thresholds,

5.5. Results

previously defined in section 5.5.3, was achieved within 20 days. The evolution of the SSIs are characterised by dry and wet cycles with the dry conditions showing more extreme negative anomalies.

The blue, orange and green markers in Figure 5.31 represent the flash drought onset in SPI, EDDI and ESI respectively. Figure 5.32 shows the SSIs for the two soil depths as in Figure 5.31, but with the time series of EDDI, ESI and SPI added. In the period encompassed by the figure (December 2016 to December 2018), four flash droughts were identified in both the upper and deeper level soil moisture. There were three events recorded in both soil moisture levels, Feb-Mar 2017, Jun-Jul 2017, Jan 2018. Additional events were recorded independently in each level, namely May 2018 for SSI 1m and Aug 2018 for SSI 0.1m.



**Figure 5.31:** Times series for 0-10cm (brown) and 0-100cm (darkred) SSI from November 2016 to December 2018 for the location  $26^{\circ}S$  and  $144^{\circ}E$  that was affected by a flash drought in that time period according to [Nguyen et al. \(2019\)](#). Markers show timing of flash drought onset for SSIs, SPI, ESI and EDDI. The dot-dashed line represents their  $40^{th}$  and the dashed line their  $20^{th}$  percentile. Light grey shaded area covers an eight week time period prior to the onset of a flash drought in the 1m SSI. Dark grey shaded area two week time period after the event onset.

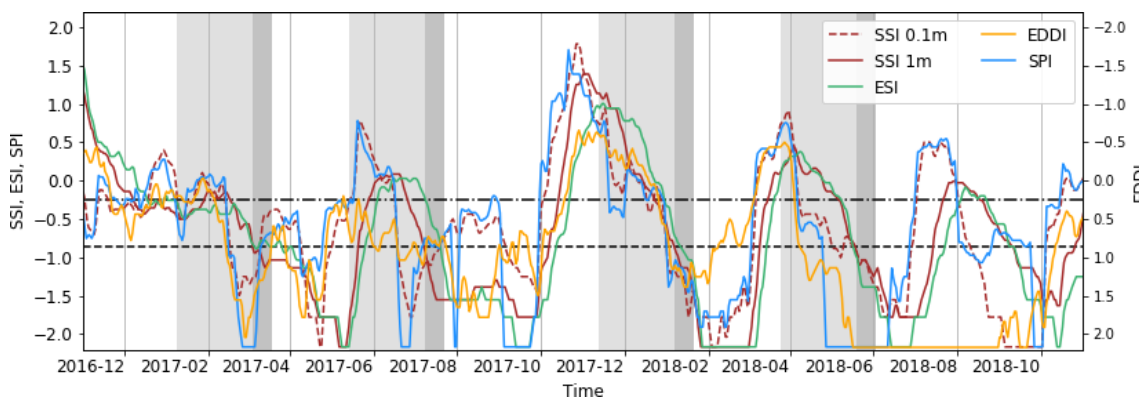


**Figure 5.32:** As figure 5.31 above but with markers removed and time series of SPI, EDDI and ESI added.

Figures 5.31 and 5.32 show that both EDDI and ESI register all four flash droughts that are detected in the 1m SSI. However, only the flash drought in May 2018 is successfully predicted by the ESI prior to its onset in the 1m SSI. In contrast, for all except the May 2018 flash drought, the EDDI displays a flash drought signal three to six weeks prior to the onset registered by the 1m SSI. The SPI detects three of the four flash droughts in the 1m soil layer prior to the onset as defined using the 1m SSI, but also raises two false alarms. Of these, one false alarm is associated with a flash drought in the top 10cm soil layer, but none of the ESI or EDDI flag this as an event.

This case study highlights the potential benefits and limitations of using the SPI, EDDI and ESI for early detection and/or monitoring. The SPI is not as reliable as EDDI and ESI for flash drought in the 1m soil layer. Yet, the ESI is not useful for early prediction due to its significant lag behind flash drought identification in the soil moisture. However, this does make the index useful for flash drought monitoring (Otkin et al., 2013, 2018; Nguyen et al., 2019). In this case, the EDDI seems to be the more capable tool for early flash drought detection in the relevant 1m soil layer. While these results for southeast Queensland are consistent with the results previously presented, this could vary for other locations. For example, the interior of southern Queensland is characterised by persistently hot and dry conditions with only little rainfall and EDDI has proven to be more reliable in those water-limited environments (McEvoy et al., 2016). However, the spatially consistent results presented in section 5.5.3.1 suggest that this framework is applicable Australia wide.

## 5.6 Discussion

In this chapter, we have examined the occurrence of flash drought in observations and reanalysis over Australia and compared the results to those from the CMIP5 models from Chapter 4. This comparison provides further insight into flash drought dynamics, their representation in the models, and thus, the utility of the drought indices as a tool for detection and monitoring compared to the "real world". We further used the root-zone layer soil moisture level from 0-100cm from AWRA-L to determine how the detection performance of EDDI, ESI and SPI change when flash drought is defined by soil moisture depletion in deeper soil layers.

The results show differences between observations/reanalysis and global coupled climate models in; i) the flash drought event frequency of ESI, EDDI, SPI and SSI and ii) the coupling of soil moisture to drought indices. This leads to the conclusion that the processes responsible for starting and continuing flash drought in AWRA-L and CMIP5 are different. The differences in the processes means that each data set provides different information utility of the various indices as tools for flash drought prediction and monitoring. Consequently, the models have serious limitations in the way they simulate flash droughts which can be caused by a too strong land-atmosphere coupling compared to the reanalysis from AWRA-L.

About twice as many flash droughts are observed in the top 10cm soil layer of AWRA-L using the same definition as the CMIP5 models in Chapter 4. Further, there are stark differences in how each of the SPI, EDDI and ESI represented flash drought. The SPI computes a similar event frequency to the SSI in the AWRA-L/AWAP data for the upper level soil moisture (0-10cm). In contrast, both EDDI and ESI register fewer flash droughts in AWRA-L than in the climate models. The higher frequency of flash drought in the ET-based indices in the CMIP5 models suggests that the land-atmosphere coupling of the surface to atmosphere moisture flux is too strong in the models compared to the reanalysis (Seneviratne et al., 2013; Ukkola et al., 2016b, 2018b). This is shown in the timing of the strongest responses between precipitation, ET and PET to soil moisture between models and observations/reanalysis. The results show shorter response times for the SPI to the top 10cm soil layer in the observations/reanalysis than the models. The AWRA-L and AWAP data represent physical processes realistically as past studies show that the top 10cm layer receives precipitation without any delay (Ford and Quiring, 2014). The response of EDDI and ESI is mostly lagging soil moisture and the lag is longer in the model data than in the AWRA-L reanalysis.

The reanalysis show that ET continues to occur even when soil moisture in the top layer is almost completely depleted. This is due to transpiration from plants which access available moisture from deeper soil layers Seneviratne et al. (2010). Consequently, ET does not decline rapidly in AWRA-L to fulfil our definition of a flash drought. Current global coupled climate models also include a biophysical land surface model, which considers a canopy, distinction into multiple soil layers and accounts for the main physical processes relevant for vegetation and soil (Pitman, 2003). However, on-going uncertain-

ties exist regarding parametrisations and representations of geographical details for soil and vegetation parameters, such as water holding capacity, vegetation feedbacks and rooting depth (Seneviratne et al., 2006, 2010; Anders and Rockel, 2009; Pitman et al., 2009). Differences in these parameters impact the water and energy fluxes under water stressed conditions (Ukkola et al., 2016a; De Kauwe et al., 2017; Mu et al., 2020). For example, Huang et al. (2016) found a large spread of model sensitivity to extreme dry events when investigating drought response of modelled gross primary production in nine CMIP5 models. They concluded that this largely stems from differences in the water stress function, moisture availability for plants or both.

These known issues in model representation of land surface characteristics, described above, are represented in our results when comparing CMIP5 to AWRA-L and AWAP. An earlier onset of decreasing ET when vegetation is water stressed could explain the shorter response time of ET to soil moisture found in the models. This impacts EDDI to some extent since the energy for the latent heat flux now goes into PET as sensible heat flux and EDDI spikes, ultimately leading to a strong overestimation of EDDI flash drought in many CMIP5 models, especially CanESM2. As described in the previous chapter, the GFDL models behave differently to the rest of our ensemble suite. These models do not show such large overestimations of ET, which is closer to the observations/reanalysis. However, there is still an overestimation and so the GFDL models also substantially underestimate the drying of the upper layer soil moisture.

The differences in land surface models, and their coupling to the atmosphere, have an inevitable effect on the detection skill of each of EDDI, ESI and SPI for flash drought. In dry regions the models' ET is strongly controlled by soil moisture (Koster et al., 2004). Since Australia is dominated by a dry climate, the lag in the ESI in particular, over the EDDI (which has a smaller lag) indicate that ET is changing in response to depleting soil moisture. Due to ET being a response to a reduction in soil moisture in a coupled system, there is a lag in the detection of flash drought by the ESI and EDDI. The potential of EDDI for flash drought early warning is manifested by strong, transient meteorological and radiative changes, which drive PET (Hobbins et al., 2016). The EDDI is able to do so in some occasions, which could be referred to heatwave driven flash drought as characterised by Mo and Lettenmaier (2015). The overly strong land atmosphere coupling in CMIP5 ascribes both indices more skill than in the AWRA-L

reanalysis. The SPI on the other hand shows some skill in early detection for both models and observations. However, the SPI also suffers from a high false alarm rate in its detection of flash drought.

The results from the observations and reanalysis show that the top 10cm soil layer is not necessarily indicative of flash drought in the deeper soil moisture layer. Different processes are important in the different layers and this provides information on the predictability of flash drought in each layer. For example, the stronger atmospheric coupling in the upper layer means that the SPI has the highest forecast skill there (Ford and Quiring, 2014). In the deeper soil layer, rapid depletion of soil moisture can be caused by increased plant transpiration due to an enhancement in PET (Otkin et al., 2018). This is best represented by the ESI. However, there is still a lag in the timing of flash drought in the ESI, suggesting it is a response to a reduction of soil moisture, not a cause, which makes the index best for monitoring rather than prediction. The complementary relationship of ET and PET could mean that EDDI can be used as a predictor of flash drought (Hobbins et al., 2016; Otkin et al., 2018). The skill of the EDDI indeed increases slightly for the deeper layer, yet, precipitation remains the most important driver also for root-zone layer flash drought (Koster et al., 2019). The SPI is good for early detection in both layers, however, is accompanied by high FARs. The results suggest that a range of indices would be useful for different purposes and that any forecast/monitoring tool would require a multi-variate approach, for example SPI to flag flash drought risk and then onto monitoring by the ESI to determine whether its consolidated into a true flash drought. Such an approach is used in the US drought monitor (Svoboda et al., 2002).

It is important to highlight that the soil moisture and ET data in AWRA-L we are referring to are also outputs from a LSM that is driven by observations interpolated onto a high resolution grid spanning the Australian domain (Frost et al., 2018). Even though AWRA-L is highly correlated to *in situ* measurements of ET and soil moisture observations from flux towers (Holgate et al., 2016), the results presented here need to take the uncertainties associated with the AWRA-L data into consideration. Particular scrutiny needs to be given to remote, inner continental regions of Australia that have only a few monitoring sites and so AWRA-L and AWAP data are deemed to be less reliable here (Jones et al., 2009). Also, a lot of information is lost through the interpolation to

CMIP5s' common grid cell resolution of  $2.5^\circ \times 2.5^\circ$  which is much coarser than AWRA-L's native resolution of  $0.05^\circ \times 0.05^\circ$ . Future analyses on the native resolution would provide more information about the spatial distribution of flash drought event frequency and the regional predictive or monitoring skill of ESI, EDDI and SPI.

## 5.7 Conclusion

This chapter has examined the flash drought event frequency in Australia using reanalysis and observational data from AWRA-L and AWAP. Flash droughts were identified in a shallow soil layer (0-10 cm) and total column soil moisture (0-100 cm) from AWRA-L. Flash droughts detected from an index using soil moisture were compared with flash droughts detected from drought indices based on precipitation, evaporative demand and the ratio of evapotranspiration and evaporative demand. The ability of the indices to detect flash droughts in the shallow soil layer were compared to the results from Chapter 4 where the same analyses were performed using data from CMIP5 models. The results from the total column soil moisture could not be compared to CMIP5 data as soil moisture data is not provided for deeper layers at daily resolution, only monthly. The analyses of the total column soil moisture showed different dynamics at play between the different soil layers. There was a weaker relationship with precipitation due to a less erratic variability compared to the upper soil layer but in turn a stronger relationship to ET making the ESI markedly more skilful for flash drought monitoring in the deeper soil layer.

Our results show that the LSMs in CMIP5 are systematically overestimating evaporation in flash drought. This supports previous findings that CMIP5 models overestimate evaporative droughts on monthly time scales (Ukkola et al., 2016a,b). The overestimation is manifested in the up to three-fold higher flash drought event frequency in the EDDI and ESI in the CMIP5 models as compared to the AWRA-L. The excessive evaporation does not stem from an accelerated drying of the land's surface since flash drought frequency in the top 10cm soil layer is, in contrast, underestimated in the CMIP5 models. Rather, the CMIP5 models underestimate the component of transpiration from vegetation accessed by deeper layer soil moisture, which, in reality, slows down the transition from an energy-limited to a water-limited environment during the transition to drought

conditions. This leads to an overestimation of the sensible heat flux and eventually to an increase in PET resulting in a misrepresentations of flash drought in EDDI and ESI (Ukkola et al., 2016a,b).

The CMIP5 models and AWRA-L/AWAP also show differences in response times of land-atmosphere interactions. The shorter response time of ET to changes in the top 10cm soil moisture layer shows that the land-atmosphere coupling is too strong in the CMIP5 models when compared to reanalysis. Although there are clearly problems with the representation of ET in CMIP5 LSMs, and the associated land-atmosphere coupling, the relationship between top layer soil moisture and precipitation is well represented in the CMIP5 models. This is reflected in a similar flash drought event frequency in the SPI between CMIP5 and AWAP.

The lagging or leading relationship of the drought indices to soil moisture is also embedded in their detection skills. The SPI is in both models and observations the index with the highest predictive skill in flash drought early warning, followed by the EDDI, though with significantly lower skill. However, both are accompanied by a high false alarm ratio caused by their high frequency variability. The ESI is not suitable as a predictive tool due to the delayed response of ET to decreasing soil moisture. Instead, it shows a strong potential for flash drought monitoring with high skill in the deeper soil layer and a low FAR. In regards to the top 10cm soil moisture layer, the SPI provides the skill to detect flash droughts in this layer in advance, while both ESI and EDDI are able to do so in some CMIP5 models but do not have this predictive skill in the observations/reanalysis.

Therefore, this study advocates a multi-variate approach for flash drought identification, where a combination of SPI and EDDI serve to flag a potential development of a flash drought. The ESI can then be used to monitor the development closely and help to determine whether the drying signal consolidates into a true flash drought.

---

# Chapter 6

## Discussion and Conclusions

---

### 6.1 Thesis Summary

This thesis aimed to evaluate how precipitation and evapotranspiration based drought indices represent agricultural and flash drought in observations, reanalysis and climate models. This was explored by investigating different drought indices and evaluating their skill in comparison to soil moisture for both observations and climate models.

thesis focuses

We first investigated how three drought indices, one based on precipitation only (SPI) and another two based on a combination of ET and precipitation (PDSI and SPEI) represented agricultural drought and whether including ET had an impact. Soil moisture was in two different layer depths of 0-10 and 10-40cm from the GLDAS LSM were used as the benchmark for this assessment. Our results in Chapter 3 indicate that there are instances where there is no significant improvement in correlation through the inclusion of an estimate of ET in a drought index (i.e. PDSI or SPEI rather than SPI) relative to the modelled soil moisture reference. However, note that this assessment was of drought occurrence only, and not for other characteristics of agricultural drought, such as duration or severity.

We then tested the sensitivity of the drought indices to the choice of data sets

used to compute them. The magnitudes of the uncertainties associated with the choice of data set was then compared to magnitude of the differences between the drought indices. The choice of input data changes the skill of the SPI, PDSI and SPEI such that the differences between them for drought identification purposes become small. These findings highlight that the choice of drought index may be less important than the choice of data used to compute the index.

Chapter 4 examined how different drought indices represent flash drought in a climate models. Here, we used six models from the CMIP5 suite of models to compare the estimation of flash drought using three different drought indices, namely the SPI, EDDI (based on evaporative demand) and ESI (based on the ratio of actual ET to evaporative demand). The soil moisture from each model served as the reference. However, daily soil moisture values were only available for the top 10cm soil layer on a daily basis, which limited extensive comparisons with past observational studies that used deeper soil layers to compute flash drought (e.g. [Ford et al., 2015](#); [Otkin et al., 2016](#); [Koster et al., 2019](#)).

Our results showed moderate to strong relationships between the variations in drought indices and soil moisture, especially in drought-prone regions of the sub-tropics and mid-latitudes. All indices were able to identify flash drought sufficiently within the models' climatology. However, there was significant inter-model spread in the detection of flash drought, which is likely due to issues with land-atmosphere interactions. The differences in the coupling strength between land and atmosphere led to differences in the capacity of the drought indices' to predict (i.e. skill with the index leading soil moisture) and monitor (i.e. skill concurrent with or lagging soil moisture) flash drought. Despite the inter-model differences, the SPI and to a lesser extent, the EDDI, were consistently capable of early flash drought detection in the models. The ESI had little predictive capacity indicating it is not overly useful for early flash drought detection. However, there was skill in detecting flash drought occurrence following the onset in soil moisture, suggesting it is more useful for drought monitoring. However, all indices were accompanied by a high false alarm ratio, showing that there are many instances where the indices show a progression that is similar to that of flash drought onset, but that do not result in flash drought.

Chapter 5 examined how well climate models represent flash drought in Australia by comparing the results from Chapter 4 to those computed using AWRA-L reanalysis and AWAP observations over Australia for the upper 10cm soil moisture layer. The results

confirmed that the coupling between land and atmosphere was too strong in the CMIP5 models compared to AWRA-L reanalysis. This led to the overestimation of flash drought in the models in the EDDI and ESI but to fewer flash drought events in the soil moisture. For the SPI, the skill of the models and observations in capturing flash drought mainly agreed. Compared to the CMIP5 models, AWRA-L showed a longer response time of ET to decreasing soil moisture. This resulted in longer lags between flash drought detection in the soil moisture in the AWRA-L. In particular, the ESI had very little skill in flash drought detection in the upper 10cm soil layer and EDDI was only slightly better.

The results from the deeper root-zone soil moisture layer showed that the skill of ET-based drought indices markedly increased compared to the shallow 10cm soil moisture layer, especially when the detection window was extended to two weeks post-flash drought onset. With this extension, the ESI showed strong skill for flash drought detection. Further, the ESI also had a low false alarm ratio that was considerably lower than other indices. However, the lag between soil moisture and the ESI was still present, indicating that even in the deeper soil layers, the ESI had little skill in the early detection of flash drought. Instead, the SPI remained the index with the highest predictive skill and the EDDI showed some predictive skill. However, the false alarm rate for both the SPI and EDDI remained high in the deeper soil layer. Our results suggest that decision making based solely on drought indices could be maximised by combining information from the EDDI and SPI for warning of a heightened risk of flash drought, followed by close monitoring of flash drought development using the ESI.

## 6.2 Discussion and Implications

The research presented in this thesis has wide ranging implications for drought research. Although only a fraction of the available drought indices and drought types were examined, some conclusions can be drawn based on the consistency in the results. Therefore, the results from this research represent valuable information about the representation of drought in observations and climate models.

### 6.2.1 Drought indices incorporating ET

Drought indices are an important tool to predict and monitor the development of a dry spell. ET is an important part of water balance at the land's surface and is thus argued to be a necessity for drought indices (Tsakiris and Vangelis, 2005; Vicente-Serrano et al., 2010). However, we have shown in Chapter 3 that there can be considerable uncertainties in ET associated with the data used to calculate it. The magnitude of these uncertainties is often comparable to the differences between rainfall-only based indices, and those indices incorporating both rainfall and ET. However, our research only focused on the occurrence of drought and this analysis should be extended to other characteristics of drought which may benefit from the additional ET component. Regardless, our results demonstrate that in some instances, the use of simpler and less sensitive precipitation-only drought indices might provide information that is as good as more complex drought indices that use P-E balance. In this sense, Chapter 3 shows that increasing the complexity of the index to capture more of the physical processes associated with drought development does not necessarily lead to an improvement in skill and can lead to an increase in uncertainty due to data quality. Our results are congruous with other studies (e.g. Heim Jr., 2002), that conclude precipitation is the key variable in determining drought onset, duration and cessation on seasonal to annual time scales.

We have shown that the choice of input data for the computation of the SPI, SPEI and PDSI alters the representation of drought characteristics. Thus, it is imperative to know the limitations of any data set used to calculate these indices. Issues with the quality of precipitation datasets have already been outlined by Trenberth et al. (2014) showing different trends in precipitation time series from different datasets, including some of those used in this thesis, that lead to changes in the representation of drought using the same index. It is apparent that those uncertainties in precipitation data are also applicable to the SPI. Trenberth et al. (2014) examined the influence of different PET methods in the calculation of the PDSI. Here, we have provided a complementary analysis by looking at the uncertainties in the PDSI associated with the input data set while using a consistent method to calculate PET. Hu and Willson (2000) have shown that that the PDSI is equally affected by changes in temperature anomalies as it is by precipitation which implies that care should be taken when selecting the input data for

future drought predictions in a non-stationary climate. In fact, the PDSI has often been used for this purpose (Burke and Brown, 2008; Dai, 2011b; Zhao and Dai, 2015). Our work shows that the uncertainty from the input data has the capacity to overcome any benefits yielded by including ET, making the PDSI no more skilful than the simpler SPI. Hence, our results suggest that the simple SPI is a sufficient tool for identifying seasonal to annual time scale droughts, with ET adding little additional value. However, note that we limit this conclusion to the identification of drought in observations and these conclusions do not reflect the potential utility of P-E balance indices (e.g. PDSI) in other frameworks (e.g. climate models).

Flash drought has been described as a type of drought where the role of ET is more important than precipitation (Hobbins et al., 2016; Otkin et al., 2018). This type of drought is characterised on sub-seasonal time scales. In Chapters 4 and 5, we examined flash drought using indices based on precipitation or evaporation, rather than P-E balance. According to (Hobbins et al., 2016) the main driver for changes in PET during flash drought development is warm air advection as it occurs during the heat or warm waves that typically accompany flash droughts, but also due to increased sensible heat coming from a drying land surface. However, the low hit rate of EDDI to detect flash drought in the soil moisture identified in Chapters 4 and 5 suggests that PET on its own is not a major contributor to flash drought development. In contrast, the high hit rate of the SPI and its rapid rate of change in the weeks prior found in this research support the findings in Koster et al. (2019), who said that precipitation is the main contributor to flash droughts in both shallow and deep soil layers. However, the SPI also had a high false alarm rate showing that not all rapid declines in precipitation end in flash drought conditions. Actual ET changes if plant-available soil moisture approaches the wilting point (i.e., water-limited conditions) (Hunt et al., 2014). With the increases in PET, the ET/PET ratio, as included in the ESI, significantly decreases. As such, it is good indicator for soil moisture conditions at depth, as has been shown by past work (e.g. Otkin et al., 2013; Hunt et al., 2014; Otkin et al., 2015) and through comparison with the root-zone soil layer in the AWRA-L data in Chapter 5. The ESI is less appropriate for the upper soil layer (top 10 cm), which is far more responsive to rainfall. While PET can be estimated comprehensively using the Penman-Monteith approximation, for which reliable global data is difficult to obtain, actual ET is much harder to estimate because

of additional factors that must be represented, including highly spatially heterogeneous soil and plant properties. With this in mind, the ESI might be the most appropriate variable to represent flash drought, but the complex estimation of ET and access to the necessary data makes it less suitable for operational use. In contrast, the SPI has proven to be a useful index for flash drought detection with its easy calculation and good skill.

Overall, the results from this thesis have shown that a precipitation-based drought index with an adjustable time scale such as the SPI can be sufficient for subseasonal to annual drought detection and more robust when using different input sources on a global scale. However, the extension of a drought index with ET or based on ET alone can be beneficial for estimating soil moisture conditions at depth and for examination of other drought characteristics than onset.

### 6.2.2 Indices for the prediction and monitoring of drought

Drought indices serve different purposes. They are used for drought identification (Nguyen et al., 2019), but also for operational drought prediction and monitoring (Svoboda et al., 2002) or to evaluate changes in future drought development in a warming climate (Dai and Zhao, 2016). The predictive and monitoring capacities of a drought index are tightly bound to its representation of drought's physical processes and were subject of Chapters 4 and 5.

Naturally, precipitation leads soil moisture content with an increasing lead time for deeper soil layers (Ford and Quiring, 2014). A lack of precipitation over time will result in a decline in soil moisture content. Identifying this deficiency over subseasonal to seasonal time scales provides information that can be used for early warning. We showed that the SPI has skill as a predictive drought index for the upper 10cm soil layer regardless of whether modelled or observed data was employed. The skill of the SPI decreased slightly for the root-zone layer soil moisture. However, the predictive skill remained higher than the EDDI and ESI. The high predictive skill of the SPI was accompanied by high false alarm ratio, showing that most rapid dry spells do not result in a flash drought in soil moisture, especially when PET is very low or soil water retention high.

PET, as used in the EDDI, is a precursor for drought development when warm air is advected. PET can also increase as a response to drying soil due to an elevated sensible heat flux increasing the ambient temperature. Which of these processes is more

prevalent will influence the predictive skill of the EDDI. Proposed as a tool for flash drought early warning in [Hobbins et al. \(2016\)](#); [Otkin et al. \(2018\)](#); [Pendergrass et al. \(2020\)](#), we have found only a limited capability of the EDDI to detect soil moisture flash drought in real time for the upper 10 cm soil layer (i.e. exactly concurrently with the soil moisture flash drought). The skill improved slightly for the root-zone layer in the AWRA-L reanalysis but detected no more than half of the identified soil moisture flash droughts. However, relaxing the timing of the detection to within two weeks of onset in the soil moisture suggests that the increase in PET is mainly a response to drying soil, rather than the cause of the initial, rapid drying. In addition, the EDDI came with a similarly high false alarm ratio as the SPI, since not all regions experiencing abnormally high PET will enter drought conditions ([Otkin et al., 2018](#)).

During times of sufficient moisture availability and elevated PET, plants increase their rate of ET, which additionally accelerates root zone soil moisture depletion. The enhanced rate markedly decreases when water-limited conditions set in. The tight coupling of actual ET to soil moisture and interaction with PET is expressed in the potential ET fraction (ET/PET) in the ESI ([Anderson et al., 2007](#)). As actual ET is a response to soil moisture, flash drought in the ESI naturally lags flash drought in soil moisture. Therefore, the ESI is not a suitable index for flash drought prediction or early detection. Despite the identified potential capabilities of early warning from [Otkin et al. \(2013\)](#) and [Nguyen et al. \(2019\)](#), our analysis showed that the ESI's skill remained very low for the root-zone layer in the AWRA-L at the concurrent onset of flash drought in the soil moisture when compared to the other drought indices of the SPI and EDDI. In contrast, the detection skill of the ESI drastically increased when the detection interval was extended to two weeks post flash drought onset in the soil moisture, highlighting the ESI's potential as a monitoring tool. The additional low false alarm ratio makes it also a far more reliable index for regions where a flash drought has already developed.

Based on the results of this thesis, none of the indices procured are able to identify flash drought sufficiently when used as a stand-alone tool. We identified that rapid changes in evaporation, either PET or ET, appear to be a response or second order contributor to flash drought, rather than the primary cause. Our evidence shows that a sudden, rapid shut-off in precipitation that is the ultimate cause of flash droughts. However, a sudden and rapid decline in precipitation is not necessarily sufficient for a

flash drought to occur i.e. not all rapid declines result in a flash drought. The identified strengths and limitations of the SPI, EDDI and ESI suggest that a multi-variate approach is most appropriate. This is similar to the operational US Drought Monitor (Svoboda et al., 2002). Otkin et al. (2018) already suggests a combination of the EDDI and ESI for drought monitoring and prediction due to their complementary nature. However, these were suggestions only and no study has been undertaken to examine this in more detail. We support their view but provide evidence that their approach would benefit from incorporating the SPI due to its high predictive skill. Our evidence shows that, for prediction, both EDDI and SPI can be used to flag regions experiencing both unusually negative precipitation anomalies and positive PET anomalies. Subsequently, the ESI can be used track those locations where a flash drought ultimately results. Visual signs of flash drought in deteriorating vegetation health might still not be visible at the point when the ESI flags a flash drought, since soil moisture is not completely depleted according to our definition with the lowest 10<sup>th</sup> percentile as the onset threshold. Using such a framework would help to target an initial response for flash drought mitigation measures and prevent excessive crop loss by, for example, allowing agriculturalists to alter irrigation schedules.

### 6.2.3 The limitations of LSMs for drought research

Since the analysis within this thesis is primarily on the global and continental scale, the use of LSMs is inevitable as observational data of land variables is inadequate for the purposes required here (discussed in detail in Chapter 1). Two LSMs from the GLDAS were used in Chapter 3 to evaluate the performance of SPI, PDSI and SPEI. Different LSMs are embedded in the CMIP5 models procured for the flash drought analyses in Chapter 4. Even on smaller domains, e.g. Australia, soil moisture observations are sparse and don't cover long time periods. Thus, for Chapter 5 outputs from AWRA-L were used, which is, like GLDAS, a model driven by observations. All their outputs, mainly soil moisture, serve as the reference in this thesis against which the drought indices are evaluated. Though there is no targeted investigation of the efficacy of LSMs in this thesis, there are some implications about their efficacy from our results.

Offline LSMs such as NOAH and CLM from GLDAS and AWRA-L are widely used to assess the performance of drought indices. Obviously, the LSMs cannot provide an exact

representation of the diversity of soil and plant properties and will miss highly localised features. However, [Koster et al. \(2009a\)](#) argue that while the absolute values of the output variables of LSMs might differ between different models, they show very similar information about soil moisture variability to observations. Droughts are an inherent part of this variability and as long as the timing of troughs and peaks of the LSMs coincide each LSM will show drought conditions within its own climatology. LSMs have also been extensively evaluated against *in situ* soil moisture and energy fluxes where possible and can be seen as a best estimate of real-world conditions, e.g. [Liu et al. \(2009\)](#); [Wang et al. \(2016b\)](#) for GLDAS and [Frost et al. \(2015\)](#); [Holgate et al. \(2016\)](#) for AWRA-L. Therefore, their use for benchmarking drought indices on a global scale is justified.

The LSMs within the six global climate models from the CMIP5 suite showed large inter-model spread in their flash drought representation, and differences to the AWRA-L reanalysis. These differences are associated with both the LSM and the coupling to the atmospheric model within the GCM. Within the range of different models and observations/reanalysis we procured in Chapters 4 and 5, the largest uncertainties in flash drought detections are associated with ET. Due to a stronger coupling between land and atmosphere, GCMs show a higher skill for ET based drought indices EDDI and ESI than they should when compared to AWRA-L, where both have a much weaker skill than the SPI. Within the model suite some models were performing worse than others. An ensemble mean could not represent the land atmosphere coupling strength in AWRA-L either. Hence, using CMIP5 models to evaluate changes in past and future flash drought scenarios would need further evaluation against a global observed climatology of flash drought to truly determine the biases in the GCMs. Additionally, this would likely be amplified by the increasing PET in a warming climate ([Milly and Dunne, 2016](#)). These biases would also depend on how the drought indices are computed, either using offline model output for the input variables or using outputs from coupled models, e.g. latent heat flux. The former method would be subject to the biases in all those variables, whereas the latter will be internally consistent and a much better approach.

A major caveat of using CMIP5 models for flash drought research is the limitation of daily data to the upper 10cm soil layer. Deeper layers are available on a monthly time scale, but this is too temporally coarse considering a flash drought definition that is based on just two or three weeks. Compared to the root-zone layer, flash droughts happen

five to ten times more often in the upper 10cm in AWRA-L when applying the same definition. Consequently, using the upper 10cm as an indicator for flash droughts in the deeper layers proves to be unreasonable. Additionally, the physical processes relating to the development of ET in the lead-up to the onset of flash drought are not represented well by the upper 10cm soil layer. This was made clear by the larger correlations between the ESI and soil moisture in the root zone layer in Chapter 5. The ET/PET fraction is an indicator of water stress and hence, ET continues from the deeper soil even when the moisture in the upper 10cm is nearly completely depleted. Furthermore, the top soil layer will always dry out first before the deeper layers follow. This means that those indices more sensitive to variability at the surface (i.e. the SPI and EDDI) would naturally have a higher hit rate (i.e. correctly indicating) a flash drought. However, as we showed in Chapter 5, this sensitivity inevitably also has a high false alarm rate since the top soil layer moisture is often restored before the drying penetrates further into the ground. For these reasons, the shallow soil layer is less useful for flash drought research compared to deeper layers in the root zone.

### 6.3 Future Work

It is our hope that the results from this thesis prove useful for future drought research in the area of prediction and monitoring. For example, our results could be used to help guide the creation of a multi-variate tool for drought prediction and monitoring that can help to mitigate impacts from this natural hazard. Although many interesting results were found in this research many questions and research avenues remain. For example, if the output were obtainable, using root-zone layer soil moisture from global climate models and testing the procured indices SPI, EDDI and ESI on it should be the first extension of this study. The newest phase of the Coupled Model Intercomparison Project Phase 6 (Eyring et al., 2016) provides soil moisture content for various layers on a daily basis. Thus, further investigations regarding details of the underlying LSMs in CMIP6 and its components can be conducted for a deeper understanding of flash drought development in those models.

The sheer amount of drought indices available only allows to test a fraction of them. For this thesis, the most popular ones for either seasonal to annual or sub-seasonal time

scales have been chosen. Testing other indices could broaden the knowledge of suitable drought indices for flash drought. For example, recently, [Noguera et al. \(2020\)](#) has used the Standardised Precipitation Evapotranspiration Index (SPEI, [Vicente-Serrano et al., 2010](#)) to evaluate characteristics and trends of flash droughts in Spain, however these were not compared to soil moisture. Incorporating a larger suite of drought indices could help to develop a multi-variate tool not only for flash drought but for prediction and monitoring of drought on all time scales.

Further, there have been definitions and metrics developed that could be employed. [Otkin et al. \(2014\)](#) has specifically designed the rapid change index (RCI) based on the ESI to "to highlight areas undergoing rapid changes in moisture stress". [Pendergrass et al. \(2020\)](#) proposed a definition for international operation, prediction and research, which is based on a 50% increase in EDDI. However, the index itself should reach a certain drought threshold, otherwise the rapid change could also occur on the wet side of the distribution from anomalously wet to average conditions. While this thesis has adjusted and used the definition from [Ford and Labosier \(2017\)](#), using a certain change within a certain time frame and reaching a specific drought threshold, it is likely not the perfect definition for flash drought globally. Local adjustments to the time periods in which the rapid change has to occur, or to the drought threshold, could be done to closer represent different evaporative regimes.

Conducting the analyses on a higher spatial resolution than the  $2.5^{\circ} \times 2.5^{\circ}$  used in the entire thesis to match either the grid dimensions of observational data sets (Chapter 3) or the coarsest CMIP5 model (Chapters 4 and 5), would likely provide more information about regional differences. Interpolating to a coarse common grid generalises information that would otherwise provide potentially highly localised features. Especially the very high native resolution of AWAP/AWRA-L of  $0.05^{\circ} \times 0.05^{\circ}$  could be useful to further distinguish flash drought frequency and usefulness of the drought indices in different environments.

## 6.4 Conclusion

This thesis has investigated drought indices incorporating precipitation or ET or both and has shown how they represent sub-seasonal, seasonal and annual-scale drought in models

and observations. The results from this thesis show that a significant lack of precipitation is the main contributor to drought development on the time scales examined. The simplicity of an index like the SPI and the availability of, dense, long term precipitation records have proven be equally or even more skilful than its counterparts including ET and make it an attractive index for the ongoing study of drought. However, the use of precipitation for detecting drought is not flawless as it is uncoupled to land surface conditions. It is unquestionable that ET also contributes to drought development and this is particularly true for flash drought. However, our results show that the inclusion of ET in drought indices tends to be more useful for monitoring drought due to its response to drying soil moisture, than for the prediction of drought onset. In that sense, we have shown that different drought indices are useful for different aspects of a drought. For example, for flash drought, we provide evidence that the SPI and EDDI could be useful for predicting flash drought risk, but that the ESI is more appropriate for monitoring the development of a flash drought once it has onset. Additionally, this thesis has shown that the source of input data for drought indices, whether from observations, reanalysis or climate models, play a significant role in the efficacy of a drought index. Consideration of the data sets employed when computing drought indices, and their associated uncertainties, is paramount for drought research.

# Chapter 7

## Appendix

### 7.1 Appendix Chapter 3

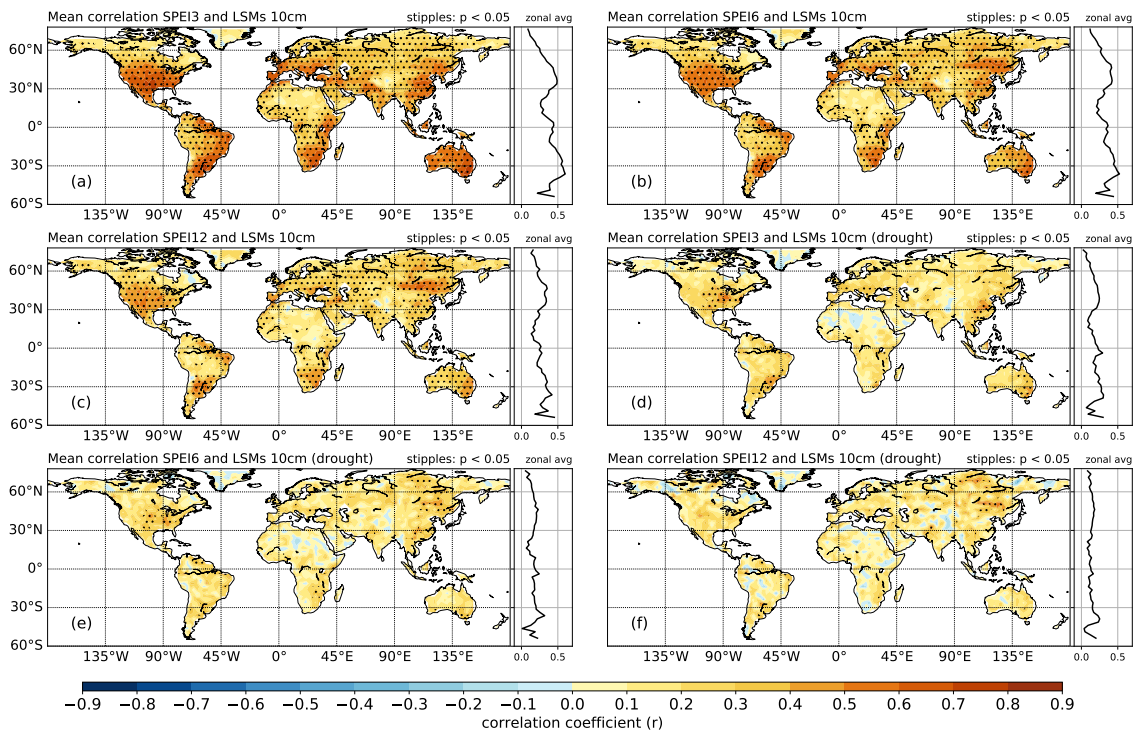


**Figure 7.1:** Mean and zonal correlation coefficients ( $r$ ) of varying GLDAS LSMs for SPEI3 (a/d), SPEI6 (b/e) and SPEI12 (c/f) for whole data distribution (a-c) and drought periods (d-f) of the 0-10cm layer. The zonal average is shown to the right of each plot. Stippling shows statistically significant correlations at the 95% level.

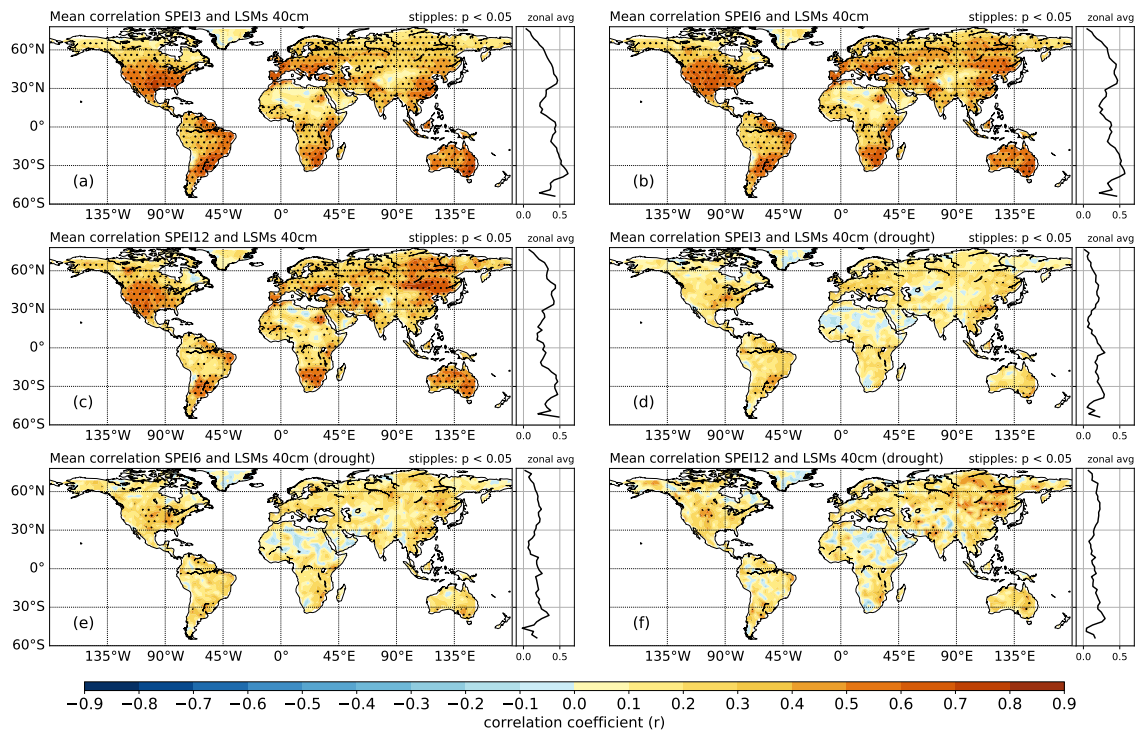


**Figure 7.2:** Mean and zonal correlation coefficients ( $r$ ) of varying GLDAS LSMs for SPEI3 (a/d), SPEI6 (b/e) and SPEI12 (c/f) for whole data distribution (a-c) and drought periods (d-f) of the 10-40cm layer. The zonal average is shown to the right of each plot. Stippling shows statistically significant correlations at the 95% level.

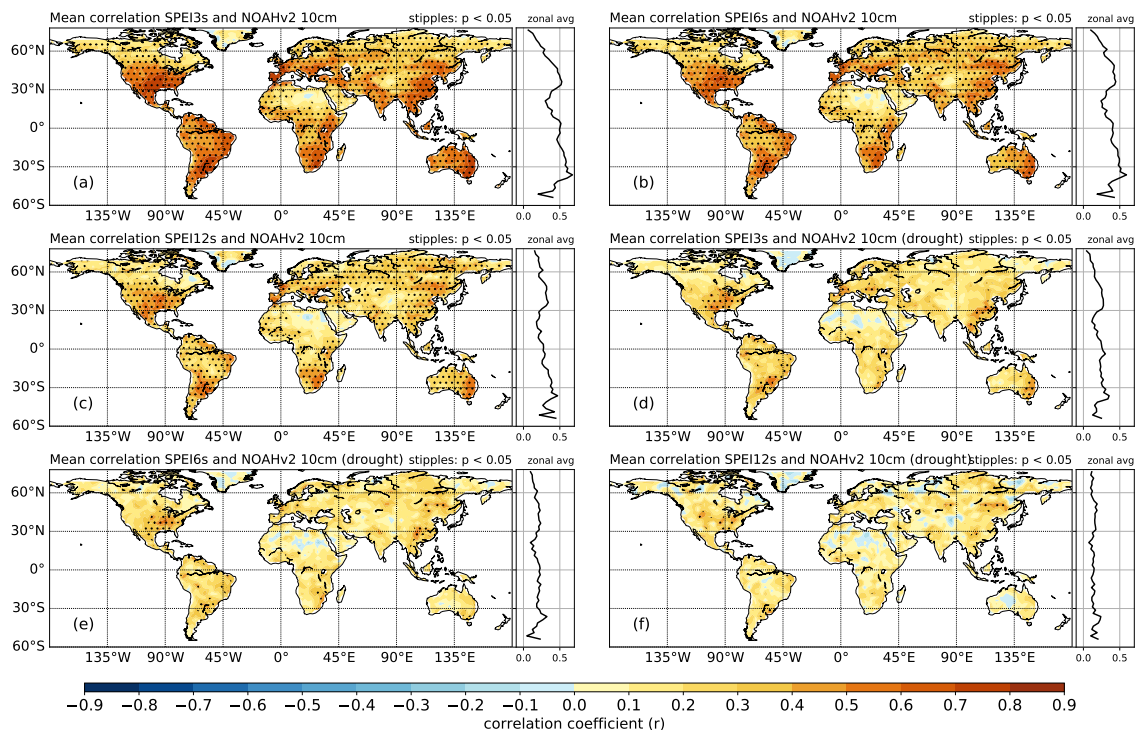


**Figure 7.3:** Mean and zonal correlation coefficients ( $r$ ) of varying input data for SPEI3 (a/d), SPEI6 (b/e) and SPEI12 (c/f) with GLDAS NOAHv2 for whole data distribution (a-c) and drought periods (d-f) of the 0-10cm layer. The zonal average is shown to the right of each plot. Stippling shows statistically significant correlations at the 95% level.

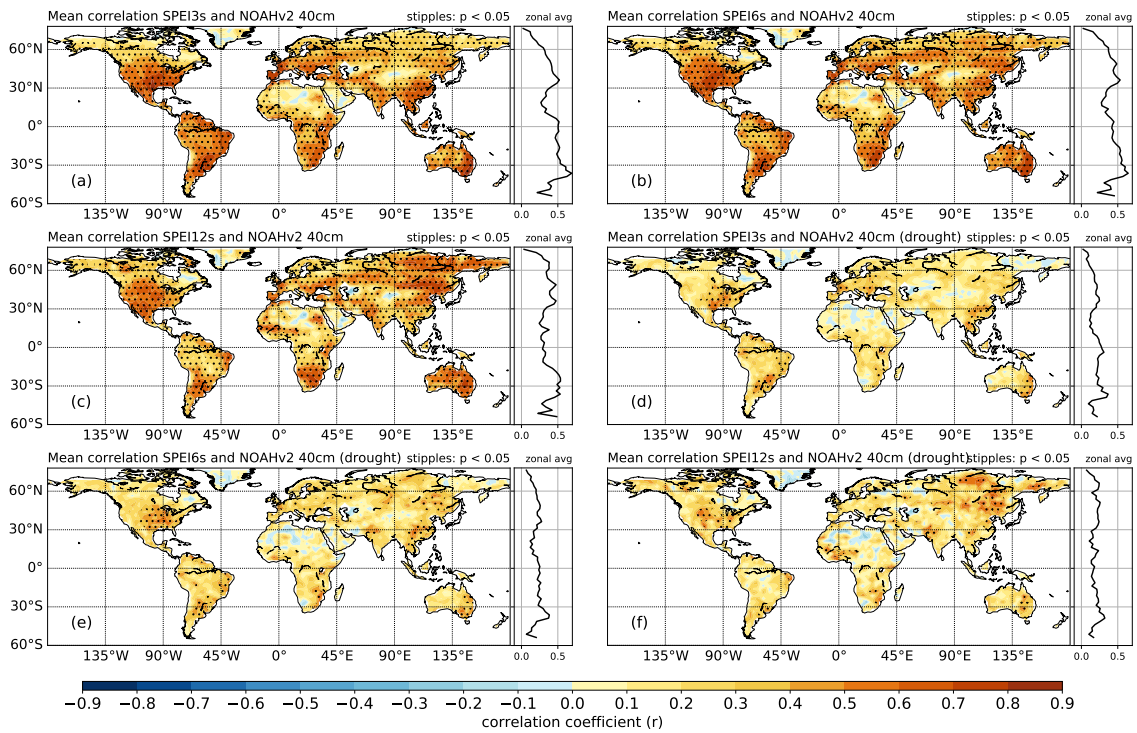


**Figure 7.4:** Mean and zonal correlation coefficients ( $r$ ) of varying input data for SPEI3 (a/d), SPEI6 (b/e) and SPEI12 (c/f) with GLDAS NOAHv2 for whole data distribution (a-c) and drought periods (d-f) of the 10-40cm layer. The zonal average is shown to the right of each plot. Stippling shows statistically significant correlations at the 95% level.

## 7.2 Appendix Chapter 5

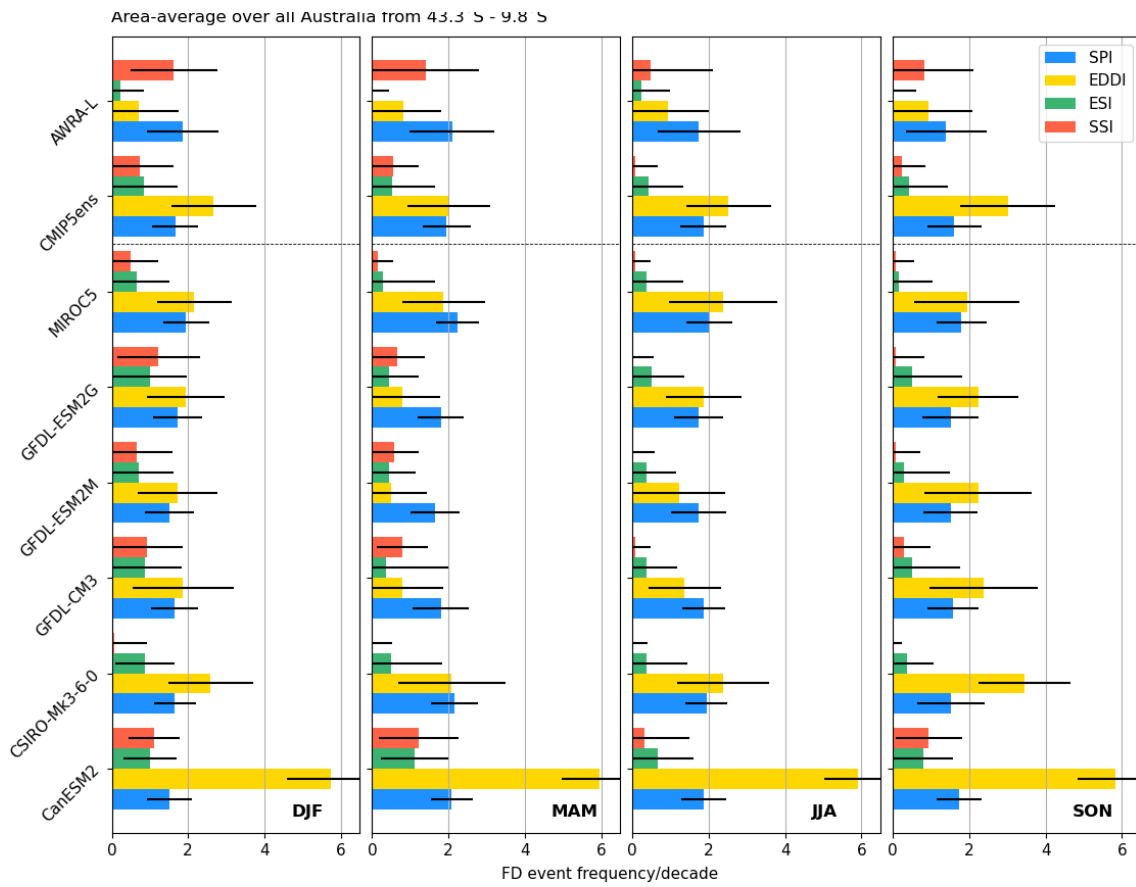


**Figure 7.5:** Area median over all of Australia of flash drought event frequency per decade for each of EDDI, ESI, SPI and SSI split into season and listed for each CMIP5 model (top to sixth row), CMIP5 ensemble (seventh row) and AWRA-L/AWAP (eighth row). Black lines represent the 90<sup>th</sup> percentile confidence interval.

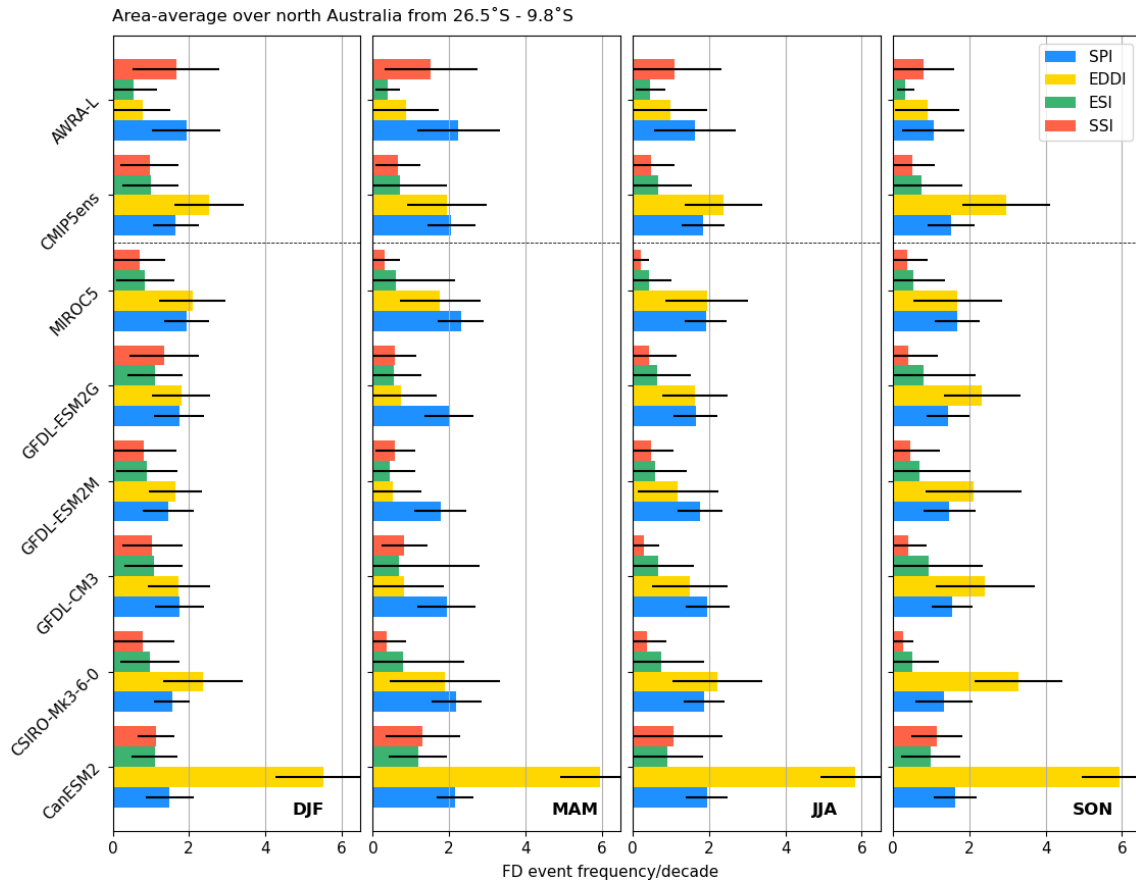


**Figure 7.6:** Area average of north Australia ( $< 27^{\circ}\text{S}$ ) of flash drought event frequency per decade for each of EDDI, ESI, SPI and SSI split into season and listed for each CMIP5 model (top to sixth row), CMIP5 ensemble (seventh row) and AWRA-L/AWAP (eighth row). Grid cells without any flash droughts occurring were masked out. Black lines represent the 90<sup>th</sup> percentile confidence interval.

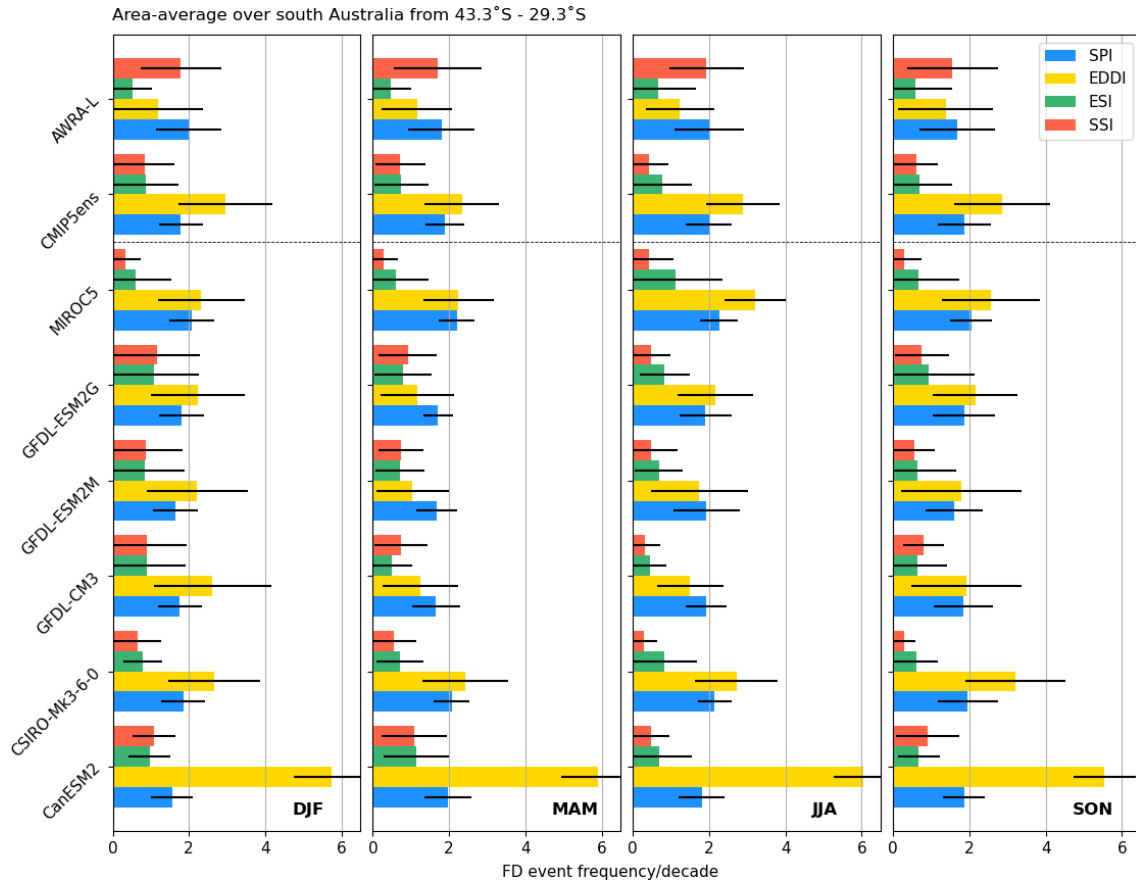


Figure 7.7: As Figure 7.6 but for south Australia ( $> 27^{\circ}S$ )

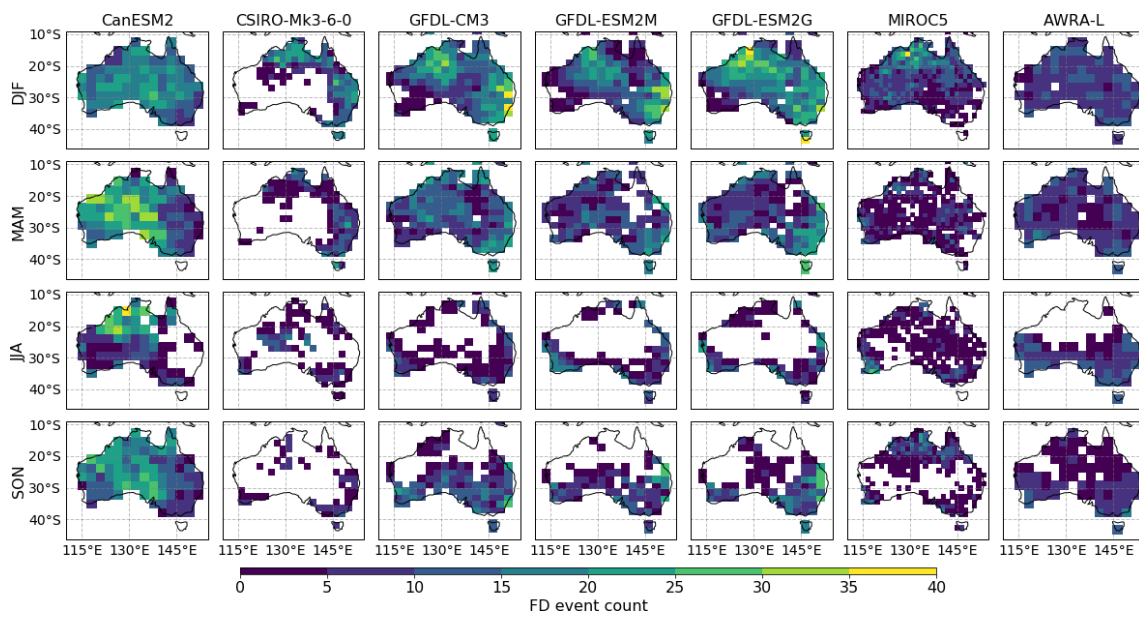


Figure 7.8: Total count of soil moisture flash drought events longer than 30 days for each season and CMIP5 model/AWRA-L observations. Grid cells with not a single flash drought occurrence are masked out.

## References

- Abramowitz, G., Pitman, A., Gupta, H., Kowalczyk, E., and Wang, Y.: Systematic Bias in Land Surface Models, *Journal of Hydrometeorology*, 8, 989–1001, <https://doi.org/10.1175/jhm628.1>, 2007.
- Adler, R., Huffman, G., Chang, A., Ferraro, R., Xie, P.-P., Janowiak, J., Rudolf, B., Schneider, U., Curtis, S., Bolvin, D., Gruber, A., Susskind, J., Arkin, P., and Nelkin, E.: The Version-2 Global Precipitation Climatology Project (GPCP) Monthly Precipitation Analysis (1979–Present), *Journal of Hydrometeorology*, 4, 1147–1167, 2003.
- Agutu, N. O., Awange, J. L., Zerihun, A., Ndehedehe, C. E., Kuhn, M., and Fukuda, Y.: Assessing multi-satellite remote sensing, reanalysis, and land surface models' products in characterizing agricultural drought in East Africa, *Remote Sensing of Environment*, 194, 287–302, <https://doi.org/10.1016/j.rse.2017.03.041>, 2017.
- Alexander, L. V. and Arblaster, J. M.: Assessing trends in observed and modelled climate extremes over Australia in relation to future projections, *International Journal of Climatology: A Journal of the Royal Meteorological Society*, 29, 417–435, 2009.
- Allen, R., Walter, I., Elliott, R., Howell, T., Itenfisu, D., and Jensen, M.: The ASCE standardized reference evapotranspiration equation. Prepared by Task Committee on Standardization of Reference Evapotranspiration. Reston, Va.: ASCE Environmental and Water Resources Institute, Reston, VA, 2005.
- Allen, R. G., Pereira, L. S., Raes, D., and Smith, M.: Crop evapotranspiration - Guidelines for computing crop water requirements - FAO Irrigation and drainage paper 56, Report, 1998.

- Anders, I. and Rockel, B.: The influence of prescribed soil type distribution on the representation of present climate in a regional climate model, *Climate dynamics*, 33, 177–186, 2009.
- Anderson, M. C., Norman, J. M., Mecikalski, J. R., Otkin, J. A., and Kustas, W. P.: A climatological study of evapotranspiration and moisture stress across the continental United States based on thermal remote sensing: 1. Model formulation, *Journal of Geophysical Research: Atmospheres*, 112, <https://doi.org/10.1029/2006jd007506>, 2007.
- Bandyopadhyay, A., Bhadra, A., Raghuwanshi, N., and Singh, R.: Estimation of monthly solar radiation from measured air temperature extremes, *Agricultural and forest meteorology*, 148, 1707–1718, 2008.
- Beaudoing, H., Rodell, M., and NASA/GSFC/HSL: GLDAS Noah Land Surface Model L4 monthly 0.25 x 0.25 degree V2.0, Greenbelt, Maryland, USA, Goddard Earth Sciences Data and Information Services Center (GES DISC), <https://doi.org/10.5067/9SQ1B3ZXP2C5>, 2015.
- Beguiría, S., Vicente-Serrano, S. M., Reig, F., and Latorre, B.: Standardized precipitation evapotranspiration index (SPEI) revisited: parameter fitting, evapotranspiration models, tools, datasets and drought monitoring, *International journal of climatology*, 34, 3001–3023, 2014.
- Best, M. J., Abramowitz, G., Johnson, H., Pitman, A., Balsamo, G., Boone, A., Cuntz, M., Decharme, B., Dirmeyer, P., Dong, J., et al.: The plumbing of land surface models: benchmarking model performance, *Journal of Hydrometeorology*, 16, 1425–1442, 2015.
- Burke, E. J. and Brown, S. J.: Evaluating uncertainties in the Projection of Future Drought, *Journal of Hydrometeorology*, 9, 292–299, <https://doi.org/10.1175/2007JHM929.1>, 2008.
- Chen, M., Xie, P., Janowiak, J. E., and Arkin, P. A.: Global Land Precipitation: A 50-yr Monthly Analysis Based on Gauge Observations, *Journal of Hydrometeorology*, 3, 249–266, [https://doi.org/10.1175/1525-7541\(2002\)003<0249:GLPAYM>2.0](https://doi.org/10.1175/1525-7541(2002)003<0249:GLPAYM>2.0).

- CO<sub>2</sub>, URL [https://doi.org/10.1175/1525-7541\(2002\)003<0249:GLPAYM>2.0.CO;2](https://doi.org/10.1175/1525-7541(2002)003<0249:GLPAYM>2.0.CO;2), 2002.
- Contractor, S., Donat, M. G., Alexander, L. V., Ziese, M., Meyer-Christoffer, A., Schneider, U., Rustemeier, E., Becker, A., Durre, I., and Vose, R. S.: Rainfall Estimates on a Gridded Network (REGEN) - A global land-based gridded dataset of daily precipitation from 1950-2013, *Hydrology and Earth System Sciences Discussions*, pp. 1–30, <https://doi.org/10.5194/hess-2018-595>, 2019.
- Cowtan, K. and Way, R. G.: Coverage bias in the HadCRUT4 temperature series and its impact on recent temperature trends, *Quarterly Journal of the Royal Meteorological Society*, 140, 1935–1944, <https://doi.org/10.1002/qj.2297>, 2014.
- Crausbay, S. D., Ramirez, A. R., Carter, S. L., Cross, M. S., Hall, K. R., Bathke, D. J., Betancourt, J. L., Colt, S., Cravens, A. E., Dalton, M. S., Dunham, J. B., Hay, L. E., Hayes, M. J., McEvoy, J., McNutt, C. A., Moritz, M. A., Nislow, K. H., Raheem, N., and Sanford, T.: Defining Ecological Drought for the Twenty-First Century, *Bulletin of the American Meteorological Society*, 98, 2543–2550, <https://doi.org/10.1175/bams-d-16-0292.1>, 2017.
- Dai, A.: Characteristics and trends in various forms of the Palmer Drought Severity Index during 1900–2008, *Journal of Geophysical Research*, 116, 1–26, <https://doi.org/doi:10.1029/2010JD015541>, 2011a.
- Dai, A.: Drought under global warming: a review, *WIREs Climate Change*, 2, 45–65, 2011b.
- Dai, A. and Zhao, T.: Uncertainties in historical changes and future projections of drought. Part I: estimates of historical drought changes, *Climatic Change*, 144, 519–533, <https://doi.org/10.1007/s10584-016-1705-2>, 2016.
- Dai, A., Fung, I. Y., and Del Genio, A. D.: Surface observed global land precipitation variations during 1900–88, *Journal of climate*, 10, 2943–2962, 1997.
- Dai, A., Trenberth, K. E., and Qian, T.: A Global Dataset of Palmer Drought Severity Index for 1870–2002: Relationship with Soil Moisture and Effects of Surface Warming, *Journal of Hydrometeorology*, 5, 1117–1130, 2004.

- De Kauwe, M. G., Zhou, S. X., Medlyn, B. E., Pitman, A. J., Wang, Y. P., Durumsma, R. A., and Prentice, I. C.: Do land surface models need to include differential plant species responses to drought? Examining model predictions across a mesic-xeric gradient in Europe, *Biogeosciences*, 12, 7503–7518, <https://doi.org/10.5194/bg-12-7503-2015>, 2015.
- De Kauwe, M. G., Medlyn, B. E., Walker, A. P., Zaehle, S., Asao, S., Guenet, B., Harper, A. B., Hickler, T., Jain, A. K., Luo, Y., et al.: Challenging terrestrial biosphere models with data from the long-term multifactor Prairie Heating and CO<sub>2</sub> Enrichment experiment, *Global change biology*, 23, 3623–3645, <https://doi.org/10.1111/gcb.13643>, 2017.
- Dee, D. P., Uppala, S. M., Simmons, A. J., Berrisford, P., Poli, P., Kobayashi, S., Andrae, U., Balmaseda, M. A., Balsamo, G., Bauer, P., Bechtold, P., Beljaars, A. C. M., van de Berg, L., Bidlot, J., Bormann, N., Delsol, C., Dragani, R., Fuentes, M., Geer, A. J., Haimberger, L., Healy, S. B., Hersbach, H., Hólm, E. V., Isaksen, I., Kållberg, P., Köhler, M., Matricardi, M., McNally, A. P., Monge-Sanz, B. M., Morcrette, J. J., Park, B. K., Peubey, C., de Rosnay, P., Tavolato, C., Thépaut, J. N., and Vitart, F.: The ERA-Interim reanalysis: configuration and performance of the data assimilation system, *Quarterly Journal of the Royal Meteorological Society*, 137, 553–597, <https://doi.org/10.1002/qj.828>, 2011.
- Dirmeyer, P. A.: A History and Review of the Global Soil Wetness Project (GSWP), *Journal of Hydrometeorology*, 12, 729–749, <https://doi.org/10.1175/jhm-d-10-05010.1>, 2011.
- Dirmeyer, P. A., Jin, Y., Singh, B., and Yan, X.: Trends in Land–Atmosphere Interactions from CMIP5 Simulations, *Journal of Hydrometeorology*, 14, 829–849, <https://doi.org/10.1175/jhm-d-12-0107.1>, 2013.
- Donohue, R. J., McVicar, T. R., and Roderick, M. L.: Assessing the ability of potential evaporation formulations to capture the dynamics in evaporative demand within a changing climate, *Journal of Hydrology*, 386, 186–197, 2010.
- Dorigo, W. A., Wagner, W., Hohensinn, R., Hahn, S., Paulik, C., Xaver, A., Gruber, A., Drusch, M., Mecklenburg, S., van Oevelen, P., Robock, A., and Jackson, T.:

- The International Soil Moisture Network: a data hosting facility for global in situ soil moisture measurements, *Hydrology and Earth System Sciences*, 15, 1675–1698, <https://doi.org/10.5194/hess-15-1675-2011>, 2011.
- Doyle, K.: What you need to know about droughts: Why they happen and how they are defined, ABC News, URL <https://www.abc.net.au/news/2018-08-01/what-you-need-to-know-about-droughts/10051956>, 2018.
- Doyle, K.: 'Flash droughts' strike fast and hard, and researchers are still racing to identify them before they happen, ABC News, URL <https://www.abc.net.au/news/2019-07-20/how-flash-droughts-strike-fast-and-hard/11320654>, 2019.
- Dracup, J. A., Seong Lee, K., and Paulsen Jr, E. G.: On the Definition of Droughts, *Water Resources Research*, 16, 297–302, 1980.
- Du, J., Fang, J., Xu, W., and Shi, P.: Analysis of dry/wet conditions using the standardized precipitation index and its potential usefulness for drought/flood monitoring in Hunan Province, China, *Stochastic Environmental Research and Risk Assessment*, 27, 377–387, <https://doi.org/10.1007/s00477-012-0589-6>, 2012.
- Edwards, D. C.: Characteristics of 20th Century drought in the United States at multiple time scales., Tech. rep., AIR FORCE INST OF TECH WRIGHT-PATTERSON AFB OH, 1997.
- Entekhabi, D., Rodriguez-Iturbe, I., and Castelli, F.: Mutual interaction of soil moisture state and atmospheric processes, *Journal of Hydrology*, 184, 3–17, 1996.
- Esfahanian, E., Nejadhashemi, A. P., Abouali, M., Daneshvar, F., Alireza, A. R., Herman, M. R., and Tang, Y.: Defining drought in the context of stream health, *Ecological Engineering*, 94, 668–681, <https://doi.org/10.1016/j.ecoleng.2016.06.110>, 2016.
- Eyring, V., Bony, S., Meehl, G. A., Senior, C. A., Stevens, B., Stouffer, R. J., and Taylor, K. E.: Overview of the Coupled Model Intercomparison Project Phase 6 (CMIP6) experimental design and organization, *Geoscientific Model Development (Online)*, 9, <https://doi.org/10.5194/gmd-9-1937-2016>, 2016.
- Fan, J., McConkey, B., Wang, H., and Janzen, H.: Root distribution by depth for temperate agricultural crops, *Field Crops Research*, 189, 68–74, 2016.

- Farahmand, A. and AghaKouchak, A.: A generalized framework for deriving nonparametric standardized drought indicators, *Advances in Water Resources*, 76, 140–145, <https://doi.org/10.1016/j.advwatres.2014.11.012>, 2015.
- Ficklin, D. L., Letsinger, S. L., Gholizadeh, H., and Maxwell, J. T.: Incorporation of the Penman–Monteith potential evapotranspiration method into a Palmer Drought Severity Index Tool, *Computers & Geosciences*, 85, 136–141, <https://doi.org/10.1016/j.cageo.2015.09.013>, 2015.
- Ford, T. W. and Labosier, C. F.: Meteorological conditions associated with the onset of flash drought in the Eastern United States, *Agricultural and Forest Meteorology*, 247, 414–423, <https://doi.org/10.1016/j.agrformet.2017.08.031>, 2017.
- Ford, T. W. and Quiring, S. M.: Comparison and application of multiple methods for temporal interpolation of daily soil moisture, *International Journal of Climatology*, 34, 2604–2621, <https://doi.org/10.1002/joc.3862>, 2014.
- Ford, T. W., McRoberts, D. B., Quiring, S. M., and Hall, R. E.: On the utility of in situ soil moisture observations for flash drought early warning in Oklahoma, USA, *Geophysical Research Letters*, 42, 9790–9798, <https://doi.org/10.1002/2015GL066600>, 2015.
- Frost, A., Ramchurn, A., Hafeez, M., Zhao, F., Haverd, V., J., B., and Briggs, P.: Evaluation of AWRA-L: the Australian Water Resource Assessment model, 2015.
- Frost, A. J., Ramchurn, A., and Smith, A.: The Australian landscape water balance model (AWRA-L v6). Technical description of the Australian water resources assessment landscape model version 6, Report, Melbourne, Australia: Bureau of Meteorology, 2018.
- Gallant, A. J. E., Reeder, M. J., Risbey, J. S., and Hennessy, K. J.: The characteristics of seasonal-scale droughts in Australia, 1911 – 2009, *International Journal of Climatology*, 33, 1658–1672, <https://doi.org/10.1002/joc.3540>, 2013.
- Giorgi, F. and Francisco, R.: Uncertainties in regional climate change prediction: a regional analysis of ensemble simulations with the HADCM2 coupled AOGCM, *Climate Dynamics* (2000), 16, 169–182, 2000.

- Guo, Z., Dirmeyer, P., Koster, R., Bonan, G., Chan, E., Cox, P., Gordon, C., Kanae, S., Kowalczyk, E., Lawrence, D., Liu, P., Malyshev, S., McAvaney, B., McGregor, J., Mitchell, K., Mocko, D., Oki, T., Oleson, K., Pitman, A., Sud, Y., Taylor, C., Verseghy, D., Vasic, R., Xue, Y., and Yamada, T.: GLACE: The Global Land-Atmosphere Coupling Experiment. Part II: Analysis, *Journal of Hydrometeorology*, 7, 611–625, <https://doi.org/10.1175/JHM511.1>, 2006.
- Guttman, N. B.: A sensitivity analysis of the Palmer hydrologic drought index, *Water Resources Bulletin*, 27, 1991.
- Guttman, N. B.: Comparing the palmer Drought Index and the Standardized Precipitation Index, *Journal of the American Water Resources Association*, 34, 113–121, 1998.
- Haile, G. G., Tang, Q., Li, W., Liu, X., and Zhang, X.: Drought: Progress in broadening its understanding, *WIREs Water*, 7, <https://doi.org/10.1002/wat2.1407>, 2019.
- Halwatura, D., McIntyre, N., Lechner, A. M., and Arnold, S.: Capability of meteorological drought indices for detecting soil moisture droughts, *Journal of Hydrology: Regional Studies*, 12, 396–412, <https://doi.org/10.1016/j.ejrh.2017.06.001>, 2017.
- Hameed, M., Ahmadalipour, A., and Moradkhani, H.: Apprehensive drought characteristics over Iraq: results of a multidecadal spatiotemporal assessment, *Geosciences*, 8, 58, 2018.
- Hao, Z. and Singh, V. P.: Drought characterization from a multivariate perspective: A review, *Journal of Hydrology*, 527, 668–678, <https://doi.org/10.1016/j.jhydrol.2015.05.031>, 2015.
- Harris, I., Jones, P. D., Osborn, T. J., and Lister, D. H.: Updated high-resolution grids of monthly climatic observations - the CRU TS3.10 Dataset, *International Journal of Climatology*, 34, 623–642, <https://doi.org/10.1002/joc.3711>, 2014.
- Harris, I., Osborn, T. J., Jones, P., and Lister, D.: Version 4 of the CRU TS monthly high-resolution gridded multivariate climate dataset, *Scientific data*, 7, 1–18, 2020.
- Hayes, M., Svoboda, M., Wall, N., and Widhalm, M.: The Lincoln Declaration on Drought Indices: Universal Meteorological Drought Index Recommended, *Bul-*

- letin of the American Meteorological Society, 92, 485–488, <https://doi.org/10.1175/2010BAMS3103.1>, 2011.
- Heim Jr., R. R.: A Review of Twentieth- Century Drought Indices Used in the United States, *Bulletin of the American Meteorological Society*, pp. 1149–1165, 2002.
- Hobbins, M., McEvoy, D., and Hain, C.: Evapotranspiration, Evaporative Demand, and Drought, in: [Wilhite and Pulwarty \(2017\)](#), pp. 259–288, <https://doi.org/10.1201/9781315265551-15>, 2017.
- Hobbins, M. T., Dai, A., Roderick, M. L., and Farquhar, G. D.: Revisiting the parameterization of potential evaporation as a driver of long-term water balance trends, *Geophysical Research Letters*, 35, 2008.
- Hobbins, M. T., Wood, A., McEvoy, D. J., Huntington, J. L., Morton, C., Anderson, M., and Hain, C.: The Evaporative Demand Drought Index. Part I: Linking Drought Evolution to Variations in Evaporative Demand, *Journal of Hydrometeorology*, 17, 1745–1761, <https://doi.org/10.1175/jhm-d-15-0121.1>, 2016.
- Hoffmann, D., Gallant, A. J. E., and Arblaster, J. M.: The sensitivity of drought variability to index and data selection, *Journal of Geophysical Research - Atmospheres*, <https://doi.org/10.1029/2019JD031946>, 2020.
- Holgate, C. M., De Jeu, R. A. M., van Dijk, A. I. J. M., Liu, Y. Y., Renzullo, L. J., Vinodkumar, Dharssi, I., Parinussa, R. M., Van Der Schalie, R., Gevaert, A., Walker, J., McJannet, D., Cleverly, J., Haverd, V., Trudinger, C. M., and Briggs, P. R.: Comparison of remotely sensed and modelled soil moisture data sets across Australia, *Remote Sensing of Environment*, 186, 479–500, <https://doi.org/10.1016/j.rse.2016.09.015>, 2016.
- Hu, Q. and Willson, G. D.: Effects of Temperature Anomalies on the Palmer Drought Severity Index in the Central United States, *International Journal of Climatology*, 20, 1899–1911, 2000.
- Huang, Y., Gerber, S., Huang, T., and Lichstein, J. W.: Evaluating the drought response of CMIP5 models using global gross primary productivity, leaf area, precipitation, and

- soil moisture data, *Global Biogeochemical Cycles*, 30, 1827–1846, <https://doi.org/10.1002/2016gb005480>, 2016.
- Huffman, G. J., Adler, R. F., Arkin, P., Chang, A., Ferraro, R., Gruber, A., Janowiak, J., McNab, A., Rudolf, B., and Schneider, U.: The Global Precipitation Climatology Project (GPCP) Combined Precipitation Dataset, *Bulletin of the American Meteorological Society*, 78, 5–20, [https://doi.org/10.1175/1520-0477\(1997\)078<0005:TGPCPG>2.0.CO;2](https://doi.org/10.1175/1520-0477(1997)078<0005:TGPCPG>2.0.CO;2), 1997.
- Hunt, E. D., Svoboda, M., Wardlow, B., Hubbard, K., Hayes, M., and Arkebauer, T.: Monitoring the effects of rapid onset of drought on non-irrigated maize with agronomic data and climate-based drought indices, *Agricultural and Forest Meteorology*, 191, 1–11, 2014.
- Hurrell, J. W., Hack, J. J., Shea, D., Caron, J. M., and Rosinski, J.: A New Sea Surface Temperature and Sea Ice Boundary Dataset for the Community Atmosphere Model, *Journal of Climate*, 21, 5145–5153, <https://doi.org/10.1175/2008jcli2292.1>, 2008.
- IPCC: Managing the Risk of Extreme Events and Disasters to Advance Climate Change adaptation. A Special Report of Working Groups I and II of the Intergovernmental Panel on Climate Change, Cambridge University Press, Cambridge, UK and New York, NY, USA, 2012.
- Jacobi, J., Perrone, D., Duncan, L. L., and Hornberger, G.: A tool for calculating the Palmer drought indices, *Water Resources Research*, 49, 6086–6089, <https://doi.org/10.1002/wrcr.20342>, 2013.
- Jones, D. A., Wang, W., and Fawcett, R.: High-quality spatial climate data-sets for Australia, *Australian Meteorological and Oceanographic Journal*, 58, 233–248, 2009.
- Jones, P., Lister, D., Osborn, T., Harpham, C., Salmon, M., and Morice, C.: Hemispheric and large-scale land-surface air temperature variations: An extensive revision and an update to 2010, *Journal of Geophysical Research*, 117, 29, <https://doi.org/10.1029/2011JD017139>, 2012.
- Kalney, E., Kanamitsu, M., Kistler, R., Collins, W., Deaven, D., Gandin, L., Iredell, M., Saha, S., White, G., Woollen, J., Zhu, Y., Chelliah, M., Ebisuzaki, W., Higgins, W.,

- Janowiak, J., Mo, K. C., Ropelewski, C., Wang, J., Leetmaa, A., Reynolds, R., Jenne, R., and Joseph, D.: The NCEP/NCAR 40-Year Reanalysis Project, *Bulletin of the American Meteorological Society*, 77, 437–471, 1996.
- Karthikeyan, L., Pan, M., Wanders, N., Kumar, D. N., and Wood, E. F.: Four decades of microwave satellite soil moisture observations: Part 1. A review of retrieval algorithms, *Advances in Water Resources*, 109, 106–120, <https://doi.org/10.1016/j.advwatres.2017.09.006>, 2017.
- Keyantash, J. and Dracup, J. A.: The Quantification of Drought: An Evaluation of Drought Indices, *Bulletin of American Meteorological Society*, pp. 1167–1180, 2002.
- Khalili, D., Farnoud, T., Jamshidi, H., Kamgar-Haghighi, A. A., and Zand-Parsa, S.: Comparability Analyses of the SPI and RDI Meteorological Drought Indices in Different Climatic Zones, *Water Resources Management*, 25, 1737–1757, <https://doi.org/10.1007/s11269-010-9772-z>, 2011.
- Kiem, A. S. and Franks, S. W.: Multi-decadal variability of drought risk, eastern Australia, *Hydrological Processes*, <https://doi.org/10.1002/hyp.1460>, 2004.
- Kistler, R., Kalnay, E., Collins, W., Saha, S., White, G., Woollen, J., Chelliah, M., Ebisuzaki, W., Kanamitsu, M., Kousky, V., et al.: The NCEP-NCAR 50-year reanalysis: monthly means CD-ROM and documentation, *Bulletin of the American Meteorological society*, 82, 247–268, 2001.
- Koster, R. D. and Suarez, M. J.: Soil Moisture Memory in Climate Models, *Journal of Hydrometeorology*, 2, 558–570, [https://doi.org/10.1175/1525-7541\(2001\)002<0558:SMMICM>2.0.CO;2](https://doi.org/10.1175/1525-7541(2001)002<0558:SMMICM>2.0.CO;2), 2001.
- Koster, R. D., Dirmeyer, P. A., Guo, Z., Bonan, G., Chan, E., Cox, P., Gordon, C. T., Kanae, S., Kowalczyk, E., Lawrence, D., Liu, P., Lu, C.-H., Malyshev, S., McAvaney, B., Mitchell, K., Mocko, D., Oki, T., Oleson, K., Pitman, A., Sud, Y. C., Taylor, C. M., Verseghy, D., Vasic, R., Xue, Y., and Yamada, T.: Regions of strong coupling between soil moisture and precipitation, *Science (New York, N.Y.)*, 305, 1138, 2004.
- Koster, R. D., Guo, Z., Yang, R., Dirmeyer, P. A., Mitchell, K., and Puma, M. J.: On the

- Nature of Soil Moisture in Land Surface Models, *Journal of Climate*, 22, 4322–4335, <https://doi.org/10.1175/2009jcli2832.1>, 2009a.
- Koster, R. D., Schubert, S. D., and Suarez, M. J.: Analyzing the Concurrence of Meteorological Droughts and Warm Periods, with Implications for the Determination of Evaporative Regime, *Journal of Climate*, 22, 3331–3341, <https://doi.org/10.1175/2008jcli2718.1>, 2009b.
- Koster, R. D., Schubert, S. D., Wang, H., Mahanama, S. P., and DeAngelis, A. M.: Flash Drought as Captured by Reanalysis Data: Disentangling the Contributions of Precipitation Deficit and Excess Evapotranspiration, *Journal of Hydrometeorology*, <https://doi.org/10.1175/jhm-d-18-0242.1>, 2019.
- Leelaruban, N., Padmanabhan, G., and Oduor, P.: Examining the Relationship between Drought Indices and Groundwater Levels, *Water*, 9, <https://doi.org/10.3390/w9020082>, 2017.
- Legates, D. R. and Willmott, C. J.: Mean seasonal and spatial variability in gauge-corrected, global precipitation, *International Journal of Climatology*, 10, 111–127, 1990.
- Liu, Y. Y., McCabe, M. F., Evans, J. P., Dijk, A. I. J. M. v., Jeu, R. A. M. d., and Su, H.: Comparison of soil moisture in GLDAS model simulations and satellite observations over the Murray Darling Basin, 18th World IMACS Congress and MODSIM09 International Congress on Modelling and Simulation: Interfacing Modelling and Simulation with Mathematical and Computational Sciences, Proceedings, pp. 2798–2804, 2009.
- Lorenz, R., Argüeso, D., Donat, M. G., Pitman, A. J., van den Hurk, B., Berg, A., Lawrence, D. M., Chéruy, F., Ducharne, A., Hagemann, S., Meier, A., Milly, P. C. D., and Seneviratne, S. I.: Influence of land-atmosphere feedbacks on temperature and precipitation extremes in the GLACE-CMIP5 ensemble, *Journal of Geophysical Research: Atmospheres*, 121, 607–623, <https://doi.org/10.1002/2015jd024053>, 2016.
- Lukas, J., Hobbins, M., and Rangwala, I.: The EDDI User Guide, Tech. rep., URL [https://psl.noaa.gov/eddi/pdf/EDDI\\_UserGuide\\_v1.0.pdf](https://psl.noaa.gov/eddi/pdf/EDDI_UserGuide_v1.0.pdf), 2017.

- Matsuura, K. and Willmott, C. J.: Terrestrial Air Temperature: 1900-2014 Gridded Monthly Time Series, Report, Department of Geography University of Delaware, URL [http://climate.geog.udel.edu/~climate/html\\_pages/Global2014/README.GlobalTsT2014.html](http://climate.geog.udel.edu/~climate/html_pages/Global2014/README.GlobalTsT2014.html), 2015.
- McEvoy, D. J., Huntington, J. L., Hobbins, M. T., Wood, A., Morton, C., Anderson, M., and Hain, C.: The Evaporative Demand Drought Index. Part II: CONUS-Wide Assessment against Common Drought Indicators, *Journal of Hydrometeorology*, 17, 1763–1779, <https://doi.org/10.1175/jhm-d-15-0122.1>, 2016.
- McKee, T. B., Doesken, N. J., and Kleist, J.: The Relationship of Drought Frequency and Duration to Time Scales, *Proceedings of the 8th Conference on Applied Climatology*, pp. 179–184, 1993.
- McMahon, T. A., Peel, M. C., Lowe, L., Srikanthan, R., and McVicar, T. R.: Estimating actual, potential, reference crop and pan evaporation using standard meteorological data: a pragmatic synthesis, *Hydrology and Earth System Sciences*, 17, 1331–1363, <https://doi.org/10.5194/hess-17-1331-2013>, 2013.
- McNeeley, S. M., Dewes, C. F., Stiles, C. J., Beeton, T. A., Rangwala, I., Hobbins, M. T., and Knutson, C. L.: Anatomy of an interrupted irrigation season: Micro-drought at the Wind River Indian Reservation, *Climate Risk Management*, 19, 61–82, 2018.
- McVicar, T. R., Van Niel, T. G., Li, L. T., Roderick, M. L., Rayner, D. P., Ricciardulli, L., and Donohue, R. J.: Wind speed climatology and trends for Australia, 1975–2006: Capturing the stilling phenomenon and comparison with near-surface reanalysis output, *Geophysical Research Letters*, 35, <https://doi.org/10.1029/2008gl035627>, 2008.
- Milly, P. and Dunne, K. A.: A hydrologic drying bias in water-resource impact analyses of anthropogenic climate change, *JAWRA Journal of the American Water Resources Association*, 53, 822–838, 2017.
- Milly, P. C. D. and Dunne, K. A.: Potential evapotranspiration and continental drying, *Nature Climate Change*, 6, 946–949, <https://doi.org/10.1038/nclimate3046>, 2016.

- Mishra, A. K. and Singh, V. P.: A review of drought concepts, *Journal of Hydrology*, 391, 202–216, 2010.
- Mo, K. C. and Lettenmaier, D. P.: Heat wave flash droughts in decline, *Geophysical Research Letters*, 42, 2823–2829, <https://doi.org/10.1002/2015GL064018>, 2015.
- Mo, K. C. and Lettenmaier, D. P.: Precipitation deficit flash droughts over the United States, *Journal of Hydrometeorology*, 17, 1169–1184, <https://doi.org/10.1175/JHM-D-15-0158.1>, 2016.
- Mo, X., Wu, J. J., Wang, Q., and Zhou, H.: Variations in water storage in China over recent decades from GRACE observations and GLDAS, *Natural Hazards and Earth System Sciences*, 16, 469–482, <https://doi.org/10.5194/nhess-16-469-2016>, 2016.
- Monteith, J.: Evaporation and Environment, *Symposia of the Society for Experimental Biology*, 19, 205–234, 1965.
- Mpelasoka, F., Hennessy, K., Jones, R., and Bates, B.: Comparison of suitable drought indices for climate change impacts assessment over Australia towards resource management, *International Journal of Climatology*, 28, 1283–1292, 2008.
- Mu, M., Kauwe, M. G. D., Ukkola, A. M., Pitman, A. J., Gimeno, T. E., Medlyn, B. E., Or, D., Yang, J., and Ellsworth, D. S.: Evaluating a land surface model at a water-limited site: implications for land surface contributions to droughts and heatwaves, *Hydrology and Earth System Sciences Discussions*, pp. 1–38, 2020.
- Mueller, B. and Seneviratne, S. I.: Systematic land climate and evapotranspiration biases in CMIP5 simulations, *Geophys Res Lett*, 41, 128–134, <https://doi.org/10.1002/2013GL058055>, 2014.
- Mukherjee, S., Mishra, A., and Trenberth, K.: Climate Change and Drought: a Perspective on Drought Indices, *Current Climate Change Reports*, 4, 145–163, <https://doi.org/10.1007/s40641-018-0098-x>, 2018.
- Narasimhan, B. and Srinivasan, R.: Development and evaluation of Soil Moisture Deficit Index (SMDI) and Evapotranspiration Deficit Index (ETDI) for agricultural drought monitoring, *Agricultural and Forest Meteorology*, 133, 69–88, <https://doi.org/10.1016/j.agrformet.2005.07.012>, 2005.

- Nguyen, H., Wheeler, M. C., Otkin, J. A., Cowan, T., Frost, A., and Stone, R.: Using the evaporative stress index to monitor flash drought in Australia, *Environmental Research Letters*, 14, <https://doi.org/10.1088/1748-9326/ab2103>, 2019.
- Noguera, I., Dominguez-Castro, F., and Vicente-Serrano, S. M.: Characteristics and trends of flash droughts in Spain, 1961-2018, *Ann N Y Acad Sci*, <https://doi.org/10.1111/nyas.14365>, URL <https://www.ncbi.nlm.nih.gov/pubmed/32406067>, 2020.
- of East Anglia Climatic Research Unit, U., Harris, I., and Jones, P.: CRU TS4.01: Climatic Research Unit (CRU) Time-Series (TS) version 4.01 of high-resolution gridded data of month-by-month variation in climate (Jan. 1901- Dec. 2016). Centre for Environmental Data Analysis, 04 December 2017., <https://doi.org/doi:10.5285/58a8802721c94c66ae45c3baa4d814d0>, 2017.
- Otkin, J. A., Anderson, M. C., Hain, C., Mladenova, I. E., Basara, J. B., and Svoboda, M.: Examining Rapid Onset Drought Development Using the Thermal Infrared-Based Evaporative Stress Index, *Journal of Hydrometeorology*, 14, 1057–1074, <https://doi.org/10.1175/jhm-d-12-0144.1>, 2013.
- Otkin, J. A., Anderson, M. C., Hain, C., and Svoboda, M.: Examining the Relationship between Drought Development and Rapid Changes in the Evaporative Stress Index, *Journal of Hydrometeorology*, 15, 938–956, <https://doi.org/10.1175/jhm-d-13-0110.1>, 2014.
- Otkin, J. A., Anderson, M. C., Hain, C., and Svoboda, M.: Using Temporal Changes in Drought Indices to Generate Probabilistic Drought Intensification Forecasts, *Journal of Hydrometeorology*, 16, 88–105, <https://doi.org/10.1175/jhm-d-14-0064.1>, 2015.
- Otkin, J. A., Anderson, M. C., Hain, C., Svoboda, M., Johnson, D., Mueller, R., Tadesse, T., Wardlow, B., and Brown, J.: Assessing the evolution of soil moisture and vegetation conditions during the 2012 United States flash drought, *Agricultural and Forest Meteorology*, 218–219, 230–242, <https://doi.org/10.1016/j.agrformet.2015.12.065>, 2016.
- Otkin, J. A., Svoboda, M., Hunt, E. D., Ford, T. W., Anderson, M. C., Hain, C., and Basara, J. B.: Flash Droughts: A Review and Assessment of the Challenges Imposed by

- Rapid-Onset Droughts in the United States, *Bulletin of the American Meteorological Society*, 99, 911–919, <https://doi.org/10.1175/bams-d-17-0149.1>, 2018.
- Palmer, W. C.: Meteorological Drought, Weather Bureau Research Paper, US Department of Commerce, Washington, DC, 45, 58, 1965.
- Pendergrass, A. G., Meehl, G. A., Pulwarty, R., Hobbins, M., Hoell, A., AghaKouchak, A., Bonfils, C. J. W., Gallant, A. J. E., Hoerling, M., Hoffmann, D., Kaatz, L., Lehner, F., Llewellyn, D., Mote, P., Neale, R. B., Overpeck, J. T., Sheffield, A., Stahl, K., Svoboda, M., Wheeler, M. C., Wood, A. W., and Woodhouse, C. A.: Flash droughts present a new challenge for subseasonal-to-seasonal prediction, *Nature Climate Change*, 10, 191–199, <https://doi.org/10.1038/s41558-020-0709-0>, 2020.
- Penman, H. L.: Natural evaporation from open water, bare soil and grass, *Proceedings of the Royal Society of London. Series A. Mathematical and Physical Sciences*, 193, 120–145, 1948.
- Pitman, A. J.: The evolution of, and revolution in, land surface schemes designed for climate models, *International Journal of Climatology*, 23, 479–510, <https://doi.org/10.1002/joc.893>, 2003.
- Pitman, A. J., de Noblet-Ducoudré, N., Cruz, F. T., Davin, E. L., Bonan, G. B., Brovkin, V., Claussen, M., Delire, C., Ganzeveld, L., Gayler, V., van den Hurk, B. J. J. M., Lawrence, P. J., van der Molen, M. K., Müller, C., Reick, C. H., Seneviratne, S. I., Strengers, B. J., and Voldoire, A.: Uncertainties in climate responses to past land cover change: First results from the LUCID intercomparison study, *Geophysical Research Letters*, 36, <https://doi.org/10.1029/2009gl039076>, 2009.
- Prudhomme, C., Parry, S., Hannaford, J., Clark, D. B., Hagemann, S., and Voss, F.: How Well Do Large-Scale Models Reproduce Regional Hydrological Extremes in Europe?, *Journal of Hydrometeorology*, 12, 1181–1204, <https://doi.org/10.1175/2011jhm1387.1>, 2011.
- Pulwarty, R. and Sivakumar, M. V. K.: Information systems in a changing climate: Early warnings and drought risk management, *Weather and Climate Extremes*, 3, 14–21, <https://doi.org/10.1016/j.wace.2014.03.005>, 2014.

- Raible, C. C., Bärenbold, O., and Gómez-navarro, J. J.: Drought indices revisited – improving and testing of drought indices in a simulation of the last two millennia for Europe, *Tellus A: Dynamic Meteorology and Oceanography*, 69, <https://doi.org/10.1080/16000870.2017.1296226>, 2017.
- Rippey, B. R.: The U.S. drought of 2012, *Weather and Climate Extremes*, 10, 57–64, <https://doi.org/10.1016/j.wace.2015.10.004>, 2015.
- Rodell, M., Houser, P., Jambor, U., Gottschalck, J., Mitchell, K., Meng, C.-J., Arsenault, K., Cosgrove, B., Radakovich, J., Bosilovich, M., Entin, J., Walker, J., Lohmann, D., and Toll, D.: The Global Land Data Assimilation System, *Bulletin of the American Meteorological Society*, 85, 381–394, <https://doi.org/10.1175/BAMS-85-3-381>, 2004.
- Rodell, M., Beaudoin, H. K., and NASA/GSFC/HSL: GLDAS Noah Land Surface Model L4 Monthly 1.0 x 1.0 degree V001, Greenbelt, Maryland, USA, Goddard Earth Sciences Data and Information Services Center (GES DISC), <https://doi.org/10.5067/G6ON3ZR1EUIJ>, 2007.
- Roderick, M. L., Rotstayn, L. D., Farquhar, G. D., and Hobbins, M. T.: On the attribution of changing pan evaporation, *Geophysical research letters*, 34, 2007.
- Roderick, M. L., Hobbins, M. T., and Farquhar, G. D.: Pan evaporation trends and the terrestrial water balance. II. Energy balance and interpretation, *Geography Compass*, 3, 761–780, 2009.
- Rui, H.: README Document for Global Land Data Assimilation System Version 1 (GLDAS-1) Products, Report, Goddard Earth Sciences Data and Information Service Center (GES DISC), 2017.
- Rui, H.: README Document for NASA GLDAS Version 2 Data Products, Report, Goddard Earth Sciences Data and Information Service Center (GES DISC), 2018.
- Samani, Z.: Estimating solar radiation and evapotranspiration using minimum climatological data, *Journal of irrigation and drainage engineering*, 126, 265–267, 2000.
- Schneider, U., Becker, A., Finger, P., Meyer-Christoffer, A., Ziese, M., and Rudolf, B.: GPCP's new land surface precipitation climatology based on quality-controlled in situ

- data and its role in quantifying the global water cycle, *Theoretical Applied Climatology*, 115, 15–40, <https://doi.org/10.1007/s00704-013-0860-x>, 2014.
- Schubert, S. D., Suarez, M. J., Pegion, P. J., Koster, R. D., and Bacmeister, J. T.: On the cause of the 1930s Dust Bowl, *Science (New York, N.Y.)*, 303, 1855, <https://doi.org/10.1126/science.1095048>, 2004.
- Seneviratne, S., Nicholls, N., Easterling, D., Goodess, C., Kanae, S., Kossin, J., Luo, Y., Marengo, J., McInnes, K., Rahimi, M., Reichstein, M., Sorteberg, A., Vera, C., and Zhang, X.: Changes in climate extremes and their impacts on the natural physical environment, in: *A Special Report of Working Groups I and II of the Intergovernmental Panel on Climate Change (IPCC)*, edited by Field, C., Barros, V., Stocker, T., Qin, D., Dokken, D., Ebi, K., Mastrandrea, M., Mach, K., Plattner, G.-K., Allen, S., Tignor, M., and Midgley, P., pp. 109–230, Cambridge University Press, Cambridge, UK, and New York, NY, USA, 2012.
- Seneviratne, S. I., Koster, R. D., Guo, Z., Dirmeyer, P. A., Kowalczyk, E., Lawrence, D., Liu, P., Mocko, D., Lu, C.-H., Oleson, K. W., et al.: Soil moisture memory in AGCM simulations: analysis of global land–atmosphere coupling experiment (GLACE) data, *Journal of Hydrometeorology*, 7, 1090–1112, 2006.
- Seneviratne, S. I., Corti, T., Davin, E. L., Hirschi, M., Jaeger, E. B., Lehner, I., Orlowsky, B., and Teuling, A. J.: Investigating soil moisture–climate interactions in a changing climate: A review, *Earth-Science Reviews*, 99, 125–161, 2010.
- Seneviratne, S. I., Wilhelm, M., Stanelle, T., Hurk, B., Hagemann, S., Berg, A., Cheruy, F., Higgins, M. E., Meier, A., Brovkin, V., Claussen, M., Ducharne, A., Dufresne, J., Findell, K. L., Ghattas, J., Lawrence, D. M., Malyshev, S., Rummukainen, M., and Smith, B.: Impact of soil moisture–climate feedbacks on CMIP5 projections: First results from the GLACE-CMIP5 experiment, *Geophysical Research Letters*, 40, 5212–5217, <https://doi.org/10.1002/grl.50956>, 2013.
- Sheffield, J. and Wood, E. F.: *Drought - Past Problems and Future Scenarios*, Earthscan, London, 2011.
- Sheffield, J., Goteti, G., and Wood, E. F.: *Development of a 50-yr high-resolution*

- global dataset of meteorological forcings for land surface modeling, *JOURNAL OF CLIMATE*, 19, 3088–3111, 2006.
- Sheffield, J., Wood, E. F., and Roderick, M. L.: Little change in global drought over the past 60 years, *Nature*, 491, 435–8, <https://doi.org/10.1038/nature11575>, 2012.
- Spennemann, P., Rivera, J., Saulo, A., and Penalba, O.: A Comparison of GLDAS Soil Moisture Anomalies against Standardized Precipitation Index and Multisatellite Estimations over South America, *Journal of Hydrometeorology*, 16, 158–171, <https://doi.org/10.1175/JHM-D-13-0190.1>, 2015.
- Stahl, K., Moore, R., Floyer, J., Asplin, M., and McKendry, I.: Comparison of approaches for spatial interpolation of daily air temperature in a large region with complex topography and highly variable station density, *Agricultural and forest meteorology*, 139, 224–236, 2006.
- Sun, Q., Miao, C., Duan, Q., Ashouri, H., Sorooshian, S., and Hsu, K.: A Review of Global Precipitation Data Sets: Data Sources, Estimation, and Intercomparisons, *Reviews of Geophysics*, 56, 79–107, <https://doi.org/10.1002/2017rg000574>, 2018.
- Svoboda, M., Lecomte, D., Hayes, M., Heim, R., Gleason, K., Angel, J., Rippey, B., Tinker, R., Palecki, K., Stooksbury, D., Miskus, D., and Stephens, S.: The Drought Monitor, *BULLETIN OF AMERICAN METEOROLOGICAL SOCIETY*, pp. 1181–1190, 2002.
- Swann, A. L., Hoffman, F. M., Koven, C. D., and Randerson, J. T.: Plant responses to increasing CO<sub>2</sub> reduce estimates of climate impacts on drought severity, *Proc Natl Acad Sci U S A*, 113, 10019–24, <https://doi.org/10.1073/pnas.1604581113>, 2016.
- Syed, T. H., Famiglietti, J. S., Rodell, M., Chen, J., and Wilson, C. R.: Analysis of terrestrial water storage changes from GRACE and GLDAS, *Water Resources Research*, 44, <https://doi.org/10.1029/2006wr005779>, 2008.
- Taylor, K. E., Stouffer, R. J., and Meehl, G. A.: An overview of CMIP5 and the experiment design, *American Meteorological Society*, April, 485–498, <https://doi.org/10.1175/BAMS-D-11-00094.1In>, 2012.

- Thornthwaite, C. W.: An approach toward a rational classification of climate, *Geographical review*, 38, 55–94, 1948.
- Trenberth, K. E., Dai, A., van der Schrier, G., Jones, P. D., Barichivich, J., Briffa, K. R., and Sheffield, J.: Global warming and changes in drought, *Nature Climate Change*, 4, 17–22, <https://doi.org/10.1038/nclimate2067>, 2014.
- Tsakiris, G. and Vangelis, H.: Establishing a Drought Index Incorporating Evapotranspiration, *European Water*, 9, 3–11, 2005.
- Ukkola, A. M., De Kauwe, M. G., Pitman, A. J., Best, M. J., Abramowitz, G., Haverd, V., Decker, M., and Haughton, N.: Land surface models systematically overestimate the intensity, duration and magnitude of seasonal-scale evaporative droughts, *Environmental Research Letters*, 11, <https://doi.org/10.1088/1748-9326/11/10/104012>, 2016a.
- Ukkola, A. M., Pitman, A. J., Decker, M., De Kauwe, M. G., Abramowitz, G., Kala, J., and Wang, Y.-P.: Modelling evapotranspiration during precipitation deficits: identifying critical processes in a land surface model, *Hydrology and Earth System Sciences*, 20, 2403–2419, <https://doi.org/10.5194/hess-20-2403-2016>, 2016b.
- Ukkola, A. M., Haughton, N., De Kauwe, M. G., Abramowitz, G., and Pitman, A. J.: FluxnetLSM R package (v1. 0): A community tool for processing FLUXNET data for use in land surface modelling, *Geoscientific Model Development*, 10, 3379, 2017.
- Ukkola, A. M., Pitman, A. J., De Kauwe, M. G., Abramowitz, G., Herger, N., Evans, J. P., and Decker, M.: Evaluating CMIP5 Model Agreement for Multiple Drought Metrics, *Journal of Hydrometeorology*, 19, 969–988, <https://doi.org/10.1175/jhm-d-17-0099.1>, 2018a.
- Ukkola, A. M., Pitman, A. J., Donat, M. G., De Kauwe, M. G., and Angéilil, O.: Evaluating the Contribution of Land-Atmosphere Coupling to Heat Extremes in CMIP5 Models, *Geophysical Research Letters*, 45, 9003–9012, <https://doi.org/10.1029/2018gl079102>, 2018b.
- Ummenhofer, C. C., England, M. H., McIntosh, P. C., Meyers, G. A., Pook, M. J., Risbey, J. S., Sen Gupta, A., and Taschetto, A. S.: What causes southeast Australia's

- worst droughts?, *Geophysical Research Letters*, 36, 1–5, <https://doi.org/doi:10.1029/2008GL036801>, 2009.
- Ummenhofer, C. C., Sen Gupta, A., Briggs, P. B., England, M. H., Macintosh, P. C., Meyers, G. A., Pook, M. J., Raupach, M. R., and Risbey, J. S.: Indian and Pacific Ocean Influences on Southeast Australian Drought and Soil Moisture, *Journal of Climate*, 24, 1313–1336, <https://doi.org/DOI:10.1175/JCLI-D-11-00229.1>, 2011.
- Van Dijk, A., Bacon, D., Barratt, D., Crosbie, R., Daamen, C., Fitch, P., Frost, A., Guerschman, J., Henderson, B., King, E., McVicar, T., Renzullo, L., Stenson, M., and Viney, N.: Design and development of the Australian Water Resources Assessment system.pdf, *Water Information Research and Development Alliance (WIRADA) Science Symposium Proceedings*, 2011.
- van Dijk, A. I. J. M., Beck, H. E., Crosbie, R. S., de Jeu, R. A. M., Liu, Y. Y., Podger, G. M., Timbal, B., and Viney, N. R.: The Millennium Drought in south-east Australia (2001–2009): Natural and human causes and implications for water resources, ecosystems, economy, and society, *Water Resources Research*, 49, 1040–1057, <https://doi.org/doi:10.1002/wrcr.20123>, 2013.
- Van Lanen, H. A. J. and Peters, E.: Definition, effects and assessment of groundwater droughts, in: *Drought and Drought Mitigation in Europe. Advances in Natural and Technological Hazards Research*, edited by J.V., V. and F., S., pp. 49–61, Springer, Dordrecht, [https://doi.org/10.1007/978-94-015-9472-1\\_4](https://doi.org/10.1007/978-94-015-9472-1_4), 2000.
- Van Loon, A. F.: Hydrological drought explained, *Wiley Interdisciplinary Reviews: Water*, 2, 359–392, <https://doi.org/10.1002/wat2.1085>, 2015.
- Van Loon, A. F., Kumar, R., and Mishra, V.: Testing the use of standardised indices and GRACE satellite data to estimate the European 2015 groundwater drought in near-real time, *Hydrology and Earth System Sciences*, 21, 1947–1971, <https://doi.org/10.5194/hess-21-1947-2017>, 2017.
- Van Looy, K., Bouma, J., Herbst, M., Koestel, J., Minasny, B., Mishra, U., Montzka, C., Nemes, A., Pachepsky, Y. A., Padarian, J., et al.: Pedotransfer functions in Earth system science: challenges and perspectives, *Reviews of Geophysics*, 55, 1199–1256, 2017.

- Verdon-Kidd, D. C. and Kiem, A. S.: Nature and causes of protracted droughts in south-east Australia: Comparison between the Federation, WWII, and Big Dry droughts, *Geophysical Research Letters*, 36, 1–6, <https://doi.org/doi:10.1029/2009GL041067>, 2009.
- Vicente-Serrano, S. M., Beguería, S., and López-Moreno, J. I.: A Multiscalar Drought Index Sensitive to Global Warming: The Standardized Precipitation Evapotranspiration Index, *Journal of Climate*, 23, 1696–1718, <https://doi.org/10.1175/2009jcli2909.1>, 2010.
- Vicente-Serrano, S. M., Beguería, S., Lorenzo-Lacruz, J., Camarero, J. J., López-Moreno, J. I., Azorin-Molina, C., Revuelto, J., Morán-Tejeda, E., and Sanchez-Lorenzo, A.: Performance of Drought Indices for Ecological, Agricultural, and Hydrological Applications, *Earth Interactions*, 16, 1–27, <https://doi.org/10.1175/2012ei000434.1>, 2012.
- Wang, H., Rogers, J. C., and Munroe, D. K.: Commonly Used Drought Indices as Indicators of Soil Moisture in China, *Journal of Hydrometeorology*, 16, 1397–1408, <https://doi.org/10.1175/jhm-d-14-0076.1>, 2015.
- Wang, L., Yuan, X., Xie, Z., Wu, P., and Li, Y.: Increasing flash droughts over China during the recent global warming hiatus, *Scientific Reports*, 6, <https://doi.org/10.1038/srep30571>, 2016a.
- Wang, W., Cui, W., Wang, X., and Chen, X.: Evaluation of GLDAS-1 and GLDAS-2 Forcing Data and Noah Model Simulations over China at the Monthly Scale, *Journal of Hydrometeorology*, 17, 2815–2833, <https://doi.org/10.1175/jhm-d-15-0191.1>, 2016b.
- Webb, R. S. and Rosenzweig, C. E.: Specifying Land Surface Characteristics in General Circulation Models: Soil Profile Data Set and Derived Water-Holding Capacity, *Global Biogeochemical Cycles*, 7, 97–108, 1993.
- Wells, N. and Hayes, M. J.: A Self-Calibrating Palmer Drought Severity Index, *Journal of Climate*, 17, 2335–2351, 2004.

- Weymouth, G. and Le Marshall, J. F.: Estimation of daily surface solar exposure using GMS-5 stretched-VISSR observations: The system and basic results, *Australian Meteorological Magazine*, 50, 263–278, 2001.
- Wilhite, D. and Pulwarty, R., eds.: *Drought and Water Crises*, CRC Press, Boca Raton, USA, <https://doi.org/10.1201/9781315265551-15>, 2017.
- Wilhite, D. A.: *Drought*, Drought Mitigation Center Faculty Publications, 64, URL <http://digitalcommons.unl.edu/droughtfacpub/64>, 1992.
- Wilhite, D. A. and Glantz, M. H.: Understanding the Drought Phenomenon: The Role of Definitions, *Water International*, 10, 111–120, 1985.
- WMO: Standardized Precipitation Index User Guide (M. Svoboda, M. Hayes and D. Wood), Report, World Meteorological Organization, WMO-No. 1090, Geneva, URL [http://www.wamis.org/agm/pubs/SPI/WMO\\_1090\\_EN.pdf](http://www.wamis.org/agm/pubs/SPI/WMO_1090_EN.pdf), 2012.
- Wu, H., Hayes, M. J., Wilhite, D. A., and Svoboda, M. D.: The effect of the length of record on the standardized precipitation index calculation, *International Journal of Climatology*, 25, 505–520, <https://doi.org/10.1002/joc.1142>, 2005.
- Xie, P. and Arkin, P. A.: Global Precipitation: A 17-Year Monthly Analysis Based on Gauge Observations, Satellite Estimates, and Numerical Model Outputs, *Bulletin of the American Meteorological Society*, 78, 2539–2558, 1997.
- Yang, T., Wang, C., Yu, Z., and Xu, F.: Characterization of spatio-temporal patterns for various GRACE- and GLDAS-born estimates for changes of global terrestrial water storage, *Global and Planetary Change*, 109, 30–37, <https://doi.org/10.1016/j.gloplacha.2013.07.005>, 2013.
- Yuan, S. and Quiring, S. M.: Evaluation of soil moisture in CMIP5 simulations over the contiguous United States using in situ and satellite observations, *Hydrology and Earth System Sciences*, 21, 2203–2218, <https://doi.org/10.5194/hess-21-2203-2017>, 2017.
- Zargar, A., Sadiq, R., Naser, B., and Kahn, F. I.: A review of drought indices, *Environmental Review*, 19, 333–349, <https://doi.org/10.1139/A11-013>, 2011.

- Zhan, W., Guan, K., Sheffield, J., and Wood, E. F.: Depiction of drought over sub-Saharan Africa using reanalyses precipitation data sets, *Journal of Geophysical Research: Atmospheres*, 121, 10,555–10,574, <https://doi.org/10.1002/2016jd024858>, 2016.
- Zhang, Y., You, Q., Chen, C., and Li, X.: Flash droughts in a typical humid and subtropical basin: A case study in the Gan River Basin, China, *Journal of Hydrology*, 551, 162–176, <https://doi.org/10.1016/j.jhydrol.2017.05.044>, 2017.
- Zhang, Y., You, Q., Chen, C., Ge, J., and Adnan, M.: Evaluation of downscaled CMIP5 Coupled with VIC model for flash drought simulation in a humid subtropical basin, China, *Journal of Climate*, 31, 1075–1090, <https://doi.org/10.1175/JCLI-D-17-0378.1>, 2018.
- Zhao, M., A, G., Velicogna, I., and Kimball, J. S.: A Global Gridded Dataset of GRACE Drought Severity Index for 2002–14: Comparison with PDSI and SPEI and a Case Study of the Australia Millennium Drought, *Journal of Hydrometeorology*, 18, 2117–2129, <https://doi.org/10.1175/jhm-d-16-0182.1>, 2017.
- Zhao, T. and Dai, A.: The Magnitude and Causes of Global Drought Changes in the Twenty-First Century under a Low–Moderate Emissions Scenario, *Journal of Climate*, 28, 4490–4512, <https://doi.org/10.1175/jcli-d-14-00363.1>, 2015.